

**Solid Solution/Aqueous Solution Partitioning of Cadmium to Calcite:
Thermodynamics and Transport**

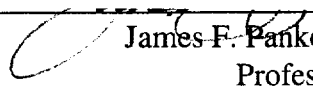
Andrea Pavlick

B.S. magna cum laude, Allegheny College, 1993

A thesis presented to the faculty of the
Oregon Graduate Institute of Science and Technology
in partial fulfillment of the
requirements for the degree
Doctor of Philosophy
in
Environmental Science and Engineering

August 1999

The dissertation "Solid Solution/Aqueous Solution Partitioning of Cadmium to Calcite: Thermodynamics and Transport" by Andrea Pavlick has been examined and approved by the following Examination Committee:

 James F. Pankow, Advisor
Professor

William Fish
Associate Professor

Carl D. Palmer
Associate Professor

Patricia L. Toccalino
Assistant Professor

Acknowledgments

First, I would like to acknowledge Jim Pankow who agreed to take me on as a student in 1993. I consider Jim to be an exceptional advisor and will always appreciate the great deal of freedom that he allowed me to have while I was a student in his research group. Jim also provided me with opportunities to participate in research planning, proposal writing, project management, and manuscript review not available to every graduate student. As a result, I have developed a more complete understanding of science in the modern world.

I would also like to recognize the following individuals who provided technical assistance over the course of this research project: Lorne Isabelle and Graham Tewksbury from OGI; Don Bear, Mark Englehardt and Dave McCready from the Environmental Molecular Sciences Laboratory National Scientific User Facility; and finally, David Brush and Neil Thompson from the University of Waterloo.

I would like to thank those individuals in addition to my advisor who over the course of my dissertation provided guidance, advice and a kick in the head when necessary. This group includes the remainder of my committee, Bill Fish, Carl Palmer and Patty Toccalino, Wentai Luo who had the dubious honor of sharing a cubicle with me for many years, and nearly the entire faculty of the ESE Department. Thanks to Rob, Sharon and Rachel for a home away from home away from home in Richland, and to family and friends for near unlimited support over the past years.

Finally, I would like to thank everyone who made my time here in the Pacific Northwest a joy. This includes the staff and students of the ESE Department past and present, the members of the OGI Aikido club (who ensured that I slept well at least two nights a week), the river people, the card players, and everyone who got up early on a

weekend to come hiking with me. A special thank you goes out to those brave few who entertained the knuckle headed beastie when I was sick, injured or away, everyone who got up before sunrise to get me to the airport for those 6:30 AM flights, and those of you who supported my sugar habit. I'm going to cut back now, honest.

Table of Contents

Acknowledgments	iii
Table of Contents	v
List of Tables	vii
List of Figures	x
Abstract	xii
Chapter 1: Introduction	1
1.1 Background	1
1.2 Solid Solutions in the Environment	3
1.3 Calcite in Natural Systems	5
1.4 Objectives	7
Chapter 2: Solid Solution Theory and Representation	8
2.1 Introduction	8
2.2 Thermodynamic Mixing	8
2.3 Miscibility Gaps	11
2.4 Solid Solution/Aqueous Solution Equilibria	12
2.5 Distribution Coefficients	13
2.6 Stoichiometric Saturation Model	15
2.7 Total Solubility Product Model	16
2.8 Reaction Paths	18
Chapter 3: Determination of Thermodynamic Parameters for the Calcite/Otavite Solid Solution Series	19
3.1 Objectives	19

3.2	Seed Material Characterization	20
3.3	SSAS Partitioning of Cadmium to Calcite	26
3.4	SSAS Partitioning of Calcium to Otavite	51
3.5	XPS	70
3.6	XRD	79
3.7	Discussion	80
Chapter 4: Mixing Behavior of the Calcite/Otavite Solid Solution Series		89
4.1	Introduction	89
4.2	Literature Values for Interaction Parameters	91
4.3	Estimation of Mixing Parameters from Measured D_{eq} and ζ Values	93
4.4	Discussion	98
Chapter 5: SSAS Partitioning as a Retardation Mechanism in Subsurface Transport ...		105
5.1	Introduction	105
5.2	Transport Studies	105
5.3	Modeling Attempts	107
5.4	MeTran Model.....	109
5.5	Diagnostic Modeling	115
5.6	Column Experiment Design	123
Chapter 6: Summary and Conclusions		124
References		130
Appendix A: Data from Constant Composition Experiments		138
Appendix B: Data from XPS Analyses		156
Appendix C: Data from XRD Analyses		163
Appendix D: MeTran Source Code		167
Biography		193

List of Tables

Table 3.1	Trace composition of calcite seed material.....	20
Table 3.2	Calcite solubility data.....	23
Table 3.3	Otavite solubility data.....	24
Table 3.4	G series precipitation rate data.....	32
Table 3.5	G series solid solution compositions.....	33
Table 3.6	G series distribution coefficient data.....	34
Table 3.7	H series precipitation rate data.....	43
Table 3.8	H series solid solution compositions.....	44
Table 3.9	H series distribution coefficient data.....	45
Table 3.10	E series precipitation rate data.....	54
Table 3.11	E series solid solution compositions.....	56
Table 3.12	E series distribution coefficient data.....	57
Table 3.13	F series precipitation rate data.....	63
Table 3.14	F series solid solution compositions.....	64
Table 3.15	F series distribution coefficient data.....	65
Table 3.16	Mole fraction comparison from washed and unwashed samples.....	76
Table 3.17	XRD unit cell volumes.....	80
Table 4.1	Endmember properties.....	91
Table 4.2	Mole fraction, distribution coefficient, and solid phase activity coefficient data.....	96
Table 4.3	Interaction parameters for the $\text{CaCO}_{3(s)}/\text{CdCO}_{3(s)}$ solid solution series.....	98
Table A.1	Data from experiment E1.....	138

Table A.2	Data from experiment E2.....	138
Table A.3	Data from experiment E3.....	139
Table A.4	Data from experiment E4.....	139
Table A.5	Data from experiment E5.....	140
Table A.6	Data from experiment E6.....	140
Table A.7	Data from experiment E7.....	140
Table A.8	Data from experiment E8.....	141
Table A.9	Data from experiment E9.....	141
Table A.10	Data from experiment E10.....	141
Table A.11	Data from experiment E11.....	142
Table A.12	Data from experiment E12.....	142
Table A.13	Data from experiment E13.....	142
Table A.14	Data from experiment E14.....	143
Table A.15	Data from experiment F1.....	143
Table A.16	Data from experiment F2.....	143
Table A.17	Data from experiment F3.....	144
Table A.18	Data from experiment F4.....	144
Table A.19	Data from experiment F5.....	144
Table A.20	Data from experiment F6.....	145
Table A.21	Data from experiment F7.....	145
Table A.22	Data from experiment F8.....	145
Table A.23	Data from experiment F9.....	146
Table A.24	Data from experiment F10.....	146
Table A.25	Data from experiment F11.....	146
Table A.26	Data from experiment F12.....	147
Table A.27	Data from experiment F13.....	147
Table A.28	Data from experiment F14.....	147
Table A.29	Data from experiment G1.....	148
Table A.30	Data from experiment G2.....	148

Table A.31	Data from experiment G3.....	149
Table A.32	Data from experiment G4	149
Table A.33	Data from experiment G5.....	149
Table A.34	Data from experiment G6	150
Table A.35	Data from experiment G7.....	150
Table A.36	Data from experiment G8.....	150
Table A.37	Data from experiment G9.....	151
Table A.38	Data from experiment G10.....	151
Table A.39	Data from experiment G11.....	151
Table A.40	Data from experiment G12.....	152
Table A.41	Data from experiment H1.....	152
Table A.42	Data from experiment H2.....	152
Table A.43	Data from experiment H3.....	153
Table A.44	Data from experiment H4.....	153
Table A.45	Data from experiment H5.....	153
Table A.46	Data from experiment H6.....	154
Table A.47	Data from experiment H7.....	154
Table A.48	Data from experiment H8.....	154
Table A.49	Data from experiment H9.....	155
Table A.50	Data from experiment H10.....	155
Table A.50	Data from experiment H12.....	155
Table B.1	XPS atomic concentration table, multiplex scans.....	156
Table B.2	XPS atomic concentration table, survey scans.....	159
Table C.1	D-spacings for calcite seed material.....	163
Table C.2	D-spacings for otavite seed material.....	164
Table C.3	D-spacings for sample G4.....	164
Table C.4	D-spacings for sample F13.....	165

List of Figures

Figure 1.1	Schematic representation of a $\text{Ca}_{1-x}\text{Cd}_x\text{CO}_3$ solid solution.....	2
Figure 1.2	Areas of carbonate rock in the near surface of the continental United States.....	5
Figure 2.1	Lippmann phase diagram for the calcite/otavite solid solution series assuming regular behavior, $a_m = 0.8$	17
Figure 3.1	SEM image of calcite seed material.....	21
Figure 3.2	SEM image of otavite seed material.....	21
Figure 3.3	Schematic diagram of apparatus used during experiments discussed in Chapter 3.....	28
Figure 3.4	$[\text{Ca}^{2+}]$ vs. log precipitation rate and $[\text{Cd}^{2+}]$ vs. log precipitation rate for G series experiments.....	36
Figure 3.5	$D_{\text{Cd}^{2+}, \text{titrant}}$ vs. log precipitation rate for G series experiments.....	38
Figure 3.6	$D_{\text{Cd}^{2+}, \text{mass balance}}$ vs. log precipitation rate for G series experiments.....	39
Figure 3.7	$D_{\text{Cd}^{2+}, \text{XPS}}$ vs. log precipitation rate for G series experiments.....	40
Figure 3.8	$[\text{Ca}^{2+}]$ vs. log precipitation rate and $[\text{Cd}^{2+}]$ vs. log precipitation rate for H series experiments.....	47
Figure 3.9	$D_{\text{Cd}^{2+}, \text{titrant}}$ vs. log precipitation rate for H series experiments.....	48
Figure 3.10	$D_{\text{Cd}^{2+}, \text{mass balance}}$ vs. log precipitation rate for H series experiments.....	49
Figure 3.11	$D_{\text{Cd}^{2+}, \text{XPS}}$ vs. log precipitation rate for H series experiments.....	50
Figure 3.12	$[\text{Ca}^{2+}]$ vs. log precipitation rate and $[\text{Cd}^{2+}]$ vs. log precipitation rate for E series experiments.....	58
Figure 3.13	$D_{\text{Ca}^{2+}, \text{AAS}}$ vs. log precipitation rate for E series experiments.....	60

Figure 3.14	$D_{Ca^{2+}, XPS}$ vs. log precipitation rate for E series experiments.....	61
Figure 3.15	$[Ca^{2+}]$ vs. log precipitation rate and $[Cd^{2+}]$ vs. log precipitation rate for F series experiments.....	66
Figure 3.16	$D_{Ca^{2+}, AAS}$ vs. log precipitation rate for F series experiments.....	68
Figure 3.17	$D_{Ca^{2+}, XPS}$ vs. log precipitation rate for F series experiments.....	69
Figure 3.18	XPS survey scan of sample G10.....	74
Figure 3.19	XPS multiplex scan of sample E13 showing separation of C1s and adventitious carbon peaks.....	75
Figure 3.20	Comparison of XPS X values to mass balance values from G and H series experiments and to AAS values from E and F series experiments....	78
Figure 3.21	SEM images of sample G4 at high and low magnification.....	83
Figure 3.22	SEM images of sample G10 at high and low magnification.....	84
Figure 3.24	SEM images of E series solid materials.....	85
Figure 4.1	Comparison of experimental ζ values to regular solid solution model with $a_m = 1.04$	100
Figure 4.2	Comparison of experimental ζ values to regular solid solution model with $a_m = -1.26$	101
Figure 4.3	Comparison of experimental ζ values to sub-regular solid solution model with $a_0 = 0.17$ and $a_1 = 1.27$	102
Figure 4.4	Comparison of measured $D_{Ca^{2+}, eq}$ values to model predictions.....	103
Figure 4.5	Comparison of measured $D_{Cd^{2+}, eq}$ values to model predictions.....	104
Figure 5.1	MeTran input file.....	114
Figure 5.2	Breakthrough curves for increasing weight fractions of calcite with no solid state diffusion.....	118
Figure 5.3	Breakthrough curves for $f_{calcite} = 0.05$ with increasing solid state diffusion depths.....	119
Figure 5.4	Column profile for continuous source, $f_{calcite} = 0.05$, calcite depth = 200 Å.....	120
Figure 5.5	Pulsed source with increasing solid state diffusion depth.....	121
Figure C.1	XRD spectra for samples G4 and F13.....	166

Abstract

Solid Solution/Aqueous Solution Partitioning of Cadmium to Calcite: Thermodynamics and Transport

Andrea Pavlick

James F. Pankow, Advisor

Solid solution formation allows the precipitation of otavite ($\text{CdCO}_{3(s)}$) under conditions when the solution is not saturated with respect to pure $\text{CdCO}_{3(s)}$. Since Cd^{2+} and other divalent metals partition readily into calcite ($\text{CaCO}_{3(s)}$), solid solution/aqueous solution (SSAS) partitioning may play a significant role in the transport of metals in the environment. In order to understand this process in a natural water context, equilibrium constants for the SSAS partitioning process need to be determined and the ability of SSAS partitioning to retard the movement of metal contaminants in the environment needs to be evaluated.

A constant composition method was used to precipitate calcite/otavite solid solutions of known composition on seed material via the controlled addition of titrant solutions. Solid solution/aqueous solution distribution coefficient D values were found to be dependent on precipitation rate with equilibrium behavior occurring at the slowest precipitation rates. $D_{\text{Ca}^{2+}\text{eq}}$ values near the otavite endmember ranged from 0.007 to 0.0019 depending on solid solution composition. Near the calcite endmember, $D_{\text{Cd}^{2+}\text{eq}}$ values ranged from 1200 to 2400 depending on solid solution composition.

D_{eq} values were used to calculate solid phase activity coefficient ζ values for the trace components of the various solid solutions. The measured D_{eq} and calculated ζ values indicated that the $\text{CaCO}_{3(s)}/\text{CdCO}_{3(s)}$ solid solution series follows sub-regular mixing behavior described by dimensionless Guggenheim interaction parameters of $a_0 = 0.17$ and $a_1 = 1.27$.

Diagnostic transport modeling that incorporated SSAS partitioning indicated that solid solution formation can have a major impact on the transport of Cd^{2+} in saturated media that contains even small amounts of calcite. The model was used to design a column experiment that can be used to evaluate the importance of SSAS partitioning as a retardation mechanism in advective-dispersive transport.

Chapter 1

Introduction

1.1 Background

The behavior of chemical species in natural systems is often controlled by the solid phases present in those systems. Adsorption, ion-exchange, precipitation/dissolution of nearly pure phases, and precipitation/dissolution of solid solutions are common processes by which solid phases effect the compositions of ground and surface waters. An understanding of these processes is fundamental to our ability to predict the transport of contaminants in the environment and the effect of those contaminants on water quality and the general health of ecosystems. Of the processes mentioned above, the role of solid solutions in the fate and transport of metal contaminants is the least understood.

The term solid solution refers to a single-phase mixture of two or more pure solid phases which are referred to as end-members. In many cases, solid solutions are ionic solids where a common anion is shared by two or more metal cations. When one of the cations is present at low levels, a binary solid solution may be conceptualized as a foreign cation partitioning into an existing mineral structure. Figure 1.1 is a schematic diagram for a calcite/otavite ($\text{CaCO}_{3(s)}/\text{CdCO}_{3(s)}$) solid solution showing the substitution of Cd^{2+} for some of the Ca^{2+} in the calcite lattice. A general chemical formula for this solid solution can be written as $\text{Ca}_{1-x}\text{Cd}_x\text{CO}_3$ where x refers to the number of sites where Cd^{2+} has replaced Ca^{2+} in the crystal lattice.

Although the existence of solid solutions in natural systems is evidenced by the rarity of pure mineral phases under natural conditions (Garrels and Christ, 1965), the

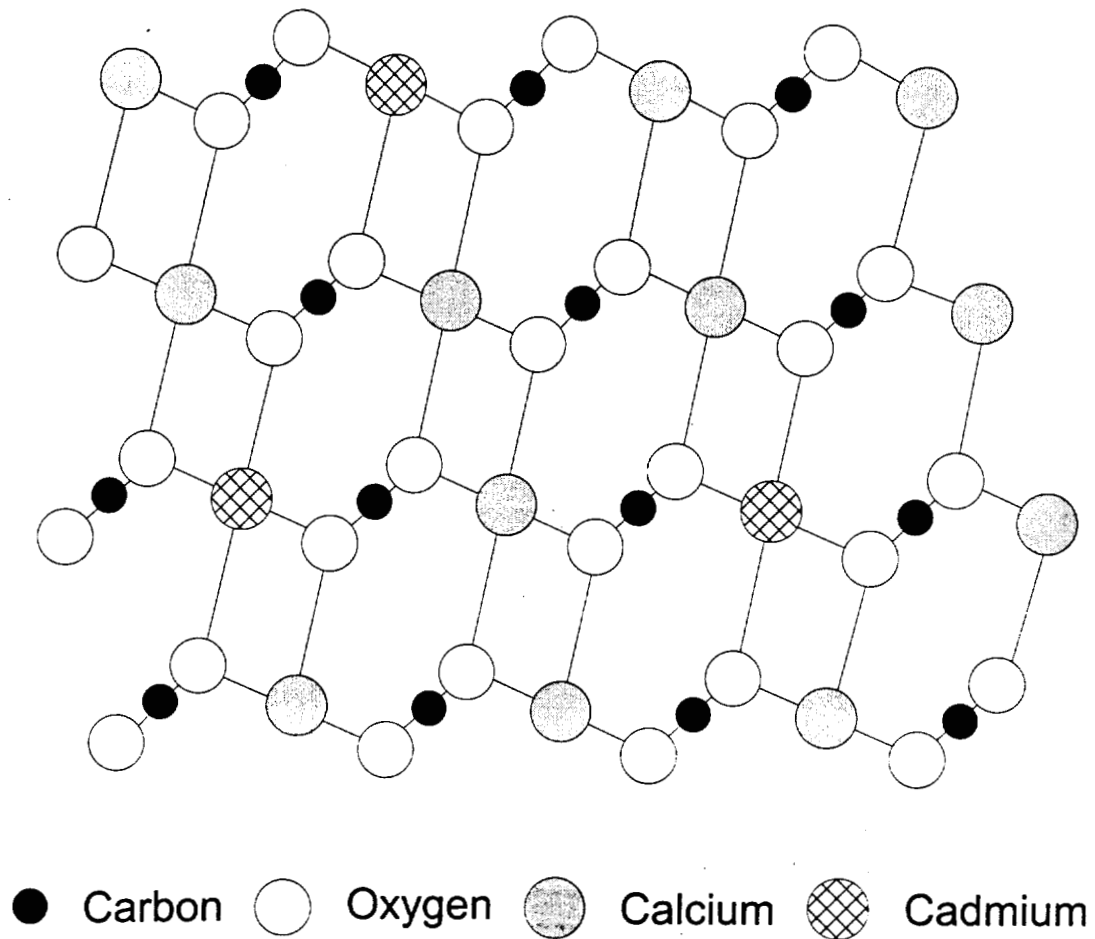


Figure 1.1 Schematic representation of a $\text{Ca}_{1-x}\text{Cd}_x\text{CO}_3$ solid solution.

formation of solid solutions is rarely accounted for when predicting the fate and transport of metals in the environment. This discrepancy is due in part to a lack of information concerning the thermodynamic and kinetic properties of solid solutions in low temperature systems. For low and "trace" levels of divalent metals in water, the approaches currently used to predict partitioning rely almost exclusively on surface adsorption models. For example, MINTEQA2 (Allison *et al.*, 1991) and other similar geochemistry models assume that Cd^{2+} will not begin to precipitate as a carbonate solid until the aqueous conditions exceed saturation with respect to pure $\text{CdCO}_{3(s)}$. Contaminant transport models which employ speciation models like MINTEQA2 are bound by the same assumptions.

There is a growing body of evidence that indicates surface adsorption, ion-exchange and pure phase precipitation are inadequate for describing the partitioning of metal trace constituents to solid phases including carbonates, oxy-hydroxides and clays (Lornes, 1981; Davis *et al.*, 1987; Tesoriero and Pankow, 1996; Friedl *et al.*, 1997; Scheidegger *et al.*, 1997; Ford *et al.*, 1997; Martínez and McBride, 1998). Solid solution/aqueous solution (SSAS) partitioning, also called “coprecipitation”, is a mechanism which may play a significant role in the fate and transport of chemical constituents, particularly the long term uptake of ions into solid phases. With respect to accurately predicting the behavior of trace metals, failure to account for solid solution formation can result in under predictions of the amounts of trace metals associated with the solid phase, and over predictions of the mobilities of trace metals in the environment.

1.2 Solid Solutions in the Environment

Ample evidence exists to indicate that carbonate solid solutions play a role in the cycling of metals in the environment. In the case of surface waters, whitening events in lakes (Stabel *et al.*, 1986; Kleiner and Stabel, 1989), and the growth of marine aquatic organisms that construct shells and skeletons from calcite and aragonite (Hirao *et al.*, 1994; McCulloch *et al.*, 1994; Mashiotto *et al.*, 1997) are common processes by which solid solutions are formed. In ground waters, solid solutions can be observed in calcite deposits along fractures (Erel and Katz, 1990; Denniston *et al.*, 1997) and in cave formations where ground water re-equilibrates with atmospheric levels of carbon dioxide resulting in the precipitation of carbonate rock (Holland *et al.*, 1964). Calcite solid solutions have even been found along road sides where the degradation of calcium magnesium acetate, a deicing compound, leads to precipitation of mixed carbonates (Amrhein *et al.*, 1994). Since a solid solution contains information about the aqueous solution with which it was in contact when it was formed, the analysis of natural solid solutions may also provide information about the evolution of sediments and the compositions of ancient seas (McCulloch *et al.*, 1994; Riciputi *et al.*, 1994; Mashiotto *et al.*, 1997).

It has been well documented that coprecipitation with calcium carbonate is a significant mechanism for the loss of both strontium and phosphorus from the aqueous phase in Lake Constance (Stabel *et al.*, 1986; Kleiner and Stabel, 1989). During the summer months, authigenically formed calcite is a major component of the material settling out of the water column. It is estimated that the sedimentation of calcite solid solutions accounts for an average removal of 50% of the strontium and phosphorus during whitening events (Stabel *et al.*, 1986; Kleiner and Stabel, 1989). This type of process is not unique to Lake Constance. Friedl *et al.* (1997) have shown that Ca/Mn/CO₃ solid solutions play an important role in the cycling of manganese in Lake Sempach, Switzerland. Approximately 55-60% of the Mn in the sediment was found to be incorporated in a carbonate solid solution with most of the remainder in a (FeMn)₃(PO₄)_{2(s)} solid solution.

The ability of calcite to sorb divalent metals has led to speculation that, as in the case of Lake Constance, solid solutions may mitigate pollution in the environment. One attempt to study if SSAS partitioning could scavenge metal ions from surface waters was carried out at the Elbe River where a mixed calcite solid solution involving Cd, Pb, Co, Zn and Cu was found to have formed on a man-made concrete block submerged in the river (Patchineelam, 1978). Cd, Zn, Cu and Co were found to be enriched in the surface of the concrete relative to a standard carbonate rock while Pb and Mn were not. Although the formation of solid solutions in the environment was confirmed in this case, it was determined that sorption to oxides and complexation with organic matter were the significant mechanisms by which the metals were being transported in the river.

The importance of solid solution formation to the overall transport of metals can vary depending on environmental conditions. Factors which can influence the role that carbonate solid solutions play in the fate and transport of metals in the environment include reaction rates, the presence of other competing phases/processes, and the contact time between the aqueous and solid phases. While calcite is not the only mineral that can have impacts on the behavior of metals in the environment through the formation of solid solutions, the potential for mixed calcite solid solutions to be widespread is significant due to the abundance and behavior of calcite in natural systems.

1.3 Calcite in Natural Systems

Calcite is one of the most common and widespread minerals in the environment. As shown in Figure 1.2, carbonate rock (predominately calcite and dolomite) is present at or near the surface throughout the continental United States. Calcite is often present in sedimentary rock and is by far the dominant mineral in limestone and marble. Although most calcite rock is sedimentary in origin, calcite can be found in all rock types and can form by authigenic precipitation.

The formation of shells and skeletons from biological activity plays a significant role in calcite formation in ocean surface waters. This biological activity keeps ocean surface

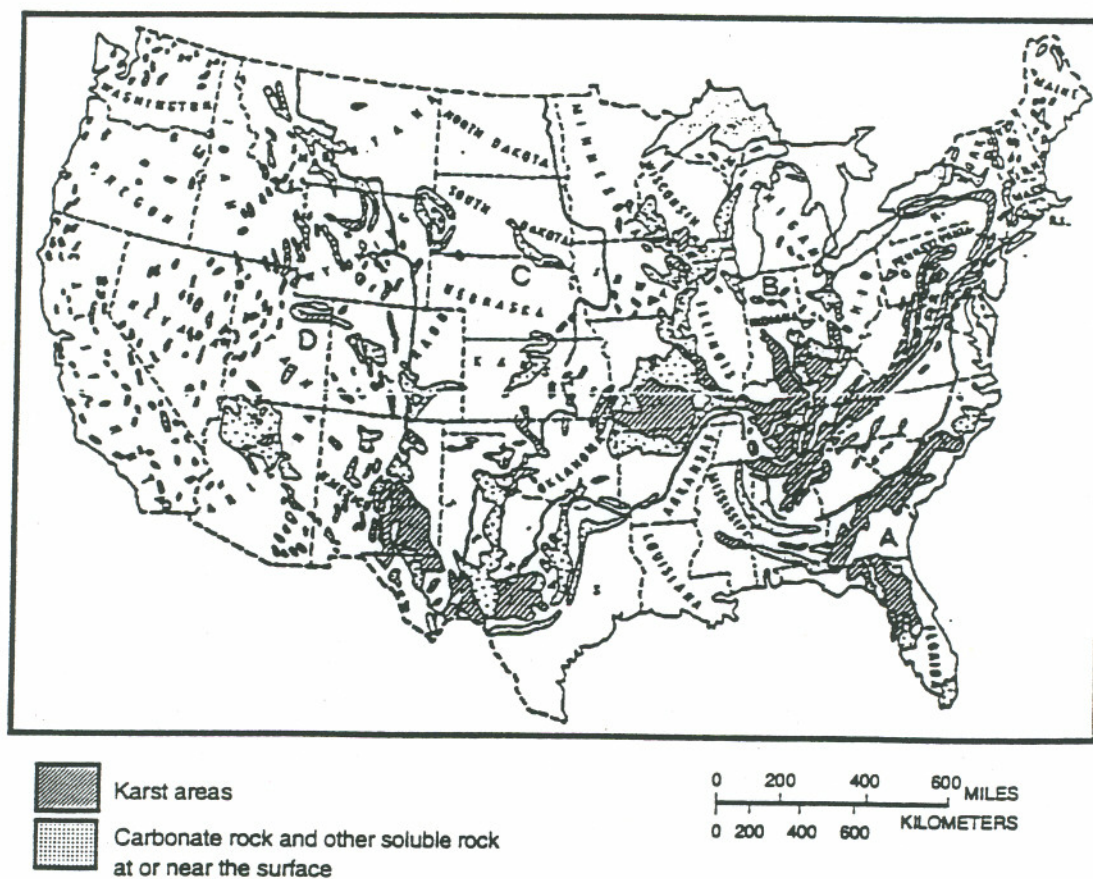


Figure 1.2 Areas of carbonate rock in the near surface of the continental United States (Komatina, 1975).

waters in near saturated conditions while deep ocean waters remain undersaturated with respect to calcite. In fresh surface waters, the rapid consumption of CO_2 that occurs during algal blooms can lead to a rapid precipitation of calcite. These episodes are often called "whiting events" due to the white color that the water body develops during the calcite precipitation. Since the precipitation and dissolution of calcite affects the alkalinity of water systems, carbonate minerals play an important role in the pH buffering of both surface and ground waters.

In the environment, the kinetics of CaCO_3 precipitation and dissolution vary widely from the relatively fast precipitation that occurs during whiting events in surface waters, to the relatively slow reaction rates that occur under near equilibrium conditions. The extent to which a trace metal will be incorporated into a host lattice is related to the precipitation rate. Therefore, determining the rate of reaction of carbonate minerals in natural systems is a key factor in applying solid solution chemistry to real world problems.

The use of calcite as host lattice in environmentally-directed solid solution studies is logical for several reasons. First, as noted above, calcite is abundant in surface and subsurface water systems. Second, waters are often saturated with respect to this mineral phase, and almost all ground waters have encountered carbonate minerals at some point in their evolution (Freeze and Cherry, 1979). Third, the dependence of precipitation rate on saturation state allows a range of precipitation rates to be studied in the laboratory. (A range of reaction rates can therefore be observed over reasonable time scales. It should be noted, however, that a rapidly-formed solid solution containing calcite most likely does not represent thermodynamic equilibrium.) Finally, calcite acts as an efficient sorbent for many divalent metals, rare earth elements and radionuclides (Rimstidt *et al.*, 1998). Otavite (CdCO_3) is believed to form an ideal or nearly ideal solid solution series with calcite (Papadopoulos and Rowell, 1988; Königsberger *et al.*, 1991); as a result, the two minerals should be completely miscible over all proportions.

1.4 Objectives

Although research in aqueous geochemistry has been conducted for decades, solid solution geochemistry, particularly the role of solid solution/aqueous solution partitioning in the fate and transport of metals in the environment, remains one of the least understood areas in this field. Almost nothing is understood in practical terms about how the movement of divalent metal ions in groundwater is affected by sorption to carbonate minerals, even though divalent metal ions such as Cd^{2+} , Sr^{2+} and Pb^{2+} are common groundwater contaminants at many sites in the U.S.

It is the objective of this work to encourage the informed application of solid solution/aqueous solution partitioning to the prediction of metal transport in the environment. This research will have three main goals:

- 1) determination of general and equilibrium distribution coefficients and equilibrium solid phase activity coefficients for the calcite/otavite solid solution series over a range of precipitation rates and solid solution compositions;
- 2) determination of mixing parameters that describe the solid solution thermodynamics for the calcite/otavite solid solution series, and classification of that behavior as ideal, regular or sub-regular; and
- 3) improved understanding of the transport of divalent metal ions in porous media which contain calcite as a component phase through diagnostic modeling and comparison of two incorporation mechanisms, surface partitioning with subsequent solid state diffusion or more rapid incorporation into a surface layer that isolates the bulk material from the aqueous solution.

Chapter 2

Solid Solution Theory and Representation

2.1 Introduction

A stable binary solid solution forms when a mixture of two solids results in a lower free energy for the system than would be set by the presence of either of the two pure endmembers, or near-end member mixtures. When a system mixes ideally, the interactions between the end members are equal to the interactions within the end members, and the driving force for mixing is simply the increase in the overall disorder of the mixed system. However, differences in electronegativity, ionic charge and ionic radius between a substituting and host lattice ion often make the incorporation of a foreign metal ion into a mineral structure occur non-ideally. Since the behavior of a non-ideal solid solution varies with composition, it is important to understand how non-ideal behavior, described by solid phase activity coefficients, varies with mole fraction.

2.2 Thermodynamic Mixing

The mixing of two solids is governed by the same basic thermodynamic principles commonly used to describe the mixing of two liquids (Gresens, 1981; Lippmann, 1982; Pankow, 1991). In order to have a favorable thermodynamic driving force for mixing, the free energy of mixing ΔG_{mixg} must be negative where

$$\Delta G_{\text{mixg}} = \Delta H_{\text{mixg}} - T\Delta S_{\text{mixg}} \quad (2-1)$$

The entropy of mixing ΔS_{mixg} is favorable when two pure phases mix to form one more disordered phase. Therefore, it is the enthalpy of mixing ΔH_{mixg} which determines the extent to which a given solid solution can form.

The change in the molar free energy of mixing for a binary solid solution of calcite and otavite is given by

$$\Delta \bar{G}_{\text{mixg}} = X_{\text{CdCO}_3(\text{s})} RT \ln X_{\text{CdCO}_3(\text{s})} + X_{\text{CdCO}_3(\text{s})} RT \ln \zeta_{\text{CdCO}_3(\text{s})} + X_{\text{CaCO}_3(\text{s})} RT \ln X_{\text{CaCO}_3(\text{s})} + X_{\text{CaCO}_3(\text{s})} RT \ln \zeta_{\text{CaCO}_3(\text{s})} \quad (2-2)$$

where each X is a solid phase mole fraction, and each ζ is a solid phase activity coefficient. The terms in the above equation that involve solid phase mole fractions make up ΔS_{mixg} , while the terms containing solid phase activity coefficients make up ΔH_{mixg} . In an ideal solid solution, the activity coefficients of both components equal unity, and the enthalpy of mixing is zero. In this case, mixing is due only to entropy effects.

In order to understand the behavior of non-ideal solid solutions, it is necessary to understand how the excess free energy of mixing, *i.e.*, the deviation of the free energy of mixing from that of an ideal solid solution, varies with composition. Since it is a measure of the non-ideality of the solid solution, the excess free energy of mixing can be related to solid phase activity coefficients by the following relation (Mukhopadhyay *et al.*, 1993)

$$RT \ln(\zeta_i) = \frac{\partial (MG^{\text{xs}})}{\partial m_i} \quad (2-3)$$

where ζ_i is the solid phase activity coefficient of component i , M is the total number of moles, G^{xs} is the excess free energy of mixing, and m_i is the number of moles of component i in the solid solution. Taylor series expansion of Equation 2-3 results in expressions that can be used to determine the activity coefficient of each of the components of the solid solution. Several equations relating the solid phase activity coefficient to the composition of the solid solution have been developed including the Guggenheim expansion (Guggenheim, 1952), the Margules equations (Helffrich and Wood, 1989) and the Thompson equation (Thompson,

1967). Although these equations are functionally equivalent (Glynn and Reardon, 1990; Glynn, 1991), they do differ in their derivation. Therefore, the interaction parameters for the different equations are not directly interchangeable, although it is possible to convert one type of mixing parameter into another (Glynn, 1991).

The Guggenheim expansion is often used to determine solid phase activity coefficients for binary solid solutions. Based on the Guggenheim excess free energy model, the solid phase activity coefficients for a binary $\text{Ca}_{1-x}\text{Cd}_x\text{CO}_{3(s)}$ solid solution can be predicted from the composition of the solid solution.

$$\ln \zeta_{\text{CaCO}_{3(s)}} = X_{\text{CdCO}_{3(s)}}^2 [a_0 + a_1(3X_{\text{CaCO}_{3(s)}} - X_{\text{CdCO}_{3(s)}}) \dots] \quad (2-4)$$

$$\ln \zeta_{\text{CdCO}_{3(s)}} = X_{\text{CaCO}_{3(s)}}^2 [a_0 - a_1(3X_{\text{CdCO}_{3(s)}} - X_{\text{CaCO}_{3(s)}}) \dots] \quad (2-5)$$

The variables a_0 , a_1 , etc. are dimensionless interaction parameters which can be determined experimentally (Glynn, 1990).

In some cases, the first term of the above expansion is sufficient to describe non-ideal solid solution behavior. This type of solid solution is called “regular”, and the dependence of the solid phase activity coefficient (and the free energy of mixing) on composition is symmetric about mole fraction 0.5. The Guggenheim equations for a regular solid solution are shown below. They are identical to the two-suffix Margules equations.

$$\ln \zeta_{\text{CaCO}_{3(s)}} = a_0 X_{\text{CdCO}_{3(s)}}^2 \quad (2-6)$$

$$\ln \zeta_{\text{CdCO}_{3(s)}} = a_0 X_{\text{CaCO}_{3(s)}}^2 \quad (2-7)$$

When the first two terms of the Guggenheim expansion are necessary to describe the dependence of the solid phase activity coefficient on the composition of the solid, the solid solution is referred to as “sub-regular”. In this case the dependence of solid phase activity

coefficient and the free energy of mixing is not symmetric with respect to a mole fraction of 0.5. The sub-regular Guggenheim equations for a binary solid solution are shown below.

$$\ln \zeta_{\text{CaCO}_3(\text{s})} = X_{\text{CdCO}_3(\text{s})}^2 [a_0 + a_1(3 - 4X_{\text{CdCO}_3(\text{s})})] \quad (2-8)$$

$$\ln \zeta_{\text{CdCO}_3(\text{s})} = X_{\text{CaCO}_3(\text{s})}^2 [a_0 - a_1(3 - 4X_{\text{CaCO}_3(\text{s})})] \quad (2-9)$$

Although higher order equations can be used to describe non-ideal solid solution behavior, the experimental data used to determine interaction parameters is not usually detailed enough to warrant the use of more complicated equations (Smith, 1992; Mukhopadhyay *et al.*, 1993).

2.3 Miscibility Gaps

When two solids mix non-ideally, there may be certain compositions where the resulting pure solid solution is unstable relative to two solid solution phases in mutual equilibrium. The range of compositions where this type of phase separation occurs for a given system is called the “miscibility gap”. At full thermodynamic equilibrium, it is not possible to have a solid solution with a composition that is inside a miscibility gap. This is simply because the free energy of the system will be lowered by phase separation. A more detailed treatment of miscibility gaps can be found in Urusov (1975) and Pankow (1991).

As mentioned earlier, differences in ionic radii and electronegativities between a host lattice and a substituting ion contribute to ΔH_{mixg} . Since ΔH_{mixg} restricts miscibility in a solid solution, the more similar the host and substituting ion are, the more likely that the solid solution series will be fully miscible. There is little agreement in the literature about the presence of a *miscibility gap* in the calcite/otavite solid solution series (Chang *et al.*, 1971; Urusov, 1975; Königsberger *et al.*, 1991; Rock *et al.*, 1994). Although, Ca^{2+} and Cd^{2+} are of similar size, and calcite and otavite are isostructural (two factors which favor miscibility), there is a significant difference in the electronegativities of the two ions. The difference in

electronegativities could result in lattice strain sufficiently high enough to result in a miscibility gap. This topic will be treated in more detail in Chapter 4.

2.4 Solid Solution/Aqueous Solution Equilibria

One of the main factors controlling the precipitation/dissolution of carbonate minerals in solution is the degree of supersaturation/undersaturation that exists with respect to the mineral phase (Xyla *et al.*, 1991). In general, the greater the degree of supersaturation or undersaturation, the more rapidly the precipitation or dissolution occurs. The saturation index Ω is a convenient measure of both solution properties. For a pure solid phase it is given by

$$\Omega = \frac{IAP}{K_{s0}} \quad (2-10)$$

where IAP is the ion activity product of the solution for the pure phase solid, and K_{s0} is the solubility constant of the pure solid. When $\Omega > 1$ the solution is supersaturated with respect to the given mineral phase. When $\Omega < 1$ the solution is undersaturated. The solution is in equilibrium with the solid when $\Omega = 1$.

SSAS equilibria are only slightly more complicated than the equilibria between a pure solid and an aqueous phase. In the case of a solid solution, the activity of each solid phase in the solution must be treated explicitly (in a pure phase solid, the activity of the solid is unity). For a calcite/otavite solid solution in contact with an aqueous phase, the two basic equations which describe equilibrium are

$$\{Cd^{2+}\}\{CO_3^{2-}\} = K_{s0,CdCO_3(s)} X_{CdCO_3(s)} \zeta_{CdCO_3(s)} \quad (2-11)$$

$$\{Ca^{2+}\}\{CO_3^{2-}\} = K_{s0,CaCO_3(s)} X_{CaCO_3(s)} \zeta_{CaCO_3(s)} \quad (2-12)$$

where each K_{s0} refers to a pure end member solubility constant. As shown by these equations, equilibrium between a solid solution series and an aqueous solution is not characterized by a single ion activity product as is the case for a pure solid phase.

When only a trace amount of cadmium partitions into the calcite lattice, the resulting solution is near infinite dilution. In this case, both the mole fraction and the activity coefficient of the bulk phase, $\text{CaCO}_{3(s)}$, are approximately unity. Therefore, the solubility properties of the major constituent of a solid solution are largely the same as for the corresponding pure component.

2.5 Distribution Coefficients

Driessens (1986) provides a detailed overview of SSAS distribution coefficients. In general, distribution coefficients are useful for describing the extent to which ions will partition into a given solid structure. The equilibrium distribution coefficient for a system can also be used to obtain a measure of the distance of the system from equilibrium. The Berthelot-Nernst distribution coefficient for Cd^{2+} partitioning into calcite, assuming a homogeneous solid, is defined as

$$D_{\text{Cd}^{2+}} = \frac{\frac{X_{\text{CdCO}_3(s)}}{\{\text{Cd}^{2+}\}}}{\frac{X_{\text{CaCO}_3(s)}}{\{\text{Ca}^{2+}\}}} \quad (2-13)$$

Substitution of Equations 2-11 and 2-12 into the above expression for the distribution coefficient yields an expression for the equilibrium distribution coefficient (Equation 2-14). As shown by this equation, the equilibrium distribution coefficient for an ideal solid solution is simply the ratio of the endmember K_{s0} values.

$$D_{\text{Cd}^{2+}, \text{eq}} = \frac{K_{\text{s0, CaCO}_3(\text{s})} \zeta_{\text{CaCO}_3(\text{s})}}{K_{\text{s0, CdCO}_3(\text{s})} \zeta_{\text{CdCO}_3(\text{s})}} \quad (2-14)$$

The Doerner-Hoskins approach to the formation of a solid solution assumes that an incremental precipitation process occurs as a series of equilibrium states which change as the composition of the aqueous phase changes. The result is a solid composed of layers of varying composition. The Doerner-Hoskins distribution coefficient λ is defined as

$$\ln\left(\frac{\text{Cd}^{2+}_{\text{aq, i}}}{\text{Cd}^{2+}_{\text{aq, f}}}\right) = \lambda \ln\left(\frac{\text{Ca}^{2+}_{\text{aq, i}}}{\text{Ca}^{2+}_{\text{aq, f}}}\right) \quad (2-15)$$

Terms with "i" in the subscript refer to initial concentrations, and terms with "f" in the subscript refer to final concentrations.

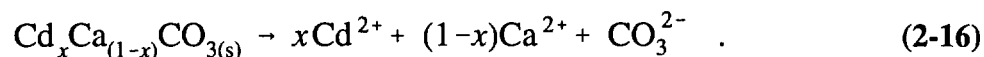
D values have been shown to vary with precipitation rate (Lorens, 1981; Mucci, 1988; Dromgoole and Walter, 1990; Tesoriero and Pankow, 1996). As the precipitation rate increases, D will approach unity indicating a less selective mode of incorporation of ions into the crystal structure. For laboratory experiments, it has been assumed that equilibrium partitioning behavior occurs when the observed D remains constant as the precipitation rate is decreased.

The main drawback with distribution coefficients is that when both end members share a common anion, information regarding the overall solubility of the solid solution is lost because all of the terms involving the anion have canceled. Alternative methods for describing solid solution behavior can be used when information about the solubility of a solid solution is important. For example, the "stoichiometric saturation" model can be used in cases where the dissolution of the solid solution is congruent. This model does not require that the solution reach full thermodynamic equilibrium, it only requires that the composition of the initial solid remain invariant. In contrast, the "equilibrium saturation model" which

is more rigorously based in thermodynamics can be used only when the SSAS system is at full thermodynamic equilibrium.

2.6 Stoichiometric Saturation Model

In low-temperature geologic systems, solid solutions often do not achieve thermodynamic equilibrium on observable time scales. Therefore, a non-equilibrium solid solution composition may appear invariant over a given time scale of interest. Thorstenson and Plummer (1977) suggest that due to kinetic limitations, the dissolution of a solid solution can remain congruent. The dissolution of ions from the solid to the aqueous phase then occurs according to the same ratio exhibited by the ions present in the solid. In the case of a solid solution of $\text{CdCO}_{3(s)}$ in $\text{CaCO}_{3(s)}$, the dissolution reaction is given by



Under the conditions of stoichiometric saturation, the solid solution may be treated as a one component solid with unit activity. An ion activity product (*IAP*) for the case of stoichiometric saturation can then be defined in a manner that is analogous to the definition of that for a pure solid so that

$$IAP_{ss} = \{\text{Cd}^{2+}\}^x \{\text{Ca}^{2+}\}^{(1-x)} \{\text{CO}_3^{2-}\} \quad (2-17)$$

The value of the IAP_{ss} that results when the solution is at saturation with the invariant composition solid solution is called the stoichiometric saturation constant, K_{ss} . It should be noted that this K_{ss} depends on the composition of a given solid solution.

Stoichiometric saturation is valid only as long as the solid remains homogeneous and of constant composition. In contrast, if the solid can dissolve incongruently, then the key assumptions made in developing the K_{ss} approach are violated and the K_{ss} expression will not be satisfied. The stoichiometric saturation concept has been criticized by Lafon (1978) and

later by Lippmann (1980). Both challenged the validity of the K_{ss} expression as a mass action law since it is not strictly based in thermodynamics. As an alternative to this special case model, equilibrium models have also been developed based more rigorously on the appropriate mass action laws (*e.g.*, Equations 2-11 and 2-12 in the case of $\text{CdCO}_{3(s)}$ in $\text{CaCO}_{3(s)}$).

2.7 Total Solubility Product Model

In contrast to the stoichiometric saturation model, Lippmann's total solubility product model recognizes that a binary solid solution is a mixture of two distinct solids and assumes full thermodynamic equilibrium. A requirement of this model is therefore that the chemical potential of each species in the solid phase has the same value as the chemical potential of the corresponding constituent in the aqueous phase.

For the case of a solid solution of $\text{CdCO}_{3(s)}$ in $\text{CaCO}_{3(s)}$, the total solubility product $\Sigma\Pi$ is defined as

$$\Sigma\Pi = (\{\text{Ca}^{2+} + \{\text{Cd}^{2+}\})\{\text{CO}_3^{2-}\} . \quad (2-18)$$

Expansion of the RHS of Equation 2-18 in terms of the solid components results in the equilibrium relationship

$$\Sigma\Pi_{\text{eq}} = K_{s0, \text{CaCO}_{3(s)}} X_{\text{CaCO}_{3(s)}} \zeta_{\text{CaCO}_{3(s)}} + K_{s0, \text{CdCO}_{3(s)}} X_{\text{CdCO}_{3(s)}} \zeta_{\text{CaCO}_{3(s)}} . \quad (2-19)$$

A plot of $\Sigma\Pi_{\text{eq}}$ as described by Equation 2-19 vs. the mole fraction in the solid phase produces a curve known as the "solidus" (Figure 2.1).

When the RHS of Equation 2-18 is expanded in terms of the aqueous species, a different equilibrium equation is produced namely,

$$\Sigma\Pi_{\text{eq}} = \left(\frac{X_{\text{Ca}^{2+}, \text{aq}}}{K_{s0, \text{CaCO}_3(s)} \zeta_{\text{CaCO}_3(s)}} + \frac{X_{\text{Cd}^{2+}, \text{aq}}}{K_{s0, \text{CdCO}_3(s)} \zeta_{\text{CdCO}_3(s)}} \right)^{-1} \quad (2-20)$$

Based on Equation 2-20, a plot of $\Sigma\Pi_{\text{eq}}$ versus mole fraction of one of the two metal ions in the aqueous phase results in a curve called the "solutus" (Figure 2.1).

Plotting $\Sigma\Pi$ vs. the mole fraction in the solid phase and the mole fraction in the aqueous phase for a binary solid solution system yields a phase diagram similar to the isothermal vapor pressure diagram for a binary liquid mixture (Lippmann, 1980). Lippmann phase diagrams provide information about the composition of primary saturation states and can also be used to propose equilibrium endpoints in reactions. Figure 2.1 is a proposed Lippmann phase diagram for the calcite/otavite solid solution series assuming regular solid solution behavior with $a_m = -0.8$ (Glynn and Reardon, 1990).

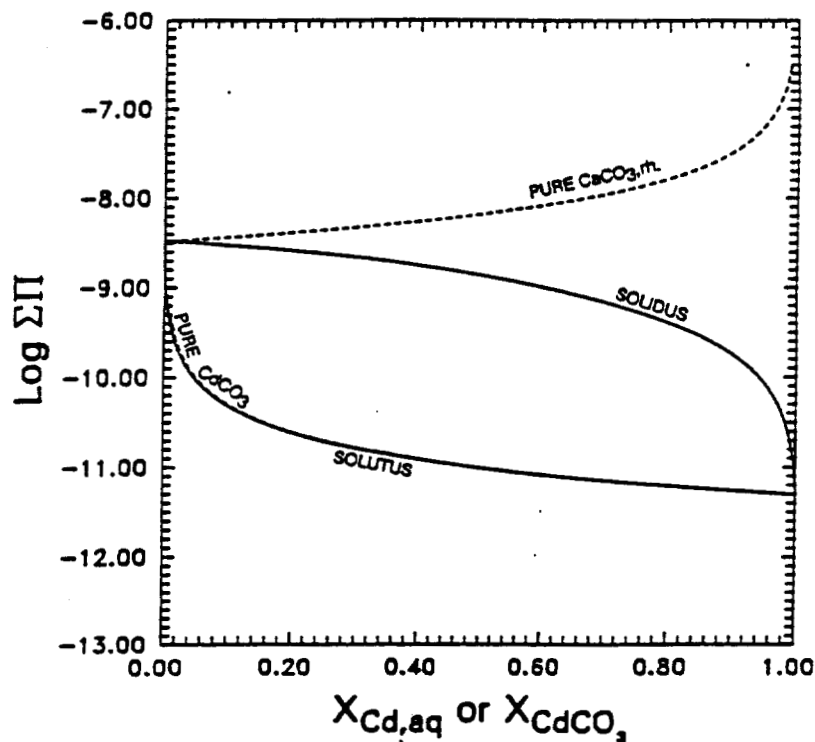


Figure 2.1 Lippmann phase diagram for the calcite/otavite solid solution series assuming regular behavior, $a_m = -0.8$ (Glynn and Reardon, 1990).

2.8 Reaction Paths

Although many factors may control the reaction path of a solid solution, the most significant factors appear to be the solid to solution ratio, the overall solubility of the dominant endmember, the composition of the solid solution, and the kinetics of precipitation and dissolution. Dissolution of a solid solution is initially congruent until primary saturation is reached. At this point, the solution has become saturated with respect to a secondary mineral phase. Further incongruent dissolution of the solid phase is thermodynamically possible although it may be limited by kinetic factors. As the system moves towards full equilibrium, the solid phase is enriched in the less soluble end member while the solution is enriched in the more soluble end member.

When a secondary mineral phase coats the original solid and isolates it from the solution, it is possible to have a SSAS system in partial equilibrium. This occurs when the system is at equilibrium with respect to the outer secondary mineral layer, but not at equilibrium with respect to the inner, bulk solid. The solutus corresponds to the minimum-solubility reaction-path for a partial equilibrium SSAS while the stoichiometric saturation curve represents the upper limiting solubility for a given, fixed mineral composition (Glynn *et al.*, 1990).

During precipitation, the composition of the aqueous phase can vary with the extent of the reaction. Regardless of whether the precipitation is of the Berthelot-Nerst or Doerner-Hoskins type, several general principles are followed during solid solution formation. First, precipitation always tends to enrich the solution in the more soluble end member. Second, at equilibrium, the composition of the solution is located on the solutus. Third, the actual reaction path is generally controlled by reaction kinetics. Since the kinetics of precipitation affects the distribution coefficient, knowledge of the distribution coefficient as a function of precipitation rate is important when describing a SSAS system.

Chapter 3

Determination of Thermodynamic Parameters for the Calcite/Otavite Solid Solution Series

3.1 Objectives

Distribution coefficients are functions of the compositions of aqueous and solid phases. Changes in aqueous or solid compositions due to changes in saturation state, pH, or depletion/enrichment of key constituents in the solid or aqueous phase affect the observed distribution coefficient value. Therefore, it can be difficult to generate thermodynamic information for SSAS systems that is not limited in application to the conditions under which it was measured. The first objective of this research was to determine distribution coefficients for the $\text{CaCO}_{3(s)}/\text{CdCO}_{3(s)}$ solid solution series over a range of precipitation rates and solid compositions using an experimental procedure that controls the precipitation rate, the composition of the aqueous phase, and the composition of the solid phase. By observing the dependence of the general distribution coefficient D (see Equation 2.13) on precipitation rate, the equilibrium distribution coefficient D_{eq} (see Equation 2.14) for a given solid composition can be determined. Once the D_{eq} for a given solid composition has been determined, the solid phase activity coefficient for the trace constituent can be calculated. The distribution coefficients and solid phase activity coefficients determined during this research provide a more complete understanding of the behavior of this system at ambient temperatures than provided by previous research. This data will also be used in Chapter 4 to determine mixing parameters for the system and to classify the behavior of the system as ideal, regular, or subregular.

3.2 Seed Material Characterization

Calcite and otavite powders were used as seed materials in the distribution coefficient experiments. These powders were subjected to routine characterization including x-ray diffraction (XRD), x-ray photoelectron spectroscopy (XPS), scanning electron microscopy (SEM) and solubility tests. The calcite powder (EM Science, lot number 37286) was reported to contain no more than 0.01 ppm Cd. The compositional information from the certificate of guarantee is listed in Table 3.1. The otavite powder (Alfa Aesar, lot number F25D04) was 99+% pure (metals basis); no additional compositional information was provided by the manufacturer. XRD analysis of the seed material confirmed that neither the calcite nor otavite contained detectable trace phases. XPS analysis of the seed materials also showed no detectable trace contamination. Except where noted, all other chemicals used in the course of this research were ACS reagent grade.

Figures 3.1 and 3.2 are SEM images of the calcite and otavite seed materials. The powders in these images had not been exposed to solution. Although the rough surfaces of the calcite and otavite would have been smoothed over after equilibration with an

Table 3.1 Trace composition of calcite seed material.
Assay (chelometric) min. 99%.
Listed values are maximum ppm levels.

Cl	5	Mg	5	Li	5
SO ₄	20	Mn	0.05	Pb	0.01
Al	0.1	Hg	0.05	Zn	0.05
Ba	10	Ni	0.01	Fe	0.05
Cd	0.01	K	5	Tl	0.01
Cs	50	Rb	50	Cu	0.01
Co	0.01	Na	1	Sr	100

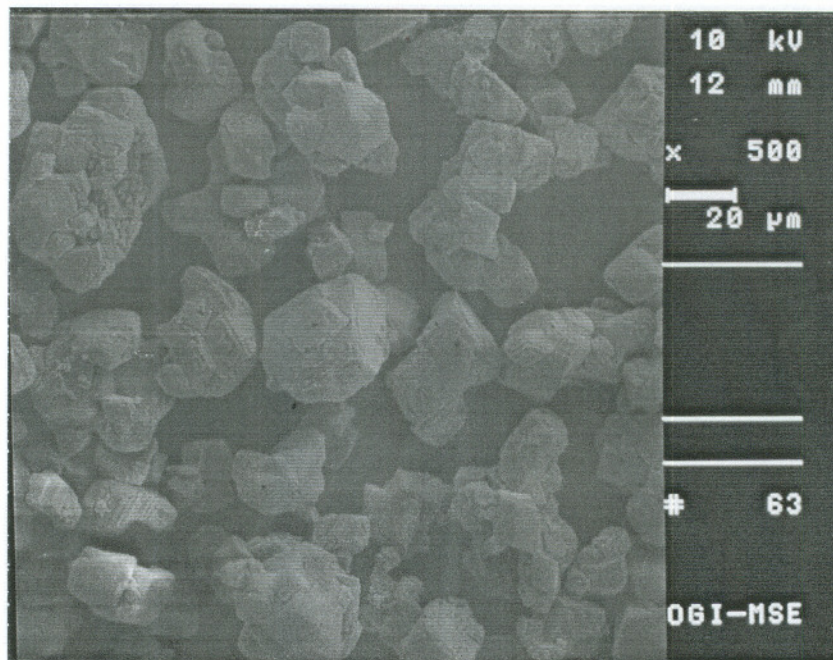


Figure 3.1 SEM image of calcite seed material.

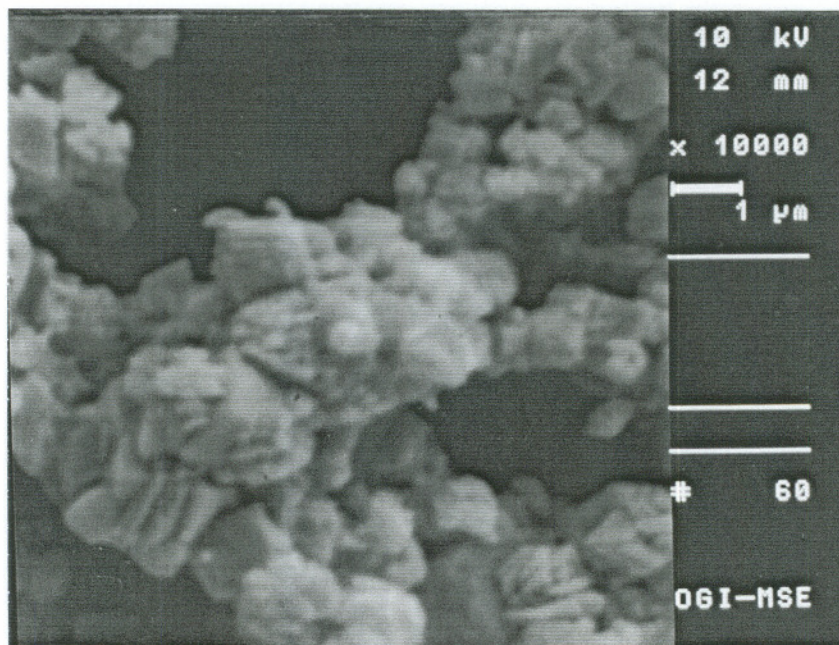


Figure 3.2 SEM image of otavite seed material.

aqueous phase, a grain size difference between the seed materials remained throughout the experiments. (The calcite seed material grain size was approximately 10 times greater than the otavite seed material grain size.) Precipitation rates were calculated on a mass basis during the course of this research. Since the experimental precipitation rates were not normalized to surface area, direct comparison of D values at a given precipitation rate from experiments that used different seed materials is not strictly valid. It is however, valid to compare mass-based precipitation rates between samples grown on the same seed material (Weichers, 1975).

3.2.1 Seed Material Solubility Measurement

Solubility tests were run under experimental conditions similar to those used in the distribution coefficient experiments. In each case, 400 mL of 0.25 F NaCl solution was kept at 25°C in a water jacketed beaker with a recirculating water bath. Humidified CO₂ gas (99.5% pure) was bubbled through the solutions throughout the experiments. After allowing time for the water to become equilibrated with CO₂, the seed material was added to the solution. For the calcite test, 900 mg of CaCO_{3(s)} was added as seed material. For the otavite test, 500 mg of CdCO_{3(s)} was added as seed material. The solutions were kept well mixed with a suspended magnetic stir bar. After addition of the seed material, the pH was monitored with a Ross Sure-Flow semi-micro combination electrode. The solutions were allowed to equilibrate for three days. After this time, the aqueous phase was sampled. The sample was filtered through a 0.45 μm cellulose nitrate membrane syringe tip filter. The aqueous portion of the sample was acidified to pH < 2 to prevent precipitation as CO₂ degassed from the sample. Atomic absorption spectroscopy (AAS) was used to measure the amount of calcium and/or cadmium in the samples.

After the seed material had reached equilibrium, pure phase solid of the same type as the seed material was precipitated onto the seed material using a dual syringe pump which simultaneously added a 0.25 F Na₂CO₃ solution and either a 0.25 F CaCl₂ or a 0.25 F CdCl₂ solution to each reaction vessel at a constant rate. After approximately 0.003 to

Table 3.2 Calcite solubility data.

Sample	pH	Ca _T mg/L	{Ca ²⁺ } M	{CO ₃ ²⁻ } M	measured log K _{s0}
Casat-1	6.07	615.2	3.969x10 ⁻³	9.597x10 ⁻⁷	-8.45
Casat-2	6.17	623.8	3.958x10 ⁻³	1.507x10 ⁻⁶	-8.22
Casat-3	6.09	618.1	3.974x10 ⁻³	1.062x10 ⁻⁶	-8.37
Casat-4	6.09	623.7	4.014x10 ⁻³	1.033x10 ⁻⁶	-8.38

0.005 mols of pure phase material was precipitated onto the seed material, the titration was stopped and the pH was monitored while the system returned to equilibrium. Both solutions were allowed to equilibrate for 3 days after the precipitation portion of the experiment. Three calcite samples and four otavite samples were taken after the precipitation phase of the experiment. Table 3.2 contains the data collected from the calcite solubility experiments. Table 3.3 contains the otavite solubility data.

Solubility constants for the two solids were determined from the aqueous phase compositions measured by AAS. Aqueous speciations were calculated using MINTEQA2 (Allison *et al.*, 1991) with the restriction that no solids be allowed to precipitate from solution during the calculation. Several minor changes were made to the MINTEQA2 database including different values for the CdHO₃⁺_(aq) and CdCO₃⁰_(aq) cadmium ion pairs and the K_{s0} of otavite. The new values were taken from the Stipp *et al.* (1993). No changes were made to the database concerning the calcium species. As suggested by Plummer and Busenberg (1982), the CaHCO₃⁺_(aq) and CaCO₃⁰_(aq) ion pairs were included in the aqueous speciation calculations.

There are several sources of error in the measured K_{s0} values listed in Tables 3.2 and 3.3. First, the purity of CO₂ from a general grade gas tank has an uncertainty of ~1% (Plummer and Busenberg, 1982). Therefore, the pCO₂ in the reaction vessel could be as low as 0.985. Second, changes in barometric pressure over the course of the experiments also affect the pCO₂ in the reaction vessel. A characteristic barometric pressure range for ambient conditions is 0.982 atm to 1.004 atm. Under low barometric pressure conditions,

Table 3.3 Otavite solubility data.

Sample	pH	Cd _T mg/L	{Cd ²⁺ } M	{CO ₃ ²⁻ } M	measured log K _{s0}
Cdsat-1	5.21	171.4	3.662x10 ⁻⁵	1.771x10 ⁻⁸	-12.18
Cdsat-2	5.20	192.9	4.129x10 ⁻⁵	1.723x10 ⁻⁸	-12.15
Cdsat-3	5.20	182.2	3.757x10 ⁻⁵	1.739x10 ⁻⁸	-12.18
Cdsat-4	5.28	175.8	3.750x10 ⁻⁵	2.479x10 ⁻⁸	-12.03
Cdsat-5	5.14	177.1	3.791x10 ⁻⁵	1.331x10 ⁻⁸	-12.29

the $p\text{CO}_2$ in the reaction vessel will be less than it would be under high pressure conditions. Third, measurement of pH in a suspension is inherently difficult. Of these sources of error, the uncertainty in the pH measurement is the most significant source of error in the measured K_{s0} values. According to the manufacturer's specifications, the Ross Sure-Flow electrode used throughout the experiments is accurate to ± 0.03 pH units when using a two buffer calibration. The uncertainty in the pH measurement due to the electrode affects the calculated $\{\text{CO}_3^{2-}\}$ values leading to an uncertainty of ± 0.04 log units in the reported log K_{s0} values.

3.2.2 Comparison of Measured K_{s0} Values to Literature Values

The thermodynamic solubility of calcite has been determined by numerous investigators including Langmuir (1968), Nakayama (1968), Jacobson and Langmuir (1974), Christ *et al.* (1974), Berner (1976), Plummer and Busenberg (1982), Mucci (1983), and Sass *et al.* (1983). Early attempts to calculate a K_{s0} value for calcite were limited by the large uncertainties in the aqueous dissociation constants for several aqueous species including $\text{CaHCO}_3^+_{(\text{aq})}$ and $\text{CaCO}_3^0_{(\text{aq})}$. Although experimental evidence confirmed the presence of the ion pairs in solution, early attempts to include the ion pairs in speciation calculations led to a dependence of the calculated solubility on ionic

strength and $p\text{CO}_2$ (Langmuir, 1968; Jacobson and Langmuir, 1974). Because the measured solubility determined by the mass of calcite that dissolved in a given volume of liquid did not vary with changes in ionic strength or $p\text{CO}_2$, it was concluded that the equilibrium constants for the ion pairs were inaccurate, and the ion pairs were often omitted from solubility calculations. Jacobson and Langmuir (1974) calculated the solubility of calcite both neglecting and incorporating the ion pairs. The calculated $\log K_{s0}$ when neglecting the ion pairs was -8.42. When the ion pairs were included in the calculation, the $\log K_{s0}$ dropped to -8.47. Plummer and Busenberg (1982) determined equilibrium constants for the ion pairs as well as the K_{s0} values for calcite, aragonite, and vaterite. Their experiments showed that inclusion of the ion pairs in speciation calculations using the more accurate equilibrium constants did not affect the apparent solubilities of these three calcium carbonate solids. Plummer and Busenberg's (1982) -8.48 ± 0.02 value for the $\log K_{s0}$ of calcite is in good agreement with almost all of the literature values for the solubility of calcite at infinite dilution.

For the data in Table 3.2, there is good agreement between the calculated $\log K_{s0}$ for sample Casat-1 and the literature values. The Casat-2 value may be too large due to the solution not yet reaching equilibrium after the precipitation of calcite onto the seed material, or due to an inaccurate pH measurement. In fact, the measured pH values of Casat-1, Casat-3 and Casat-4 are about 0.05 to 0.07 pH units too basic relative to what has been observed for calcite saturated solutions in equilibrium with 1 atm CO_2 . Literature values for the equilibrium pH of calcite solutions where $p\text{CO}_2$ is approximately unity are consistently reported as pH of 6.02 (Berner, 1967; Jacobson and Langmuir, 1974; Plummer and Busenberg, 1982). The measured pH values from the SSAS distribution coefficient experiments after overnight equilibration but before any precipitation had been initiated are very similar to this literature value. The average pH value for the initial conditions of the distribution coefficient experiments that used calcite seed material (G and H series) was 6.02 ± 0.01 . If it is assumed that the pH measurements in Table 3.2 are inaccurate and a pH of 6.02 is used in the calculations, the measured $\log K_{s0}$ for each sample is -8.52 ± 0.04 . Taking into consideration error in the pH

measurements during the calcite solubility experiments, the experimental $\log K_{s0}$ values in Table 3.2 are within the range of values expected for calcite when considering the $\text{CaHCO}_3^+_{(aq)}$ and $\text{CaCO}_3^0_{(aq)}$ ion pairs. The $\log K_{s0}$ for calcite of -8.48 ± 0.02 (Plummer and Busenberg, 1982) will be used in all subsequent calculations.

Few independent solubility measurements for otavite exist in the literature. However, there is good agreement among the reported values. Gamsjäger *et al.* (1965) reported a $\log K_{s0}$ for otavite of -12.0 ± 0.15 . More recent measurements, $\log *K_{s0} = 6.41 \pm 0.02$ (Könseberger *et al.*, 1991), $\log K_{s0} = -12.24 \pm 0.1$ (Rai *et al.*, 1991) and $\log K_{s0} = -12.1 \pm 0.1$ (Stipp *et al.*, 1993) are not significantly different from the earlier value. One literature value that differs is $\log K_{s0}$ of -11.3 used by Fuller and Davis (1987), and Davis *et al.* (1987). The experimental solubility constants listed in Table 3.3 are in good agreement with the values reported in the literature. The $\log K_{s0}$ for otavite of -12.1 ± 0.1 (Stipp *et al.*, 1993) will be used in all subsequent calculations.

Solubility constants were also calculated from the initial conditions of each distribution coefficient experiment. For calcite (G and H series experiments), the calculated average $\log K_{s0}$ value from the initial samples after overnight equilibration was -8.60 ± 0.04 . For otavite (E and F series experiments), the average $\log K_{s0}$ value after overnight equilibration was -12.28 ± 0.04 . In both cases, these observed values are close to the literature values but slightly smaller than the values measured during the actual solubility experiments. This is may be due to the system not reaching equilibrium when given only 24 hours in which to equilibrate.

3.3 SSAS Partitioning of Cadmium to Calcite

Three different procedures have been used to determine SSAS distribution coefficients for the $\text{CaCO}_{3(s)}/\text{CdCO}_{3(s)}$ solid solution series near the calcite end member. Lorens (1978, 1981) used the radioactive isotope ^{109}Cd so that low levels of Cd could be measured with a scintillation counter. The pH-stat experimental method allowed the precipitation rate to be controlled by the addition of a Na_2CO_3 solution. All of the

cadmium was added to the solution before precipitation was initiated. Because cadmium partitions favorably into calcite, the aqueous concentration of cadmium decreased as the precipitation progressed resulting in a layered precipitate. Therefore, the SSAS partitioning was of the Doerner-Hoskins type (see Equation 2.15).

Davies *et al.* (1987) allowed a solid solution to form by recrystallization without inducing net calcite precipitation. Therefore, the total amount of solid solution formed in these recrystallization experiments was small. Because cadmium partitions so strongly to calcite, total aqueous cadmium levels were maintained at measurable levels by complexing the cadmium with ethylenediaminetetraacetic acid (EDTA). When EDTA was not used in the experiments, aqueous levels of cadmium quickly dropped to below detectable levels. The composition of the solid phase was estimated from the relative long term loss of Cd and ^{45}Ca from solution.

Tesoriero and Pankow (1996) determined a distribution coefficient and solid phase activity coefficient for trace amounts of cadmium in calcite using a constant composition method. In this method, a surface coating of a known composition is precipitated onto seed material. Because cadmium partitions favorably into the solid solution, cadmium was added to the reaction vessel at a constant rate throughout the experiment. This allowed Tesoriero and Pankow (1996) to achieve steady state conditions during experiments that were not possible using the Lorens (1981) or Davies *et al.* (1987) methods. Therefore, the SSAS partitioning was of the Berthelot-Nerst type (see Equation 2.13).

3.3.1 G Series Experiments

A constant composition method similar to that of Tesoriero and Pankow (1996) for the case when $D > 1$ was used in all of the experiments where Cd partitioned into calcite. Figure 3.3 shows a schematic of the experimental apparatus used to precipitate the $\text{CaCO}_{3(s)}/\text{CdCO}_{3(s)}$ solid solutions. Solid solutions were formed over a range of precipitation rates. The range of precipitation rates demonstrated the dependence of the

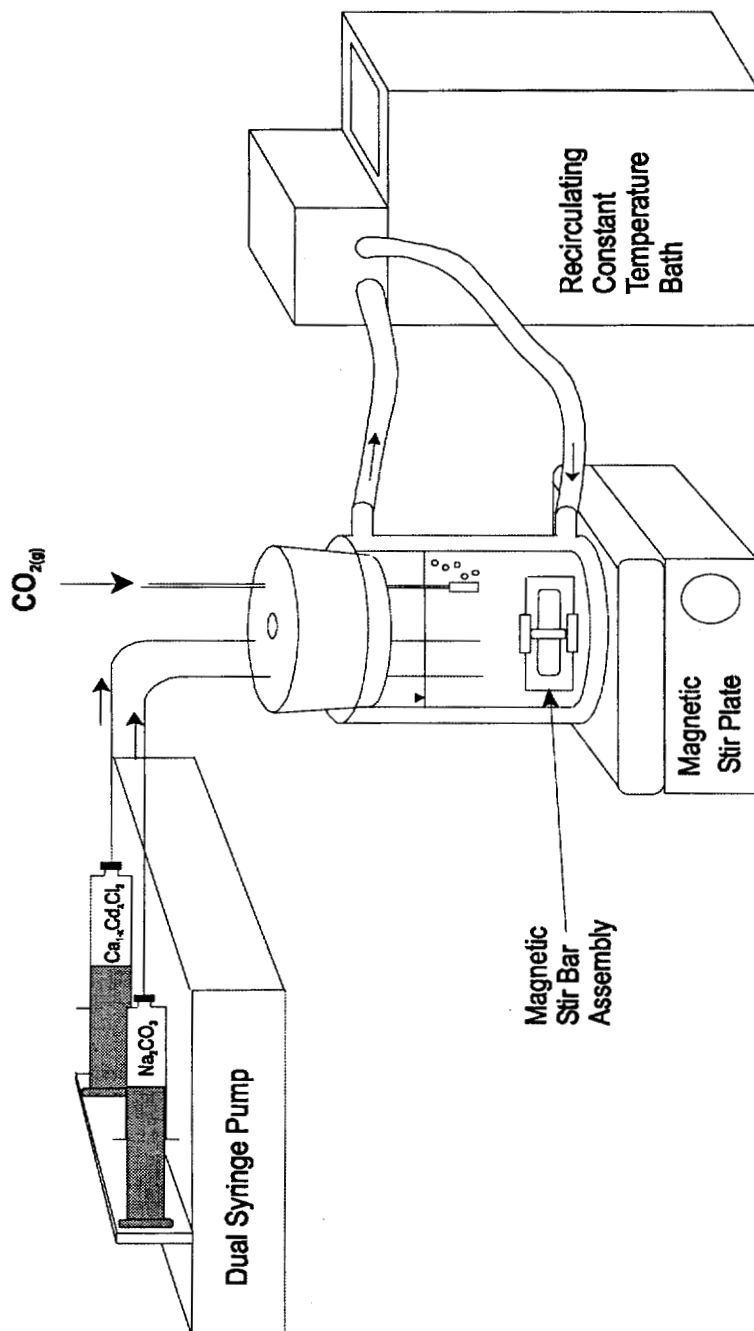


Figure 3.3 Schematic diagram of apparatus used during experiments discussed in Chapter 3.

distribution coefficient on precipitation rate and allowed the equilibrium distribution coefficient to be determined.

3.3.1.1 Procedure

500 mL of a 0.25 *F* NaCl solution was maintained at 25°C using a water-jacketed beaker and a recirculating constant temperature water bath. The solution was equilibrated with $p\text{CO}_2 \approx 1$ atm by bubbling humidified CO_2 gas (99.5% pure) into the solution through a glass bubbler. Calcite was added to the beaker to equilibrate the solution with calcite and to provide seed material for the precipitation. The amount of seed material varied depending on the desired precipitation rate. Usually, 1.25 - 1.50 g of calcite was added for experiments at faster precipitation rates, and 5.0 g of calcite was added for experiments at slower precipitation rates. The solution was stirred with a Teflon stir bar to keep the solid phase suspended. Stirring the solution also helped to prevent localized precipitation during the addition of titrant solutions and kept the system well mixed. A suspended stir bar was used to prevent the precipitate from being ground against the sides of the container.

A dual syringe pump outfitted with gas tight syringes was used to maintain a near constant precipitation rate by adding titrants to the reaction vessel at a constant rate. The syringe pump also allowed the precipitation rate to be varied between experiments by varying the rate at which the titrants were added to the reaction vessel. One of the syringes contained a 0.5 *F* Na_2CO_3 titrant solution and the other contained a 0.5 *F* $\text{Ca}_{0.905}\text{Cd}_{0.095}\text{Cl}_2$ titrant solution. The titrants were added to the solution through narrow bore poly ether ether ketone (PEEK) tubing that was attached to the gas tight syringes with high pressure liquid chromatography (HPLC) fittings. The use of narrow bore tubing ensured that the solutions entered the reaction vessel with a high linear velocity encouraging mixing and minimizing localized precipitation at the titrant inlets. PEEK tubing and HPLC fittings were chosen because they could withstand the high pressures that were generated when forcing the titrant solutions through the narrow bore tubing. In

addition, the tubing and fittings were not a source of trace metal contamination and were not affected by the high pH of the concentrated Na_2CO_3 titrant solution.

The addition of the titrants to the reaction vessel caused the pH to rise and the solution to become increasingly over saturated with respect to calcite. When the precipitation rate equaled the titration rate, the aqueous composition including pH remained nearly constant. At this point, a solid solution of constant known composition was precipitating onto the seed material. The $X_{\text{CdCO}_3(\text{s})}$ in the solid solution during the steady state portion of the precipitation experiments should be the same as the X_{CdCl_2} in the titrant solution since, under steady state conditions, the rate at which Cd, Ca and CO_3 were added by titration was equal to the rate at which Cd, Ca and CO_3 were removed by precipitation.

The use of only a $\text{Ca}_{1-x}\text{Cd}_x\text{Cl}_2$ solution syringe deviates from the Tesoriero (1994) method for the determination of the partitioning of trace levels of Cd into calcite. That method first achieved steady state precipitation of calcite then introduced cadmium to the system by changing from a CaCl_2 syringe to a $\text{Ca}_{0.973}\text{Cd}_{0.063}\text{Cl}_2$ syringe. This procedure required the attainment of a second steady state as the concentration of Cd in the solution increased until it reached a steady state concentration. This method works best near the calcite end member. When working away from the calcite end member, the difference in the rate of addition of Ca between the CaCl_2 syringe and the $\text{Ca}_{1-x}\text{Cd}_x\text{Cl}_2$ syringe is significant and results in the system needing to reach a new steady state with respect to the aqueous concentrations of both Ca and Cd. To avoid the interruption of steady state precipitation that occurred when changing from a CaCl_2 syringe to a mixed chloride syringe, the step of first reaching end member steady state conditions was removed from the experimental procedure. Instead, precipitation experiments were run with only the mixed chloride syringe. This procedural change had the added benefit of decreasing the overall experiment time and allowed pH to be used as an indication of the attainment of steady state precipitation conditions, thereby reducing the number of samples that needed to be taken over the course of an experiment.

The pH of the aqueous solution in the reaction vessel was monitored throughout an experiment using a Ross Sure-Flow semi-micro combination pH electrode. Immediately before starting the titration and periodically throughout the experiment, 5-7 mL of solution was removed and filtered through a 0.45 μm cellulose nitrate membrane syringe tip filter to remove the solid phase. The aqueous portion of the sample was acidified to $\text{pH} < 2$ to prevent precipitation as CO_2 degassed from the sample. Aqueous phase samples were analyzed for calcium and cadmium by AAS. Due to the presence of NaCl in the samples, the AAS analysis was performed by either the method of standard additions or with standards prepared in an appropriate NaCl solution. Aqueous composition, pH, and titration rate data for G series experiments can be found in Appendix A.

After reaching steady state conditions, each experiment was run until approximately 0.005 mols of solid solution precipitated onto the seed material. Immediately after an experiment was finished, the solid phase was collected by vacuum filtering the entire solution volume through a 0.45 μm filter. Although Tesoriero (1994) washed the solid phase with a calcite saturated aqueous solution after collection, the solid phase materials from G series experiments were not washed with calcite-saturated water due to concerns that the surface of the more concentrated G series solid solutions might have been altered by the calcite saturated wash. Solids were then dried in a 105°C oven for 24 hours and weighed. Comparison of washed and unwashed samples by XPS indicated that washing the calcite based solids did not affect $X_{\text{CdCO}_3(\text{s})}$ values for G series compositions.

Precipitation of unwanted minerals, like aragonite and otavite, was avoided by keeping the solution undersaturated with respect to those phases. XRD was used to identify the mineral phases in select solid samples. Tesoriero (1994) used routine XRD analysis with a similar experimental procedure and did not find evidence of trace phases except when the aqueous phase supersaturated with respect to aragonite. SEM images of select precipitated solids gave a visual indication of the effects of the precipitation rate on the distribution of crystal growth sites. XPS was used to directly measure the surface

composition of the solid solutions. A complete discussion of the XPS analysis is located in Section 3.5.

3.3.1.2 Experimental Precipitation Rates

The precipitation rate for each experiment was determined as the average of the initial and final precipitation rates for the steady state portion of the experiment. Since the amount of solid phase increased throughout the experiment due to active precipitation, the mass based precipitation rate decreased over the course of the experiment. The variation between initial and final precipitation rates was most significant when titration rates were high and the initial amount of seed material was low. Table 3.4 lists the initial, final, and average precipitation rates for G series experiments.

Table 3.4 G series precipitation rate data.

Experiment	titration rate (mL/min)	initial precipitation rate (nmol/mg-min)	final precipitation rate (nmol/mg-min)	average precipitation rate (nmol/mg-min)
G1	0.349	138	74.1	106
G2	0.00203	1.82	0.988	1.40
G3	0.0176	6.44	3.49	4.97
G4	0.00501	3.00	1.68	2.34
G5	0.00180	1.15	0.967	1.06
G6	0.00140	0.920	0.600	0.760
G7	0.00216	0.216	0.201	0.210
G8	0.00145	0.151	0.144	0.147
G9	0.00343	0.447	0.327	0.387
G10	0.000739	0.0811	0.0771	0.0791
G11	0.00360	0.366	0.332	0.349
G12	0.00125	0.156	0.154	0.155

3.3.1.3 $D_{\text{Cd}^{2+}}$ Values

To calculate $D_{\text{Cd}^{2+}}$ for each experiment according to Equation 2.13, the composition of both the aqueous and solid phases was determined. The aqueous speciation was calculated using MINTEQA2 in the same manner as described for the endmember solubility experiments. The calculated $[\text{Ca}^{2+}]$ and $[\text{Cd}^{2+}]$ values for G series experiments can be found in Appendix A. The $X_{\text{CdCO}_3(\text{s})}$ in the solid solution layer precipitated onto the calcite seed material was determined by three methods for G series experiments. The $X_{\text{CdCO}_3(\text{s})}$ values are listed in Table 3.5.

Table 3.5 G series solid solution compositions.

Experiment	$X_{\text{CdCO}_3(\text{s})}$, titrant	$X_{\text{CdCO}_3(\text{s})}$, mass balance	$X_{\text{CdCO}_3(\text{s})}$, XPS
G1	0.0946	0.138	NA
G2	0.0946	0.0960	0.279
G3	0.0946	0.0968	NA
G4	0.0946	0.100	0.264
G5	0.0946	0.0960	0.296
G5	-	-	0.304
G6	0.0946	0.109	0.265
G7	0.0946	0.0996	0.148
G8	0.0946	0.119	0.161
G8	-	-	0.165
G9	0.0946	0.0966	0.186
G10	0.0946	0.0841	0.125
G11	0.0946	0.0995	0.187
G12	0.0946	0.102	0.126

NA - not analyzed

Due to the experimental design, the ratio of Ca to Cd in the solid solution should be the same as the ratio of Ca to Cd in the $\text{Ca}_{0.905}\text{Cd}_{0.095}\text{Cl}_2$ titrant solution. This is due to the fact that under steady state conditions, Ca and Cd must be removed from the solution by precipitation at the same rate and in the same ratio as Ca and Cd are being added to the solution by titration. By this method, $X_{\text{CdCO}_3(\text{s})} = 0.0946$. The composition of the solid phase can also be determined from the total number of mols of Ca and Cd precipitated during the steady state portion of the experiment. The mols of Ca and Cd precipitated were calculated from mass balance considerations once $[\text{Ca}_T]_{(\text{aq})}$ and $[\text{Cd}_T]_{(\text{aq})}$ at the beginning and end of the steady state period were determined along with the number of mols of Ca and Cd that were added to the reaction vessel by titration during the steady

Table 3.6 G series distribution coefficient data.

Experiment	log precipitation rate (nmol/mg-min)	$D_{\text{Cd}^{2+}, \text{titrant}}$	$D_{\text{Cd}^{2+}, \text{mass balance}}$	$D_{\text{Cd}^{2+}, \text{XPS}}$
G1	2.03	NC	NC	NC
G2	0.146	640±80	650±80	2400±300
G3	0.696	170±60	170±60	NC
G4	0.369	570±50	600±50	1900±200
G5	0.0263	800±60	800±60	3200±200
G6	-0.119	1330±5	1560±6	4560±20
G7	-0.678	1600±100	1600±100	2600±200
G8	-0.833	1210±60	1570±70	2200±100
G9	-0.412	1000±100	1000±100	2200±200
G10	-1.10	1900±300	1700±300	2600±400
G11	-0.457	1180±80	1250±80	2600±200
G12	-0.810	1500±400	1600±400	2000±600

NC - not calculated

state period. XPS analysis of the solids provided a third and direct measurement of the solid solution compositions (see Section 3.5).

Log precipitation rates and three sets of distribution coefficients for the G series experiments are listed in Table 3.6. $D_{\text{Cd}^{2+}}$ values were calculated using the aqueous speciations from Appendix A and the solid solution compositions from Table 3.5. The $D_{\text{Cd}^{2+}}$ value for a given experiment listed in Table 3.6 is the average of $D_{\text{Cd}^{2+}}$ values from each sample taken during the steady state portion of that experiment. Log precipitation rate values were taken from the average precipitation rate values in Table 3.4.

3.3.1.4 Equilibrium Partitioning Region

In order to determine the region where equilibrium partitioning is occurring, the region where the observed distribution coefficient no longer changes with decreasing precipitation rate must be determined. One way to determine this region is to identify when the aqueous composition remains nearly constant with decreasing precipitation rate. This is essentially looking for the region where the saturation state of the aqueous solution remains constant with decreasing precipitation rate.

Figure 3.4 contains plots of $[\text{Ca}^{2+}]$ and $[\text{Cd}^{2+}]$ vs. log precipitation rate for the G series experiments. In these plots, each sample from the steady state portion of a given experiment is plotted individually at the average precipitation rate of the experiment to give a measure of the scatter in the data. The expected behavior of the $[\text{Ca}^{2+}]$ and $[\text{Cd}^{2+}]$ vs. log precipitation rate plots is an asymptotic approach to equilibrium values as the precipitation rate is decreased. The plot of $[\text{Ca}^{2+}]$ vs. log precipitation rate does not clearly demonstrate an approach to equilibrium values given the scatter in the data. However, it should be noted that the precipitation rate data is plotted on a log scale which covers a range of three orders of magnitude. At slower precipitation rates (around 0.25 nmol/mg-min), the growth rate of the solid phase is so slow that the observed behavior is most likely representative of near equilibrium values even without a clear approach to an asymptotic limit. Therefore, it can be argued that the $[\text{Ca}^{2+}]$ values begin to level off

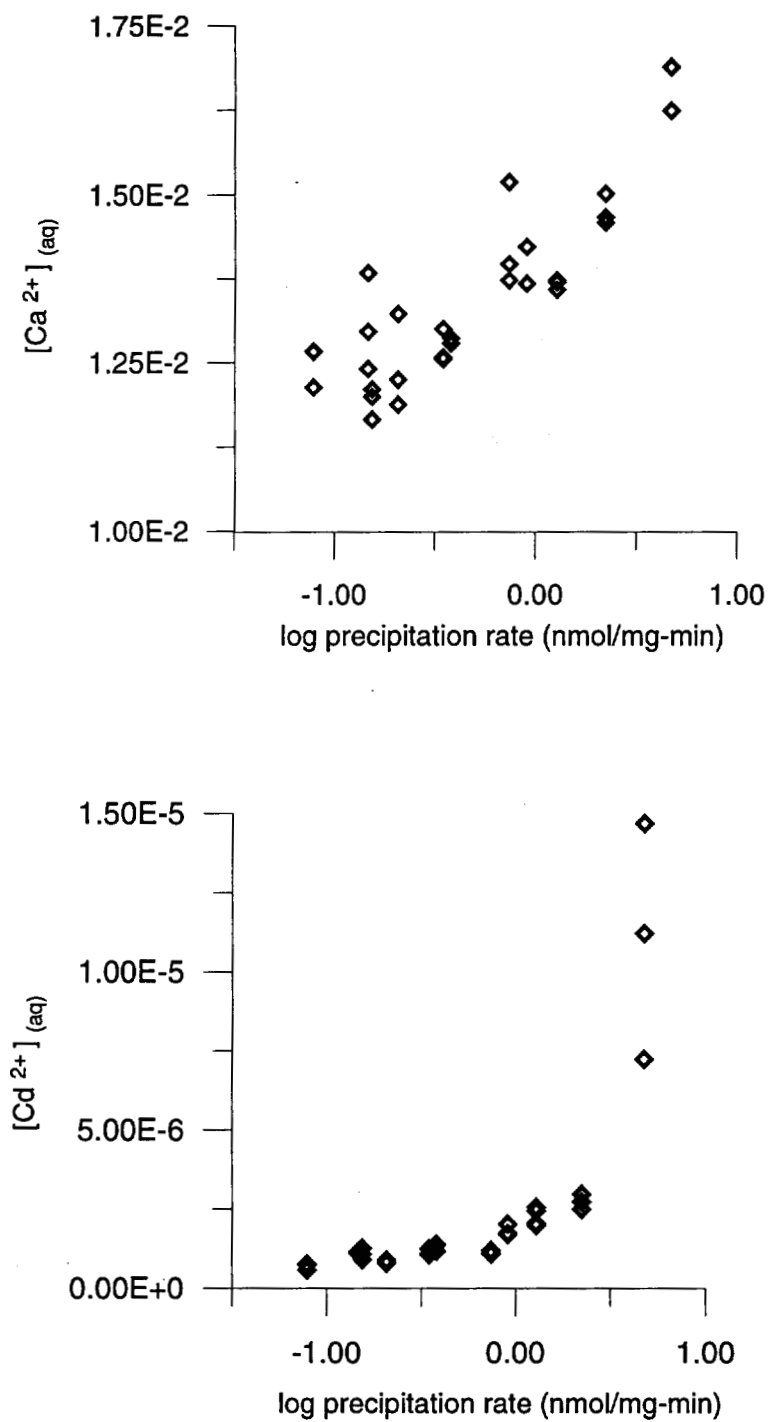


Figure 3.4 $[Ca^{2+}]$ vs. log precipitation rate (top) and $[Cd^{2+}]$ vs. log precipitation rate (bottom) for G series experiments.

below log precipitation rate -0.6. $[\text{Cd}^{2+}]$ values appear to level off below log precipitation rates -0.5. These plots indicate that the equilibrium partitioning region does not extend to precipitation rates faster than log precipitation rate -0.6.

The overall behavior of the data for the G series experiments, decreasing concentration with decreasing precipitation rate, is expected from the experimental design. Indeed, when adding titrants at a faster rate, the system is perturbed farther from equilibrium. This is characterized by higher saturation states and aqueous concentrations. Since both Ca and Cd are added to the reaction vessel throughout the experiment, the trend is seen for both aqueous phase constituents. Plots of pH, Ca_T , and Cd_T vs. log precipitation rate would all show similar trends, *i.e.* an approach to equilibrium values as the precipitation rate is decreased.

3.3.1.5 $D_{\text{Cd}^{2+}, \text{eq}}$ and $\zeta_{\text{CdCO}_3(\text{s})}$ Values

The data from Table 3.6 are plotted as $D_{\text{Cd}^{2+}}$ vs. log precipitation rate in Figures 3.5, 3.6 and 3.7. The expected behavior in these plots is an increase in $D_{\text{Cd}^{2+}}$ as precipitation rate is decreased until the equilibrium partition region is reached. In the equilibrium partitioning region, the observed $D_{\text{Cd}^{2+}}$ is independent of precipitation rate which is observed by a leveling off in the $D_{\text{Cd}^{2+}}$ vs. log precipitation rate curve at slow precipitation rates. As shown in Figure 3.5, when using the composition of the titrant solution to approximate the solid phase mole fraction in order to calculate $D_{\text{Cd}^{2+}}$ values, $D_{\text{Cd}^{2+}}$ increases as the precipitation rate decreases. In contrast, when the mass balance calculation is used to determine $X_{\text{CdCO}_3(\text{s})}$, $D_{\text{Cd}^{2+}}$ values appear to reach a maximum value at log precipitation rate -0.60 and remain nearly constant as the precipitation rate decreases (see Figure 3.6). When the $X_{\text{CdCO}_3(\text{s})}$ determined by XPS is used to calculate $D_{\text{Cd}^{2+}}$, the region where $D_{\text{Cd}^{2+}}$ appears independent of precipitation rate extends to log precipitation rates as high as -0.41 (see Figure 3.7). The datum point at log precipitation rate 0.7, shown in grey in Figure 3.7, is an approximate value since the solid phase material from experiment G3 was not analyzed by XPS.

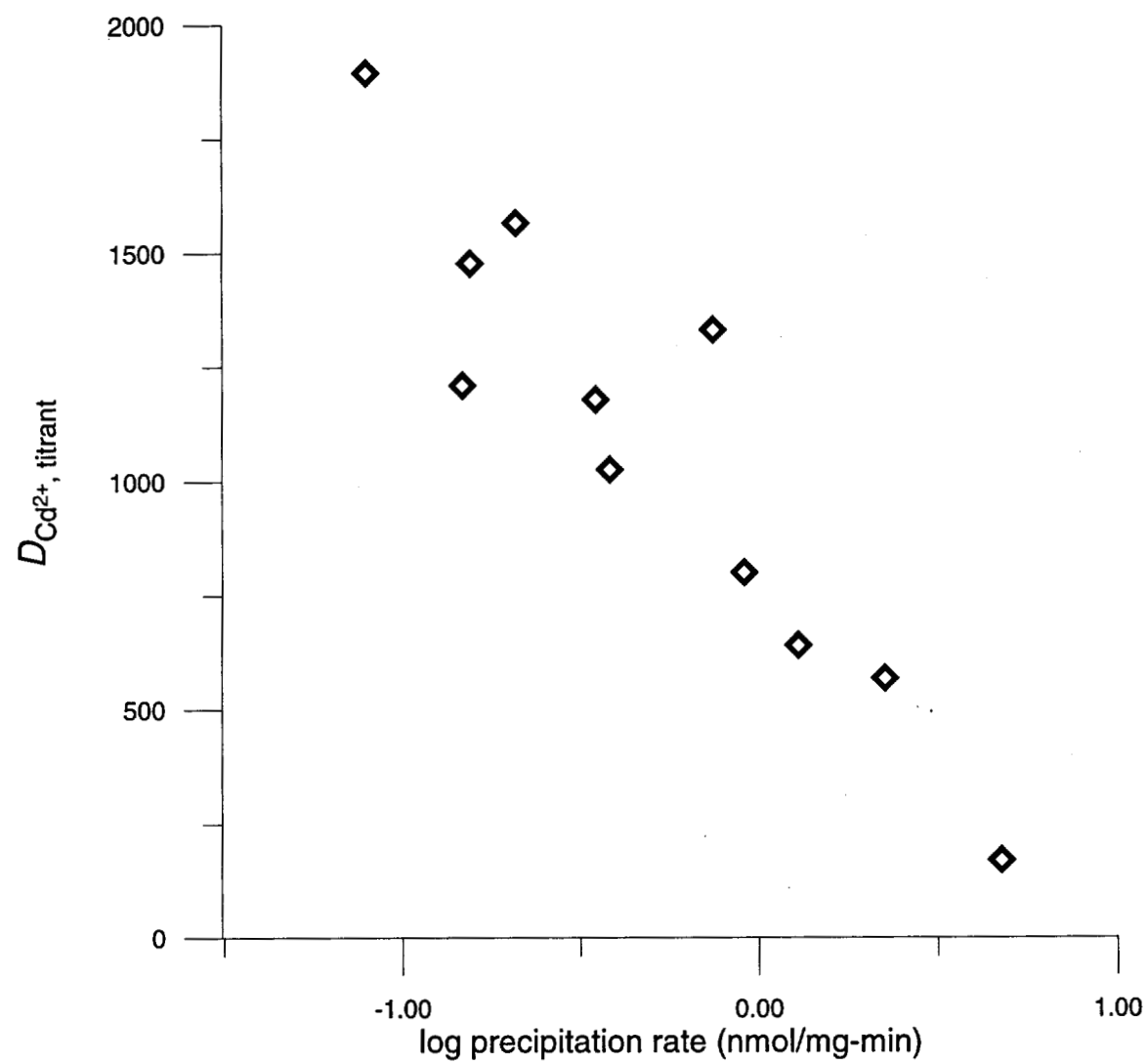


Figure 3.5 $D_{\text{Cd}^{2+}, \text{titrant}}$ vs. log precipitation rate for G series experiments.

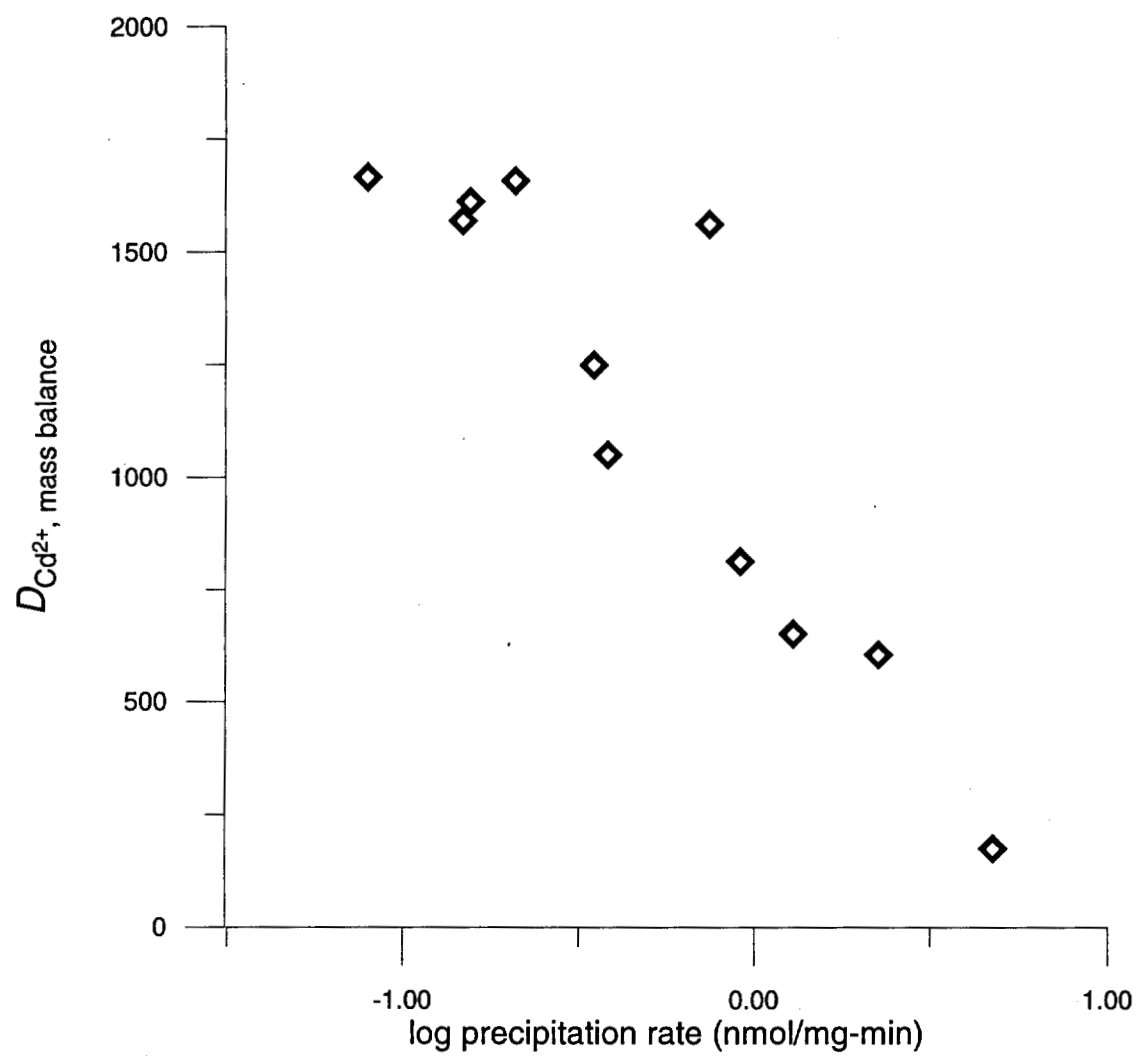


Figure 3.6 $D_{Cd^{2+}}$, mass balance vs. log precipitation rate for G series experiments.

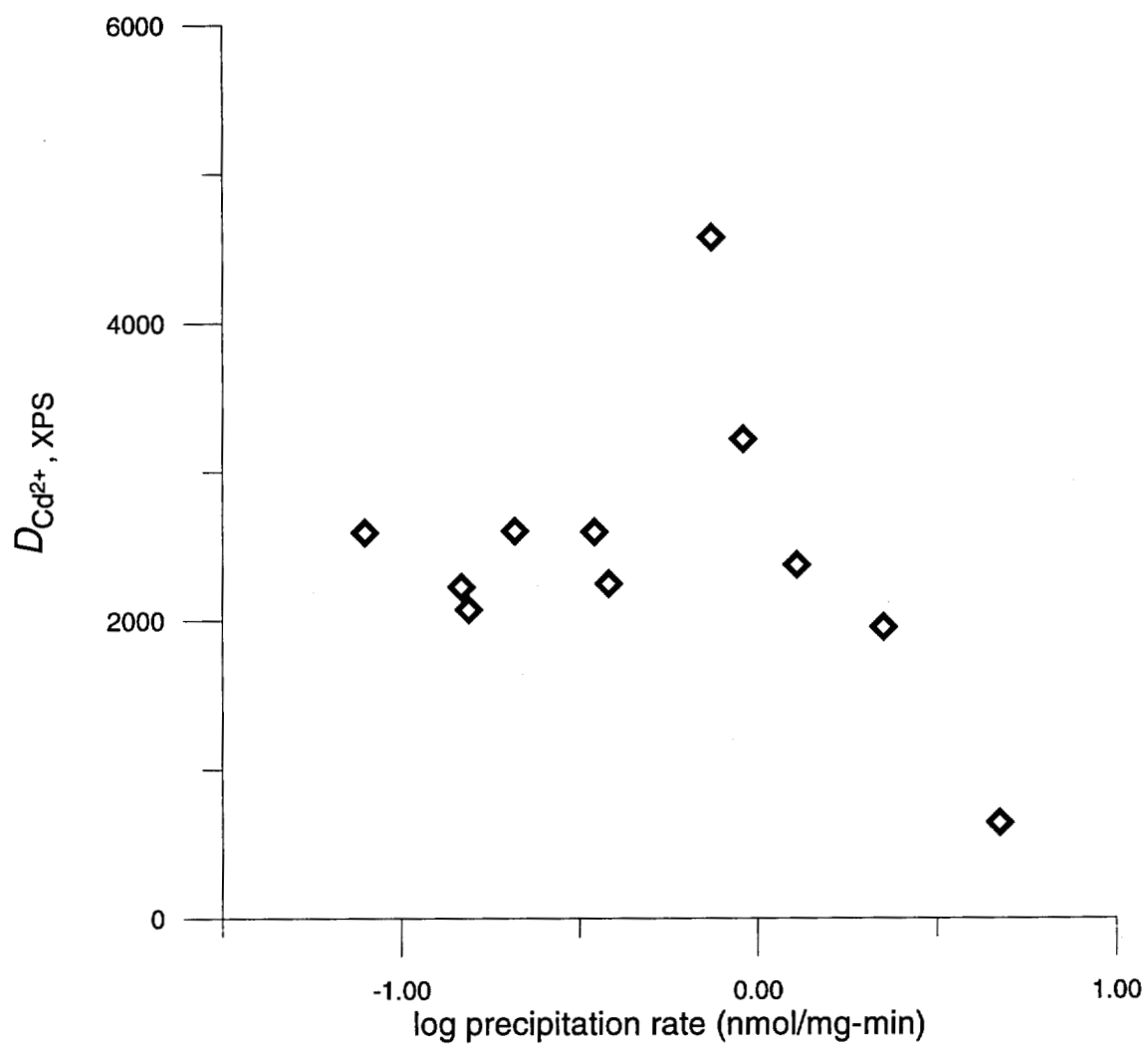


Figure 3.7 $D_{Cd^{2+}, XPS}$ vs. log precipitation rate for G series experiments.

$D_{\text{Cd}^{2+}, \text{eq}}$ values were calculated as the average of the $D_{\text{Cd}^{2+}}$ values located within the equilibrium partitioning region determined in Section 3.3.1.4. The $D_{\text{Cd}^{2+}, \text{eq}}$ values for G series experiments were 1500 ± 300 (titrant), 1620 ± 40 (mass balance) and 2400 ± 300 (XPS). If the additional 2 points that had leveled off on the (XPS) $D_{\text{Cd}^{2+}}$ vs. log precipitation rate plot located outside the equilibrium partitioning region are included in the average, the $D_{\text{Cd}^{2+}, \text{eq}}$ is 2400 ± 200 (extended XPS).

Once the $D_{\text{Cd}^{2+}, \text{eq}}$ has been determined, the solid phase activity coefficient for the trace constituent, $\zeta_{\text{CdCO}_3(\text{s})}$, can be calculated from Equation 2.14 using -8.48 ± 0.02 for the log $K_{\text{s}0}$ of calcite, and -12.1 ± 0.1 for the log $K_{\text{s}0}$ of otavite, if it is assumed that $\zeta_{\text{CaCO}_3(\text{s})} = 1$. This calculation yields $\zeta_{\text{CdCO}_3(\text{s})} = 2.7 \pm 0.5$ (titrant), $\zeta_{\text{CdCO}_3(\text{s})} = 2.6 \pm 0.2$ (mass balance) and $\zeta_{\text{CdCO}_3(\text{s})} = 1.8 \pm 0.2$ (XPS).

3.3.2 H Series Experiments

The same constant composition method used for the G series experiments was used for H series experiments. The main difference between the two series was the composition of the mixed chloride titrant solution. Due to the similarities between the two experimental procedures, an abbreviated procedure is given below.

3.3.2.1 Procedure

500 mL of a 0.25 *F* NaCl solution was maintained at 25°C and equilibrated with $p\text{CO}_2 \approx 1 \text{ atm CO}_2$. Calcite was added to the beaker to equilibrate the solution with calcite and to provide seed material for the precipitation. The amount of seed material varied depending on the desired precipitation rate. The solution was stirred with a suspended magnetic stir bar to keep the system well mixed.

A dual syringe pump outfitted with gas tight syringes was used to maintain a near constant precipitation rate by adding titrants to the reaction vessel at a constant rate. The precipitation rate could be varied between experiments by changing the titration rate.

One of the syringes contained a 0.5 *F* Na₂CO₃ titrant solution and the other contained a 0.5 *F* Ca_{0.991}Cd_{0.009}Cl₂ titrant solution. The titrants were added to the solution through narrow bore PEEK tubing that was attached to the gas tight syringes with HPLC fittings. The use of narrow bore tubing ensured that the solutions entered the reaction vessel with a high linear velocity encouraging mixing and minimizing localized precipitation at the titrant inlets.

The addition of the titrants to the reaction vessel caused the pH to rise and the solution to become increasingly oversaturated with respect to calcite. When the precipitation rate equaled the titration rate, the aqueous composition including pH remained nearly constant. At this point, a solid solution of constant known composition was precipitating onto the seed material. The composition of this solid solution should be set by the composition of the mixed chloride syringe.

The pH of the aqueous solution was monitored throughout an experiment. The aqueous phase was sampled immediately before starting the titration and periodically throughout the experiment. Aqueous phase samples were analyzed for calcium and cadmium by AAS. Aqueous composition, pH, and titration rate data for H series experiments can be found in Appendix A.

After reaching steady state conditions, each experiment was run until approximately 0.005 mols of solid solution precipitated onto the seed material. Immediately after an experiment was finished, the solid phase was collected by vacuum filtering the entire solution volume through a 0.45 μm filter. The solid phase materials from H series experiments were washed with calcite-saturated water as described in Tesoriero (1994) to remove any Cd that might be present in the interstitial waters or adsorbed to the solid surface. Solids were then dried in a 105°C oven for 24 hours and weighed.

Precipitation of unwanted minerals, such as aragonite and otavite, was avoided by keeping the solution undersaturated with respect to those phases. XPS was used to directly measure the surface composition of the solid solutions.

Table 3.7 H series precipitation rate data.

Experiment	titration rate (mL/min)	initial precipitation rate (nmol/mg-min)	final precipitation rate (nmol/mg-min)	average precipitation rate (nmol/mg-min)
H1	0.00369	0.381	0.348	0.365
H2	0.301	32.5	29.3	30.9
H3	0.00153	0.168	0.154	0.161
H4	0.281	192	119	155
H5	0.00358	1.27	1.03	1.15
H7	0.0476	24.7	16.6	20.6
H8	0.00396	1.54	1.23	1.42
H9	0.0174	6.02	4.68	5.35
H10	0.00359	0.367	0.330	0.349

3.3.2.2 Experimental Precipitation Rates

The initial, final, and average precipitation rates for H series experiments are given in Table 3.7. H series precipitation rates were determined in the same manner as G series precipitation rates (see Section 3.3.1.2).

3.3.2.3 $D_{\text{Cd}^{2+}}$ Values

In order to calculate a distribution coefficient for each experiment using Equation 2.13, the composition of both the aqueous and solid phases was determined (see Section 3.3.1.3). The calculated $[\text{Ca}^{2+}]$ and $[\text{Cd}^{2+}]$ values for H series experiments can be found in Appendix A. As with the G series experiments, $X_{\text{CdCO}_3(\text{s})}$ was determined by three methods. Using the titrant method, $X_{\text{CdCO}_3(\text{s})} = 0.0091$ for H series experiments. The

Table 3.8 H series solid solution compositions.

Experiment	$X_{\text{CdCO}_{3(s)}, \text{ titrant}}$	$X_{\text{CdCO}_{3(s)}, \text{ mass balance}}$	$X_{\text{CdCO}_{3(s)}, \text{ XPS}}$
H1	0.0091	0.00952	0.0143
H2	0.0091	0.00987	0.0188
H3	0.0091	0.00989	0.00738
H4	0.0091	0.00970	0.0193
H5	0.0091	0.00858	0.0115
H7	0.0091	0.00873	0.0224
H8	0.0091	0.00990	0.0161
H9	0.0091	0.00960	0.0227
H10	0.0091	0.00938	0.0108

solid phase composition was also determined by a mass balance calculation and by XPS. The solid phase composition data for H series experiments is listed in Table 3.8. Table 3.9 lists log precipitation rates and $D_{\text{Cd}^{2+}}$ values for the H series experiments.

3.3.2.4 Equilibrium Partitioning Region

The equilibrium partitioning region was determined by observing when the aqueous composition remained nearly constant with decreasing precipitation rate. The overall behavior of the data for the H series experiments is the same as the behavior seen in the G series experiments (see Section 3.3.1.4). In Figure 3.8 which contains plots of $[\text{Ca}^{2+}]$ and $[\text{Cd}^{2+}]$ vs. log precipitation rate for the H series experiments, the approach to an asymptotic value for aqueous concentration as precipitation rate is decreased is more apparent. This is due in large part to less scatter in the observed data. As shown in Figure 3.8, $[\text{Ca}^{2+}]$ values appear to level off around log precipitation rate of 0. The low outlier point at log precipitation rate 0.1 is experiment H8 which was run with a mixed

Table 3.9 H series distribution coefficient data.

Experiment	log precipitation rate (nmol/mg-min)	$D_{\text{Cd}^{2+}, \text{titrant}}$	$D_{\text{Cd}^{2+}, \text{mass balance}}$	$D_{\text{Cd}^{2+}, \text{XPS}}$
H1	-0.438	900±30	950±30	1430±50
H2	1.49	330±20	360±20	700±40
H3	-0.793	1600±300	1700±300	1300±200
H4	2.19	181±1	193±1	388±1
H5	0.0607	900±100	900±100	1200±200
H7	1.31	261±8	250±8	650±20
H8	0.152	530±40	580±40	950±70
H9	0.728	353±8	372±9	890±20
H10	-0.457	1200±50	1240±50	1430±60

chloride syringe that leaked around the plunger. Since the $\text{Ca}_{0.991}\text{Cd}_{0.009}\text{Cl}_2$ and Na_2CO_3 solutions were not being added at the same rate through the course of the experiment, steady state conditions were not met. Therefore, experiment H8 was removed from the data set due to the faulty syringe. The $[\text{Cd}^{2+}]$ values level off around log precipitation rate of 0 indicating that this value is the upper boundary of the equilibrium partitioning region.

3.3.2.5 $D_{\text{Cd}^{2+}, \text{eq}}$ and $\zeta_{\text{CdCO}_{3(s)}}$ Values

Plots of $D_{\text{Cd}^{2+}}$ vs. log precipitation rate for H series experiments can be found in Figures 3.9 (titrant), 3.10 (mass balance) and 3.11 (XPS). Experiment H8 was omitted from these plots for reasons explained in Section 3.3.2.4. The plots of $D_{\text{Cd}^{2+}}$ vs. log precipitation rate calculated from the titrant composition and from the mole balance calculation continue to increase as log precipitation rate is decreased with no indication of

an equilibrium partitioning region as shown by a leveling off of $D_{\text{Cd}^{2+}}$ values. However, $D_{\text{Cd}^{2+}}$ values appear to level off around the expected log precipitation rate value of 0 when $D_{\text{Cd}^{2+}}$ values are calculated with the $X_{\text{CdCO}_3(s)}$ values determined by XPS. Although it would have been advantageous to collect additional data from experiments run at slow precipitation rates to confirm the presence of an equilibrium partitioning region, the observed $[\text{Cd}_T]$ values from experiments run at slow precipitation rates approached the detection limit of the available instrumentation. The ability to accurately measure $[\text{Cd}_T]$ placed a lower boundary on the precipitation rate range of the H series experiments.

$D_{\text{Cd}^{2+}, \text{eq}}$ and $\zeta_{\text{CdCO}_3(s)}$ values for the H series experiments were determined in the same manner as for the G series experiments (see Section 3.3.1.5). The $D_{\text{Cd}^{2+}, \text{eq}}$ values are 1100 ± 300 (titrant), 1200 ± 400 (mass balance) and 1300 ± 100 (XPS). The $\zeta_{\text{CdCO}_3(s)}$ values are 4 ± 1 (titrant), 3 ± 1 (mass balance) and 3.2 ± 0.4 (XPS).

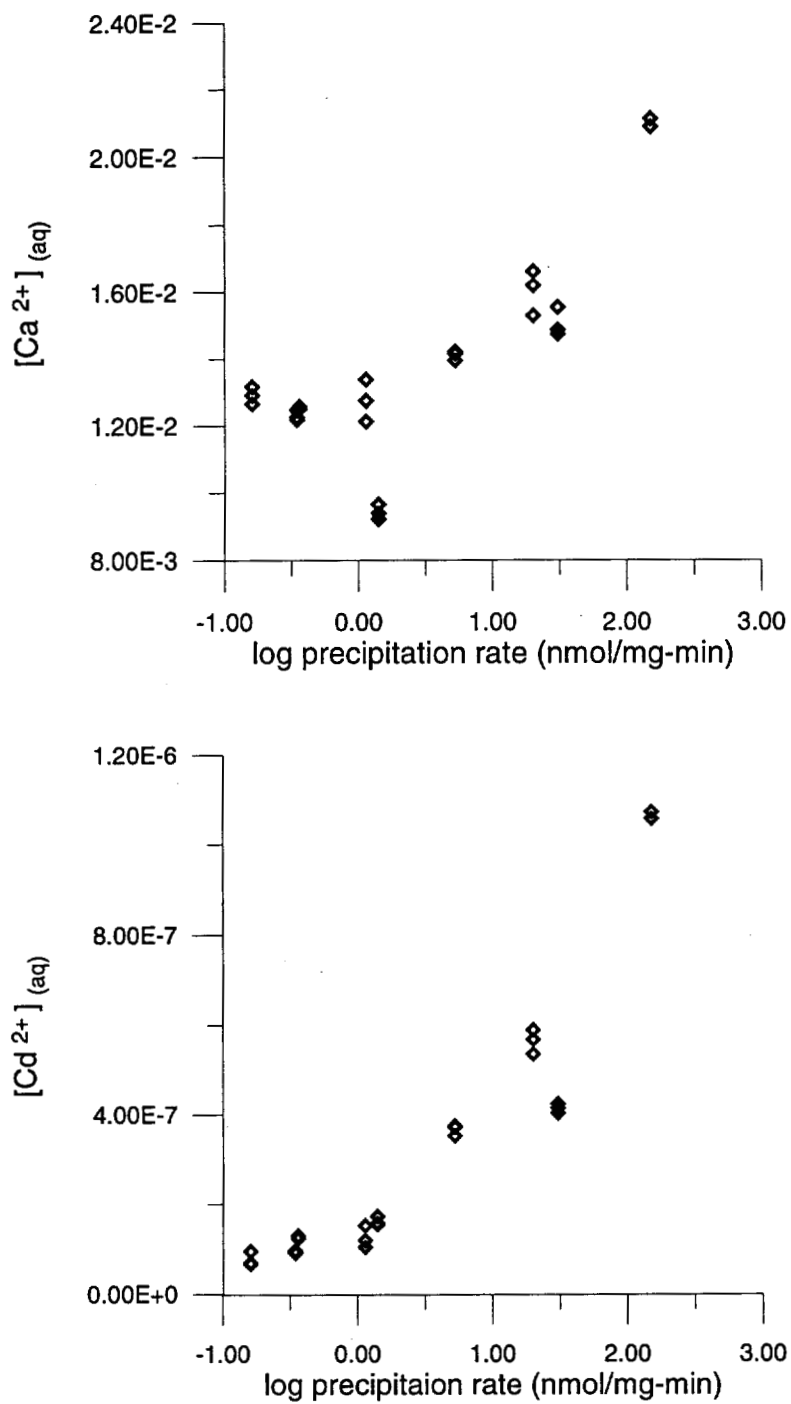


Figure 3.8 [Ca²⁺] vs. log precipitation rate (top) and [Cd²⁺] vs. log precipitation rate (bottom) for H series experiments.

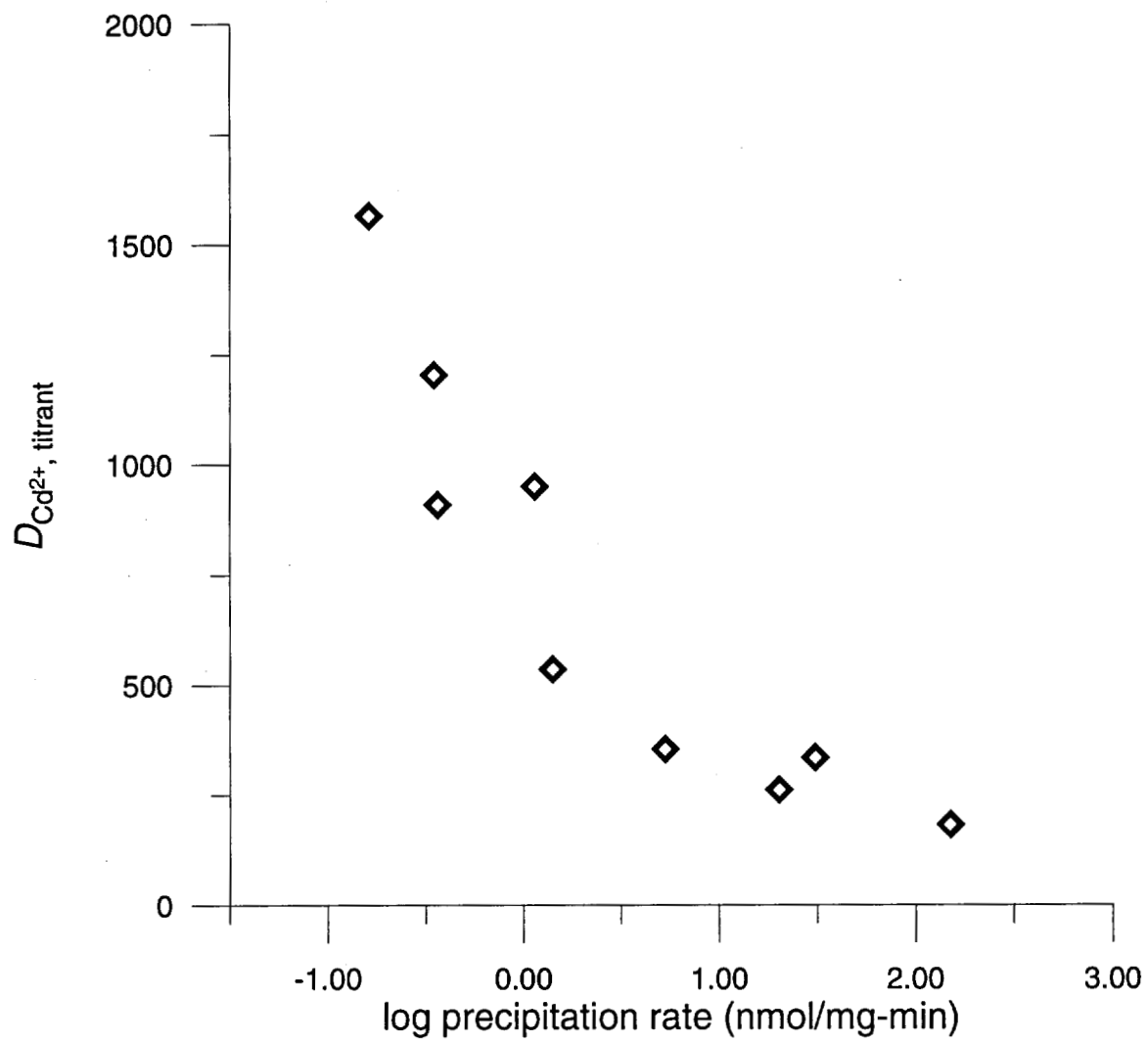


Figure 3.9 $D_{\text{Cd}^{2+}, \text{titrant}}$ vs. log precipitation rate for H series experiments.

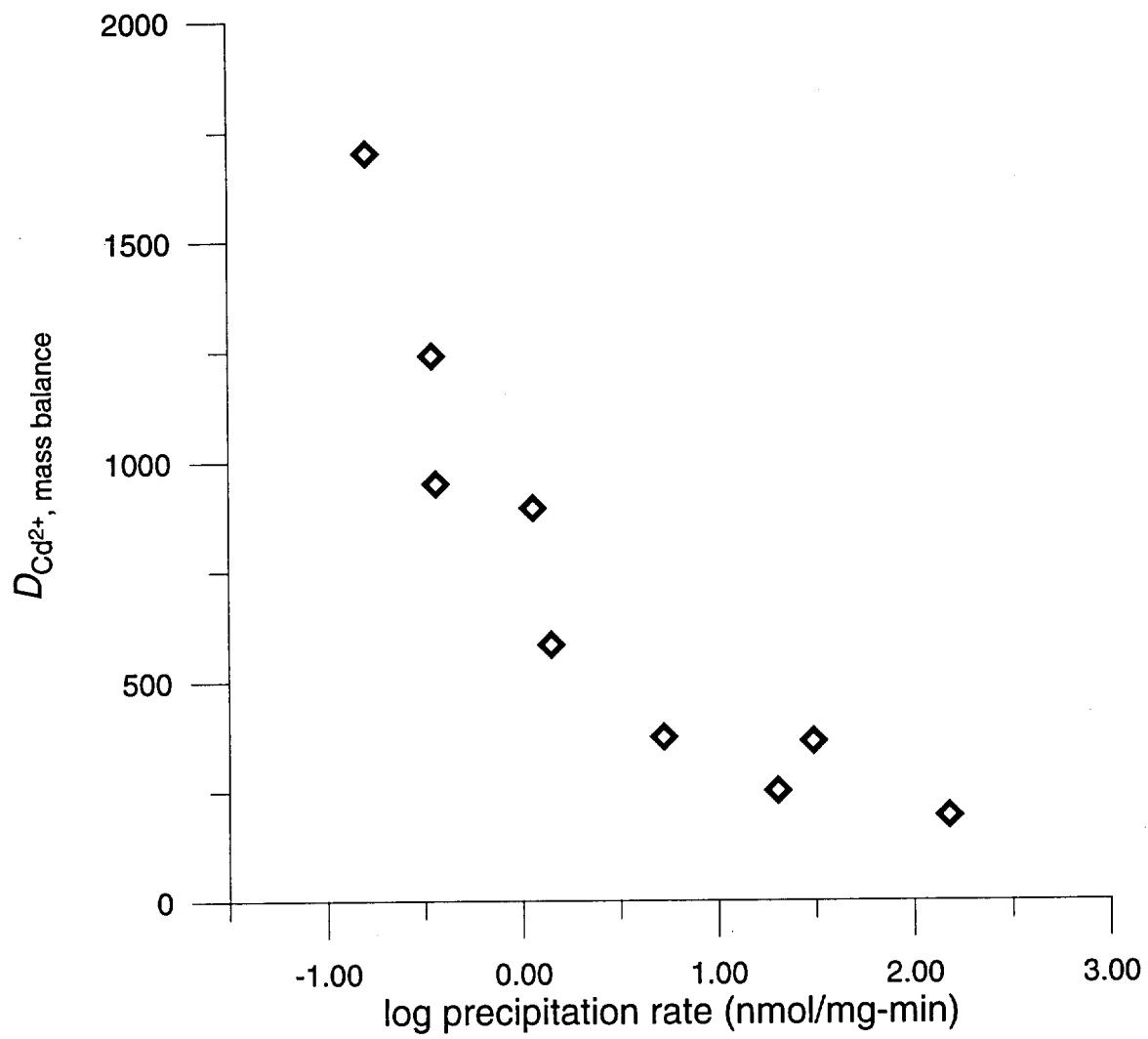


Figure 3.10 $D_{\text{Cd}^{2+}}$, mass balance vs. log precipitation rate for H series experiments.

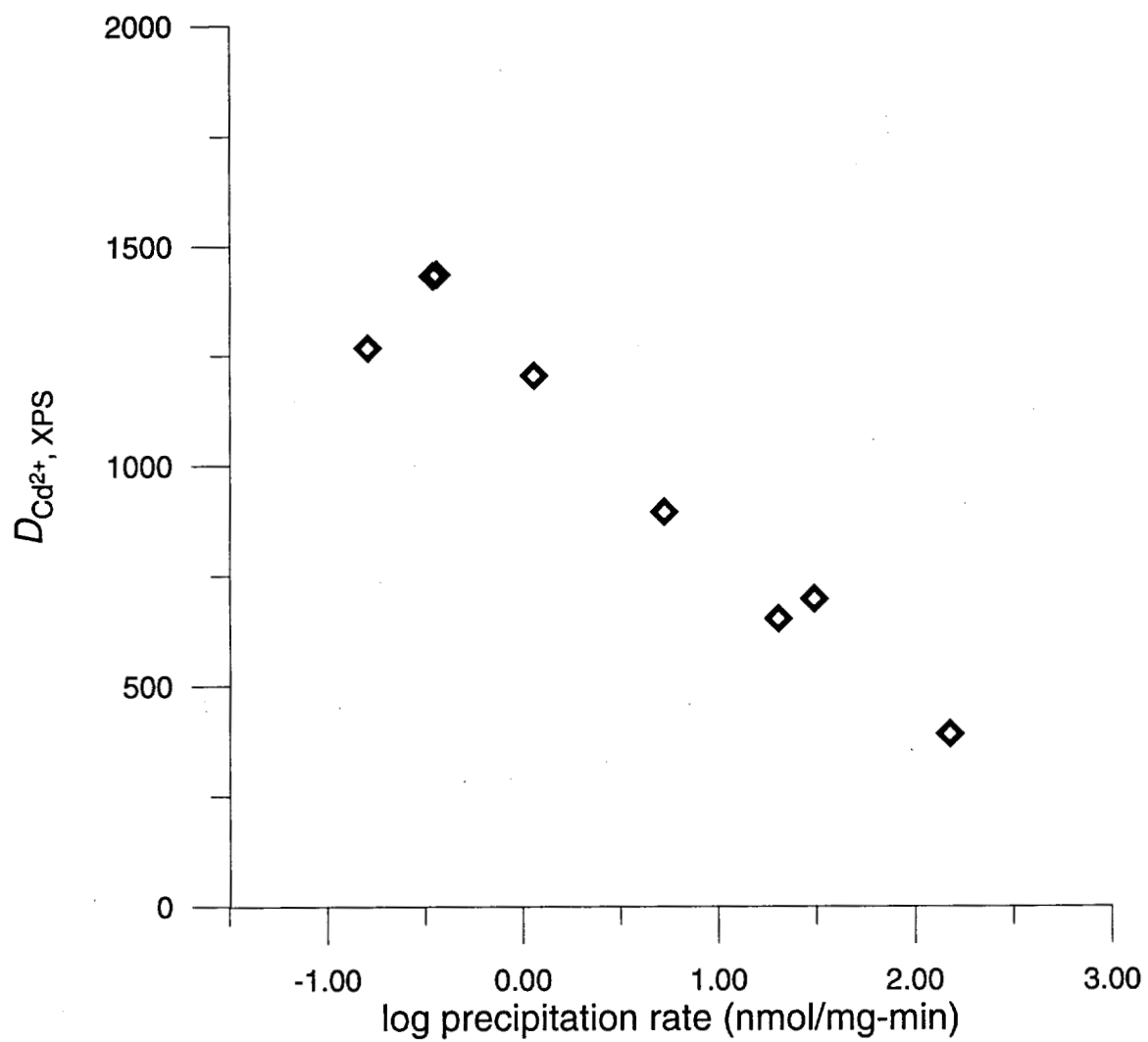


Figure 3.11 $D_{\text{Cd}^{2+}}$, XPS vs. log precipitation rate for H series experiments.

3.4 SSAS Partitioning of Calcium to Otavite

There is essentially no literature concerning the partitioning behavior of calcium to otavite and the resulting solid solutions in low temperature SSAS systems. However, because only one ion in a binary system can partition favorably into a solid, and $D_{\text{Cd}^{2+}} > 1$ for Cd partitioning from the aqueous phase to a $\text{CaCO}_{3(\text{s})}/\text{CdCO}_{3(\text{s})}$ solid solution, $D_{\text{Ca}^{2+}}$ is expected to be less than unity. The experimental procedure used for the G and H series experiments cannot be used when the trace metal ion of interest (Ca^{2+} in this case) does not partition favorably into a solid solution. This difficulty results because the aqueous concentration of the trace ion will increase over the course of the experiment if it is continually added to the solution, and steady state conditions will not be achieved. The expected $D_{\text{Ca}^{2+}} < 1$ partitioning behavior of Ca to otavite is similar to that displayed by the partitioning of metals like Sr and Ba to calcite. Therefore, the constant composition method of Mucci and Morse (1983) used by Tesoriero and Pankow (1996) to investigate the partitioning of Sr and Ba to calcite was used to investigate the partitioning of Ca to otavite. This procedure allows precipitation of a homogenous solid solution onto seed material when the trace metal ion of interest does not partition favorably into the host lattice.

3.4.1 E Series Experiments

A constant composition method similar to that used by Tesoriero and Pankow (1996) for the case when $D < 1$ was used in all of the precipitation batch experiments where Ca partitioned into otavite. The schematic of the experimental apparatus shown in Figure 3.3 is accurate for E series experiments with the exception of the mixed chloride syringe which was replaced by a CdCl_2 syringe. Solid solutions were formed over a range of precipitation rates. The range of precipitation rates demonstrated the dependence of $D_{\text{Ca}^{2+}}$ on precipitation rate and allowed $D_{\text{Ca}^{2+}, \text{eq}}$ values to be determined. Since the experimental procedure for E series experiments was similar to the procedure

for G series experiments described in Section 3.3.1.1, an abbreviated version of the procedure is provided below.

3.4.1.1 Procedure

500 mL of a 0.25 *F* NaCl solution was maintained at 25°C and equilibrated with $p\text{CO}_2 \approx 1$ atm. 1.00 - 1.25 g of otavite was added to the beaker to equilibrate the solution with respect to otavite and to provide seed material for the precipitation. The solution was stirred with a suspended stir bar to keep the solid phase suspended and the system well mixed.

A dual syringe pump outfitted with gas tight syringes was used to add a 0.5 *F* Na_2CO_3 solution and a 0.5 *F* CdCl_2 solution to the reaction vessel through narrow bore PEEK tubing at a constant rate. The addition of the titrants caused the pH to rise and the solution to become increasingly over saturated with respect to otavite. When the precipitation rate equaled the titration rate, the aqueous composition and the pH remained nearly constant. At this point, a small volume of a concentrated CaCl_2 solution was spiked into the reaction vessel. The aqueous level of Ca remained nearly constant over the course of an experiment since the amount of Ca lost to the solid solution was insignificant compared to the total amount of Ca in the solution. After the reaction vessel was spiked with Ca, a homogenous solid solution was precipitated on the seed material.

The pH of the aqueous solution in the reaction vessel was monitored throughout the experiment. 5 to 7 mL of solution was removed and filtered through a 0.45 μm cellulose nitrate membrane syringe tip filter at three points during the experiment: 1) after the initial equilibration time but before titration began; 2) immediately after the addition of Ca; and 3) at the end of the experiment. The aqueous portion of the sample was acidified to $\text{pH} < 2$ to prevent the precipitation of solids as CO_2 degassed from the sample. Aqueous phase samples were analyzed for Ca and Cd by AAS. Due to the presence of NaCl in the samples, the AAS analysis was performed by either the method of standard additions or with standards prepared in an appropriate NaCl solution. Several duplicate

samples were taken and filtered through 0.2 μm filters. It was determined that the 0.45 μm filters were adequately separating the aqueous and solid phases. Aqueous composition, pH, and titration rate data for E series experiments can be found in Appendix A.

After reaching steady-state conditions, the experiment continued until approximately 0.005 mols of solid solution was precipitated onto the seed material. At this point, the experiment was terminated. The solid phase was collected by vacuum filtration through a 0.45 μm filter. The solid-phase materials were washed with an aqueous solution that was saturated with otavite to remove any Ca that might have been present in the interstitial waters or adsorbed to the surface. Samples were then dried for 24 hours in a 105°C oven and weighed. A small portion of the solid phase was dissolved in trace metal grade HCl and analyzed for Ca by AAS.

Precipitation of unwanted minerals, like calcite, was avoided by keeping the solution undersaturated with respect to those phases. SEM images of several precipitated solids provided a visual indication of the effects of the precipitation rate on the distribution of crystal growth sites. XPS was used to directly measure the surface composition of the solid solutions.

3.4.1.2 Experimental Precipitation Rates

The reported precipitation rate for each experiment was determined as the average of the initial and final precipitation rates from the steady-state portion of that experiment. Because the amount of solid phase increased throughout the experiment, the precipitation rate decreased over the course of the experiment. Table 3.10 lists the initial, final, and average precipitation rates for the E series experiments.

Table 3.10 E series precipitation rate data.

Experiment	titration rate (mL/min)	initial precipitation rate (nmol/mg-min)	final precipitation rate (nmol/mg-min)	average precipitation rate (nmol/mg-min)
E1	0.0416	10.7	6.24	8.47
E2	0.00318	5.56	2.91	4.23
E3	0.0137	2.40	1.51	1.95
E4	0.00396	0.888	0.610	0.749
E5	0.397	77.2	50.2	63.7
E6	0.159	38.6	26.4	32.5
E7	0.0135	3.52	1.89	2.71
E8	0.00397	1.63	1.14	1.38
E9	0.00145	0.543	0.360	0.451
E10	0.00283	0.979	0.668	0.824
E11	0.00202	0.781	0.511	0.646
E12	0.00103	0.332	0.235	0.284
E13	0.000739	0.272	0.185	0.228
E14	0.000732	0.332	0.194	0.263

3.4.1.3 $D_{Ca^{2+}}$ Values

A general distribution coefficient for Ca^{2+} partitioning to a $CaCO_{3(s)}/CdCO_{3(s)}$ solid solution was calculated for every E series steady state sample according to Equation 3.1. This equation is simply the inverse of Equation 2.13, the distribution coefficient for Cd^{2+} partitioning to a $CaCO_{3(s)}/CdCO_{3(s)}$ solid solution.

$$D_{Ca^{2+}} = \frac{\frac{X_{CaCO_3(s)}}{[Ca^{2+}]}}{\frac{X_{CdCO_3(s)}}{[Cd^{2+}]}} \quad (3-1)$$

The aqueous composition data for E series experiments are given in Appendix A. Solid phase mole fractions were determined by two methods for E series. Due to the experimental design, the composition of each solid solution layer should be nearly homogenous over its entire depth. This is due to the fact that Ca was not added to the reaction vessel until the precipitation of otavite had reached steady state conditions. Because Ca does not partition favorably into otavite, $[Ca_T]$ remained nearly constant throughout the steady-state portion of the experiment which allowed a homogeneous solid solution to form. The composition of this solid solution layer can be calculated by knowledge of the initial mass of seed material, the amount of material precipitated until the addition of Ca, the amount of material precipitated after the addition of Ca and the amount of Ca in the solid as determined by AAS. Equations 3.2 and 3.3 describe the calculation.

$$\left[\frac{g Ca}{g CdCO_{3(s)}}\right]_{sp} = \frac{\left[\frac{g Ca}{g CdCO_{3(s)}}\right]_{total} - F_{seed} \left[\frac{g Ca}{g CdCO_{3(s)}}\right]_{seed}}{F_{sp}} \quad (3-2)$$

$$X_{CaCO_3(s)} = \left[\frac{g Ca}{g CdCO_{3(s)}}\right]_{sp} \left[\frac{172 g CdCO_3}{mol CdCO_3}\right] \left[\frac{mol CaCO_3}{40 g Ca}\right] \quad (3-3)$$

In the above equations, sp refers to the homogeneous surface precipitate layer and F refers to weight fractions. It should be noted that this calculation is an approximation because it assumes that the mean formula weight of the solid solution is the same as the molecular weight of the pure phase endmember. However, since the solid concentrations of Ca are so dilute, this approximation is fairly accurate. Comparison of the approximation to an iterative calculation showed percent differences between the two techniques of ~1%. XPS analysis of the solids was used as an additional and direct measurement of the solid solutions composition. Table 3.11 lists the E series solid solution compositions for each method. Table 3.12 lists the $D_{Ca^{2+}}$ and log precipitation

Table 3.11 E series solid solution compositions.

Experiment	$X_{CaCO_3(s)}$, AAS	$X_{CaCO_3(s)}$, XPS
E1	0.0103	0.00404
E2	0.00827	NA
E3	0.00986	0.00840
E4	0.0222	0.00793
E5	0.00700	NA
E6	0.00762	0.00403
E7	0.00728	0.00806
E8	0.00958	0.00832
E9	0.0133	0.00883
E10	0.00978	0.00987
E11	0.00907	0.00990
E12	0.0114	0.00544
E13	0.0139	0.00498
E14	0.0147	0.0109

NA - not analyzed

Table 3.12 E series distribution coefficient data.

Experiment	log precipitation rate (nmol/mg-min)	$D_{Ca^{2+}, AAS}$	$D_{Ca^{2+}, XPS}$
E1	0.928	0.002810±0.00004	0.001096±0.000003
E2	0.626	0.0023±0.0007	NC
E3	0.290	0.0016±0.0002	0.0014±0.0002
E4	-0.125	0.0029±0.0009	0.0010±0.003
E5	1.80	0.0046±0.0005	NC
E6	1.51	0.0038±0.0003	0.0020±0.002
E7	0.433	0.0020±0.0001	0.0022±0.001
E8	0.140	0.0016±0.0004	0.00142±0.00003
E9	-0.346	0.0014±0.0001	0.00091±0.00007
E10	-0.0841	0.0016±0.0002	0.0016±0.0002
E11	-0.190	0.0012±0.0001	0.0013±0.0001
E12	-0.547	0.0012±0.0002	0.000564±0.0001
E13	-0.642	0.0016±0.0001	0.00056±0.00003
E14	-0.580	0.0027±0.0004	0.0020±0.0003

NC- not calculated

rate data for the E series experiments. The reported $D_{Ca^{2+}}$ values are the average of the initial and final steady state values for each experiment. Log precipitation rate values are taken from the average value listed in Table 3.10.

3.4.1.4 Equilibrium Partitioning Region

The equilibrium partitioning region for E series experiments was identified by observing when a plot of $[Cd^{2+}]$ vs. log precipitation rate approached an asymptotic value

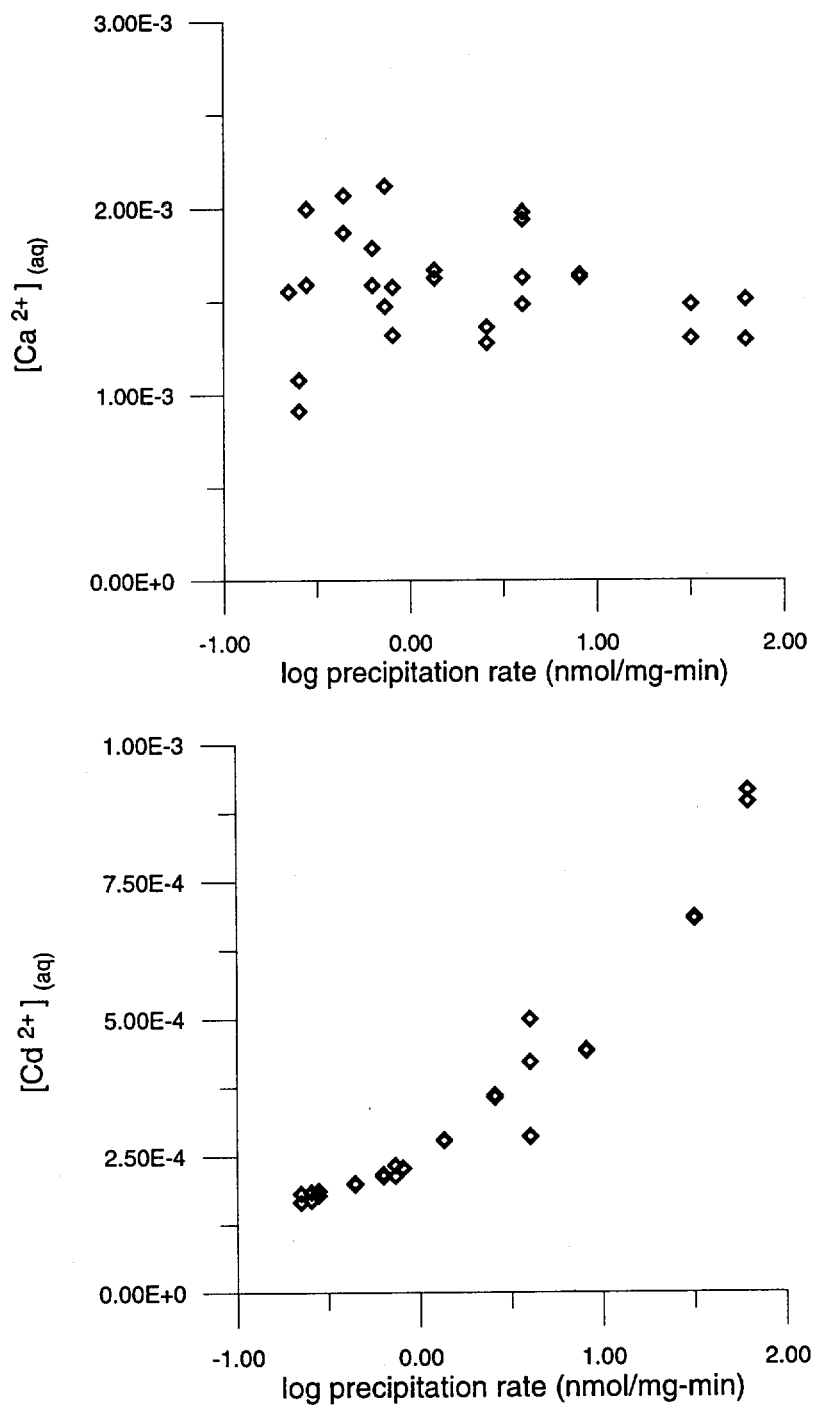


Figure 3.12 [Ca²⁺] vs. log precipitation rate (top) and [Cd²⁺] vs. log precipitation rate (bottom) for E series experiments.

with decreasing precipitation rate. Figure 3.12 shows the plots of $[Ca^{2+}]$ and $[Cd^{2+}]$ vs. log precipitation rate for the E series experiments. The $[Cd^{2+}]$ data follows the same behavior seen in the G and H series experiments (see Sections 3.3.1.4 and 3.3.2.4). However, the $[Ca^{2+}]$ data shows no trend with precipitation rate. Since Ca was spiked into the reaction vessel, and Ca does not partition favorably into a $CaCO_{3(s)}/CdCO_{3(s)}$ solid solution, if the same amount of Ca was spiked into the reaction vessel each time, the $[Ca^{2+}]$ should be independent of precipitation rate and constant across the series. Although there is a fair amount of scatter in the E series data, one experiment, E14, has $[Ca^{2+}]$ levels slightly lower than the others. This slightly low $[Ca^{2+}]$ and some of the scatter among the $[Ca^{2+}]$ values for the remaining E series experiments is due in part to the addition of inconsistent volumes of the concentrated $CaCl_2$ spiking solution from experiment to experiment. There is significantly less scatter in the $[Cd^{2+}]$ data. The $[Cd^{2+}]$ values in Figure 3.12 begin to level off at log precipitation rates less than -0.50.

3.4.1.5 $D_{Ca^{2+}, eq}$ and $\zeta_{CaCO_{3(s)}}$ Values

Figures 3.13 and 3.14 show the $D_{Ca^{2+}}$ vs. log precipitation rate plots for E series experiments (AAS and XPS respectively). The data from these plots can be found in Table 3.12. As shown in these figures, when using the AAS-based method to calculate $X_{CaCO_{3(s)}}$ the subsequent $D_{Ca^{2+}}$ values follow the expected trend of decreasing and leveling off with decreasing precipitation rate. The outlier at log precipitation rate -0.58, experiment E14, results from the comparatively lower levels of Ca in the aqueous phase compared to the other experiments. The outlier at log precipitation rate -0.125, experiment E4, has an AAS solid composition that is significantly more concentrated than the other solids in the E series (see Table 3.10). Notice that in the $D_{Ca^{2+}}$ vs. log precipitation rate plot where XPS was used to calculate $X_{CaCO_{3(s)}}$ (Figure 3.14), the E14 point remains high while the E4 point falls into place with the other data.

Based on Figure 3.12, the E series $D_{Ca^{2+}, eq}$ values should be calculated from the 3 to 4 experiments run at the slowest precipitation rates. This would include experiment E14

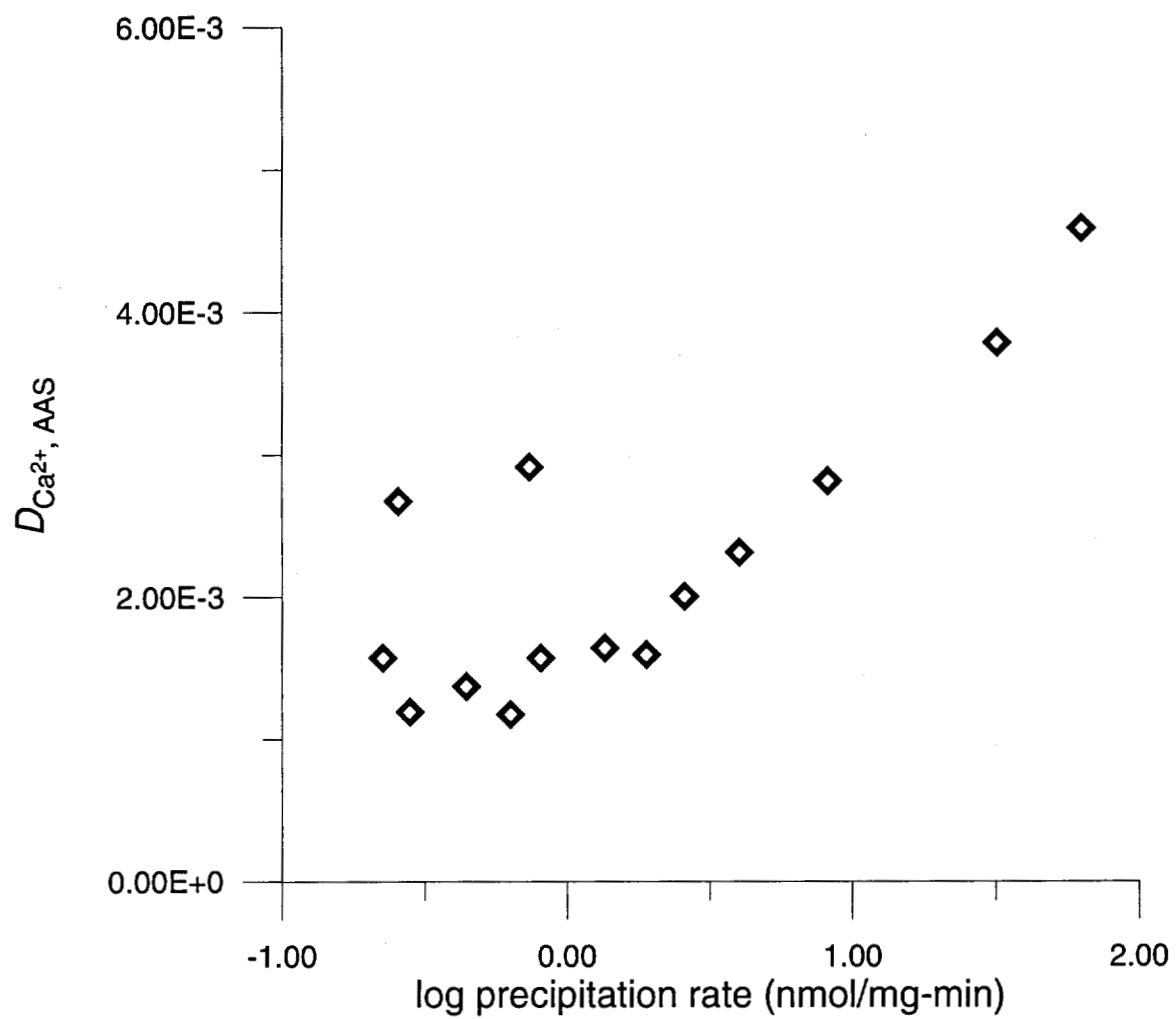


Figure 3.13 $D_{Ca^{2+}, AAS}$ vs. log precipitation rate for E series experiments.

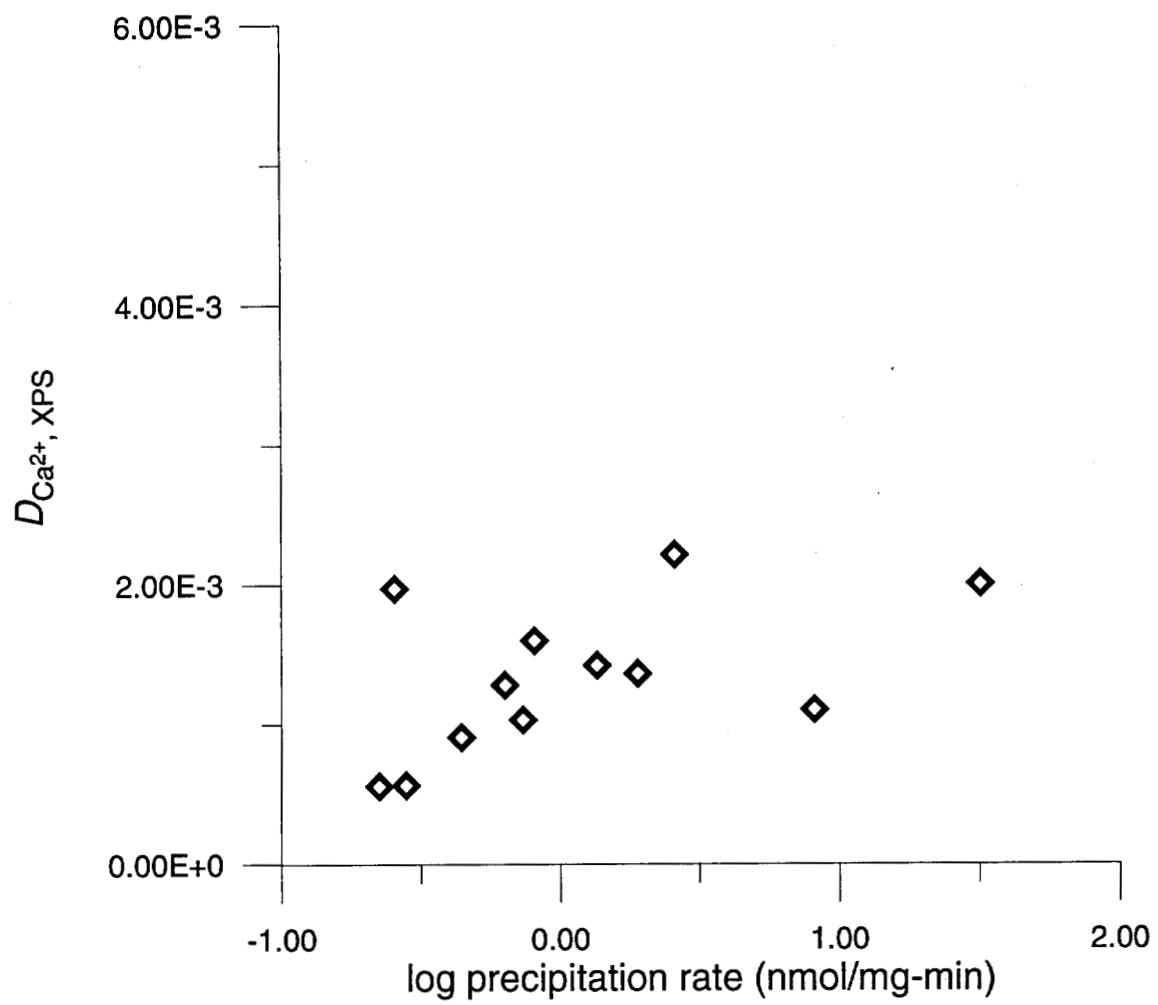


Figure 3.14 $D_{Ca^{2+}, XPS}$ vs. log precipitation rate for E series experiments.

which was discarded as an outlier. If the $D_{Ca^{2+}, eq}$ is taken to be only the three most slowly precipitated experiments neglecting experiment E14, $D_{Ca^{2+}, eq} = 0.0014 \pm 0.0002$ (AAS). If all the points that leveled off in the AAS $D_{Ca^{2+}}$ vs. log precipitation rate plot are included in the average neglecting E4 and E14, $D_{Ca^{2+}, eq} = 0.0014 \pm 0.0002$ (extended AAS). In the XPS plot, $D_{Ca^{2+}}$ appears to consistently decrease with log precipitation rate. Taking the same points for the calculation of $D_{Ca^{2+}, eq}$ gives a value of 0.0007 ± 0.0002 (XPS) for the three slowest precipitation rates neglecting experiment E14.

After the equilibrium distribution coefficient was determined, the solid phase activity coefficient for the trace constituent was calculated according to the following equation.

$$D_{Ca^{2+}, eq} = \frac{K_{s0, CdCO_{3(s)}} \zeta_{CdCO_{3(s)}}}{K_{s0, CaCO_{3(s)}} \zeta_{CaCO_{3(s)}}} \quad (3-4)$$

This equation is simply the inverse of Equation 2.14. The solid phase activity coefficient calculation for E series experiments is very similar to the calculation used for the G and H series experiments (see Section 3.3.1.5) except that otavite is now the bulk phase. Therefore, the approximation $\zeta_{CdCO_{3(s)}} = 1$ is used in this calculation. Calculation of $\zeta_{CaCO_{3(s)}}$ values for the E series experiments yields 0.17 ± 0.03 (AAS) and 0.3 ± 0.1 (XPS) when using the $D_{Ca^{2+}, eq}$ values determined by the equilibrium partitioning region.

3.4.2 F Series Experiments

3.4.2.1 Procedure

The experimental procedure used for F series experiments was virtually identical to the procedure used for E series experiments (see Section 3.4.1.1). The only difference

between the two procedures was that the F series experiments were spiked with more Ca than the E series experiments.

3.4.2.2 Experimental Precipitation Rates

The initial, final and average precipitation rates for F series experiments are given in Table 3.13. They were determined in the same manner as for the E series experiments (see Section 3.4.1.2).

Table 3.13 F series precipitation rate data.

Experiment	titration rate (mL/min)	initial precipitation rate (nmol/mg-min)	final precipitation rate (nmol/mg-min)	average precipitation rate (nmol/mg-min)
F1	0.382	46.6	35.6	41.1
F2	0.160	61.6	44.7	53.2
F3	0.0138	3.18	1.94	2.56
F4	0.00145	0.481	0.331	0.406
F5	0.00203	0.665	0.456	0.561
F6	0.00392	1.55	0.860	1.21
F7	0.00103	0.386	0.266	0.326
F8	0.0415	14.4	9.31	11.9
F9	0.00556	2.02	1.36	1.69
F10	0.456	97.7	66.7	82.2
F11	0.00284	1.30	0.816	1.06
F12	0.00546	2.12	1.22	1.67
F13	0.0167	3.26	1.89	2.58
F14	0.0260	10.8	5.71	8.25

3.4.2.3 $D_{Ca^{2+}}$ Values

$D_{Ca^{2+}}$ values for each F series steady-state sample were calculated according to Equation 3.1 in the same manner as the E series $D_{Ca^{2+}}$ values were calculated in Section 3.4.1.3. Aqueous composition, pH, and titration rate data for F series experiments can be found in Appendix A. The composition of the solid phase was determined by the same means described in Section 3.4.1.3. Table 3.14 contains the F series solid composition data. Table 3.15 contains the log precipitation rate and corresponding $D_{Ca^{2+}}$ values.

Table 3.14 F series solid solution compositions.

Experiment	$X_{CaCO_{3(s)}, AAS}$	$X_{CaCO_{3(s)}, XPS}$
F1	0.0802	0.0473
F2	0.0174	0.0225
F3	0.0253	0.0204
F4	0.0273	0.0159
F5	0.0481	0.0206
F6	0.0252	0.0170
F7	0.0539	0.0154
F8	0.0245	0.0190
F9	0.0544	0.00414
F10	0.0206	0.0101
F11	0.0352	0.0189
F12	0.0344	0.0207
F13	0.0294	0.0151
F14	0.0238	0.0176

Table 3.15 F series distribution coefficient data.

Experiment	log precipitation rate (nmol/mg-min)	$D_{Ca^{2+}, AAS}$	$D_{Ca^{2+}, XPS}$
F1	1.61	0.0038±0.0004	0.0022±0.0002
F2	1.72	0.0029±0.0002	0.0030±0.0003
F3	0.408	0.0021±0.0003	0.0016±0.0003
F4	-0.391	0.0012±0.0002	0.0007±0.0001
F5	-0.251	0.0022±0.0001	0.00093±0.00005
F6	0.0828	0.0012±0.0001	0.0008±0.0001
F7	-0.487	0.0023±0.0003	0.0006±0.0001
F8	1.07	0.0024±0.0002	0.0018±0.0002
F9	0.228	0.0031±0.0004	0.00023±0.00003
F10	1.91	0.0044±0.0001	0.00213±0.00006
F11	0.0253	0.0018±0.0003	0.0010±0.0001
F12	0.233	0.0023±0.0005	0.0014±0.0003
F13	0.412	0.0029±0.0006	0.0015±0.0003
F14	0.916	0.0021±0.0005	0.0015±0.0004

3.4.2.4 Equilibrium Partitioning Region

Figure 3.15 contains the $[Ca^{2+}]$ and $[Cd^{2+}]$ vs. log precipitation rate plots for F series experiments. The plot of $[Ca^{2+}]$ vs. log precipitation rate for the F series experiments shows scatter similar to the E series plot (see Figure 3.12). However, in this case, the low outlier at log precipitation rate 1.70 is due to intentionally spiking experiment F2 with less Ca than the other F series experiments. The $[Cd^{2+}]$ values in series F experiments level off around log precipitation rate -0.25. Experiments run at precipitation rates slower

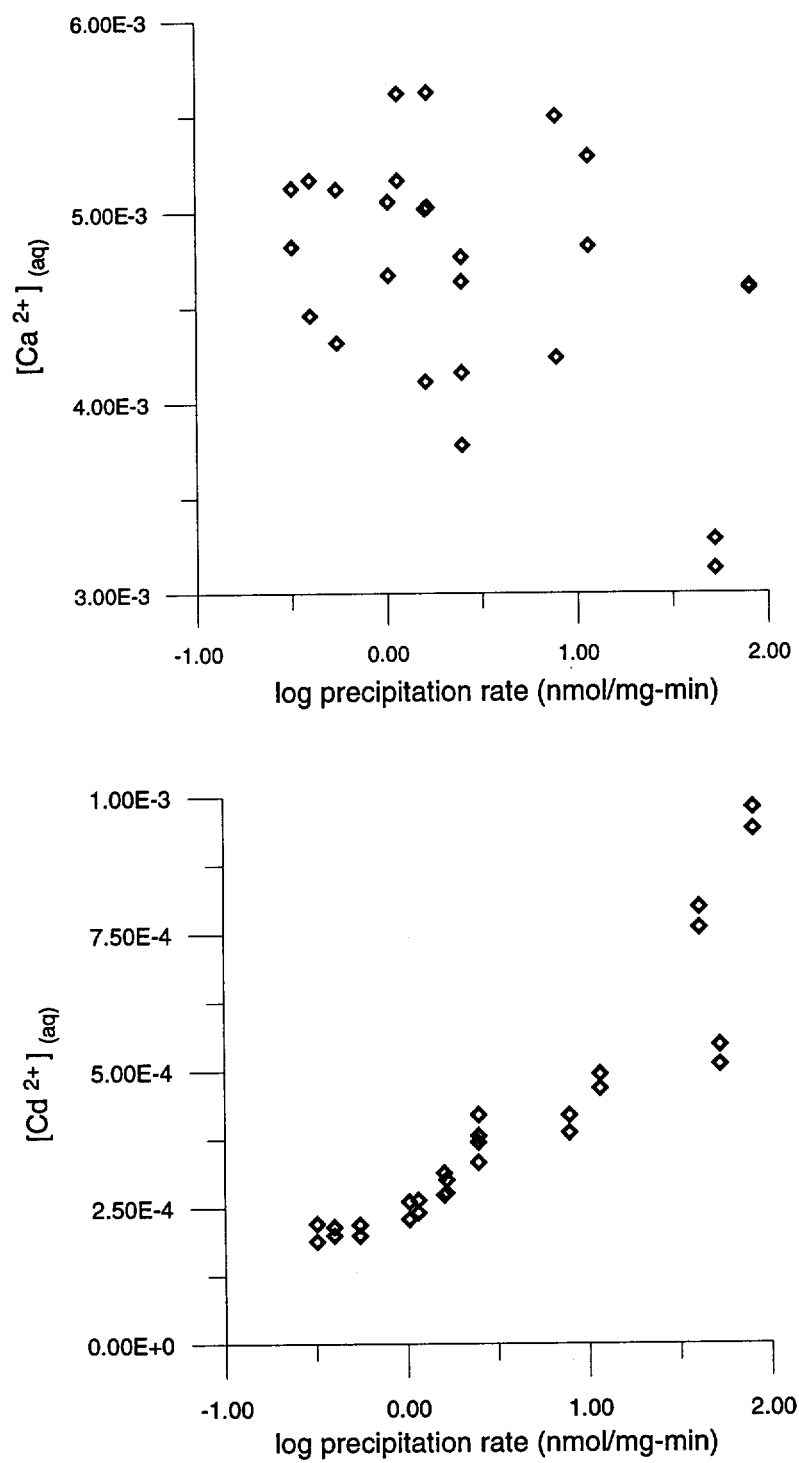


Figure 3.15 $[Ca^{2+}]$ vs. log precipitation rate (top) and $[Cd^{2+}]$ vs. log precipitation rate (bottom) for F series experiments.

than log precipitation rate -0.25 are considered to be within the equilibrium partitioning region for F series experiments.

3.4.2.5 $D_{Ca^{2+}, eq}$ and $\zeta_{CaCO_3(s)}$ Values

$D_{Ca^{2+}, eq}$ and $\zeta_{CaCO_3(s)}$ values for F series experiments were determined in the same manner as for E series experiments (see Section 3.4.1.5). Figure 3.16 is the plot of $D_{Ca^{2+}}$ vs. log precipitation rate for AAS-determined values. Figure 3.17 is a similar plot for XPS-determined $D_{Ca^{2+}}$ values. The data for these plots are listed in Table 3.15. Figures 3.16 and 3.17 show similar behavior to the $D_{Ca^{2+}}$ vs. log precipitation rate plots for E series experiments (see Figures 3.13 and 3.14). The $D_{Ca^{2+}}$ values in Figure 3.16 decrease with decreasing precipitation rate and then level off, although with considerably more scatter than the E series data. Again, the XPS determined $D_{Ca^{2+}}$ values shown in Figure 3.17 decrease with no apparent leveling off at slow precipitation rates. Using the proposed equilibrium partitioning region determined in Section 3.4.2.4, the $D_{Ca^{2+}, eq}$ value determined for F series experiments is 0.0019 ± 0.0006 (AAS). If data points with log precipitation rates as fast as 0 that appeared to have leveled off in the of $D_{Ca^{2+}}$ vs. log precipitation rate plot (Figure 3.16) are included in the average, the $D_{Ca^{2+}, eq}$ value is 0.0018 ± 0.0005 (extended AAS). For $D_{Ca^{2+}}$ values calculated using XPS $X_{CaCO_3(s)}$, the $D_{Ca^{2+}, eq}$ value is 0.0008 ± 0.0001 (XPS). Calculation of $\zeta_{CaCO_3(s)}$ values yields 0.12 ± 0.04 and 0.13 ± 0.04 for the AAS $D_{Ca^{2+}, eq}$ values and 0.31 ± 0.07 for the XPS $D_{Ca^{2+}, eq}$ value.

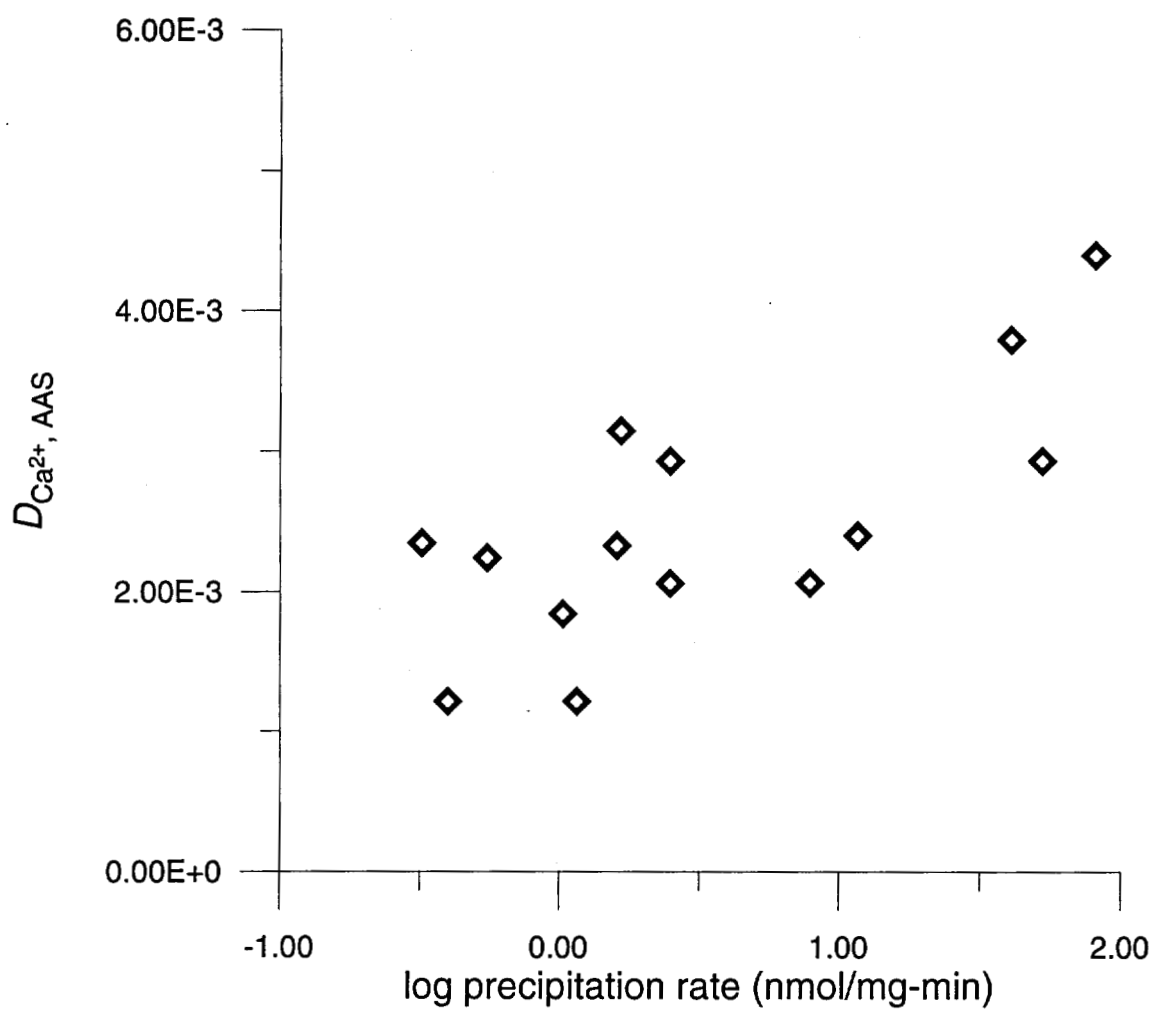


Figure 3.16 $D_{Ca^{2+}, AAS}$ vs. log precipitation rate for F series experiments.

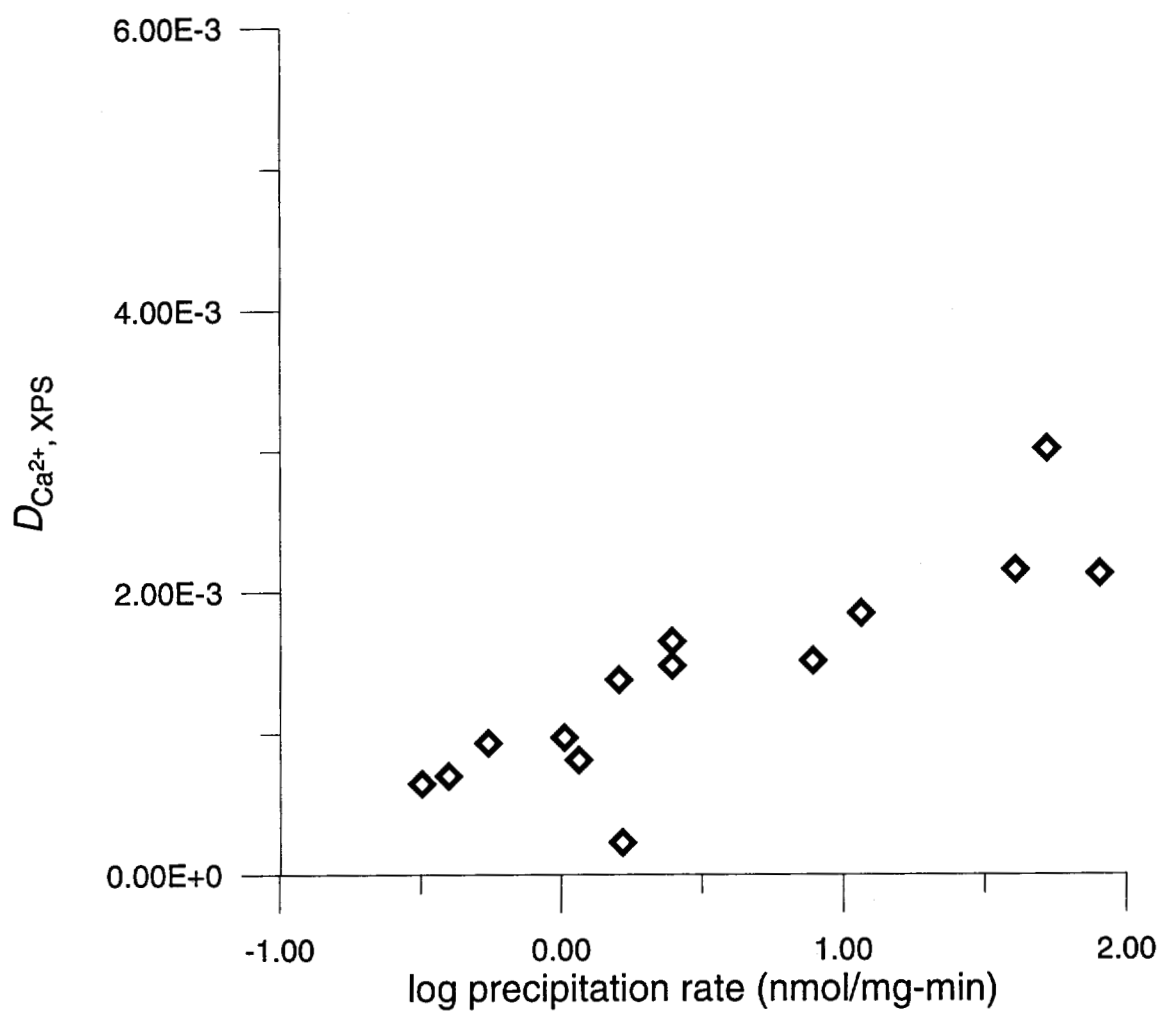


Figure 3.17 $D_{Ca^{2+}, XPS}$ vs. log precipitation rate for F series experiments.

3.5 XPS

3.5.1 Background

X-ray photoelectron spectroscopy (XPS) is a non destructive, surface-sensitive technique that allows compositional and to a certain extent chemical information to be determined from the surface of a sample without interference from the bulk of the sample. A detailed overview of the XPS technique with emphasis on geochemical applications can be found in Spectroscopic Methods in Mineralogy and Geology, Chapter 13 (Hochella, 1988). In short, the technique uses x-rays of known energy to eject photoelectrons from the inner orbitals of atoms in a sample. The kinetic energies of the ejected photoelectrons are related to their binding energies which are unique for each element. Therefore, XPS can be used to identify all elements up to U with the exception of H and He. The surface-sensitive nature of this technique is due to the fact that an ejected photoelectron cannot travel long distances through a solid without significant energy loss. Therefore, only photoelectrons ejected from atoms near the surface can escape the sample and be detected. The escape depth, which is roughly equivalent to the analysis depth, varies among different materials. For mineral solids, the analysis depth is 10-50 Å.

3.5.2 XPS Analyses

XPS has been used to study calcite consistently over the past 20 years (Bancroft *et al.*, 1977; Hochella *et al.*, 1988; Baer *et al.*, 1991; Stipp and Hochella, 1991; Blanchard and Baer, 1992; Stipp *et al.*, 1992; Baer and Moulder, 1993; Xu *et al.*, 1996). Since all of the solids in the G, H, E and F series consist of pure phase material covered with a layer of homogeneous solid solution, the ability of XPS to characterize the surface of a solid with minimal interference from any underlying material makes it an ideal technique with which to obtain a direct measurement of the solid solution compositions from this research. XPS scans were run on the seed materials, most G, H, E and F series samples, test sample A3 of

similar composition to the G series solid solutions, test sample A4 of similar composition to the F series solid solutions, and two samples from Tesoriero (1994), #37 and #40. XPS scans were run in two modes, survey scans over a wide energy range to look for any possible contamination in the solid solutions, and multiplex scans to accurately determine the relative amounts of key elements in the overgrowths.

The XPS analyses were run at the Environmental Molecular Sciences Laboratory (EMSL) National Scientific User Facility in eastern Washington. Spectra were collected with a Phi Quantum 2000 Scanning ESCA Microprobe using a focused monochromatic Al K α x-ray source for excitation (1486.6 eV), a spherical section analyzer and a 16 element multichannel detection system. For both survey and multiplex scans, 100.5 W of power was used on the anode, producing a 100 μ m diameter x-ray beam that was rastered over a 1.5 mm by 0.2 mm section of the sample. The x-ray beam was incident normal to the sample surface and the detector was at 45° away from normal. Since carbonates tend to be insulators, the charge build up on the samples was neutralized during the analyses with low energy ions and electrons. Samples were mounted on platens using double sided tape and molybdenum masks attached to the platen with screws. Survey scans were run over a relatively wide energy window, 700.00 eV to 0.00 eV in increments of -1.00 eV. A pass energy of 117.40 eV was used in the survey scans, producing an energy resolution in the data of approximately 1.6 eV. Multiplex scans were run over 4 smaller energy windows, 298.00 to 278.00 eV for C1s, 420.00 to 400.00 eV for Cd3d5, 539.00 to 525.00 eV for O1s, and 362.00 to 342.00 eV for Ca2p. Multiplex scans were run in increments of -0.10 eV. A pass energy of 23.50 eV was used in the multiplex scans producing an energy resolution in the data of approximately 0.7 eV.

Atomic concentration data from the survey and multiplex scans are listed in Appendix B. The atomic concentration of a given element is related to the peak area for a specific photoelectron ejected from the element by an atomic sensitivity factor and a spectrometer work function (see Hochella, 1998 for details). Atomic concentrations are essentially percent concentrations since the sum of the atomic concentrations over all elements in a given analysis equals 100. It is straightforward to calculate mole fractions from

atomic concentration data. The mole fraction of Cd in a given solid solution sample is simply the atomic concentration of Cd divided by the sum of the atomic concentrations of Ca and Cd. Atomic concentration data can also be used in a self check of the analysis if the structure of the solid surface is known. For example, in a $\text{CaCO}_{3(s)}/\text{CdCO}_{3(s)}$ solid solution there is one metal atom (Ca or Cd) for every carbonate C atom. Therefore, the sum of atomic concentrations of Ca and Cd should equal the atomic concentration of C, and the atomic concentration of O should be three times the atomic concentration of C.

XPS measurements are most accurate when atomic concentrations for the atoms of interest are greater than 1. As shown from the data in Appendix B, only the G series samples and #37 and #40 from Tesoriero (1994) meet this guideline for both Ca and Cd atomic concentrations. Duplicate measurements on samples G5 and G8 have excellent reproducibility as shown by the $X_{\text{CdCO}_{3(s)}}$ values in Table 3.5. Solid phase mole fractions calculated from XPS atomic concentration data for H, E and F series experiments are not as accurate as the G series data due to the low levels of trace atoms in the solid solutions. However, in this analysis numerous individual measurements were averaged to obtain the final spectra which significantly improved the signal to noise ratio. This allowed the small amounts of Cd in the H series samples and the small amounts of Ca in the E and F series samples to be measured. Since no $\text{CaCO}_{3(s)}/\text{CdCO}_{3(s)}$ solid solution standards were available, it was not possible to measure the exact error in the XPS measurements for this analysis. However, the error in a given XPS measurement can be as high as 5%-10% depending on the structure of the solid.

3.5.3 Sample Contamination

All of the analyzed samples were remarkably clean with respect to surface contamination. This is important because if a sample surface is contaminated due to poor storage and handling, the XPS analysis will provide information about the contamination on the surface instead of the underlying material of interest. The surfaces of all the samples contained adventitious carbon, hydrocarbon contamination from the ambient atmosphere that

partitions to solid surfaces. However, the contamination was not present in amounts that would interfere with the analysis as it was possible to resolve the carbonate carbon peak and the adventitious carbon peak in all of the carbon multiplex spectra. Inorganic contaminants were limited to Na and Cl from the ionic strength buffer, Si (from glass surfaces, particularly the Na_2CO_3 titrant syringe barrel) and sometimes S, which is another common contaminant on surfaces exposed to the atmosphere. Figure 3.18 is a survey scan of the solid phase from experiment G10. All of the major peaks including contaminants are labeled. In this spectra, the binding energy resolution is such that the adventitious carbon peak overlaps with the inorganic carbon peak. With multiplex scans it was possible to completely resolve the carbonate carbon from the adventitious carbon. Figure 3.19 is the carbon multiplex scan of sample E13 showing the separation of the two carbon peaks.

3.5.4 Effects of Washing Samples

Both the survey and multiplex scans provide information about the effects of washing the solid solutions after collection by vacuum filtration. From the survey scans it can be seen that the G series solids (which were not washed) contain more Na, Cl and Si than the H, E and F series solids (which were washed after collection). This is reasonable since the contaminants were most likely adsorbed to the calcite surface or present in the interstitial waters.

Multiplex scans of washed and unwashed samples from the same solid solution material gave some indication of the effects of washing the solid solutions on the mole fraction of the trace component in the solid solution surface. Table 3.16 lists mole fractions from the washed and unwashed samples. From this table it can be seen that washing the samples had little effect on the measured $X_{\text{CdCO}_3(s)}$ values of the A3 sample which was of a similar composition to the G series samples. In contrast, the $X_{\text{CaCO}_3(s)}$ for sample A4, which was of a similar composition to the F series samples, had decreased after the sample had been washed. This decreased $X_{\text{CaCO}_3(s)}$ after washing is most likely due to the removal of surface-adsorbed Ca. The more dilute samples show significant differences between the

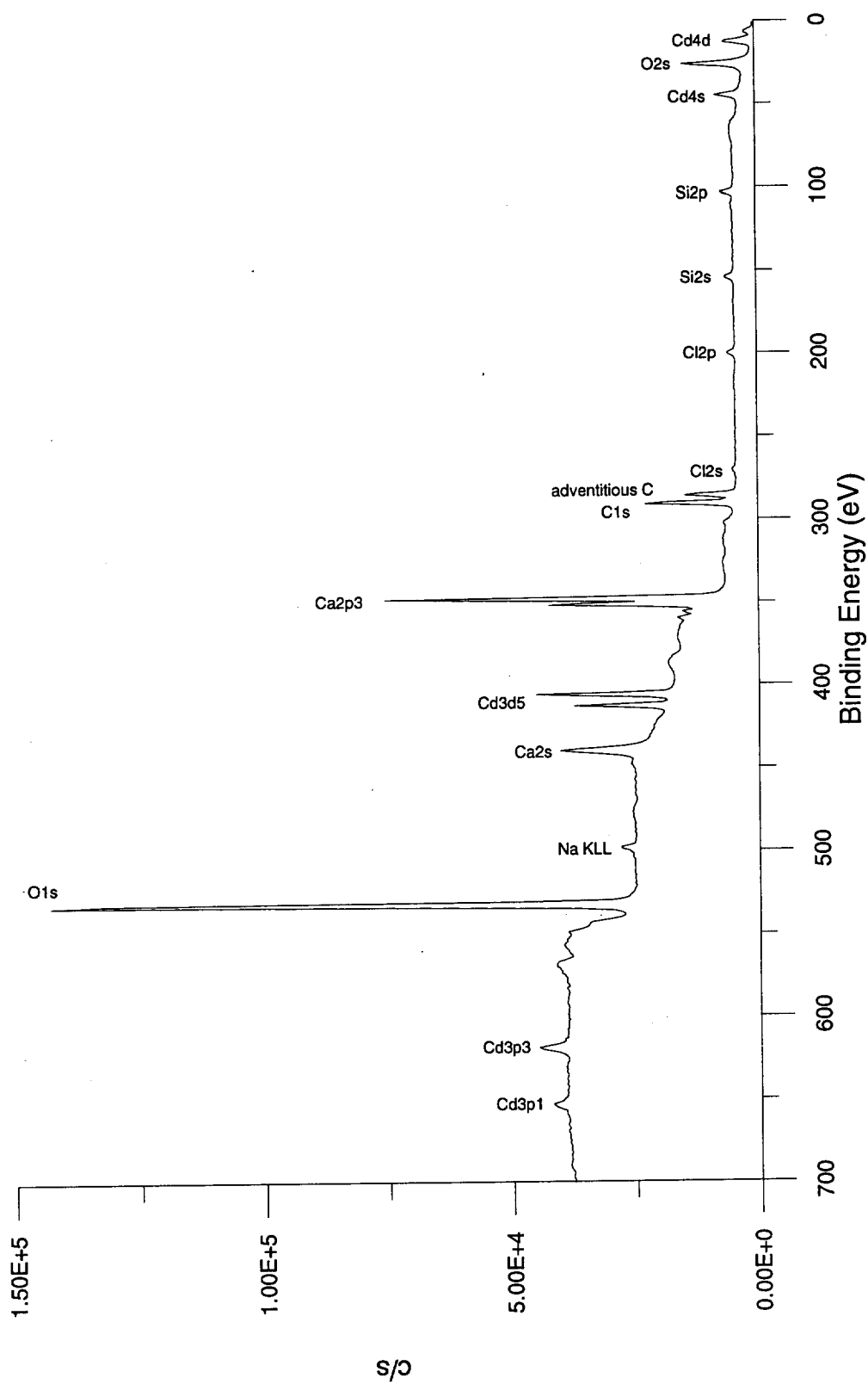


Figure 3.18 XPS survey scan of sample G10.

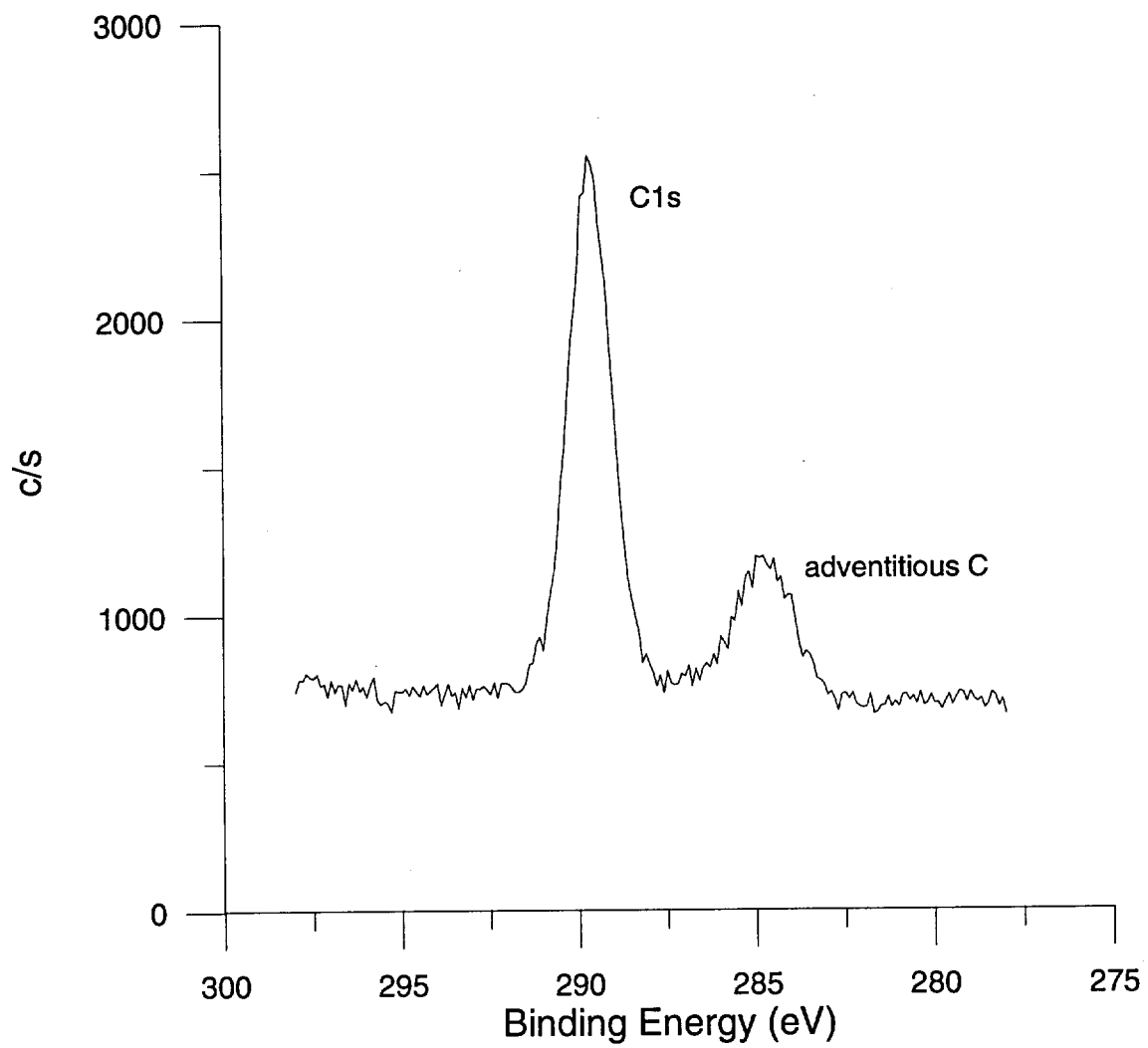


Figure 3.19 XPS multiplex scan of sample E13 showing separation of C1s and adventitious carbon peaks.

washed and unwashed values. This is due in part to increased error in the analysis when the levels of trace ion in the solid solutions are extremely low. However, the E12 sample that was washed contained less Ca in the surface than the unwashed sample. This behavior is similar to that seen for sample A4. In contrast, the H12 washed sample appears to contain more Cd than the unwashed sample. This unexpected result is most likely due to an inaccurate measurement of the atomic concentrations for the H12uw sample because no other H series solid had a $X_{\text{CdCO}_{3(s)}}$ value less than 0.00738 (see Table 3.8).

Table 3.16 Mole fraction comparison from washed and unwashed samples.

Sample	$X_{\text{CaCO}_{3(s)}}$	Sample	$X_{\text{CdCO}_{3(s)}}$
E12w	0.00544	H12w	0.00872
E12uw	0.00946	H12uw	0.00574
A4w	0.0124	A3w	0.166
A4uw	0.0151	A3uw	0.172

w - washed

uw - unwashed

3.5.6 Comparison of XPS to Mass Balance Calculation and AAS

Although it is not necessary to use standards in an XPS analysis, the use of standards always improves the quality of the data. Calcite/otavite solid solution standards were not available. However, because the composition of all the samples could be identified by other means, it was possible to compare XPS values to either mass balance or AAS determined values. XPS and mass balance $X_{\text{CdCO}_{3(s)}}$ values were compared for G and H series experiments. XPS and AAS $X_{\text{CaCO}_{3(s)}}$ values were compared for E and F series experiments. Tables 3.5, 3.8, 3.11 and 3.13 contain this data.

If two methods report the same value for a given measurement, a plot of the measured values from one method vs. the other method should yield a straight line with a slope of 1 and a zero intercept. Figure 3.20 contains such plots for the data in Tables 3.5, 3.8, 3.11 and 3.13. As shown in this figure, XPS $X_{\text{CaCO}_{3(s)}}$ values are slightly depleted with Ca compared to the AAS values and there is no obvious distinction between the E and F series data. In contrast, the XPS $X_{\text{CdCO}_{3(s)}}$ values are enriched with Cd compared to the mass balance values for G and H series experiments. It is interesting to note that the H series data points (open circles), the G series data points (open squares), and samples #37 and #40 (open triangles) from Tesoriero (1994) appear to fall on vertical lines. In all three cases, the experiments run at faster precipitation rates have more concentrated surface $X_{\text{CdCO}_{3(s)}}$ values than experiments run at slower precipitation rates.

3.5.7 XPS Analysis for Solid Solution Identification

As discussed by Stipp *et al.* (1992), the characteristic binding energies for elements in a solid solution will vary with composition across a solid solution series. Therefore, the absolute binding energies determined by XPS analysis can be used as evidence of solid solution formation. For a calcite/otavite solid solution series the largest shift in binding energies across the series occurs for the C1s photoelectron. However, this binding energy shift is small, only 0.6 eV, and requires careful analysis and use of an accurate reference if it is to be measured. One reference of choice for this type of analysis is a small amount of gold evaporated onto the sample surface. The solid samples from this research were referenced with the adventitious carbon peak, a common practice in XPS analysis, but not accurate enough for the determination of small shifts in absolute binding energies. Therefore, it was not possible to measure the shift in the C1s photoelectron binding energy between the G, H, E and F series samples and the pure phase endmembers.

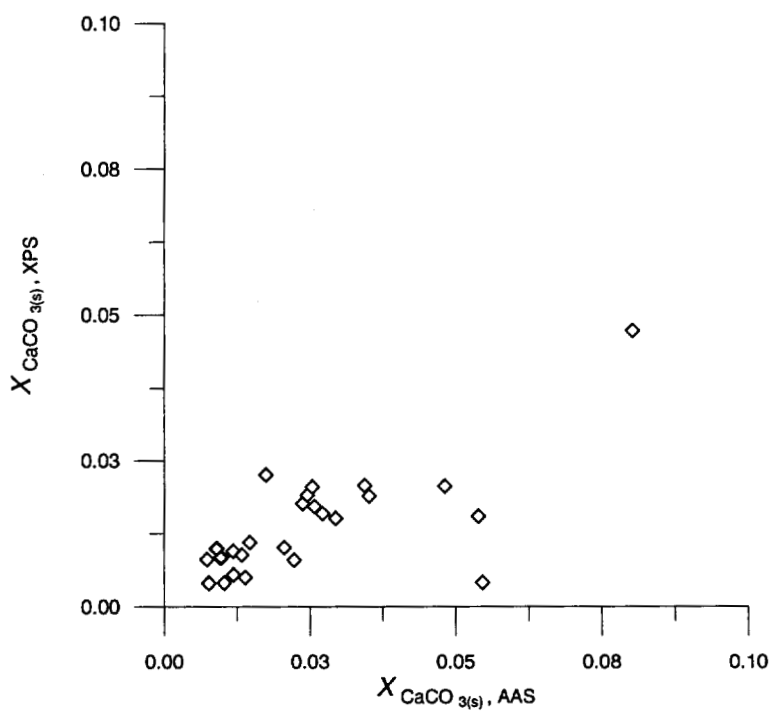
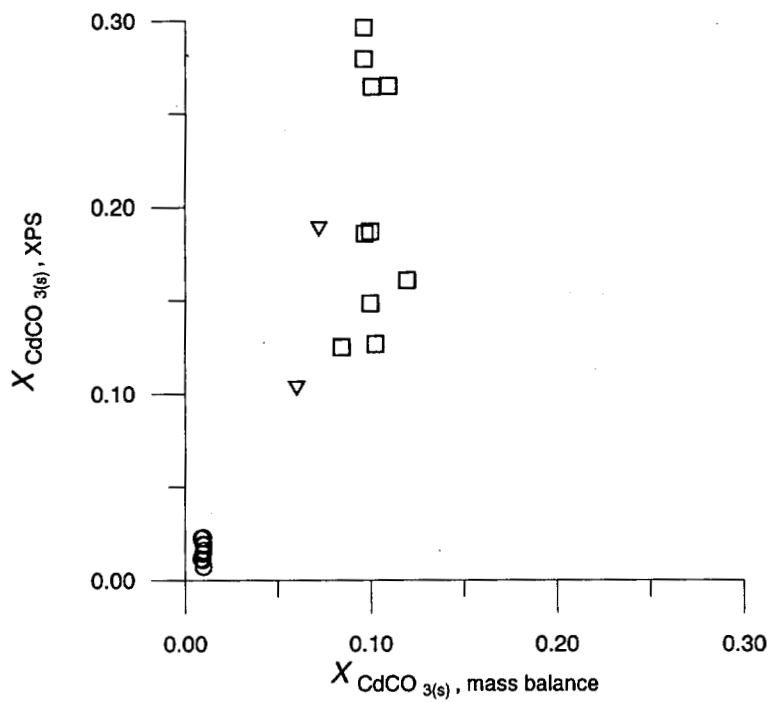


Figure 3.20 Comparison of XPS X values to mass balance values from G and H series experiments (top) and to AAS values from E and F series experiments (bottom).

3.6 XRD

X-ray diffraction (XRD) is commonly used for the routine characterization of mineral phases. In addition to the identification of mineral phases in a given sample, XRD is a useful tool for the identification of solid solutions because the unit cell volume of a solid solution will have a value that is in between the unit cell volumes of the pure phase endmembers. The variation of unit cell volume between the endmember values should be uniform with concentration of the solid solution. Several researchers have demonstrated this type of behavior for calcite solid solutions (Chang and Brice, 1971; Könseberger *et al.*, 1991; Rock *et al.*, 1994; Casey *et al.*, 1996).

A similar analysis of the solid solutions from this research is complicated by the layered structure of the solids. Since XRD is a bulk technique, the measured signal is an average of both the seed and solid solution materials in the G, H, E and F series samples. However, calcite, G4, F13, and otavite were analyzed by XRD in order to see if the analysis could provide evidence of solid solution formation in the samples. The XRD analyses were run at the EMSL National Scientific User Facility. Spectra were collected with a Philips PW3040/00 X'Pert MPD system with a PW3050/10 vertical Θ - Θ goniometer and a PW3373 long fine focus, ceramic x-ray tube with a Cu anode. Samples were run using the primary optical train with the x-ray source operated at 40 kV, 50 mA (2000 W). The divergence and anti-scatter slits were operated in the automatic (2 Θ -compensating) mode which combined with a beam mask resulted in a 10 mm by 10 mm study area. The receiving slits height was 0.2 mm. The scan range was from $2\Theta = 5^\circ$ to 75° . The scan rate was a continuous $0.04^\circ/2.5$ sec. The samples were mounted in a shallow front loading cavity (12 mm by 0.5 mm) in an off-axis single-crystal quartz plate. The detection limit of the analysis was $\sim 1\%$ by weight.

XRD analysis of the samples found no evidence of any trace phases. In addition, the spectra for samples G4 and F13 were close to but shifted from the patterns of the bulk endmember phases. This shift from the pure phase endmember spectra is an indication of solid solution formation. Table 3.17 shows the measured unit cell volumes for the two

Table 3.17 XRD unit cell volumes.

Sample	measured unit cell volume (Å ³)
calcite	367.87±0.04
G4	366.24±0.06
F13	342.77±0.05
otavite	343.23±0.02

endmember and two solid solution samples. The measured unit cell volume of the calcite and otavite seed materials compare favorably with standard values, 367.78 Å³ for calcite and 342.46 Å³ for otavite. The unit cell volume of sample G4 falls within the two endmember phases as expected for a solid solution. The unit cell volume of sample F13 falls outside of the range set by the two pure phase endmember measurements. However, the unit cell volume of sample F13 falls within the range set by the standard values. Spectra and related data can be found in Appendix C.

3.7 Discussion

The mechanisms believed to control the partitioning of an ion between the aqueous phase and a solid solution fall into two classifications, solution boundary layer processes and surface site related processes (Rimstidt *et al.*, 1998). Although the two types of processes can occur simultaneously, Rimstidt argues that surface site related processes would tend to occur at faster precipitation rates where high energy sites are more common in a crystal's structure, while solution boundary layer processes are more important at slow growth rates when crystals are more perfectly formed.

3.7.1 Boundary Layer Processes

Davis *et al.* (1987) reported that the sorption of Cd to calcite in calcite saturated aqueous solutions appeared to be a three stage process, rapid adsorption followed by a slower uptake believed to be diffusion through a hydrated boundary layer, and finally a slow long term uptake of Cd due to solid solution formation during the recrystallization process. The presence of a diffusion limiting hydrated boundary layer at the calcite water interface was later challenged by Stipp and Hochella (1991) and van Cappellen *et al.* (1993). Stipp and Hochella (1991) found spectroscopic evidence of hydrated surface species using surface sensitive techniques and determined that the presence of a hydrated layer on the surface of calcite does not distort the underlying crystal structure for more than one to two atomic layers. In contrast to the diffuse hydrated layer postulated by Davis *et al.* (1987), the model described by van Cappellen *et al.* (1993) proposes a defined boundary between a carbonate surface and an aqueous phase where the solid surface is covered with a monolayer of dissociated water molecules in two primary binding sites and the underlying solid is undisturbed.

Rimstidt *et al.* (1998) proposed a slightly different boundary layer process, arguing that when $D > 1$, the near surface is depleted with the trace ion compared to bulk values, and when $D < 1$ the near surface is enriched with the trace ion compared to bulk values. Therefore, D values calculated with bulk aqueous concentrations may not represent the actual partitioning process. Although the fact that many carbonate solid solutions do not appear to form ideal solid solutions was acknowledged, Rimstidt *et al.* (1998) did not address the fact that non ideal behavior in the solid phase mixture could account for the discrepancy between theoretical values assuming ideal behavior and experimentally determined values. Tesoriero (1994) addressed the possibility of near surface concentration gradients in detail and determined that for Sr partitioning to calcite, the presence of a concentration gradient near the solid surface during precipitation did not significantly affect the observed distribution coefficient values indicating that the error due to using bulk aqueous concentrations to calculate D values instead of near surface aqueous concentrations was small.

3.7.2 Surface Site Related Processes

The dependence of D on precipitation rate has been well documented in the literature (Lornes, 1981; Mucci, 1998; Dromgoole and Walter, 1990; Tesoriero and Pankow, 1996). In a most general sense, the precipitation rate dependence of D values has been attributed to a balance between selective and non selective partitioning mechanisms. At fast precipitation rates, ions that have sorbed to a mineral surface may be incorporated into the growing solid without regard to thermodynamic favorability. As the precipitation rate decreases, more selective processes are allowed to occur and the observed D values begin to approach equilibrium values. Tesoriero (1994) argued that saturation state Ω (see Equation 2-10) may be a more appropriate parameter by which to characterize the degree of solid solution partitioning because the Ω of a solution has been more closely related to the occurrence of kink sites, multiple step migration, and other crystal structures than precipitation rate. Steps, edges, kinks, and other high energy binding sites are strong adsorption sites for aqueous ions. When these features are abundant during crystal growth, the overall incorporation of foreign ions into the growing crystal may be determined more by the kinetics of sorption and precipitation than by the thermodynamic driving force for mixing. In contrast, a crystal that grows slowly is characterized by smooth surfaces and minimal high energy binding sites which favors selective partitioning processes.

SEM images can provide a visual indication of the relative abundance of kinks, steps and other high energy sites on the surface of a given crystal. Figure 3.21 contains two SEM images of sample G4 formed at a relatively fast precipitation rate. The Ω for this sample was 1.43. Figure 3.22 contains two similar images for sample G10 which was precipitated at a slower rate. The Ω for sample G10 was 0.96. Although a $\Omega < 1$ normally indicates that the solution is undersaturated with respect to the given solid phase, this apparent undersaturation is due to experimental error since calcite was precipitating throughout the experiment. As shown by the comparison of these images, the G4 sample precipitated at the faster rate, contains more high energy sites binding sites on the solid surface than the G10 sample.

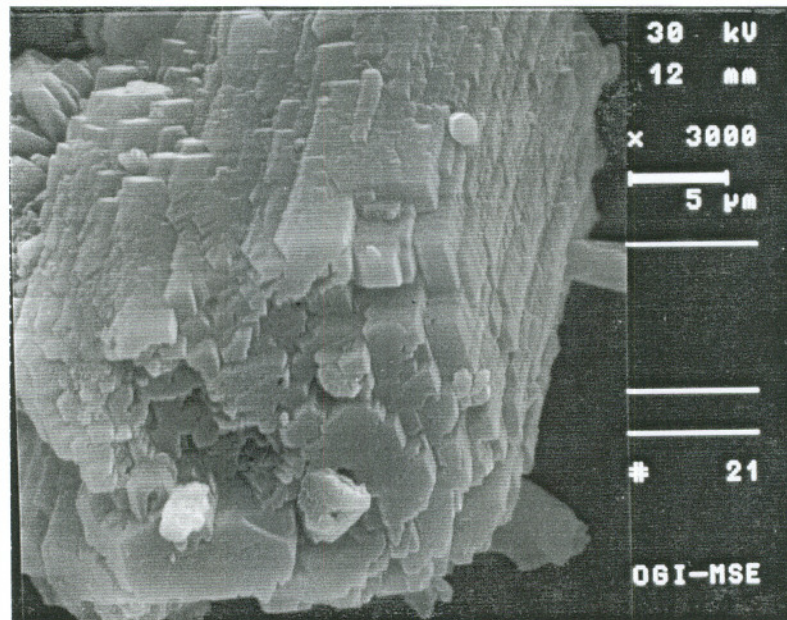
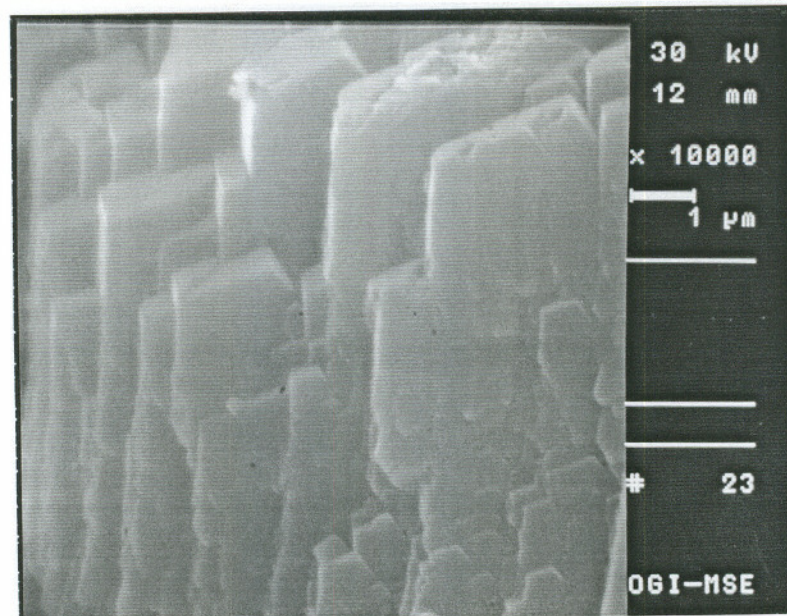


Figure 3.21 SEM images of sample G4 at high (top) and low (bottom) magnification.

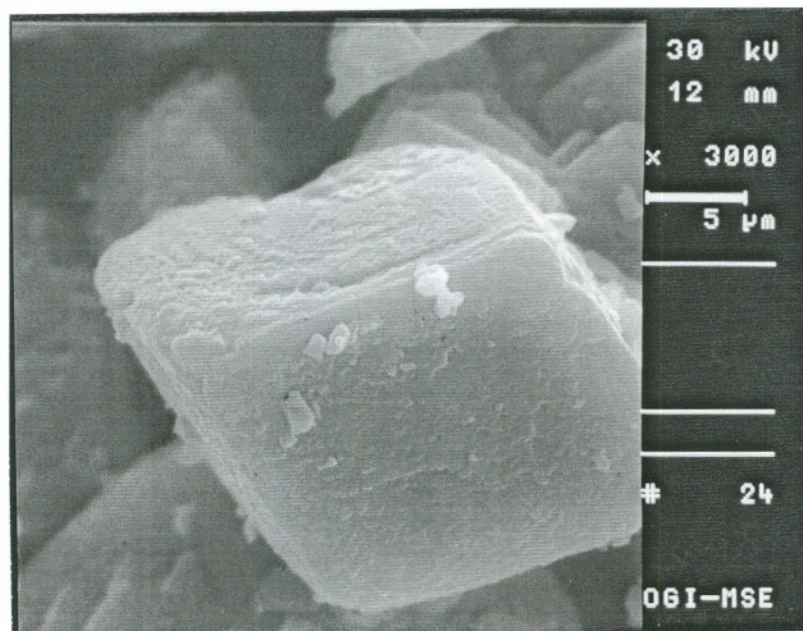
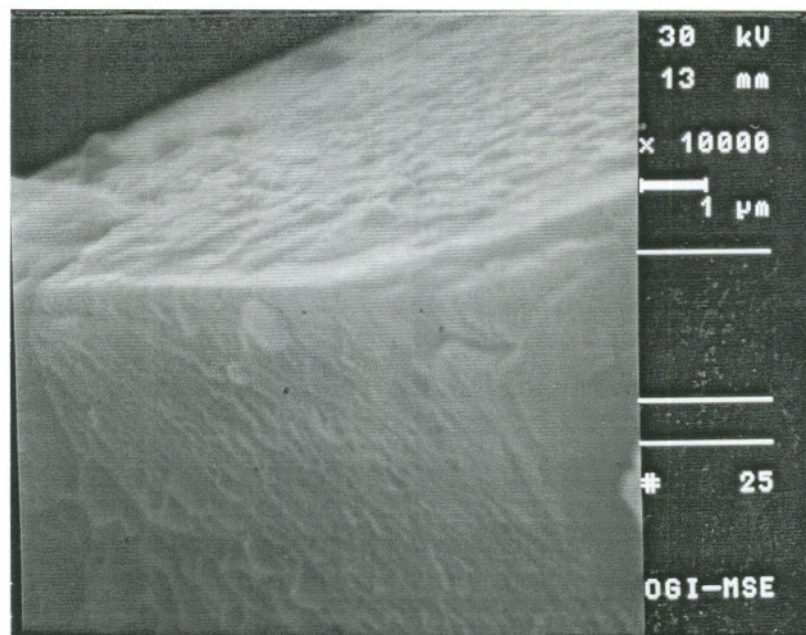


Figure 3.22 SEM images of sample G10 at high (top) and low (bottom) magnification.

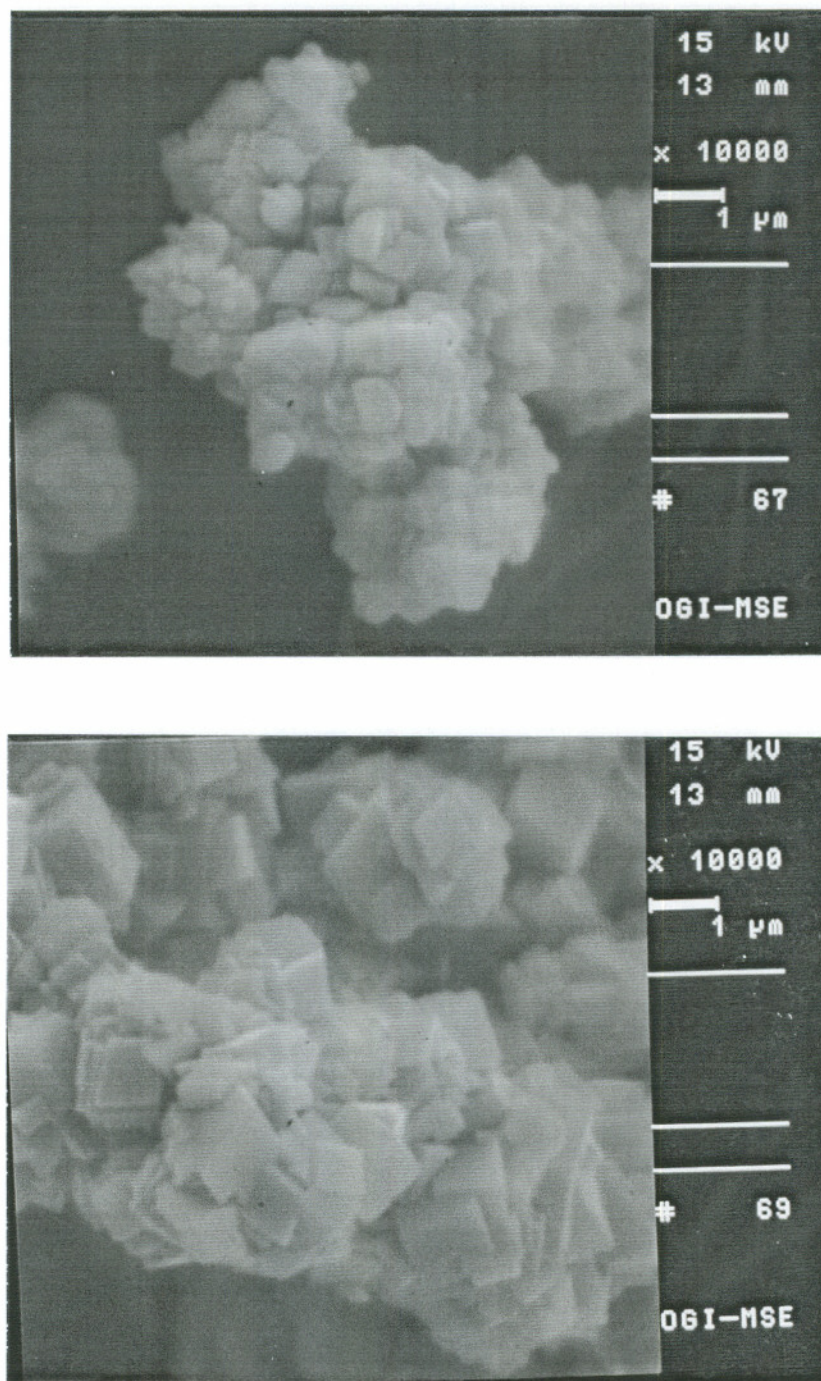


Figure 3.23 SEM images of E series solid materials. Sample E12w (top) formed at a relatively slow precipitation rate and sample E5 (bottom) formed at a relatively fast precipitation rate.

Figure 3.23 contains two SEM images from the E series experiments. The solid from experiment E5 was formed at a relatively fast precipitate rate (Ω of 133), while the solid from experiment E12 was formed at a slower precipitation rate (Ω of 1.55). Comparison of fast to slow precipitation rates does not yield the dramatic differences in crystal structure seen in the G series experiments. This is due in part to the surface structure being too fine to resolve by SEM on the smaller crystal size. However, it appears that the crystals that were precipitated quickly tended to form plate like structures while the crystals that were precipitated more slowly formed more block like structures.

Recently, the effects of fine scale surface structures on the incorporation of trace metals into a solid solution has been recognized (Reeder and Grams, 1987; Paquette and Reeder, 1995). These fine scale effects fall into two types, compositional sector zoning where compositional differences are seen between crystallographically non equivalent faces in the same sample, and intrasectoral zoning where compositional differences are seen on equivalent portions of a crystal. Compositional sector zoning is believed to be due to differences in growth rates of different crystal faces at a given supersaturation and different lattice sites sizes in the different crystal faces. Intrasectoral zoning is believed to be due to different step structures growing on one crystal face. While sector zoning can account for variations in partitioning among a given sample and indicates that many experimentally determined D_{eq} values may not represent true equilibrium values, this fine scale partitioning behavior is not common in coprecipitation experiments that employ constant composition techniques and the use seed material (Paquette and Reeder, 1995). Since the experimental procedures used in the course of this research were constant composition techniques employing seed material, the likelihood of compositional zoning in the precipitated solid solution overgrowths is small.

3.7.3 Indication of Surface Phenomena by XPS

The determination of different surface compositions by XPS for fast and slow precipitation rate samples seen in G series experiments indicates more complicated surface

chemistry than the non equilibrium entrapment of ions into a rapidly growing crystal described above. Finding a Cd enriched solid at faster precipitation rates would not be unusual if the enrichment could be attributed to the formation of an additional Cd phase. The fact that no such phase was detected in the XRD analysis of sample G4 is not sufficient evidence for the lack of an additional phase as some possible phases, like vaterite may have been present in the reaction vessel but were too unstable to remain in the solid until the XRD analysis was performed. However, since the aqueous phase was kept undersaturated with respect to all mineral phases except calcite, it is unlikely that any additional solid phases were formed over the course of the experiments.

Additional support against the formation of an additional cadmium rich phase at high precipitation rates is the disparity between XPS mole fractions and those from the mass balance calculation. Since ~25-40% of the solid phase was formed through precipitation of solid solution material, the presence of an additional Cd rich phase should have been evident in the mass balance calculations through increased $X_{\text{CdCO}_3(s)}$ values for solids formed at fast precipitation rates. As can be seen from Table 3.5 there is no increase in mass balance $X_{\text{CdCO}_3(s)}$ values at faster precipitation rates. It could be argued that failure to wash the G series samples after vacuum filtration lead to the enhanced surface concentrations. However, a similar trend is seen in the H series samples which were all washed after collection (see Table 3.8).

What seems likely is the existence of additional surface binding sites at faster precipitation rates that do not result in the incorporation of Cd into the structure as crystal growth proceeds. Since the Ω values in G series experiments were relatively low even at fast precipitation rates, it is likely that a fair amount of selective partitioning could occur even though, as shown by comparison of Figures 3.21 and 3.22, the crystal surface contained more high energy binding sites at faster precipitation rates. Therefore, the enhanced surface concentration of Cd in G and H series samples observed by XPS may be due to chemisorption of the Cd to high energy surface binding sites while the incorporation of Cd into the growing crystal was controlled by more selective processes.

3.7.4 Comparison of Measured $D_{\text{Cd}^{2+}}$ Values to Literature Values

The majority of the measured $D_{\text{Cd}^{2+}}$ values from this research are in good agreement with existing literature values for relatively dilute mixtures of Cd in calcite. For constant composition experiments, Tesoriero and Pankow (1996) report a $D_{\text{Cd}^{2+}}$ of 1250 ± 300 at slow precipitation rates for a solid solution composition of $\text{Ca}_{0.973}\text{Cd}_{0.063}\text{CO}_3$. Davis *et al.* (1987) report an average $D_{\text{Cd}^{2+}}$ of 1510 ± 300 for their recrystallization experiments. The solid solution compositions in their experiments was estimated to be $\text{Ca}_{0.999}\text{Cd}_{0.001}\text{CO}_3$. The λ_{Cd} values reported by Lornes (1981) for precipitation experiments are also in reasonable agreement with values reported in Tesoriero and Pankow (1996), Davis *et al.* (1987) and this research. Since the SSAS partitioning was of the Dorener-Hoskins type in during the precipitation experiments performed by Lornes (1981), it was not possible to determine accurate solid phase compositions for those experiments. However, based on the data, it can be assumed that the solid solutions contained only trace amounts of Cd in calcite. The D value of 3500 ± 1350 from Lornes (1981) for a recrystallization experiment is significantly larger than the other literature values. This value is similar to the G series XPS $D_{\text{Cd}^{2+},\text{eq}}$ from this research for a solid solution more concentrated with respect to Cd than the other literature or measured values. The composition of the solid phase in the equilibrium partitioning region for XPS G series experiments was $\text{Ca}_{0.86}\text{Cd}_{0.14}\text{CO}_3$. Since D values vary with solid solution composition, it may be that the larger D values from Lornes (1981) and this research represent partitioning behavior for more concentrated solid solutions.

Chapter 4

Mixing Behavior of the Calcite/Otavite Solid Solution Series

4.1 Introduction

With respect to thermodynamics, it is the ΔH_{mix} which controls the extent to which a solid solution will form (see Chapter 2). The factors believed to have the largest effect on the ΔH_{mix} when two ionic solids mix to form a solid solution are the crystal structure of the two endmembers, the valencies of the substituting ions, the electronegativity difference between the substituting ions, and the ionic radii of the substituting ions. All of these factors influence the ability of a foreign ion to partition into a given lattice.

Ursov (1975) presents a detailed look at the theory of miscibility gaps in mineral solid solutions. According to this theory, the ΔH_{mix} can be conceptualized as the sum of two factors, deformation energy and chemical energy. The deformation energy results from distortion in the lattice structure due to solid solution formation and is primarily related to the size differences between the host and substituting ions. The chemical energy, which is a measure of the difference in the nature of the chemical bonds between atoms in a solid solution compared to pure phase material, is primarily a function of the electronegativity difference between the host and substituting ions.

The effects of ionic size differences on solid solution formation are more easily quantified than the effects of electronegativity differences (Ursov, 1975). With respect to size differences, a general rule of thumb for the substitution of one ion for another in a mineral lattice is Goldschmidt's 15% criterion. If the two ions are more than 15% different with respect to their effective ionic size, substitution is prohibited. Another rule of thumb

for substitution based on size is the Goldschmidt-Fersman "polarity" rule which simply states that the substitution of a smaller ion for a large one is favored over the substitution of a larger ion for a smaller one.

The primary affect of an electronegativity difference between substituting ions in a solid solution is alteration of the bond character or "ionicity" in the solid phase. According to Pauling (1960), the covalent character of a chemical bond can be estimated from the electronegativity difference between the atoms that form the bond. Therefore, when one ion substitutes for another in a solid solution and the two ions of interest have significantly different electronegativities, the chemical bonds in the solid solution may be more ionic or covalent in nature than the bonds in the pure phase endmembers. In many cases, this change in ionicity tends to destabilize the crystal lattice. Unfortunately, there is no simple electronegativity analog to Goldschmidt's criterion for ionic size differences. However, Ursov (1975) states that if the change in ionicity due to solid solution formation is small the contribution to the overall ΔH_{mix} due to chemical energy can be neglected. Since the electronegativity difference between the atoms in a bond is related to the ionicity of the bond, the contribution of chemical energy to the ΔH_{mix} can be neglected if the electronegativity difference between two substituting ions is ≤ 0.05 .

Table 4.1 lists some relevant physical and chemical properties for the calcite/otavite solid solution series. As can be seen from this table, $\text{CaCO}_{3(s)}$ and $\text{CdCO}_{3(s)}$ are similar in a number of ways that would tend to favor the formation of a solid solution of these two minerals. $\text{CaCO}_{3(s)}$ and $\text{CdCO}_{3(s)}$ have the same type of crystal structure and the valences of Ca and Cd are similar. Because the ionic radii of Ca^{2+} and Cd^{2+} differ by only 5%, the size difference between the two ions is not significant and should not inhibit the formation of a $\text{CaCO}_{3(s)}/\text{CdCO}_{3(s)}$ solid solution. However, the system does appear to follow the Goldschmidt-Fersman rule. Cd^{2+} , the smaller ion, partitions favorably in the calcite lattice as shown by $D_{\text{Cd}^{2+}}$ values > 1 while Ca^{2+} , the larger ion, does not partition favorably into the otavite lattice as shown by $D_{\text{Ca}^{2+}}$ values < 1 (see Chapter 3). Of the properties listed in Table 4.1, only the electronegativities of Ca and Cd are significantly different. Since the absolute value of the electronegativity difference between the two ions is much larger than 0.05, the

Table 4.1 Endmember properties.

Mineral	Crystal Class	$\log K_{s0}$
Calcite	Rhombohedral	-8.48 ^a
Otavite	Rhombohedral	-12.1 ^b
Cation	Ionic Radius ^c (Å)	Electronegativity ^d
Ca ²⁺	1.00	1.0
Cd ²⁺	0.95	1.7

^aPlummer and Busenberg (1982)

^bStipp et al. (1993)

^cShannon (1976)

^dPauling (1960)

contribution of chemical energy to the ΔH_{mix} for this system should not be dismissed. It is primarily this difference that leads to non-ideality in the mixing behavior of this system.

4.2 Literature Values for Interaction Parameters

Calcite and otavite have been considered to form an ideal or nearly ideal solid solution series based on the fact that calcite and otavite have similar structures and the ionic radii of Ca²⁺ and Cd²⁺ are very similar. It was therefore felt that Cd²⁺ could replace Ca²⁺ in calcite with minimal strain on the lattice as a result of the substitution. The fact that Ca²⁺ and Cd²⁺ have different electronegativities was for the most part ignored even though the difference between the electronegativity of Ca and Cd is significant.

Early experimental evidence indicating ideal solid solution behavior consisted of the observation that CaCO_{3(s)} and CdCO_{3(s)} formed a fully miscible solid solution series with the lattice parameters of the solid solutions varying almost linearly with composition between the endmember values. For these measurements, the endmember solids were mixed under high temperature conditions in order to ensure homogeneous mixing over short time scales (Chang and Brice, 1971). One of the first attempts to study the thermodynamics of this solid

solution series at low temperatures was conducted by Könseberger *et al.* (1991). A potentiometric technique was used to measure the dissolution of several different $\text{CaCO}_{3(s)}/\text{CdCO}_{3(s)}$ solid solutions allowing the determination of three points located along the solidus. Assuming a regular solid solution model, an interaction parameter of -0.035 ± 0.074 was estimated from the three solidus points. Since the value of the estimated interaction parameter was not significantly different from zero, it was concluded that the system behaved ideally. However, it was observed that the initial solid solution materials used in the dissolution experiments were quickly “armored” with secondary solid solutions via incongruent dissolution. Precipitation of secondary phases onto the initial solid solution material was believed to have prevented the system from reaching equilibrium and made direct calculation of an interaction parameter for the system difficult.

Papadopoulos and Rowell (1988) speculated that calcite and otavite formed an ideal solid solution series based on the observation that estimated $D_{\text{Cd}^{2+}}$ values calculated from sorption experiments were “similar” to an ideal value. However, the method used in the sorption experiments allowed the pH and the composition of the aqueous phase to vary over the course of the experiment. In addition, the solid phase composition was estimated by assuming that all Cd lost from solution partitioned in a two dimensional manner to the calcite surface. These factors made the calculations of accurate Berthelot-Nerst type D values difficult. Therefore, it is uncertain if the experimental data did in fact indicate ideal partitioning behavior.

SSAS partitioning studies provide an additional means by which interaction parameters can be determined because the D_{eq} and ζ values generated from SSAS partitioning studies can be fit to a regular or sub-regular model if the corresponding X values for the solid phase are known. In almost all cases, a limited number of data points allows only the regular solid solution model to be considered. Reported values include -0.8 (Davis *et al.*, 1987) and 1.2 (Pankow and Tesoriero, 1996) for experiments run at trace levels of Cd in calcite. The disparity in the two values is due to alternate choices of the K_{s0} for otavite which is used in the calculation of the solid phase activity coefficient. One criticism of this approach to estimate interaction parameters is that measured D values from SSAS partitioning studies

may not represent equilibrium conditions. Another criticism is the use of a D measured at one solid solution composition to describe the mixing behavior across the entire solid solution series.

Rock *et al.* (1994) used a double cell electrochemical method to observe mixing behavior across the $\text{CaCO}_{3(s)}/\text{CdCO}_{3(s)}$ solid solution series. The double cell method attempts to compensate for some of the limitations encountered in the Könesberger *et al.* (1991) study, namely the armoring of the original solid solution with secondary phases. Unlike the Könesberger *et al.* (1991) study, Rock *et al.* (1994) found no evidence of ideal behavior in the $\text{CaCO}_{3(s)}/\text{CdCO}_{3(s)}$ solid solution series. In fact, measured $\Delta G_f^\circ [\text{Ca}_x\text{Cd}_{1-x}\text{CO}_{3(s)}]$ values were in excellent agreement with values predicted from the sub-regular solid solution model. Calculation of the G^{xs} across the solid solution series also indicated sub-regular behavior since the excess free energy curve was asymmetric with respect to solid solution composition. Estimation of Waldbaum-Thompson interaction parameters from the data yielded $w_1 = -9.065 \pm 20$ kJ/mol and $w_2 = -46.7 \pm 21$ kJ/mol. The large uncertainties in these values were due to errors associated with the experimental data and the value of $\Delta G_f^\circ [\text{CdCO}_{3(s)}]$ which was used in the calculation of the interaction parameters. It is interesting to note that the calculated Waldbaum-Thompson interaction parameters from Rock *et al.* (1994) predict a significant miscibility gap in the $\text{CaCO}_{3(s)}/\text{CdCO}_{3(s)}$ solid solution series. The presence of such a miscibility gap is not supported by experimental evidence.

4.3 Estimation of Mixing Parameters from Measured D_{eq} and ζ Values

The Guggenheim expansion (see Chapter 2, Section 2.2) can be used to describe the dependence of solid phase activity coefficients on mole fraction for regular and sub-regular solid solution behavior. When a binary solid solution mixes ideally, both solid phase activity coefficients equal unity across the entire solid solution series. In terms of the Guggenheim expansion, ideal behavior occurs when all of the interaction parameters equal zero. If the solid solution is regular, then only the first term of the Guggenheim expansion is necessary to describe the dependence of the solid phase activity coefficient on mole fraction. Equations

4-1 and 4-2 are the forms of the Guggenheim expansion for a $\text{CaCO}_{3(s)}/\text{CdCO}_{3(s)}$ solid solution assuming regular behavior. From these equations, it can be seen that ζ values in a regular solid solution are symmetric about $X = 0.5$.

$$\ln \zeta_{\text{CdCO}_{3(s)}} = a_m X^2_{\text{CaCO}_{3(s)}} \quad (4-1)$$

$$\ln \zeta_{\text{CaCO}_{3(s)}} = a_m X^2_{\text{CdCO}_{3(s)}} \quad (4-2)$$

If the behavior is sub-regular, then the first two terms of the Guggenheim expansion need to be included in order to describe the dependence of ζ values on X . Equations 4-3 and 4-4 illustrate this dependence for sub-regular solid solution behavior which allows for asymmetric dependence of ζ on X .

$$\ln \zeta_{\text{CdCO}_{3(s)}} = X^2_{\text{CaCO}_{3(s)}} [a_0 - a_1(3 - 4X_{\text{CaCO}_{3(s}}))] \quad (4-3)$$

$$\ln \zeta_{\text{CaCO}_{3(s)}} = X^2_{\text{CdCO}_{3(s)}} [a_0 + a_1(3 - 4X_{\text{CdCO}_{3(s}}))] \quad (4-4)$$

It should be mentioned that the a_m in Equations 4-1 and 4-2 is not the same as the a_0 in Equations 4-3 and 4-4. To avoid confusion, the interaction parameter for the regular case will be referred to as a_m , and the interaction parameters for the sub-regular case will be referred to as a_0 and a_1 .

Expressions that describe the dependence of D on X can be generated by substitution of the above expressions into the expressions for D_{eq} . For Cd^{2+} partitioning into calcite, the equilibrium distribution coefficient is defined as

$$D_{\text{Cd}^{2+}, \text{eq}} = \frac{K_{s0, \text{CaCO}_{3(s)}} \zeta_{\text{CaCO}_{3(s)}}}{K_{s0, \text{CdCO}_{3(s)}} \zeta_{\text{CdCO}_{3(s)}}} \quad (4-5)$$

The expression for the equilibrium distribution coefficient of Ca^{2+} is simply inverse of Equation 5.

$$D_{\text{Ca}^{2+},\text{eq}} = \frac{K_{s0,\text{CdCO}_{3(s)}} \zeta_{\text{CdCO}_{3(s)}}}{K_{s0,\text{CaCO}_{3(s)}} \zeta_{\text{CaCO}_{3(s)}}} \quad (4-6)$$

If the mixing behavior is ideal, D_{eq} values are simply the ratio of the endmember K_{s0} values. In an ideal solid solution there is no dependence of D on X . Using a $\log K_{s0}$ for calcite of -8.48 ± 0.02 , and a $\log K_{s0}$ of -12.1 ± 0.1 for otavite, $D_{\text{Cd}^{2+},\text{ideal}} = 4170 \pm 1000$ and $D_{\text{Ca}^{2+},\text{ideal}} = 0.00024 \pm 0.00006$.

If the dependence of ζ on X is assumed to be regular, Equations 4-1 and 4-2 can be substituted into Equations 4-5 and 4-6 to yield expressions for the dependence of D on X for the $\text{CaCO}_{3(s)}/\text{CdCO}_{3(s)}$ solid solution series.

$$D_{\text{Cd}^{2+},\text{eq}} = 4170 e^{a_m(1-2X_{\text{CaCO}_{3(s)}})} \quad (4-7)$$

$$D_{\text{Ca}^{2+},\text{eq}} = 2.40 \times 10^{-4} e^{a_m(1-2X_{\text{CdCO}_{3(s)}})} \quad (4-8)$$

If the system is assumed to follow sub-regular behavior, then Equations 4-3 and 4-4 can be substituted into Equations 4-5 and 4-6 to yield expressions that describe the dependence of D on X .

$$D_{\text{Cd}^{2+},\text{eq}} = 4170 e^{-a_0(2X_{\text{CaCO}_{3(s)}} - 1) - a_1(6(X_{\text{CaCO}_{3(s)}}^2 - X_{\text{CaCO}_{3(s)}}) + 1)} \quad (4-9)$$

$$D_{\text{Ca}^{2+},\text{eq}} = 2.40 \times 10^{-4} e^{a_0(2X_{\text{CdCO}_{3(s)}} - 1) + a_1(6(X_{\text{CdCO}_{3(s)}}^2 - X_{\text{CdCO}_{3(s)}}) + 1)} \quad (4-10)$$

Using the data set of D_{eq} , ζ and corresponding X values determined in Chapter 3, it was possible to estimate interaction parameters assuming regular and sub-regular mixing behavior. A summary of the final D_{eq} , ζ and X values is listed in Table 4.2. Only one X value is listed for each experimental series in Table 4.2. The X of the bulk constituent is easily calculated from the X of the trace constituent because the sum of the two X values must equal unity. Similarly, only the D_{eq} for the trace constituent is listed in Table 4.2. The D_{eq} for the bulk constituent is simply the inverse of the trace constituent D_{eq} . Finally, ζ values are listed only for the trace constituents in Table 4.2. The ζ values for the bulk phases were all assumed to be unity.

Table 4.2 Mole fraction, distribution coefficient and solid phase activity coefficient data.

Series	$X_{\text{CaCO}_3(s)}$	$D_{\text{Ca}^{2+}, eq}$	$\zeta_{\text{CaCO}_3(s)}$
E			
AAS	0.0013±0.001	0.0014±0.0002	0.17±0.03
XPS	0.007±0.003	0.0007±0.0002	0.3±0.1
F			
AAS	0.04±0.01	0.0019±0.0006	0.13±0.04
XPS	0.017±0.003	0.0008±0.0001	0.31±0.07
Series	$X_{\text{CdCO}_3(s)}$	$D_{\text{Cd}^{2+}, eq}$	$\zeta_{\text{CdCO}_3(s)}$
G			
mass balance	0.10±0.01	1620±40	2.6±0.2
XPS	0.14±0.02	2400±300	1.8±0.2
H			
mass balance	0.0093±0.0005	1200±400	3±1
XPS	0.011±0.003	1300±100	3.2±0.4

Interaction parameters for the regular solid solution model were estimated from the best fit of the ζ vs. X data to Equations 4-1 and 4-2. Sigma Plot 4.0 was used for all curve fitting. Five data points were used in these fits, one from each of the four data series and the fifth point representing the pure phase endmember ($X = 1, \zeta = 1$). Although 5 points were used in the fits, the spacing of the data points across the series was concentrated at the endmembers with no data points in the middle region. The concentration of data points near the endmembers makes the curve fitting less robust. However, if the system behaves in a regular manner, the a_m from the best fit of the $\zeta_{\text{CdCO}_3(\text{s})}$ data set and the a_m from the best fit of the $\zeta_{\text{CaCO}_3(\text{s})}$ data set should be identical.

Interaction parameters for the sub-regular solid solution model were estimated from the best fit of the D_{eq} vs. X data to Equations 4-9 and 4-10. Although there were only 4 data points in each data set with which to fit the equation (as opposed to the 5 data points in the ζ data sets), the spacing of the D_{eq} data points were such that the curve fitting was more robust than the fit of the sub-regular equations to the ζ data.

Table 4.3 lists the interaction parameters estimated by the best fits of the regular and sub-regular equations to the experimental data along with the t statistic and P value associated with each fit. The regular solid solution model was fit to the solid phase activity coefficient data, while the sub-regular model was fit to the distribution coefficient data. The t statistic is the ratio of the regression coefficient to its standard error and tests the null hypothesis that the coefficient of the independent variable is zero. A large t value is an indication that the predicted coefficient is significantly different from zero. The P value is the probability of committing a Type 1 error based on t . In general, it can be concluded that the predicted coefficient is not zero when $P < 0.05$. None of the fits summarized in Table 4.3 contained sufficient data points spaced in such a way as to provide a rigorous fit. In particular, the data sets did not contain any points at intermediate solid solution compositions. Therefore, the mixing parameter values listed in Table 4.3 should be treated cautiously.

Table 4.3 Interaction parameters for the $\text{CaCO}_{3(s)}/\text{CdCO}_{3(s)}$ solid solution series.

Regular Model		
Cadmium	a_m	
mass balance	1.14±0.01 ($t=77$; $P<0.0001$)	
XPS	1.04±0.09 ($t=11$; $P=0.0004$)	
Calcium	a_m	
AAS	-1.97±0.1 ($t=-18$; $P<0.0001$)	
XPS	-1.26±0.01 ($t=-14$; $P<0.0001$)	
Sub-regular model		
Cadmium	a_0	a_1
mass balance/AAS	-0.1±0.2 ($t=-0.6$; $P=0.6$)	2.0±0.3 ($t=5$; $P=0.03$)
XPS	0.17±0.07 ($t=2.3$; $P=0.1$)	1.27±0.09 ($t=14$; $P=0.005$)
Calcium	a_0	a_1
mass balance/AAS	0.3±0.4 ($t=0.9$; $P=0.4$)	1.7±0.4 ($t=4$; $P=0.05$)
XPS	0.03±0.07 ($t=-0.3$; $P=0.8$)	1.24±0.08 ($t=15$; $P=0.004$)

4.4 Discussion

Ideal mixing behavior is characterized by ζ values of unity and no dependence of D_{eq} on composition. Ideal behavior for the $\text{CaCO}_{3(s)}/\text{CdCO}_{3(s)}$ system is ruled out by both the calculated ζ values and measured D_{eq} values for this system. None of the solid phase activity coefficients equal unity even considering the large amount of error in the values (see Table 4.2). In addition, although the measured D_{eq} values do not appear to vary significantly with

composition, all of the observed D_{eq} values are significantly different from the ideal values of $D_{Cd^{2+}, ideal} = 4170 \pm 1000$ and $D_{Ca^{2+}, ideal} = 0.00024 \pm 0.00006$.

Although the regular solid solution model was able to fit each individual set of ζ values, as shown in Table 4.3, the a_m values determined by the best fits of Equations 4-1 and 4-2 to the $\zeta_{CdCO_{3(s)}}$ and $\zeta_{CaCO_{3(s)}}$ data were not similar, indicating that the $CaCO_{3(s)}/CdCO_{3(s)}$ solid solution does not follow regular behavior. Figure 4.1 is a plot of the measured ζ values and the predicted behavior for regular solid solution assuming an interaction parameter of 1.04. When using an a_m value of 1.04, the regular model can predict the behavior of the $\zeta_{CdCO_{3(s)}}$ values but is unable to predict the observed behavior for the $\zeta_{CaCO_{3(s)}}$ values. Figure 4.2 is a similar plot to Figure 4.1. However, in this case an a_m value of -1.26 was used to calculate the model predictions. As in Figure 4.1, the regular solid solution model can predict the behavior of only half of the measured ζ values. In contrast, the sub-regular model is able to predict the observed behavior of both the $\zeta_{CdCO_{3(s)}}$ and $\zeta_{CaCO_{3(s)}}$ with one set of interaction parameters. A plot of model predictions and observed values is shown in Figure 4.3.

The sub-regular model was also better able to predict the observed behavior of the D_{eq} values. Figure 4.4 is a plot of the measured $D_{Ca^{2+}, eq}$ values for the $CaCO_{3(s)}/CdCO_{3(s)}$ solid solution series and model predictions assuming ideal, regular and sub-regular behavior. Figure 4.5 is a similar plot for the measured $D_{Cd^{2+}, eq}$ values. In both Figures 4.4 and 4.5, only the sub-regular model is able to fit the measured distribution coefficient data.

To conclude that the $CaCO_{3(s)}/CdCO_{3(s)}$ solid solution series follows sub-regular mixing behavior would be an over statement of the data. However, it has been shown that the ideal and regular models for solid solution behavior were unable to predict the observed ζ and D_{eq} values. The indication that the system follows sub-regular behavior is consistent with the findings of Rock *et al.* (1994). However, in contrast to the findings of Rock *et al.* (1994), the sub-regular interaction parameters estimated from this research do not predict a miscibility gap in the $CaCO_{3(s)}/CdCO_{3(s)}$ solid solution series.

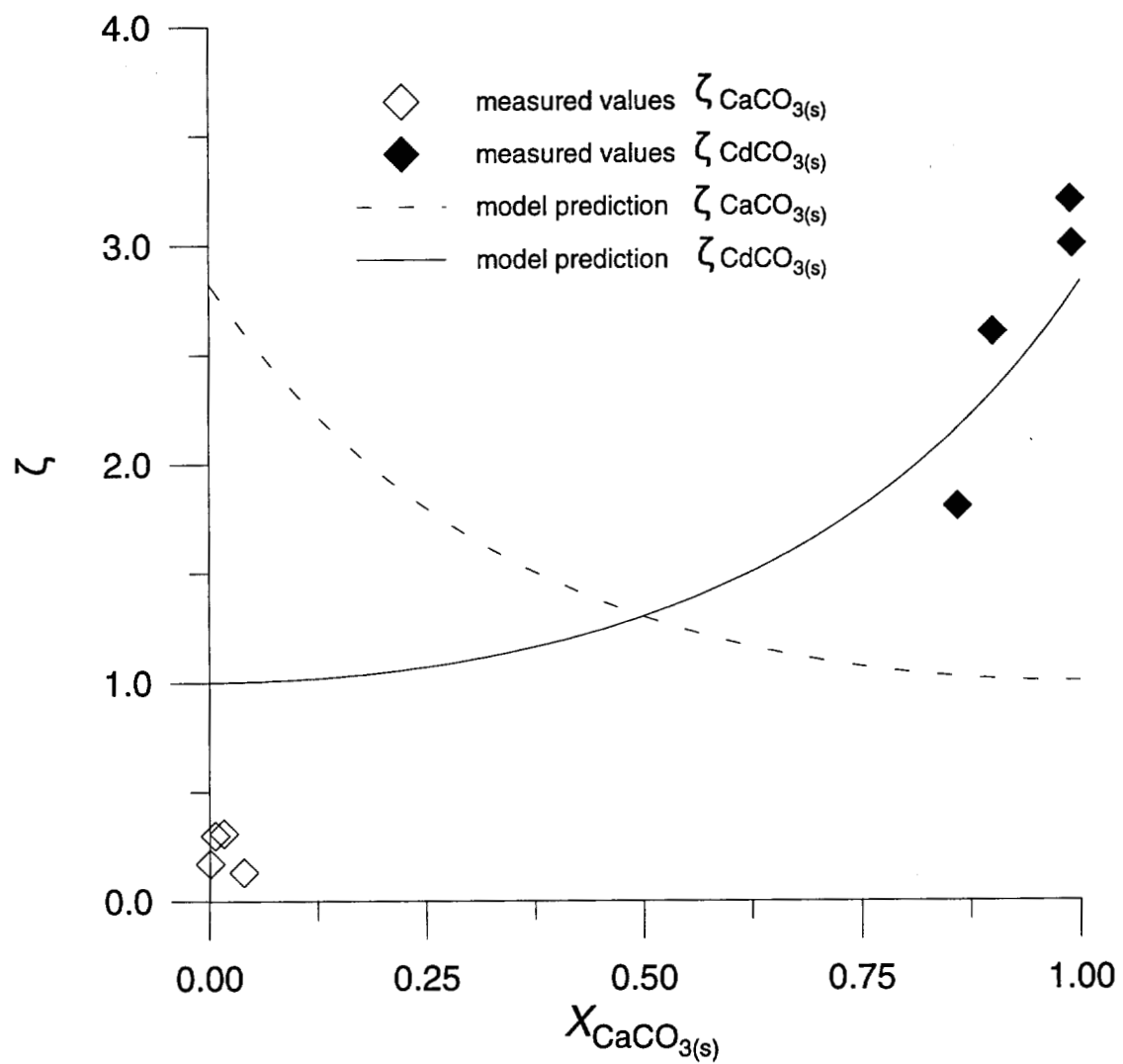


Figure 4.1 Comparison of experimental ζ values to regular solid solution model with $a_m = 1.04$.

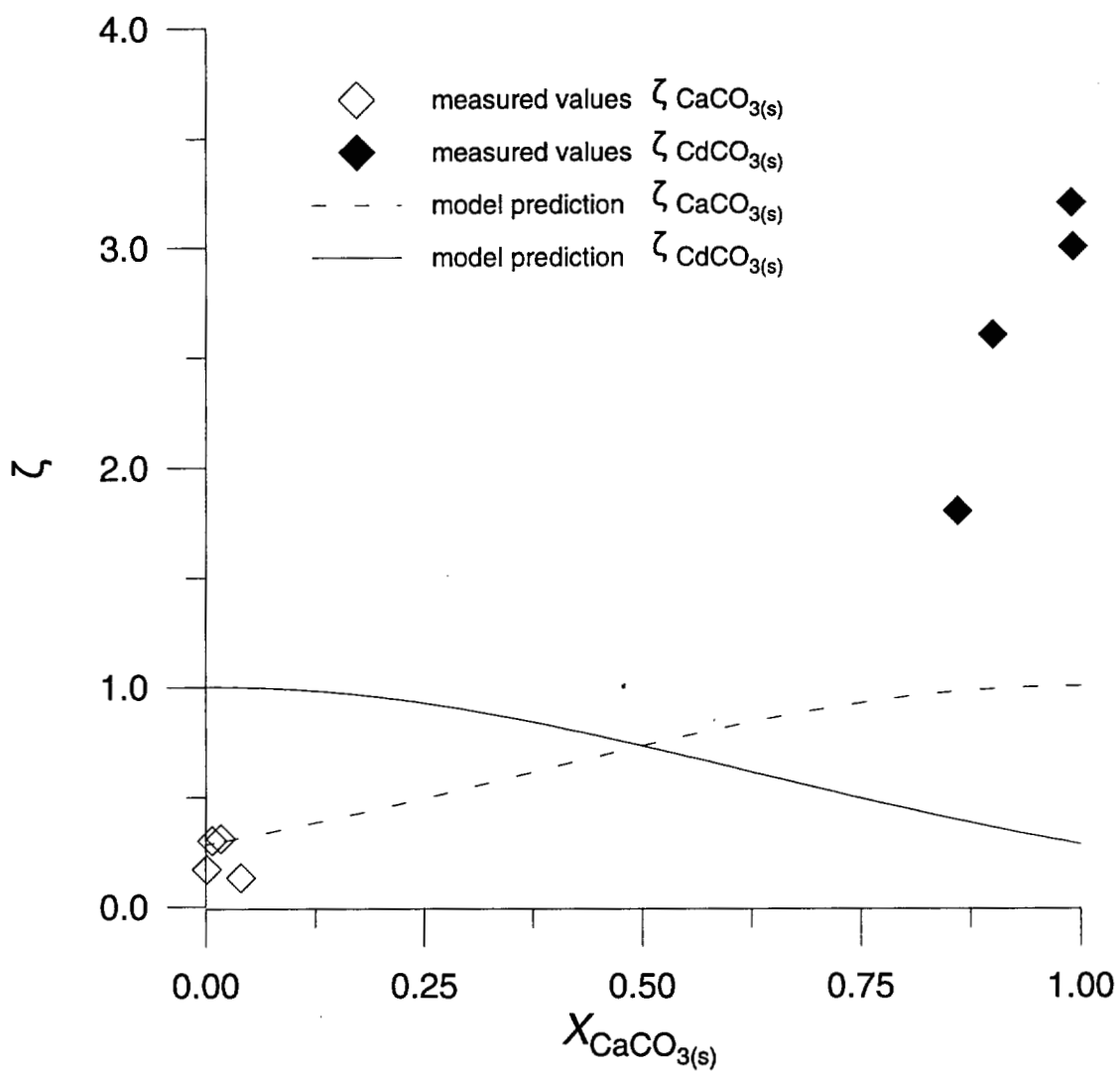


Figure 4.2 Comparison of experimental ζ values to regular solid solution model with $a_m = -1.26$.

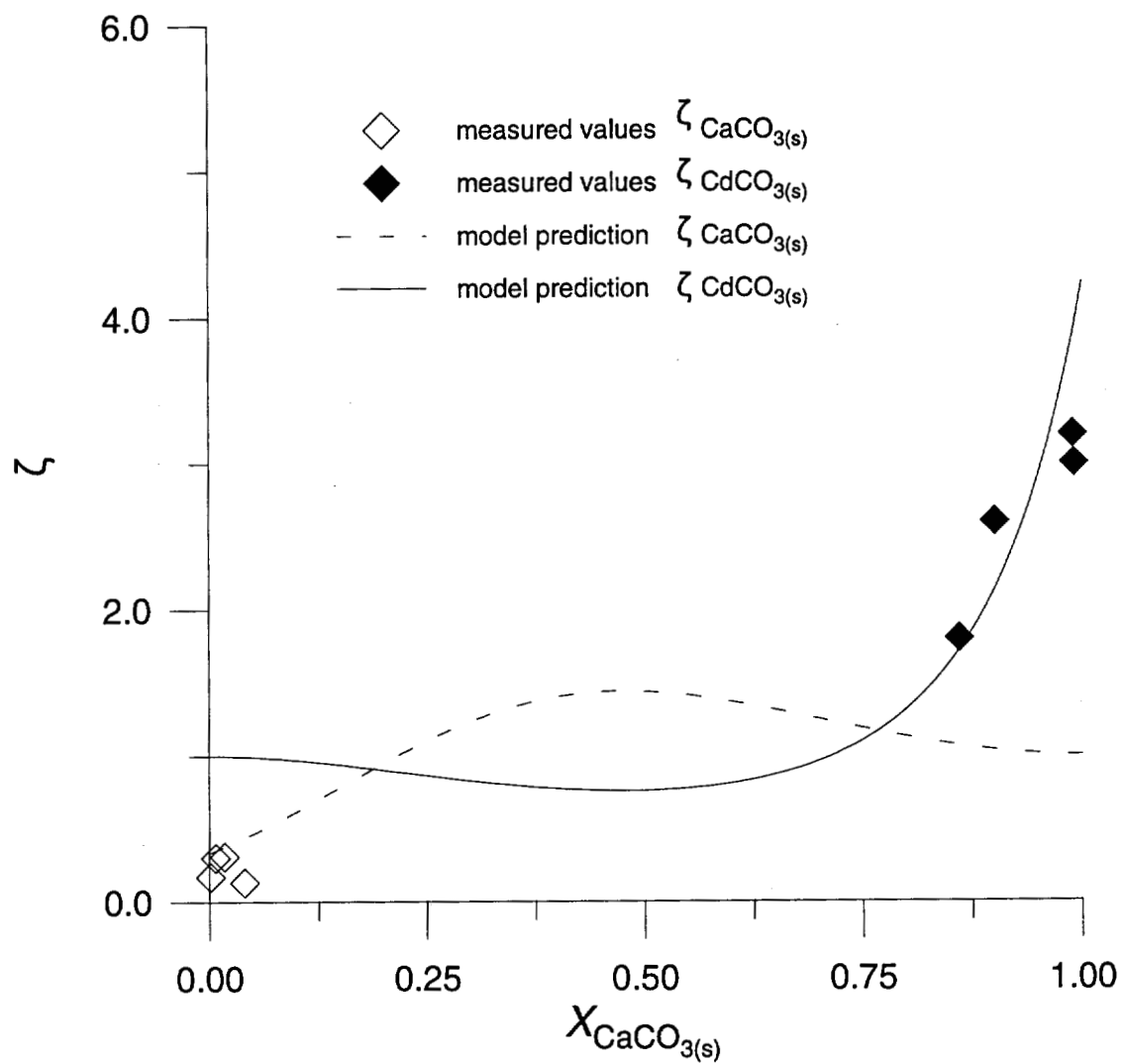


Figure 4.3 Comparison of experimental ζ values to sub-regular solid solution model with $a_0 = 0.17$ and $a_1 = 1.27$.

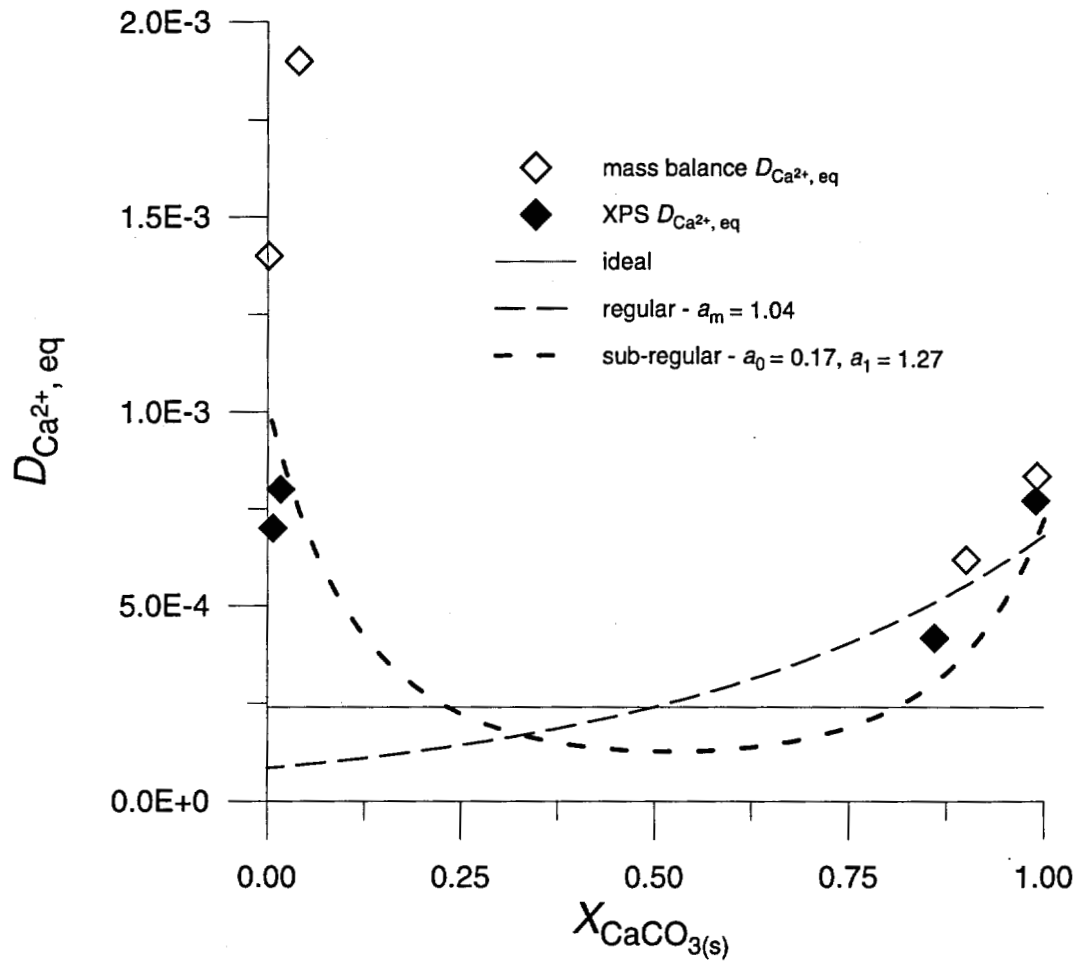


Figure 4.4 Comparison of measured $D_{Ca^{2+}, eq}$ values to model predictions.

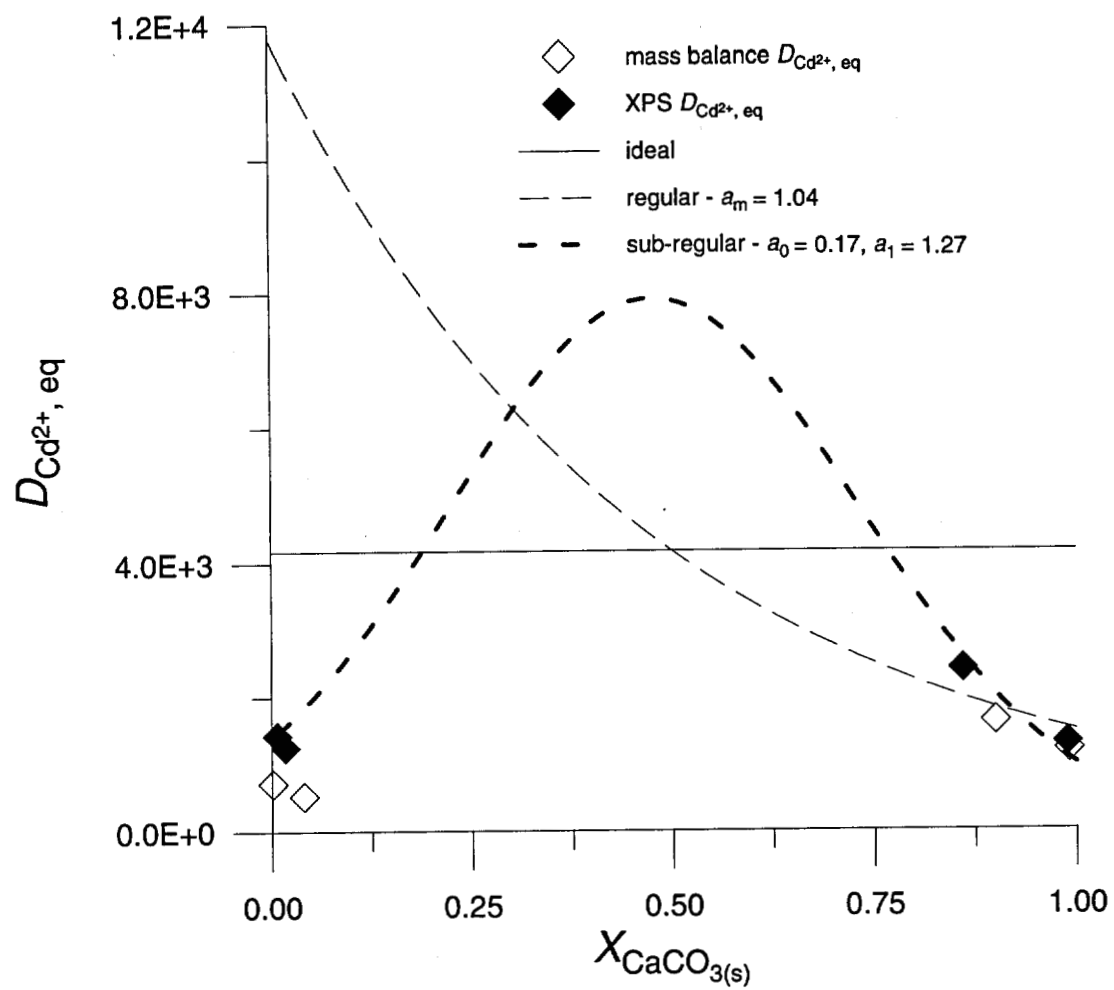


Figure 4.5 Comparison of measured $D_{\text{Cd}^{2+}, \text{eq}}$ values to model predictions.

Chapter 5

SSAS Partitioning as a Retardation Mechanism in Subsurface Transport

5.1 Introduction

While thermodynamics provides the overall driving force for solid solution formation, kinetics play an important role with respect to how fast, and by which process the mixing occurs. Unfortunately, the kinetics of solid solution formation are difficult to predict. Not only are D_{Me} values dependent on precipitation rate as demonstrated in Chapter 3, but armoring of a solid solution with secondary phases during dissolution or formation of a solid solution layer on relatively clean material may limit the interaction between solid solutions and the aqueous phase in transport scenarios due to isolation of the underlying solid.

5.2 Transport Studies

Isenbeck *et al.* (1987) conducted one of only a few transport studies that attempted to determine how the chemical properties of groundwater and aquifer materials could affect the transport of Cd. When using non-calcareous sand and acid groundwater (pH = 4.6), 95% of the Cd introduced to the column was recovered in the column effluent. When non-calcareous sand and neutral, carbonate rich ground water (pH = 7.4, $[HCO_3^-] = 341$ mg/l) was used, only 6% of the injected Cd was recovered in the column effluent. Finally, when a 0.35% by weight $CaCO_3$ sand was used as the solid phase in conjunction with neutral

groundwater, all of the injected Cd was retained on the column over the course of the relatively short experiment. What makes this study even more interesting is the sequential extraction that was performed on the column material from the calcareous sand/neutral groundwater case. Extraction of Cd from the solid phase using a cation exchange reagent recovered only 3% of the total Cd while extraction with HCl recovered 80% of the total Cd. The largest amounts of HCl-extracted Cd were found near the column inlet indicating that Cd was strongly retarded by the relatively small amount of calcite in the column.

The field study of Zahn and Seiler (1992) demonstrated that the migration of Cd through a carbonate aquifer can be significantly retarded by calcite even under conditions of high flow. In this case, Cd and fluorescein were injected into a carbonate gravel aquifer outside of Munich, Germany. Under high groundwater flow conditions of 1.4 to 2.2 m/h, the fluorescein, used as a conservative tracer, broke through a recovery well located 10 m from the injection well with a mean transit time of approximately 8 hours. In contrast, Cd was strongly retarded in the field study with a mean transit time of approximately 20,000 hours. Retardation factors calculated as the ratio of the mean transit time of Cd compared to the conservative tracer were in the range of 1,200 to 2,400. Over the course of the experiment, only 40% of the injected Cd was recovered normalized to the recovery of the conservative tracer. Although the Zahn and Seiler (1992) study did not incorporate solid phase characterization that could have identified the presence of solid solutions at the site, they did acknowledge that the strong retardation was likely due to precipitation of otavite at the injection site followed by a solid solution partitioning process that occurred as Cd was transported through the aquifer.

Cadmium transport through carbonate media has also been studied in an unsaturated stony soil monolith (Buchter *et al.*, 1996). The unsaturated transport of Cd through a carbonate media also demonstrated strong retention of Cd by the solid material with 30% of the injected Cd remaining on the column. Attempts to model this system with a simple reversible kinetic model and a combined equilibrium irreversible sorption kinetic model were problematic. Although the combined equilibrium irreversible sorption kinetic model could

be made to fit the breakthrough curve data, none of the test models could predict the significant amount of Cd that was retained by the column material.

5.3 Modeling Attempts

The incorporation of SSAS partitioning as a retardation mechanism in transport modeling is complicated by several factors. While the initial sorption of Cd to a calcite surface is rapid, as shown by Fuller and Davis (1987), Davis *et al.* (1987) and Stipp *et al.* (1992) the long-term uptake of Cd into pure calcite or calcite-containing subsurface material occurs over longer time scales. Therefore, any attempt to model SSAS partitioning should incorporate kinetics. In addition, familiar concepts like retardation factors which assume a fully reversible partitioning mechanism do not strictly apply to SSAS partitioning. Finally, the lack of knowledge about a formation mechanism and the amount of a solid that will participate in SSAS partitioning over a given time scale is perhaps the largest impediment facing the incorporation of solid solution processes in transport models.

Existing attempts to model SSAS partitioning in the subsurface (Isenbeck *et al.*, 1987; Zahn and Sieler, 1992) stress that it is inappropriate to use a classical retardation coefficient R_f

$$R_f = 1 + \frac{\rho_b}{\Theta} K_d \quad (5-1)$$

for describing retardation due to SSAS partitioning because the linear distribution coefficient K_d in Equation 5-1 is assumed to be fully reversible. (In Equation 5-1, ρ_b refers to the bulk density and Θ refers to the porosity of the solid phase.) As an alternative, Zahn and Sieler (1992) determine retardation by comparing the breakthrough time of Cd to that of a conservative tracer. Although this method can calculate retardation based on experimental observations, it not easily integrated into a numerical model.

As discussed by Tesoriero and Pankow (1996), if the mechanism of solid solution partitioning is formation of a surface layer in near equilibrium with the aqueous phase, then it is possible to develop a SSAS partitioning analog of Equation 5-1,

$$R_{f,SS} = 1 + \frac{\rho_b}{\Theta} \left(10^9 \alpha_{Me^{2+}} f_{calcite} \frac{D_{Me}}{[Ca^{2+}]} a_{calcite} m l \rho_{calcite} / FW_{calcite} \right) \quad (5-2)$$

where $\alpha_{Me^{2+}}$ is the fraction of the metal ion of interest present in the aqueous solution as Me^{2+} , $f_{calcite}$ is the calcite mass fraction of the solid phase, D_{Me} is the SSAS distribution coefficient for the metal ion of interest, $a_{calcite}$ is the specific surface area of the calcite material, m is the number of calcite monolayers involved in equilibrium, l is the monolayer thickness, $\rho_{calcite}$ is the calcite density, and $FW_{calcite}$ is the formula weight of calcite. According to this model, the retardation of a divalent metal ion due to SSAS partitioning will increase as the number of monolayers involved in the partitioning process increases. For Cd^{2+} partitioning to a medium which is 10% calcite by weight, Tesoriero and Pankow (1996) estimate a retardation factor of 71,000 assuming that 25 monolayers are involved in the partitioning process.

Leferve *et al.* (1993, 1996) used ion exchange theory combined with pure phase precipitation to model the migration of Ca and Sr in calcareous sand. Sr has been shown to form a solid solution with calcite (Tesoriero and Pankow, 1996; Lornes, 1981). However, the possibility of solid solution formation during transport in this study was not explicitly addressed. Because Sr does not partition favorably to calcite, $D_{Sr^{2+}, eq} = 0.021$ (Tesoriero and Pankow, 1996) and ion exchange may well represent the initial reaction between Sr and a calcite surface (Jensen, 1993), it is possible that the modeling approach of Leferve *et al.* (1993, 1996) may be adequate for predicting the transport of metals through calcareous media when $D < 1$ and the total amount of solid solution formed is small.

One difficulty encountered by all SSAS modeling approaches is a lack of experimental data with which to justify a given model. Existing data sets for the transport of divalent metals in a saturated media are often for experiments run at fast flow rates (Leferve *et al.*, 1993), or experiments that have no carbonate in the solid phase (Cowan *et al.*, 1992; Selim *et al.*, 1992; Hesterberg *et al.*, 1993; Roy *et al.*, 1993; Kookana *et al.*, 1994),

or there is no detailed characterization of the solid phase material to determine the extent of solid solution formation (Zahn and Seiler, 1992; Lefevre *et al.*, 1993, Buchter *et al.*, 1996). The lack of detailed experimental data concerning SSAS partitioning in transport scenarios and the strong affinity of Cd for calcite as evidenced by long transport times in the existing studies, encourages the development of a model that could be used in a diagnostic manner to evaluate SSAS partitioning as a retardation mechanism. The model could then be used to design an appropriate column study to further investigate the importance of SSAS partitioning as a fate and transport mechanism in environmental systems.

In order to incorporate SSAS partitioning into a transport model, the mechanism by which the solid solution forms should be identified. According to Stipp *et al.* (1992) solid solution formation does occur by the solid state diffusion of Cd into calcite. The identification of solid state diffusion as an incorporation mechanism combined with evidence that calcite remains well ordered during exposure to solution (Stipp *et al.* 1992; van Cappellen *et al.*, 1993), provides evidence that surface partitioning combined with solid state diffusion may be a significant process by which solid solutions form in the environment when active precipitation of calcite is limited. Therefore, SSAS partitioning of a divalent metal ion to calcite followed by solid state diffusion of the metal ion into the bulk calcite, was chosen to be the underlying solid solution formation mechanism in the MeTran model.

5.4 MeTran Model

5.4.1 General Description

MeTran simulates 1-dimensional advective-dispersive transport of a divalent metal cation through a saturated calcareous sand with partitioning to the solid material described by two different processes. The model includes reversible linear sorption to the sand surface and SSAS partitioning to the calcite surface combined with solid state diffusion of the metal cation into and out of the bulk calcite. MeTran is similar to the combined equilibrium and kinetic adsorption model described by Cameron and Klute (1977) in that it allows two

adsorption processes, one governed by equilibrium and the other governed by kinetics to be modeled at the same time with the restriction that the two adsorption processes do not interact with each other. However, MeTran is unique in that the kinetic process is the solid state diffusion of metal cations into calcite structure.

5.4.2 Governing Equations

As presented by Brush (1998), the overall mass balance for MeTran is given by Equation 5-3 where M_{pore} , M_{ads} , and M_{surf} refer to the mass of the divalent metal ion in the pore water, adsorbed to the sand surface, and sorbed to the calcite surface respectively. F_{in} , F_{out} , and F_{calcite} refer to the flux of the metal ion carried onto the column via advection/diffusion, out of the column via advection/diffusion, and into/out of the bulk calcite due to solid state diffusion.

$$\frac{\partial}{\partial t}(M_{\text{pore}} + M_{\text{ads}} + M_{\text{surf}}) = F_{\text{in}} + F_{\text{out}} + F_{\text{calcite}} \quad (5-3)$$

Substitution of expressions for the mass and flux terms for the system of interest yields Equations 5-4 through 5-8. In these equations, Θ represents the column porosity, V represents the volume of the representative element, C is the aqueous concentration of the divalent metal ion, f_{calcite} is the weight fraction of the calcite in the solid medium, ρ_d is the bulk density of the medium, K_d is a linear partition coefficient for the sand, $\text{mol}_{\text{calcite}}$ is the number of moles of calcite in the calcite surface, FW_{Me} is the formula weight of the metal ion, and X^{surf} is the mole fraction of the trace metal ion in the surface most calcite layer. D_d refers to the dispersion coefficient, and v refers the linear velocity in the aqueous phase.

$$\frac{\partial}{\partial t}(\Theta VC + (1 - f_{\text{calcite}})V\rho_b K_d + (\text{mol}_{\text{calcite}})^{\text{surf}} \text{FW}_{\text{Me}} X^{\text{surf}}) = \Theta V \frac{\partial}{\partial x} (D_d \frac{\partial C}{\partial x} - vC) - F_{\text{calcite}} \quad (5-4)$$

$$D_d = \alpha v + \omega D_{aq} \quad (5-5)$$

As shown in Equation 5-5, the dispersion coefficient D_d is comprised of diffusion and dispersion terms. In Equation 5-5, α is the dynamic dispersivity, ω is the tortuosity, and D_{aq} is the aqueous diffusion coefficient. The dispersion coefficient is normally represented by D in the literature as are diffusion coefficients. Unfortunately, this is also the variable of choice to represent the Berthelot-Nerst SSAS distribution coefficient. To minimize confusion, the dispersion coefficient will be referred to as D_d , diffusion coefficients will be identified by phase specific subscripts, and SSAS distribution coefficients will be identified by appropriate subscripts as was done in Chapter 3.

The X^{surf} for the trace metal in the calcite surface is given by rearrangement of Equation 2-13. In MeTran, the SSAS partitioning to the calcite surface described by D_{Me} is assumed to be a fast process in equilibrium with the aqueous phase. Therefore, the composition of the surface most calcite layer changes as the concentration of divalent metal ion in the aqueous phase changes. However, the D_{Me} remains constant throughout the simulation.

$$X^{surf} = \frac{C}{C + \frac{[Ca^{2+}]}{D_{Me}}} \quad (5-6)$$

The flux of calcite into the bulk material is modeled as simple diffusion with the composition of the surface most layer establishing an initial concentration gradient within the solid. Therefore, when there is sufficient Me^{2+} in the aqueous phase, the solid phase is "loaded" with Me^{2+} . When the aqueous concentration of Me^{2+} is decreased, the "loaded" Me^{2+} can diffuse out of the solid phase.

$$F_{calcite} = -\rho_{calcite} a_{calcite} D_{calcite} \left. \frac{\partial X}{\partial y} \right|_{surf} \quad (5-7)$$

In Equation 5-7, ρ_{calcite} represents the density of the calcite, a_{calcite} is the surface area of the calcite, D_{calcite} is the solid state diffusion coefficient, and y represents the direction normal to the calcite surface. In MeTran, it is assumed that the depth to which the Me^{2+} will diffuse is significantly less than the overall diameter of the particles.

Solid state diffusion within the calcite is described by Fick's second law assuming that the molar density of the calcite remains constant.

$$\frac{\partial X}{\partial y} = D_{\text{calcite}} \frac{\partial^2 X}{\partial y^2} \quad (5-8)$$

MeTran is subject to the following boundary and initial conditions where t_{off} represents the time that the contaminant source is turned off.

$$C(x, t=0) = 0 \quad (5-9)$$

$$-D \frac{\partial C}{\partial x} + vC \Big|_{x=0} = \begin{cases} vC_0 & 0 < t \leq t_{\text{off}} \\ 0 & t > t_{\text{off}} \end{cases} \quad (5-10)$$

$$\frac{\partial C}{\partial x} (x=L_{\text{column}}, t) = 0 \quad (5-11)$$

$$X(y, t=0) = 0 \quad (5-12)$$

$$\frac{\partial X}{\partial y} (y=L_{\text{calcite}}, t) = 0 \quad (5-13)$$

MeTran uses a finite volume method to approximate the governing equations. The discrete equations use the central difference scheme for all interface quantities and Crank-Nicholson for time integration. Spatial and temporal increments are automatically selected to ensure numerical stability and to limit numerical dispersion. When solid solution partitioning is active, the simulation of the equations is non-linear and a full Newton-Raphson iteration is employed using a convergence criteria of the sum of the absolute residuals having been decreased by at least 4 orders of magnitude or alternatively the sum of the absolute residuals having approached a constant value. A copy of the MeTran source code is located in Appendix D.

5.4.3 Input/Output Files

A sample MeTran input file which contains 23 variables is shown in Figure 5.1. By varying the parameters in the input file, MeTran can simulate a wide variety of transport scenarios including pulse and continuous contaminant sources, different amounts of calcite in the solid, different column sizes and transport distances, various flow rates, etc. However, a large number of fitting parameters can be problematic if the parameters are used to force a result from the model through the use of unreasonable values. Therefore, parameters like diffusion coefficients, dispersivity, and tortuosity should be set at specific values for a given transport scenario if the parameters are known and at representative values if the parameters are not well known.

MeTran output files contain a copy of the input file followed by a check of the input file for obvious errors, a listing of the control parameters for the interaction of Me^{2+} and the solid phase, and a listing of the parameters for which MeTran assigns values. The summary of input parameters is followed by three types of data tables, a time series output, a column profile at the end of the simulation, and a calcite depth profile if solid state diffusion was active during the simulation. Finally, the output file contains a short summary of the model performance during the simulation.

Figure 5.1 MeTran Input File.

```

>>> MeTran input file <<<
--- column data -----
30    velocity    average velocity [cm/day]
25    lenColum   column length [cm]
2.5   radColum   column radius [cm]
1.7   bulkDens  bulk density [g/cm^3]
0.5   bulkSurfArea bulk specific surface area [m^2/g]
.3    porosity   porosity [-]
1     dispSiv   dispersivity [cm]
0.5   tortuos   tortuosity [-]
--- Me2+ data -----
1.    aqueMe    aqueous Me2+ conc. at inflow [mg/L]
1.e-5 aqueDifus  aqueous diffusion coef. [cm^2/s]
0.2   adsorbK   linear adsorption Kd on Sand [mL/g]
1300  surfDist   surface distribution coef. [-]
2.8e-20 soliDifus solid state diffusion coef. [cm^2/s]
112.3 fwhtMe    formula weight Me2+ [g/mol]
--- calcite data -----
0.1   fraCalc   calcite fraction of bulk medium [-]
200   lenCalc   calcite diffusion length [A]
2.7   densCalc  calcite density [g/cm^3]
7.5e-10 molSurfCalc moles per unit surface area [mols/cm^2]
500   aqueCa    aqueous Ca2+ conc. [mg/L]
--- simulation data -----
5000  timeOff    time Me2+ source is turned off [d]
5000  timeEnd    end time of simulation [d]
10    delTimeOut time step for time series output [d]
10    distCalcProf column distance of Calcite profile

```

5.4.4 MeTran Validation

MeTran was validated by comparison to appropriate analytical solutions. Each portion of the model was validated individually because when the advection-dispersion equation is combined with solid-state diffusion, the system is fully nonlinear and no analytical solution exists. Comparison of MeTran simulations to analytical solutions produced remarkable agreement (Brush, 1998).

5.4.5 MeTran Limitations

MeTran is a flexible model that allows many input parameters to be altered. However, there are some underlying assumptions that restrict the application of the model. For example, MeTran does not incorporate any aqueous phase chemistry, or the effect of pH on the charge of the solid's surface, etc. However, to a certain extent these effects can be included by careful selection of the Me^{2+} and Ca^{2+} concentrations and K_d values. MeTran also does not allow for precipitation or dissolution of solids on the column. In addition, D_{Me} values are held constant throughout the simulation regardless of solid solution composition. As shown in Chapters 3 and 4, D_{Me} values are dependent on precipitation rate and composition. In a transport scenario, it is possible for D_{Me} values to vary with time and location. In order to ensure that the input D_{Me} value is valid throughout a simulation, it is best to run simulations at trace levels of the metal of interest. Finally, MeTran assumes that the surface layer formed via solid state diffusion is shallow compared to the overall diameter of the particles that make up the solid material. Therefore, MeTran should not be used to simulate experiments where diffusion should be described in radial coordinates.

5.5 Diagnostic modeling

5.5.1 Solid Solution Uptake

Before proceeding with purely diagnostic modeling, it is useful to determine if the SSAS partitioning and subsequent solid state diffusion mechanism described by MeTran are able to reproduce the uptake of Cd from aqueous solution believed to be due to solid solution formation. There are two studies in the literature that are suitable for this purpose, one for the uptake of Cd by pure phase calcite (Davis *et al.*, 1987) and the other for the uptake of cadmium by Borden Sand which is reported to be in the range of 4-10% calcite by weight (Fuller and Davis, 1987). MeBatch was used to determine if the mechanism for solid solution formation in MeTran could reproduce the data from these batch studies. MeBatch

contains the partitioning and solid state diffusion sub routines of MeTran without incorporating transport. For the simulations, a value of $2.8 \times 10^{-20} \text{cm}^2/\text{sec}$ was used for the solid state diffusion coefficient of Cd. This value was estimated from the solid state diffusion coefficient of ^{45}Ca used by Stipp *et al.* (1992).

When simulating the uptake of Cd into pure phase calcite, MeBatch overestimated the amount of Cd taken into the calcite compared to the value determined by Davis *et al.* (1987). The observed loss of Cd to calcite during what was believed to be solid solution formation was approximately $3.7 \times 10^{-11} \text{mol-Cd/g-calcite/hour}$. MeBatch simulated an uptake of approximately $1.2 \times 10^{-8} \text{mol-Cd/g-calcite/hour}$. The rate of uptake seen by Davis *et al.* (1987) could be duplicated by decreasing the solid state diffusion coefficient. However, there is no evidence that a change in the diffusion coefficient is appropriate.

When using MeBatch to simulate the uptake of Cd to Borden Sand, there was better agreement between observed and simulated values. Fuller and Davis (1987) observed loss from solution at the rate of $9.0 \times 10^{-12} \text{mol-Cd/g-sand/hour}$. MeBatch predicted an uptake rate of $5.5 \times 10^{-11} \text{mol-Cd/g-sand/hour}$. The agreement indicates that, to a first approximation, the partitioning mechanism and solid state diffusion coefficient value are appropriate for simulating the SSAS partitioning uptake when calcite is a minor component of the solid phase.

5.5.2 Formation of Solid Solution by Solid State Diffusion

MeTran was used to determine how the presence of calcite in the column material would affect the transport of Cd^{2+} . In these simulations, the concentration of Cd^{2+} in the input solution was set at 1 mg/l and the Ca^{2+} concentration at 500 mg/l. These values were chosen because they are similar to values observed in the G and H series distribution coefficient experiments. A value of 0.20 was chosen for K_d . This value was taken from a batch study partitioning study of Cd to the non-calcareous sand in acid groundwater (Isenbeck *et al.*, 1987).

Increasing the fraction of calcite in the column without allowing diffusion into the calcite has a dramatic effect on the retardation of Cd^{2+} by the column material (Figure 5.2). The presence of calcite in quantities as low as $f_{\text{calcite}} = 0.025$ increased the retardation of Cd^{2+} significantly even using a relatively fast flow rate of 100 cm/day. When solid state diffusion was allowed to occur there was also significant uptake of Cd^{2+} into the bulk of the calcite. Figure 5.3 contains breakthrough curves for a series of simulations where the $f_{\text{calcite}} = 0.05$ and the solid state diffusion depth varied from 0 to 200 Å with a flow rate of 30 cm/day. Because Cd^{2+} did not completely break through the column in all of these simulations, column profiles provided some additional information. Figure 5.4 is the column profile for the 200 Å simulation shown in Figure 5.3. This profile gives the mass of Cd^{2+} located in the pore water, the sand surface, the calcite surface, and in the bulk of the calcite along the length of the column. The strong retardation shown in Figure 5.3 and the relatively large quantity of Cd^{2+} associated with the calcite compared to the amount associated with the sand and pore water shown in Figure 5.4, indicate that even a relatively thin layer of solid solution can be a significant sink for Cd^{2+} . Figure 5.5 is a series of breakthrough curves for a pulsed contaminant source. This figure shows the significant tailing in conjunction with retardation that occurs in the breakthrough curves due to solid state diffusion.

To determine the effect of flow rate on Cd^{2+} transport, three MeTran simulations were run under identical conditions except for flow rate. The slow flow rate was chosen to be 3 cm/day, the average flow rate 30 cm/day, and the fast flow rate 300 cm/day. In the simulations, the 30 day long pulse of Cd^{2+} did not travel far along the column given a flow rate of only 3 cm/day. Over the course of 1,000 days, Cd^{2+} was predicted to migrate through only the first 2.5 cm of the column. Over the same time period, Cd^{2+} traveled 7.5 cm in the 30 cm/day flow rate simulation. During the simulation with a flow rate of 300 cm/day, Cd^{2+} was transported through all of the 25 cm column and the trailing edge of the contaminant pulse could be seen in the column profile near the inlet. In all cases, there was significant uptake of Cd^{2+} into the bulk calcite.

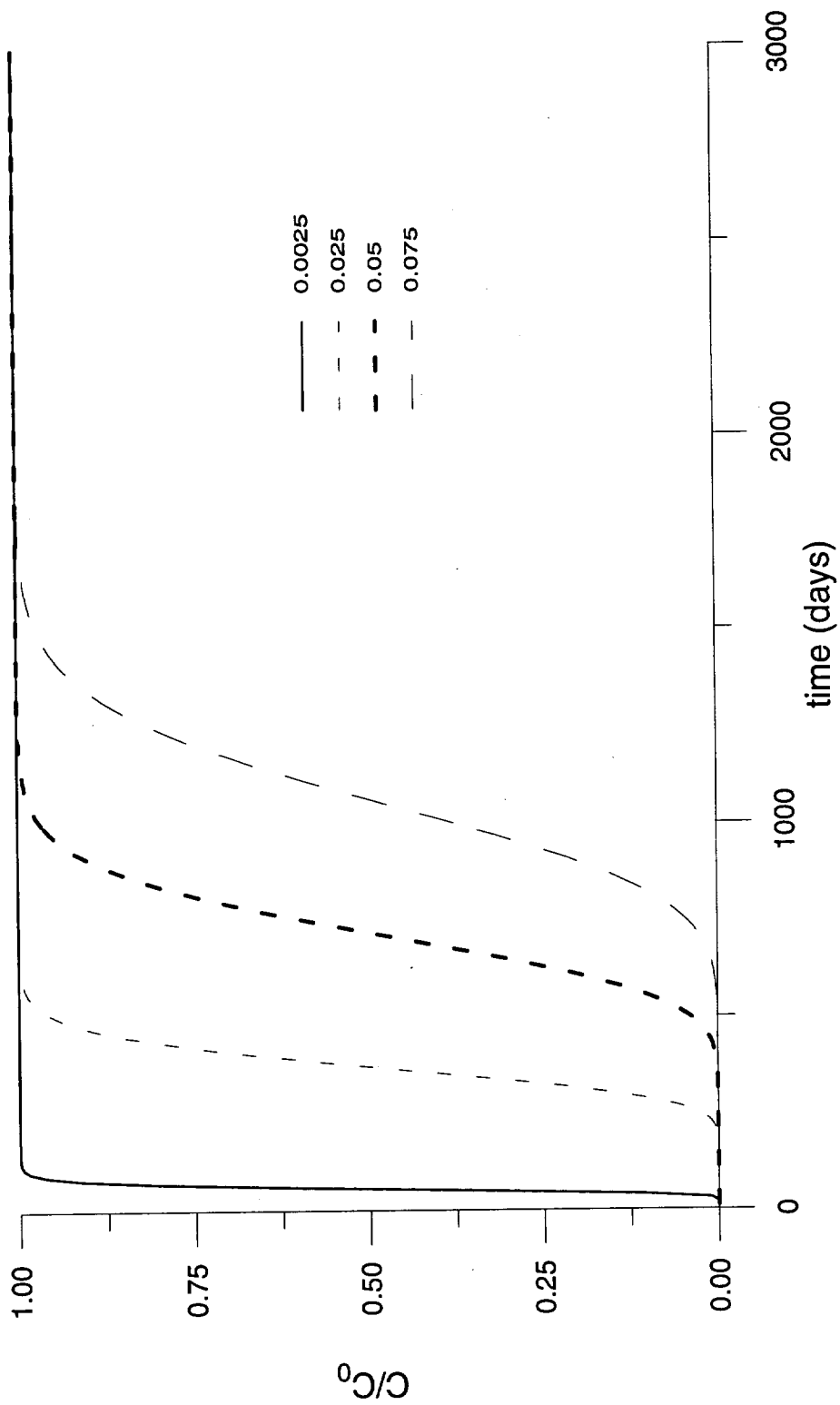


Figure 5.2 Breakthrough curves for increasing weight fractions of calcite with no solid state diffusion.

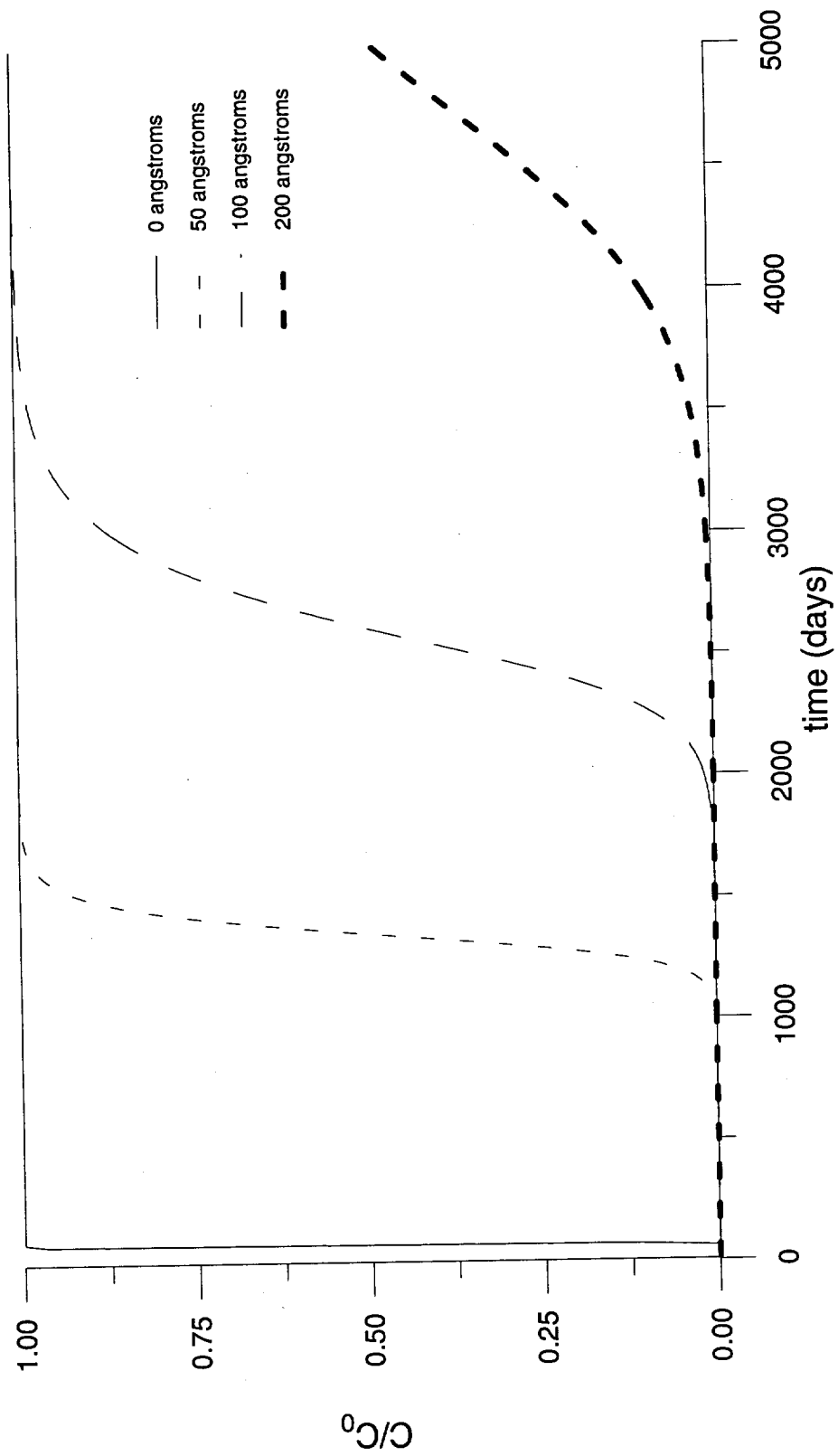


Figure 5.3 Breakthrough curves for $f_{\text{calcite}} = 0.05$ with increasing solid state diffusion depths.

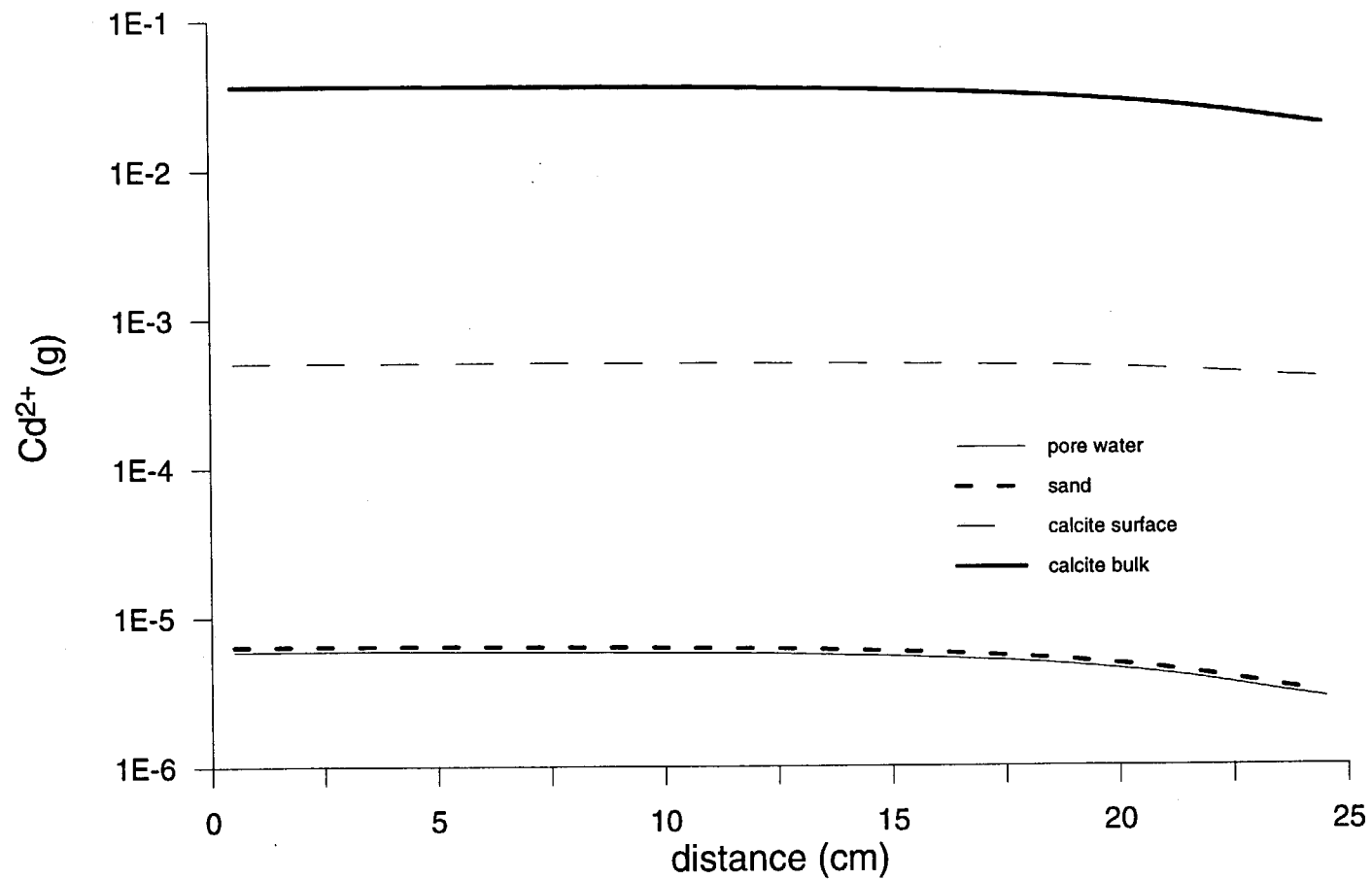


Figure 5.4 column profile for continuous source, $f_{\text{calcite}} = 0.05$, calcite depth = 200 angstroms.

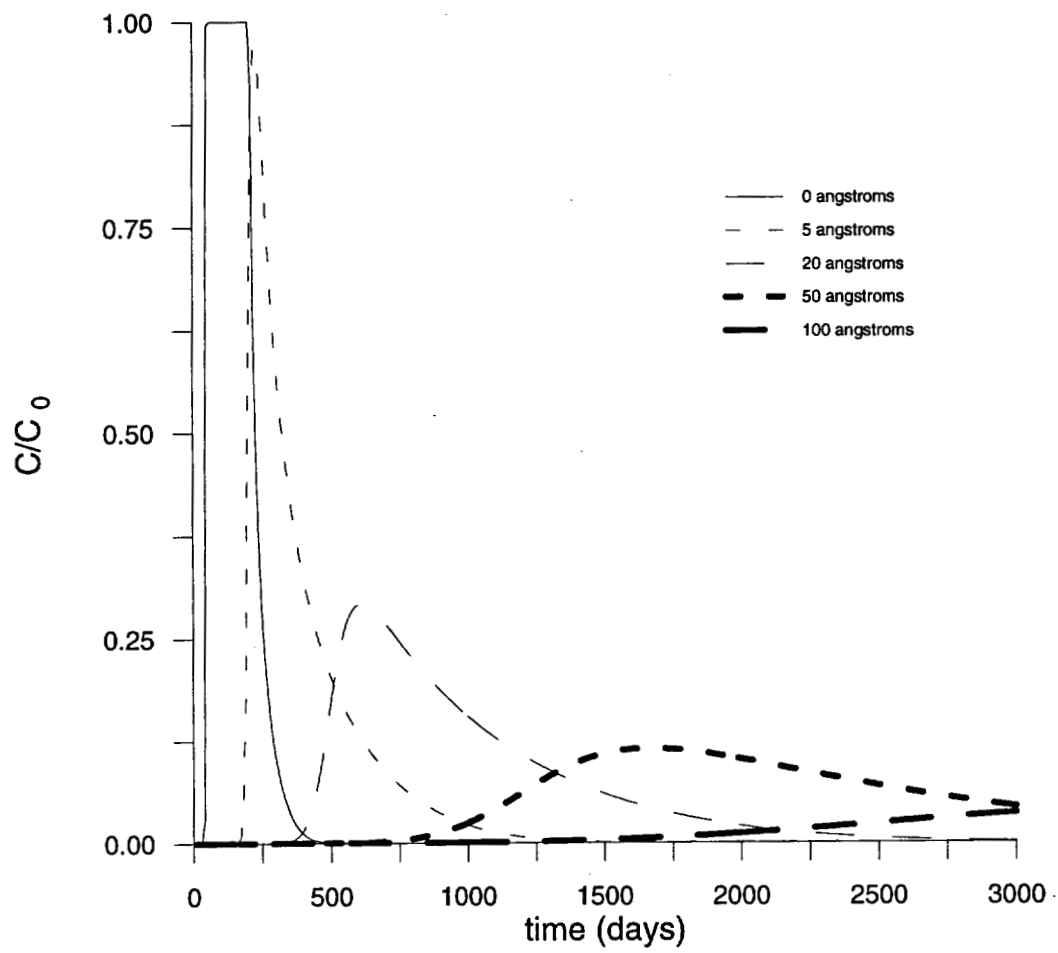


Figure 5.5 Pulsed source with increasing solid state diffusion depth of calcite.

5.5.3 Formation of Solid Solution as a Near-Equilibrium Surface Layer

Attempts to simulate a reactive boundary layer solid solution process similar to that described by Tesoriero and Pankow (1996) with MeTran were not successful. When increasing the solid state diffusion coefficient, either the magnitude of the residual was significantly larger than most of the calculated values, or the Newton-Raphson iteration did not converge. This numerical instability was due to the model being unable to incorporate a large change in solid state diffusion coefficient value. However, comparison of MeTran values for the retardation coefficient estimated from the breakthrough time of the Cd^{2+} compared to the groundwater velocity to values calculated from Equation 5-2, shows that the retardation coefficients estimated by MeTran are in better agreement for the one monolayer case than for the 25 monolayer case. MeTran predicts a retardation factor of 2,400 for the one monolayer case assuming a $D_{\text{Cd}^{2+}, \text{eq}} = 1250$. Tesoriero and Pankow (1996) predict a retardation coefficient of 2,800 for the same case. When 25 monolayers are included in the simulation, there is a large disparity between the MeTran and Tesoriero and Pankow values. MeTran simulates a retardation coefficient of 9,500 as opposed to the 71,000 calculated by Tesoriero and Pankow (1996). The larger values from the calculation of retardation coefficients according to Equation 5-2 are due to the increased capacity of the calcite to hold Cd^{2+} when the entire depth of the calcite is assumed to participate in the SSAS partitioning without a kinetic limitation.

5.5.4 Comparison of Diagnostic Modeling to Existing Transport Studies

It is difficult to model the transport studies of Isenbeck *et al.* (1987) and Zahn and Seiler (1992). In the Isenbeck case, the experiment was terminated after a very short transport time. There was no breakthrough curve provided for the experiment because all of the Cd was retained on the column throughout the course of the experiment. However, as shown by sequential extraction of the column material, the majority of the Cd was retained in the acid-soluble fraction near the column inlet. This general type of behavior is seen with

MeTran simulations run at slow flow rates and should also be seen if the simulation was run for only a short amount of time. In the Zahn and Seiler (1992) case, the concentration of Cd in the recovery well was low, $C/C_0 \approx 0.6 \times 10^{-6}$ and breakthrough occurred with significant tailing over long time periods. This type of behavior can be seen in the MeTran simulations shown in Figure 5.5.

5.6 Column Experiment Design

The main concern in the design of a column study is that the resulting experiment be able to provide information about a specific process. With respect to the SSAS partitioning of Cd to calcite, as shown by the limited transport studies that exist in the literature, the strong retention of cadmium by calcite presents some challenges. Of particular concern is the combination of column size, flow rate, and column material that will provide the best chance for the experiment to generate useful data. In addition, the overall transport time of the experiment is a concern. Transport studies that take several years to complete are not often repeated. Therefore, it is important to understand what steps can be taken to improve the chances of getting useful data from the experiment in the event that unexpected difficulties arise over the long course of the experiment.

With respect to column size, the diameter of the column within reason does not affect observed breakthrough times. However, the length of the column has a direct impact on the transport time with a short column having a shorter breakthrough time and a long column having a longer breakthrough time at the same flow rate. One advantage of a longer, larger column is the ability to install sampling ports along the length of the column. Aqueous phase measurements from along the length of the column would be advantageous since it would allow the progress of the cadmium to be monitored as it is transported through the column long before breakthrough at the column outlet would be observed.

Flow rate is another consideration. Although a fast flow rate is not necessarily a problem as shown by Zahn and Seiler (1992) for transport through an aquifer composed almost entirely of carbonates, if the flow rate is too slow the experiment may never reach

completion. However, with a column material that contains only a small fraction of calcite, a flow rate that is too fast may carry Cd through the column without allowing significant solid solution formation. 30 cm/day is generally considered average value for flow through a medium sand. Based on the diagnostic modeling, it would be acceptable to use flow rates as high as 100 cm/day for many transport studies.

Contaminant source concentrations and the length of time that a contaminant source is active provides additional concerns. If the source is too concentrated, additional undesired phases may precipitate in the column, similar to the proposed precipitation of otavite in the injection well during the Zahn and Seiler (1992) study. Because there appears to be significant spreading the peaks in both the diagnostic modeling (Figure 5.5), and in the field study of Zahn and Seiler (1992), the breakthrough curve from a pulsed source may experience intensive tailing and aqueous Cd levels may be difficult to measure accurately. A continuous source has several advantages. It eliminates the possibility of the input Cd becoming diluted by dispersion and sorption into calcite to the point that accurate detection of Cd is difficult. Because the material at the head of the column experiences a higher concentration for a longer duration, there should be a increased amounts of Cd in the calcite near the head of the column. However, the use of a continuous source over a long time period may result in the development of experimental conditions that MeTran is not equipped to model since MeTran assumes that the solid solution layer is relatively thin with respect to the overall particle size. This could be prevented if sand coated with a relatively thin layer of calcite was used in the column material.

There are two options for the composition of the solid material, a model column material, or a well characterized natural material like Borden sand. While the use of a natural material is one step closer to a real-world application, the characterization of the solid phase would be challenging. In contrast, a model material may allow easier characterization of the solid phase. Among model solids, the most appropriate choice may be a combination of clean sand and a clean sand that has been coated with a layer of calcite. This type of solid composition would allow the weight fraction of calcite in the column to be specified while the uniform coating of calcite on a portion of the sand would facilitate the use of

spectrometric methods for solid analysis because the composition of a solid phase is easier to obtain from a uniform material. It should also be possible to identify the formation of additional solid phases if any, or to observe the shift in XRD peaks due to solid solution formation after the experiment is terminated. With respect to XRD analysis the calcite solid solution would have to be at least 1% by weight to be detected in this relatively clean system.

With respect to the aqueous phase, it is important to minimize any chemical reactions that may occur in the column over the course of the experiment. The solutions will have to be equilibrated with a known $p\text{CO}_2$ and saturated with respect to calcite in an attempt to keep calcite from dissolving or precipitating on the column. Because Cd levels in the effluent may be low, the use of an analytical method with a low detection limit is essential, graphite AAS at a minimum.

The column material should be characterized before and after the experiment. Analysis of the solid phase by sequential extraction similar to Isenbeck *et al.* (1987) will be an inexpensive and useful technique. In addition, the solid phase characterization should include XRD, SEM-EDX and XPS with sputter depth profiling of calcite if possible. The resulting data from such a column experiment would include a detailed aqueous breakthrough curve from the column outlet and the sampling ports located along the column, a column profile at the end of the experiment from sequential extraction of solid materials along the column, and more detailed solid phase characterization from techniques like XRD, SEM-EDX and XPS.

Chapter 6

Summary and Conclusions

Given the increasing amount of evidence concerning the existence and formation of "impure" solids in the environment, and the effect that impure phases can have on the fate and transport of trace constituents in aqueous systems, the importance of the formation of carbonate solid solutions in ground and surface water systems cannot be doubted. However, very little is understood about how to go from a general appreciation of the importance of carbonate solid solutions to the point that retention and retardation can be predicted in a given groundwater setting. Two areas where improved understanding will eventually allow the informed application of SSAS processes to the fate and transport of metals in the environment are the compositional dependence of SSAS partitioning and an evaluation of SSAS partitioning in transport scenarios. These two areas were addressed in this study with respect to the calcite/otavite solid solution series.

SSAS distribution coefficients were measured at four different solid solution compositions across the calcite/otavite solid solution series with a constant composition precipitation method that allows the dependence of D_{Me} on precipitation rate to be observed. In order to prevent the precipitation of unwanted minerals, the aqueous phase was kept supersaturated with respect to only one endmember at any given time. This restriction placed on the experimental method resulted in the solid solution compositions being located near the pure phase endmembers.

Near the calcite endmember, the dependence of the measured $D_{Cd^{2+}}$ values on precipitation rate followed expected behavior. At fast precipitation rates, the observed distribution coefficient values approached unity indicating a less selective partitioning

process. At slower precipitation rates, the aqueous concentrations Cd^{2+} and Ca^{2+} leveled off, indicating an approach to equilibrium values. Average $D_{\text{Cd}^{2+}, \text{eq}}$ values were determined from experiments conducted in the equilibrium partitioning region. The means by which the solid solution composition was determined had an impact on the resulting $D_{\text{Cd}^{2+}, \text{eq}}$ values and the shape of the $D_{\text{Cd}^{2+}}$ vs. log precipitation rate curve. When the composition of the titrant solution was used to approximate the composition of the solid solution layer there was no apparent leveling off of $D_{\text{Cd}^{2+}}$ with decreasing precipitation rate. When a mass balance calculation was used to calculate $D_{\text{Cd}^{2+}}$ values, G series values appeared to level off in the equilibrium partitioning region while H series values did not. When XPS was used to determine the solid compositions used in the calculation of $D_{\text{Cd}^{2+}}$ values, both the G and H series curves leveled off. $D_{\text{Cd}^{2+}, \text{eq}}$ values for the G and H series experiments were in the range of 1,200 to 2,400 depending on the composition of the solid phase. The observed $D_{\text{Cd}^{2+}, \text{eq}}$ values were in good agreement with the existing literature values of Fuller and Davis (1987) and Tesoriero and Pankow (1996).

The measured $D_{\text{Ca}^{2+}}$ values for the calcite/otavite solid solution series were less than unity. This was not surprising because in a binary solid solution only one of the two partitioning ions is able to partition favorably into a lattice. At faster precipitation rates, the observed $D_{\text{Ca}^{2+}}$ values approached unity. $D_{\text{Ca}^{2+}}$ values decreased as the precipitation rate decreased. The equilibrium partitioning region was determined as the region where Cd^{2+} levels did not significantly vary as the precipitation rate was decreased. This region only included experiments conducted at the slowest precipitation rates. Solid compositions were determined by an AAS wet chemical method in addition to XPS. AAS values for the composition of the E and F series solid solutions were in reasonable agreement with the XPS values with XPS values tending to have slightly lower levels of Ca in the solid phase. It was not possible to compare observed $D_{\text{Ca}^{2+}, \text{eq}}$ values to literature values. However, the similarities between the E and F series data allows the two measurements to be treated almost as replicates improving the confidence in the precision of the data. $D_{\text{Ca}^{2+}, \text{eq}}$ values were in the range of 0.007 to 0.0019 depending on solid solution composition.

The use of XPS to measure the composition of the surface of the solid solutions indicated that the surface most layer of the G and H series solid solutions contained more Cd than was predicted by the mass balance calculation for the solid. This increased surface concentration did not appear to be due to precipitation of any additional phases as the saturation state of the aqueous solutions were relatively low (under 2) even at fast precipitation rates, and with few exceptions the aqueous phases were undersaturated with respect to all mineral phases except calcite. Dependence of the increased Cd concentrations on precipitation rate, with higher surface Cd concentrations observed at faster precipitation rates, led to the idea that the increased surface concentrations were due to the sorption of Cd to high energy binding sites on the crystal surface that were more predominant at faster precipitation rates. SEM images of a solid precipitated at fast rates compared to images of a solid formed at slow rates showed an increase in the concentration of high energy binding sites at the faster precipitation rate.

Solid phase activity coefficients were calculated for the trace component of each of the solid solutions from the observed D_{eq} values. The ζ and D_{eq} values indicated that the solid solution series was not ideal as the ζ values were not equal to unity and the observed D_{eq} values were not equal to ideal values. Regular behavior was also discarded since the regular solid solution model was unable to describe the observed behavior across the entire solid solution series with only one interaction parameter. The sub-regular model was able to predict the observed behavior across the entire series. However, the experimental data was insufficient to unequivocally determine if the calcite/otavite solid solution series follows sub-regular behavior. The indication that the calcite/otavite solid solution series follows sub-regular behavior is in agreement with the recent electrochemical measurements of Rock *et al.* (1994).

Diagnostic modeling allowed the evaluation of SSAS partitioning as a retardation mechanism in transport studies. Modeling demonstrated that even small amounts of calcite have the potential to strongly retard the migration of cadmium during a transport scenario, and that uptake of Cd into calcite during transport is significant. These conclusions are supported by the column study of Isenbeck *et al.* (1987) and the field study of Zahn and

Seiler (1992) where the migration of Cd through carbonate containing media resulted in strong retardation and low recoveries.

The use of MeTran to model existing transport experiments was limited due to sparse data sets and a lack of solid phase characterizations. It was considered more productive to use MeTran to design a column experiment that may shed some light on the role of SSAS partitioning in transport studies. The key factors in the column experiment design were the choice of column packing material, column size and flow rate.

References

- Allison, J. D., D. S. Brown and J. K. Novo-Gradac (1991) *MINTEQA2/PRODEFA2, a geochemical assessment model for environmental systems: Version 3.0 user's manual*. EPA/600/3-91-021. U. S. Environmental Protection Agency, Athens, Georgia.
- Amrhein, C., P. A. Mosher, J. E. Strong and P. G. Pacheco (1994) Heavy metals in the environment: Trace metal solubility in solids and waters receiving deicing salts. *Journal of Environmental Quality* **23**(2): 219-227.
- Baer, D. R., D. L. Blanchard, M. H. Engelhard and J. M. Zachara (1991) The interaction of water and Mn with surfaces of CaCO₃: An XPS study. *Surface and Interface Analysis* **17**(1): 25-30.
- Baer, D. R. and J. F. Moulder (1993) High resolution XPS spectrum of calcite (CaCO₃). *Surface Science Spectra* **2**(1): 1-7.
- Bancroft, M., J. R. Brown and W. S. Fyfe (1977) Quantitative X-ray photoelectron spectroscopy (ESCA): Studies of Ba²⁺ sorption on calcite. *Chemical Geology* **19**(2): 131-144.
- Berner, R. A. (1976) The solubility of calcite and aragonite in seawater at atmospheric pressure and 34.5‰ salinity. *American Journal of Science* **276**(6): 713-730.
- Blanchard, D. L. and D. R. Baer (1992) The interactions of Co, Mn and water with calcite surfaces. *Surface Science* **276**(1-3): 27-39.
- Brush, D. J. (1998) *MeTran v1.03 user's manual*. unpublished, Department of Civil Engineering, University of Waterloo.
- Buchter, B., C. Hinz, M. Gfeller and H. Flühler (1996) Cadmium transport in an unsaturated stony subsoil monolith. *Soil Science Society of America Journal* **60**(3): 716-721.

- Cameron, D. R. and A. Klute (1977) Convective-dispersive solute transport with a combined equilibrium and kinetic adsorption model. *Water Resources Research* **13**(1): 183-188.
- Casey, W. H., P. A. Rock, J.-B. Chung, E. M. Walling and M. K. McBeath (1996) Gibbs energies of formation of metal-carbonate solid solutions 2: The $CA_xSR_{1-2}CO_3(s)$ system at 298 K and 1 bar. *American Journal of Science* **296**(1): 1-22.
- Chang, L. L. Y. and W. R. Brice (1971) Subsolidus phase relations in the system calcium carbonate-cadmium carbonate. *The American Mineralogist* **56**: 338-341.
- Christ, C. L., P. B. Hostetler and R. M. Seibert (1974) Stabilities of calcite and aragonite. *Journal of Research United States Geological Survey* **2**: 175-184.
- Cowan, C. E., J. M. Zachara, S. C. Smith and C. T. Resch (1992) Individual sorbent contributions to cadmium sorption on ultisols of mixed mineralogy. *Soil Science Society of America Journal* **56**(4): 1084-1094.
- Davis, J. A., C. C. Fuller and A. D. Cook (1987) A model for trace metal sorption processes at the calcite surface: Adsorption of Cd^{2+} and subsequent solid solution formation. *Geochimica et Cosmochimica Acta* **51**(6): 1477-1490.
- Denniston, R. F., C. K. Shearer, G. D. Layne and D. T. Vaniman (1997) SIMS analyses of minor and trace element distribution in fracture calcite from Yucca Mountain, Nevada, USA. *Geochimica et Cosmochimica Acta* **61**(9): 1803-1818.
- Driessens, F. C. M. (1986) Ionic solid solutions in contact with aqueous solutions. *Geochemical processes at interfaces*. American Chemical Society: 524-560.
- Dromgoole, E. L. and L. M. Walter (1990) Iron and manganese incorporation into calcite: Effects of growth kinetics, temperature and solution chemistry. *Chemical Geology* **81**(4): 311-336.
- Erel, Y. and A. Katz (1990) Trace-element distribution across calcite veins: A tool for genetic interpretation. *Chemical Geology* **85**(3-4): 361-367.
- Ford, R. G., P. M. Bertsch and K. J. Farley (1997) Changes in transition and heavy metal partitioning during hydrous iron oxide aging. *Environmental Science and Technology* **31**: 2028-2033.
- Freeze, R. A. and J. A. Cherry (1979) *Groundwater*. Englewood Cliffs, New Jersey, Prentice-Hall.

- Friedl, G., B. Wehrli and A. Manceau (1997) Solid phases in the cycling of manganese in eutrophic lakes: New insights from EXAFS spectroscopy. *Geochimica et Cosmochimica Acta* **61**(2): 275-290.
- Fuller, C. C. and J. A. Davis (1987) Processes and kinetics of Cd²⁺ sorption by a calcareous aquifer sand. *Geochimica et Cosmochimica Acta* **51**(6): 1491-1502.
- Gamsjäger, H., H. U. Stuber and P. Schindler (1965) Thermodynamics of metal carbonates. I. Solubility constants and free energy of formation of cadmium carbonate. Thermodynamics of the ternary system Cd²⁺-H₂O-CO₂. *Helvetica Chimica Acta* **48**: 723-729.
- Garrels, R. M. and C. L. Christ (1965) *Solutions, minerals and equilibria*. San Francisco, Freeman, Cooper and Company.
- Glynn, P. D. (1990) Modeling solid-solution reactions in low-temperature aqueous systems. *Chemical modeling of aqueous systems II*. D. C. Melchior and R. L. Bassett. Washington, DC, American Chemical Society: 74-86.
- Glynn, P. D. (1991) MBSSAS: A code for the computation of Margules parameters and equilibrium relations in binary solid-solution aqueous-solution systems. *Computers & Geosciences* **17**(7): 907-966.
- Glynn, P. D. and E. J. Reardon (1990) Solid-solution aqueous-solution equilibria: Thermodynamic theory and representation. *American Journal of Science* **290**(2): 164-201.
- Glynn, P. D., E. J. Reardon, L. N. Plummer and E. Busenberg (1990) Reaction paths and equilibrium end-points in solid-solution aqueous-solution systems. *Geochimica et Cosmochimica Acta* **54**(2): 267-282.
- Gresens, R. L. (1981) The aqueous solubility product of solid solutions 2. Extension to binary solutions with stoichiometric coefficients greater than unity; analogy with vapor pressure of a binary liquid solution. *Chemical Geology* **32**(1-2): 73-86.
- Guggenheim, E. A. (1952) *Mixtures*. London, Oxford University Press.
- Helfrich, G. and B. Wood (1989) Subregular model for multicomponent solutions. *American Mineralogist* **74**: 1016-1022.
- Hesterberg, D., J. Bril and P. del Castillo (1993) Thermodynamic modeling of zinc, cadmium and copper solubilities in a munured, acidic loamy-sand topsoil. *Journal of Environmental Quality* **22**(4): 681-688.

- Hirao, Y., A. Matsumoto, H. Yamakawa, M. Maeda and K. Kimura (1994) Lead behavior in abalone shell. *Geochimica et Cosmochimica Acta* **58**(15): 3183-3189.
- Hochella, M. F. (1988) Auger electron and x-ray photoelectron spectroscopies. *Spectroscopic methods in mineralogy and geology*. F. C. Hawthorne. Chelsea, Michigan, Mineralogical Society of America. **18**: 573-638.
- Hochella, M. F., Jr, J. R. Lindsay, V. G. Mossotti and C. M. Eggleston (1988) Sputter depth profiling in mineral-surface analysis. *American Mineralogist* **73**(11-12): 1449-1456.
- Holland, H. D., T. V. Kirsipu, J. S. Huebner and U. M. Oxburgh (1964) On some aspects of the chemical evolution of cave waters. *Journal of Geology* **72**: 36-67.
- Isenbeck, M., J. Schröter, T. Taylor, M. Fic, A. Pekdeger and G. Matthes (1987) Adsorption/desorption and solution/precipitation behavior of cadmium as influenced by the chemical properties of ground water and aquifer material. *Meyniana* **39**: 7-21.
- Jacobson, R. L. and D. Langmuir (1974) Dissociation constants of calcite and CaHCO_3^+ from 0 to 50°C. *Geochimica et Cosmochimica Acta* **38**(2): 301-318.
- Jensen, B. S. (1993) The formation of solid solutions in surface layers: An important adsorption mechanism? *Journal of Contaminant Hydrology* **13**(1-4): 231-247.
- Kleiner, J. and H.-H. Stabel (1989) Phosphorus transport to the bottom of Lake Constance. *Aquatic Sciences* **51**(3): 181-191.
- Komatina, M. (1975) Development of conditions and regionalization of karst. *Hydrology of Karstic Terrains*. A. Burger and L. Dubertret. Paris, France, International Association of Hydrogeology; International Union of Geological Sciences. ser.b, no.3.
- Königsberger, E., R. Hausner and H. Gamsjäger (1991) Solid-solute phase equilibria in aqueous solution. V: The system $\text{CdCO}_3\text{-CaCO}_3\text{-CO}_2\text{-H}_2\text{O}$. *Geochimica et Cosmochimica Acta* **55**(12): 3505-3514.
- Kookana, R. S., R. Naidu and K. G. Tiller (1994) Sorption non-equilibrium during cadmium transport through soils. *Australian Journal of Soil Research* **32**(4): 635-651.
- Lafon, M. G. (1978) Discussion: Equilibria criteria for two component solids reacting with fixed composition in an aqueous phase-example: The magnesian calcites by D. C. Thoreston and L. N. Plummer. *American Journal of Science* **18**: 1455-1468.
- Langmuir, D. (1968) Stability of calcite based on aqueous solubility measurements. *Geochimica et Cosmochimica Acta* **32**: 835-851.

- Lefèvre, F., M. Sardin and D. Schweich (1993) Migration of strontium in clayey and calcareous sandy soil: Precipitation and ion exchange. *Journal of Contaminant Hydrology* **13**(1-4): 215-229.
- Lefèvre, F., M. Sardin and P. Vitorge (1996) Migration of ^{45}Ca and ^{90}Sr in a clayey and calcareous sand: calculation of distribution coefficients by ion exchange theory and validation by column experiments. *Journal of Contaminant Hydrology* **21**(1-4): 175-188.
- Lippmann, F. (1980) Phase diagrams depicting aqueous solubility of binary mineral systems. *Neues Jahrbuch für Mineralogie-Abhandlungen* **139**: 1-25.
- Lippmann, F. (1982) Stable and metastable solubility diagrams for the system $\text{CaCO}_3\text{-MgCO}_3\text{-H}_2\text{O}$ at ordinary temperature. *Bulletin de Mineralogie* **105**(3): 273-279.
- Lorens, R. B. (1981) Sr, Cd, Mn and Co distribution coefficients in calcite as a function of calcite precipitation rate. *Geochimica et Cosmochimica Acta* **45**(4): 553-561.
- Martínez, C. E. and M. B. McBride (1998) Solubility of Cd^{2+} , Cu^{2+} , Pb^{2+} and Zn^{2+} in aged coprecipitates with amorphous iron hydroxides. *Environmental Science and Technology* **32**(6): 743-748.
- Mashiotta, T. A., D. W. Lea and H. J. Spero (1997) Experimental determination of cadmium uptake in shells of the planktonic foraminifera *Orbulina universa* and *Globigerina bulloides*: Implications for surface water paleoreconstructions. *Geochimica et Cosmochimica Acta* **61**(19): 4053-4065.
- McCulloch, M. T., M. K. Gagan, G. E. Mortimer, A. R. Chivas and P. J. Isdale (1994) A high-resolution Sr/Ca and ^{18}O coral record from the Great Barrier Reef, Australia, and the 1982-1983 El Niño. *Geochimica et Cosmochimica Acta* **58**(12): 2747-2754.
- Mucci, A. (1983) The solubility of calcite and aragonite in seawater at various salinities, temperatures, and one atmosphere total pressure. *American Journal of Science* **283**(7): 780-799.
- Mucci, A. (1988) Manganese uptake during calcite precipitation from seawater: conditions leading to the formation of a pseudokutnahorite. *Geochimica et Cosmochimica Acta* **52**(7): 1859-1868.
- Mucci, A. and J. W. Morse (1983) The incorporation of Mg^{2+} and Sr^{2+} into calcite overgrowths: influences of growth rate and solution composition. *Geochimica et Cosmochimica Acta* **47**(2): 217-233.

- Mukhopadhyay, B., S. Basu and M. J. Holdaway (1993) A discussion of Margules-type formulations for multicomponent solutions with a generalized approach. *Geochimica et Cosmochimica Acta* **57**(2): 277-283.
- Nakayama, F. S. (1968) Calcium activity, complex and ion pair in saturated CaCO_3 solutions. *Soil Science* **106**: 429-434.
- Pankow, J. F. (1991) *Aquatic chemistry concepts*. Chelsea, Michigan, Lewis.
- Papadopoulos, P. and D. L. Rowell (1988) The reactions of cadmium with calcium carbonate surfaces. *Journal of Soil Science* **39**(1): 23-36.
- Paquette, J. and R. J. Reeder (1995) Relationship between surface structure, growth mechanism, and trace element incorporation in calcite. *Geochimica et Cosmochimica Acta* **59**(4): 735-749.
- Patchineelam, S. R. (1978) Coprecipitation of heavy metals with CaCO_3 : an example from polluted Elbe River (FRG). *Chemie der Erde* **37**: 221-225.
- Pauling, L. (1960) *The nature of the chemical bond*. Cornell University Press.
- Plummer, L. N. and E. Busenberg (1982) The solubilities of calcite, aragonite and vaterite in CO_2 - H_2O solutions between 0 and 90°C , and an evaluation of the aqueous model for the system CaCO_3 - CO_2 - H_2O . *Geochimica et Cosmochimica Acta* **46**(6): 1011-1040.
- Rai, D., A. R. Felmy and D. A. Moore (1991) Thermodynamic model for aqueous Cd^{2+} - CO_3^{2-} ionic interactions in high-ionic-strength carbonate solutions, and the solubility product of crystalline CdCO_3 . *Journal of Solution Chemistry* **20**(12): 1169-1187.
- Reeder, R. J. and J. C. Grams (1987) Sector zoning in calcite cement crystals: Implications for trace element distributions in carbonates. *Geochimica et Cosmochimica Acta* **51**(2): 187-194.
- Riciputi, L. R., H. Y. McSween, Jr, C. A. Johnson and M. Prinz (1994) Minor and trace element concentrations in carbonates of carbonaceous chondrites, and implications for the compositions of coexisting fluids. *Geochimica et Cosmochimica Acta* **58**(4): 1343-1351.
- Rimstidt, J. D., A. Balog and J. Webb (1998) Distribution of trace elements between carbonate minerals and aqueous solutions. *Geochimica et Cosmochimica Acta* **62**(11): 1851-1863.

- Rock, P. A., W. H. Casey, M. K. McBeath and E. M. Walling (1994) A new method for determining Gibbs energies of formation of metal-carbonate solid solutions: 1. The $\text{Ca}_x\text{Cd}_{1-x}\text{CO}_3(\text{s})$ system at 298 K and 1 bar. *Geochimica et Cosmochimica Acta* **58**(20): 4281-4291.
- Roy, W. R., I. G. Krapal and J. D. Steele (1993) Sorption of cadmium and lead by clays from municipal incinerator ash-water suspensions. *Journal of Environmental Quality* **22**(3): 537-543.
- Sass, E., J. W. Morse and F. J. Millero (1983) Dependence of the values of calcite and aragonite thermodynamic solubility products on ionic models. *American Journal of Science* **283**(3): 218-229.
- Scheidegger, A. M., G. M. Lamble and D. L. Sparks (1997) Spectroscopic evidence for the formation of mixed-cation hydroxide phases upon metal sorption on clays and aluminum oxides. *Journal of Colloid and Interface Science* **186**(1): 118-128.
- Selim, H. M., B. Buchter, C. Hinz and L. Ma (1992) Modeling the transport and retention of cadmium in soils: Multireaction and multicomponent approaches. *Soil Science Society of America Journal* **56**(4): 1004-1015.
- Shannon, R. D. (1976) Revised effective ionic radii and systematic studies of interatomic distances in halides and chalcogenides. *Acta Crystallographica*. **A32**: 751-767.
- Smith, N. O. (1992) Thermodynamics of ionic solid solutions. A new treatment of existing distribution data. *Journal of Solution Chemistry* **21**(10): 1051-1068.
- Stabel, H. H., J. K uchler-Krischun, J. Kleiner and P. Merkel (1986) Removal of strontium by coprecipitation in Lake Constance with calcite. *Naturwissenschaften* **73**(9): 551-553.
- Stipp, S. L. and M. F. Hochella, Jr (1991) Structure and bonding environments at the calcite surface as observed with X-ray photoelectron spectroscopy (XPS) and low energy electron diffraction (LEED). *Geochimica et Cosmochimica Acta* **55**(6): 1723-1736.
- Stipp, S. L., M. F. Hochella, Jr., G. A. Parks and J. O. Leckie (1992) Cd^{2+} uptake by calcite, solid-state diffusion, and the formation of solid-solution: Interface processes observed with near-surface sensitive techniques (XPS, LEED, and AES). *Geochimica et Cosmochimica Acta* **56**(5): 1941-1954.
- Stipp, S. L. S., G. A. Parks, D. K. Nordstrom and J. O. Leckie (1993) Solubility-product constant and thermodynamic properties for synthetic otavite, $\text{CdCO}_3(\text{s})$, and aqueous association constants for the $\text{Cd}(\text{II})\text{-CO}_2\text{-H}_2\text{O}$ system. *Geochimica et Cosmochimica Acta* **57**(12): 2699-2713.

- Tesoriero, A. J. (1994) *Solid solution/aqueous solution partitioning of divalent cations to calcite: Implications for the mobility of metals in natural waters*. Ph. D., Oregon Graduate Institute of Science & Technology, Beaverton, Oregon.
- Tesoriero, A. J. and J. F. Pankow (1996) Solid solution partitioning of Sr^{2+} , Ba^{2+} and Cd^{2+} to calcite. *Geochimica et Cosmochimica Acta* **60**(6): 1053-1063.
- Thompson Jr, J. B. (1967) Thermodynamic properties of simple solutions. in *Researches in geochemistry*. P. H. Abelson, John Wiley & Sons. **2**: 340-361.
- Thorstenson, D. C. and L. N. Plummer (1977) Equilibrium criteria for two-component solids reacting with fixed composition in an aqueous phase-Example: The magnesian calcites. *American Journal of Science* **277**(11): 1203-1222.
- Urusov, V. S. (1975) *Energetic theory of miscibility gaps in mineral solid solutions*. IMA 9th Meeting, Berlin-Regensburg, Germany, Stuttgart. 141-150.
- Van Cappellen, P., L. Charlet, W. Stumm and P. Wersin (1993) A surface complexation model of the carbonate mineral-aqueous solution interface. *Geochimica et Cosmochimica Acta* **57**(15): 3505-3518.
- Wiechiers, H. N. S., P. Sturrock and G. V. R. Marais (1975) Calcium carbonate crystallization kinetics. *Water Research* **9**: 835-845.
- Xu, N., M. F. Hochella, Jr, G. E. Brown, Jr and G. A. Parks (1996) Co(II) sorption at the calcite-water interface: I. X-ray photoelectron spectroscopic study. *Geochimica et Cosmochimica Acta* **60**(15): 2801-2815.
- Xyla, A., E. K. Giannimaras and P. G. Koutsoukos (1991) The precipitation of calcium carbonate in aqueous solutions. *Journal of Colloid and Interface Science* **53**: 241-255.
- Zahn, M. T. and K. P. Seiler (1992) Field studies on the migration of arsenic and cadmium in a carbonate gravel aquifer near Munich (Germany). *Journal of Hydrology* **133**(3-4): 201-214.

Appendix A
Data From Constant Composition Experiments

Table A.1 Data from experiment E1[†]

Sample #	elapsed time minutes	pH	cumulative CdCl ₂ titrated mL	[Cd _T] mg/L	[Cd ²⁺] mol/L	[Ca _T] mg/L	[Ca ²⁺] mol/L
E1-1	0.0	5.156	0.00	199	1.552x10 ⁻⁴	ND	ND
E1-2	332	5.617	14.30	558	4.434x10 ⁻⁴	67.35	1.642x10 ⁻³
E1-3	735	5.619	31.00	556	4.413x10 ⁻⁴	66.92	1.631x10 ⁻³

† 0.4 L initial volume, 0.25 M titrant solutions

ND - not detected

initial seed material 0.724 g

Table A.2 Data from experiment E2[†]

Sample #	elapsed time hours	pH	cumulative CdCl ₂ titrated mL	[Cd _T] mg/L	[Cd ²⁺] mol/L	[Ca _T] mg/L	[Ca ²⁺] mol/L
E2-1	0.0	5.161	0.00	192	1.499x10 ⁻⁴	ND	ND
E2-2	12.5	5.745	62.25	533	4.219x10 ⁻⁴	79.72	1.941x10 ⁻³
E2-3	20.1	5.665	84.50	628	4.998x10 ⁻⁴	61.12	1.485x10 ⁻³

† 0.4 L initial volume, 0.25 M titrant solutions

ND - not detected

initial seed material 0.708 g

Table A.3 Data from experiment E3

Sample #	elapsed time hours	pH	cumulative CdCl ₂ titrated mL	[Cd _T] mg/L	[Cd ²⁺] mol/L	[Ca _T] mg/L	[Ca ²⁺] mol/L
E3-1a	0.0	5.140	0.00	168	1.315x10 ⁻⁴	ND	ND
E3-1b*	0.0	5.140	0.00	173	1.354x10 ⁻⁴	ND	ND
E3-2	24.3	5.508	19.75	363	2.853x10 ⁻⁴	80.72	1.977x10 ⁻³
E3-3	48.5	5.478	39.95	364	2.864x10 ⁻⁴	66.41	1.629x10 ⁻³

† 0.4 L initial volume, 0.25 M titrant solutions

* replicate sample with 0.20 µm filter

ND - not detected

initial seed material 0.826 g

Table A.4 Data from experiment E4†

Sample #	elapsed time hours	pH	cumulative CdCl ₂ titrated mL	[Cd _T] mg/L	[Cd ²⁺] mol/L	[Ca _T] mg/L	[Ca ²⁺] mol/L
E4-1a	0.0	5.153	0.00	174	1.357x10 ⁻⁴	ND	ND
E4-1b*	0.0	5.153	0.00	174	1.354x10 ⁻⁴	ND	ND
E4-2	46.0	5.363	10.90	273	2.136x10 ⁻⁴	85.97	2.117x10 ⁻³
E4-3	98.0	5.347	23.30	297	2.331x10 ⁻⁴	59.88	1.475x10 ⁻³

† 0.4 L initial volume, 0.25 M titrant solutions

* replicate sample with 0.20 µm filter

ND - not detected

initial seed material 0.822 g

Table A.5 Data from experiment E5[†]

Sample #	elapsed time minutes	pH	cumulative CdCl ₂ titrated mL	[Cd _T] mg/L	[Cd ²⁺] mol/L	[Ca _T] mg/L	[Ca ²⁺] mol/L
E5-1	0.0	5.157	0.00	128	9.856x10 ⁻⁵	NA	NA
E5-2	72	5.862	28.65	1099	8.634x10 ⁻⁴	63.1	1.511x10 ⁻³
E5-3	117	5.857	46.40	1122	8.839x10 ⁻⁴	54.0	1.294x10 ⁻³

† 0.4 L initial volume, 0.25 M titrant solutions

NA - not analyzed

initial seed material 0.820 g

Table A.6 Data from experiment E6[†]

Sample #	elapsed time minutes	pH	cumulative CdCl ₂ titrated mL	[Cd _T] mg/L	[Cd ²⁺] mol/L	[Ca _T] mg/L	[Ca ²⁺] mol/L
E6-1	0.0	5.138	0.00	174	1.353x10 ⁻⁴	NA	NA
E6-2*	0.0	5.138	0.00	174	1.353x10 ⁻⁴	NA	NA
E6-3	83	5.813	20.70	851	6.846x10 ⁻⁴	61.85	1.487x10 ⁻³
E6-4	152	5.803	31.75	848	6.820x10 ⁻⁴	54.14	1.303x10 ⁻³

† titration rate accidentally changed during experiment and later corrected

* replicate sample with 0.20 µm filter

NA - not analyzed

initial seed material 1.002 g

Table A.7 Data from experiment E7

Sample #	elapsed time hours	pH	cumulative CdCl ₂ titrated mL	[Cd _T] mg/L	[Cd ²⁺] mol/L	[Ca _T] mg/L	[Ca ²⁺] mol/L
E7-1	0.0	5.145	0.00	167	1.303x10 ⁻⁴	NA	NA
E7-2	18.4	5.542	15.00	453	3.572x10 ⁻⁴	55.57	1.360x10 ⁻³
E7-3	42.4	5.533	34.50	457	3.609x10 ⁻⁴	52.17	1.277x10 ⁻³

NA - not analyzed

initial seed material 1.000 g

Table A.8 Data from experiment E8

Sample #	elapsed time hours	pH	cumulative CdCl ₂ titrated mL	[Cd _T] mg/L	[Cd ²⁺] mol/L	[Ca _T] mg/L	[Ca ²⁺] mol/L
E8-1	0.0	5.128	0.00	211	1.639x10 ⁻⁴	NA	NA
E8-2	24.2	5.406	5.70	356	2.785x10 ⁻⁴	67.88	1.669x10 ⁻³
E8-3	50.2	5.398	11.90	358	2.801x10 ⁻⁴	66.09	1.625x10 ⁻³

NA - not analyzed
initial seed material 1.009 g

Table A.9 Data from experiment E9

Sample #	elapsed time hours	pH	cumulative CdCl ₂ titrated mL	[Cd _T] mg/L	[Cd ²⁺] mol/L	[Ca _T] mg/L	[Ca ²⁺] mol/L
E9-1	0.0	5.158	0.00	175	1.360x10 ⁻⁴	NA	NA
E9-2	72.1	5.300	6.25	258	2.006x10 ⁻⁴	75.78	1.869x10 ⁻³
E9-3	162.8	5.299	14.15	255	1.983x10 ⁻⁴	83.75	2.066x10 ⁻³

NA - not analyzed
initial seed material 1.000 g

Table A.10 Data from experiment E10

Sample #	time hrs	pH	cumulative CdCl ₂ titrated mL	[Cd _T] mg/L	[Cd ²⁺] mol/L	[Ca _T] mg/L	[Ca ²⁺] mol/L
E10-1	0.0	5.155	0.00	180	1.397x10 ⁻⁴	NA	NA
E10-2	45.2	5.378	7.70	294	2.288x10 ⁻⁴	53.53	1.318x10 ⁻³
E10-3	91.4	5.372	15.60	293	2.280x10 ⁻⁴	60.02	1.577x10 ⁻³

NA - not analyzed
initial seed material 1.016 g

Table A.11 Data from experiment E11

Sample #	elapsed time hours	pH	cumulative CdCl ₂ titrated mL	[Cd _T] mg/L	[Cd ²⁺] mol/L	[Ca _T] mg/L	[Ca ²⁺] mol/L
E11-1	0.0	5.151	0.00	186	1.445x10 ⁻⁴	NA	NA
E11-2	24.4	5.332	5.85	274	2.131x10 ⁻⁴	72.56	1.788x10 ⁻³
E11-3	90.8	5.330	13.90	279	2.170x10 ⁻⁴	64.43	1.588x10 ⁻³

NA - not analyzed
initial seed material 1.006 g

Table A.12 Data from experiment E12

Sample #	elapsed time hours	pH	cumulative CdCl ₂ titrated mL	[Cd _T] mg/L	[Cd ²⁺] mol/L	[Ca _T] mg/L	[Ca ²⁺] mol/L
E12-1	0.0	5.155	0.00	182	1.410x10 ⁻⁴	NA	NA
E12-2	138.5	5.283	8.55	239	1.862x10 ⁻⁴	64.50	1.591x10 ⁻³
E12-3	257.8	5.282	15.90	229	1.783x10 ⁻⁴	80.84	1.995x10 ⁻³

NA - not analyzed
initial seed material 1.001 g

Table A.13 Data from experiment E13

Sample #	elapsed time hours	pH	cumulative CdCl ₂ titrated mL	[Cd _T] mg/L	[Cd ²⁺] mol/L	[Ca _T] mg/L	[Ca ²⁺] mol/L
E13-1	0.0	5.168	0.00	181	1.403x10 ⁻⁴	NA	NA
E13-2	139.0	5.263	6.25	214	1.657x10 ⁻⁴	62.93	1.554x10 ⁻³
E13-3	311.3	5.245	13.90	233	1.812x10 ⁻⁴	62.91	1.554x10 ⁻³

NA - not analyzed
initial seed material 1.006 g

Table A.14 Data from experiment E14

Sample #	elapsed time hours	pH	cumulative CdCl ₂ titrated mL	[Cd _T] mg/L	[Cd ²⁺] mol/L	[Ca _T] mg/L	[Ca ²⁺] mol/L
E14-1	0.0	5.157	0.00	173	1.343x10 ⁻⁴	ND	ND
E14-2	17.2	5.251	3.10	216	1.689x10 ⁻⁴	43.66	1.077x10 ⁻³
E14-3	284.0	5.254	12.45	235	1.831x10 ⁻⁴	37.06	9.113x10 ⁻⁴

ND - not detected

initial seed material 1.001 g

Table A.15 Data from experiment F1†

Sample #	elapsed time minutes	pH	cumulative CdCl ₂ titrated mL	[Cd _T] mg/L	[Cd ²⁺] mol/L	[Ca _T] mg/L	[Ca ²⁺] mol/L
F1-1a	0.0	5.160	0.00	168	1.301x10 ⁻⁴	ND	ND
F1-1b*	0.0	5.160	0.00	179	1.388x10 ⁻⁴	ND	ND
F1-2	126	5.836	46.50	941	7.613x10 ⁻⁴	790	1.897x10 ⁻²
F1-3	172	5.785	62.00	984	7.987x10 ⁻⁴	709	1.709x10 ⁻²

† 0.4 L initial volume, 0.25 M titrant solutions

* replicate sample with 0.20 µm filter

ND - not detected

initial seed material 0.802 g

Table A.16 Data from experiment F2

Sample #	elapsed time minutes	pH	cumulative CdCl ₂ titrated mL	[Cd _T] mg/L	[Cd ²⁺] mol/L	[Ca _T] mg/L	[Ca ²⁺] mol/L
F2-1	0.0	5.156	0.00	181	1.167x10 ⁻⁴	NA	NA
F2-2	66	5.821	10.85	801	5.113x10 ⁻⁴	191	3.281x10 ⁻³
F2-3	108	5.822	17.25	856	5.471x10 ⁻⁴	175	3.128x10 ⁻³

NA - not analyzed

initial seed material 1.002 g

Table A.17 Data from experiment F3

Sample #	elapsed time hours	pH	cumulative CdCl ₂ titrated mL	[Cd _T] mg/L	[Cd ²⁺] mol/L	[Ca _T] mg/L	[Ca ²⁺] mol/L
F3-1	0.0	5.150	0.00	181	1.409x10 ⁻⁴	NA	NA
F3-2	21.3	5.546	17.55	422	3.325x10 ⁻⁴	195	4.601x10 ⁻³
F3-3	41.5	5.540	34.30	467	3.692x10 ⁻⁴	170	4.197x10 ⁻³

NA - not analyzed

initial seed material 1.009 g

Table A.18 Data from experiment F4

Sample #	elapsed time hours	pH	cumulative CdCl ₂ titrated mL	[Cd _T] mg/L	[Cd ²⁺] mol/L	[Ca _T] mg/L	[Ca ²⁺] mol/L
F4-1	0.0	5.152	0.00	179	1.394x10 ⁻⁴	NA	NA
F4-2	96.1	5.303	8.25	254	1.990x10 ⁻⁴	209	5.165x10 ⁻³
F4-3	190.2	5.291	16.45	273	2.140x10 ⁻⁴	180	4.457x10 ⁻³

NA - not analyzed

initial seed material 1.000 g

Table A.19 Data from experiment F5

Sample #	elapsed time hours	pH	cumulative CdCl ₂ titrated mL	[Cd _T] mg/L	[Cd ²⁺] mol/L	[Ca _T] mg/L	[Ca ²⁺] mol/L
F5-1	0.0	5.161	0.00	178	1.381x10 ⁻⁴	NA	NA
F5-2	69.0	5.334	8.40	255	1.984x10 ⁻⁴	175	4.314x10 ⁻³
F5-3	138.7	5.326	16.80	280	2.186x10 ⁻⁴	207	5.117x10 ⁻³

NA - not analyzed

initial seed material 1.004 g

Table A.20 Data from experiment F6

Sample #	elapsed time hours	pH	cumulative CdCl ₂ titrated mL	[Cd _T] mg/L	[Cd ²⁺] mol/L	[Ca _T] mg/L	[Ca ²⁺] mol/L
F6-1	0.0	5.159	0.00	187	1.451x10 ⁻⁴	NA	NA
F6-2	24.3	5.411	5.80	309	2.407x10 ⁻⁴	223	5.617x10 ⁻³
F6-3	76.0	5.396	18.05	337	2.633x10 ⁻⁴	209	5.161x10 ⁻³

NA - not analyzed
initial seed material 1.003 g

Table A.21 Data from experiment F7

Sample #	elapsed time hours	pH	cumulative CdCl ₂ titrated mL	[Cd _T] mg/L	[Cd ²⁺] mol/L	[Ca _T] mg/L	[Ca ²⁺] mol/L
F7-1	0.0	5.153	0.00	183	1.418x10 ⁻⁴	NA	NA
F7-2	97.0	5.267	6.05	242	1.879x10 ⁻⁴	207	5.123x10 ⁻³
F7-3	216.4	5.260	13.45	282	2.201x10 ⁻⁴	195	4.819x10 ⁻³

NA - not analyzed
initial seed material 1.003 g

Table A.22 Data from experiment F8

Sample #	elapsed time minutes	pH	cumulative CdCl ₂ titrated mL	[Cd _T] mg/L	[Cd ²⁺] mol/L	[Ca _T] mg/L	[Ca ²⁺] mol/L
F8-1	0.0	5.144	0.00	169	1.312x10 ⁻⁴	NA	NA
F8-2	243	5.650	10.25	591	4.677x10 ⁻⁴	217	5.284x10 ⁻³
F8-3	421	5.646	20.10	623	4.938x10 ⁻⁴	198	4.818x10 ⁻³

NA - not analyzed
initial seed material 1.011 g

Table A.23 Data from experiment F9

Sample #	elapsed time hours	pH	cumulative CdCl ₂ titrated mL	[Cd _T] mg/L	[Cd ²⁺] mol/L	[Ca _T] mg/L	[Ca ²⁺] mol/L
F9-1	0.0	5.157	0.00	180	1.399x10 ⁻⁴	NA	NA
F9-2	22.6	5.436	7.55	354	2.770x10 ⁻⁴	229	5.623x10 ⁻³
F9-3	47.0	5.431	15.65	385	3.008x10 ⁻⁴	204	5.023x10 ⁻³

NA - not analyzed
initial seed material 1.005 g

Table A.24 Data from experiment F10

Sample #	elapsed time minutes	pH	cumulative CdCl ₂ titrated mL	[Cd _T] mg/L	[Cd ²⁺] mol/L	[Ca _T] mg/L	[Ca ²⁺] mol/L
F10-1	0.0	5.140	0.00	185	1.434x10 ⁻⁴	NA	NA
F10-2	60	5.955	28.75	1160	9.411x10 ⁻⁴	194	4.608x10 ⁻³
F10-3	89	5.953	43.10	1205	9.802x10 ⁻⁴	194	4.597x10 ⁻³

NA - not analyzed
initial seed material 1.003 g

Table A.25 Data from experiment F11

Sample #	elapsed time hours	pH	cumulative CdCl ₂ titrated mL	[Cd _T] mg/L	[Cd ²⁺] mol/L	[Ca _T] mg/L	[Ca ²⁺] mol/L
F11-1	0.0	5.150	0.00	185	1.435x10 ⁻⁴	NA	NA
F11-2	20.4	5.350	3.70	293	2.283x10 ⁻⁴	205	5.052x10 ⁻³
F11-3	67.1	5.344	11.65	333	2.604x10 ⁻⁴	189	4.668x10 ⁻³

NA - not analyzed
initial seed material 1.003 g

Table A.26 Data from experiment F12

Sample #	elapsed time hours	pH	cumulative CdCl ₂ titrated mL	[Cd _T] mg/L	[Cd ²⁺] mol/L	[Ca _T] mg/L	[Ca ²⁺] mol/L
F12-1	0.0	5.148	0.00	192	1.492x10 ⁻⁴	1.01	2.515x10 ⁻⁵
F12-2	19.3	5.425	6.30	349	2.728x10 ⁻⁴	182	5.016x10 ⁻³
F12-3	43.0	5.438	14.20	399	3.132x10 ⁻⁴	163	4.110x10 ⁻³

initial seed material 1.017 g

Table A.27 Data from experiment F13

Sample #	elapsed time hours	pH	cumulative CdCl ₂ titrated mL	[Cd _T] mg/L	[Cd ²⁺] mol/L	[Ca _T] mg/L	[Ca ²⁺] mol/L
F13-1	0.0	5.131	0.00	191	1.485x10 ⁻⁴	ND	ND
F13-2	22.5	5.545	22.75	484	3.807x10 ⁻⁴	163	4.634x10 ⁻³
F13-3	44.9	5.533	45.10	531	4.194x10 ⁻⁴	143	3.776x10 ⁻³

ND - not detected

initial seed material 1.002 g

Table A.28 Data from experiment F14

Sample #	elapsed time minutes	pH	cumulative CdCl ₂ titrated mL	[Cd _T] mg/L	[Cd ²⁺] mol/L	[Ca _T] mg/L	[Ca ²⁺] mol/L
F14-1	0.0	5.147	0.00	167	1.291x10 ⁻⁴	4.31	1.067x10 ⁻⁴
F14-2	208	5.568	6.80	491	3.866x10 ⁻⁴	191	5.497x10 ⁻³
F14-3	703	5.568	19.85	530	4.181x10 ⁻⁴	171	4.233x10 ⁻³

initial seed material 1.004 g

Table A.29 Data from experiment G1[†]

Sample #	elapsed time minutes	pH	cumulative CaCdCl ₂ titrated mL	[Cd _T] mg/L	[Cd ²⁺] mol/L	[Ca _T] mg/L	[Ca ²⁺] mol/L
G1-1	0	6.027	0.00	3.778	2.856x10 ⁻⁶	511	1.203x10 ⁻²
G1-2	11	6.163	3.50	40.67	3.063x10 ⁻⁵	649	1.492x10 ⁻²
G1-3	21	6.251	7.50	64.75	4.860x10 ⁻⁵	775	1.753x10 ⁻²
G1-4	36	6.343	14.50	78.51	5.859x10 ⁻⁵	954	2.110x10 ⁻²
G1-5	99	6.337	33.00	23.38	1.740x10 ⁻⁵	1129	2.499x10 ⁻²
G1-6	129	6.317	43.50	28.74	2.143x10 ⁻⁵	1124	2.504x10 ⁻²

initial seed material 1.293 g

† aqueous phase supersaturated with respect to aragonite and otavite

Table A.30 Data from experiment G2

Sample #	elapsed time hours	pH	cumulative CaCdCl ₂ titrated mL	[Cd _T] mg/L	[Cd ²⁺] mol/L	[Ca _T] mg/L	[Ca ²⁺] mol/L
G2-1	0	6.020	0.00	ND	ND	539	1.268x10 ⁻²
G2-2	21.0	6.056	2.60	3.378	2.551x10 ⁻⁶	585	1.369x10 ⁻²
G2-3	32.1	6.051	5.40	3.227	2.438x10 ⁻⁶	580	1.358x10 ⁻²
G2-4	59.6	6.057	8.70	2.725	2.057x10 ⁻⁶	586	1.372x10 ⁻²
G2-5	83.9	6.050	11.50	2.633	1.989x10 ⁻⁶	586	1.372x10 ⁻²

ND - not detected

initial seed material 1.275 g

Table A.31 Data from experiment G3†

Sample #	elapsed time hours	pH	cumulative CaCdCl ₂ titrated mL	[Cd _T] mg/L	[Cd ²⁺] mol/L	[Ca _T] mg/L	[Ca ²⁺] mol/L
G3-1	0	6.018	0.00	0.48	3.654x10 ⁻⁷	525	1.235x10 ⁻²
G3-2	20.8	6.157	21.75	19.5	1.468x10 ⁻⁵	732	1.687x10 ⁻²
G3-3	29.1	6.154	30.50	14.9	1.121x10 ⁻⁵	732	1.688x10 ⁻²
G3-4	43.3	6.115	45.50	9.61	7.241x10 ⁻⁶	699	1.623x10 ⁻²

initial seed material 1.276 g

† aqueous phase supersaturated with respect to aragonite and otavite

Table A.32 Data from experiment G4

Sample #	elapsed time hours	pH	cumulative CaCdCl ₂ titrated mL	[Cd _T] mg/L	[Cd ²⁺] mol/L	[Ca _T] mg/L	[Ca ²⁺] mol/L
G4-1	0	6.019	0.00	ND	ND	541	1.274x10 ⁻²
G4-2	25.6	6.067	7.75	3.301	2.492x10 ⁻⁶	623	1.458x10 ⁻²
G4-3	46.6	6.073	14.00	3.918	2.957x10 ⁻⁶	626	1.466x10 ⁻²
G4-4	74.8	6.076	22.50	3.611	2.725x10 ⁻⁶	643	1.501x10 ⁻²

ND - not detected

initial seed material 1.250 g

Table A.33 Data from experiment G5

Sample #	elapsed time hours	pH	cumulative CaCdCl ₂ titrated mL	[Cd _T] mg/L	[Cd ²⁺] mol/L	[Ca _T] mg/L	[Ca ²⁺] mol/L
G5-1	0	6.016	0.00	ND	ND	529	1.246x10 ⁻²
G5-2	53.5	6.045	5.50	2.250	1.700x10 ⁻⁶	583	1.367x10 ⁻²
G5-3	117.3	6.061	12.50	2.681	2.025x10 ⁻⁶	606	1.422x10 ⁻²
G5-4	145.5	6.057	15.75	2.298	1.736x10 ⁻⁶	584	1.367x10 ⁻²

ND - not detected

initial seed material 1.250 g

Table A.34 Data from experiment G6

Sample #	elapsed time hours	pH	cumulative CaCdCl ₂ titrated mL	[Cd _T] mg/L	[Cd ²⁺] mol/L	[Ca _T] mg/L	[Ca ²⁺] mol/L
G6-1	0	6.021	0.00	ND	ND	507	1.190x10 ⁻²
G6-2	53.2	6.025	4.35	1.453	1.099x10 ⁻⁶	594	1.396x10 ⁻²
G6-3	93.0	6.027	9.85	1.430	1.081x10 ⁻⁶	583	1.372x10 ⁻²
G6-4	146.0	6.033	14.35	1.570	1.187x10 ⁻⁶	643	1.518x10 ⁻²

ND - not detected

initial seed material 1.303 g

Table A.35 Data from experiment G7

Sample #	elapsed time hours	pH	cumulative CaCdCl ₂ titrated mL	[Cd _T] mg/L	[Cd ²⁺] mol/L	[Ca _T] mg/L	[Ca ²⁺] mol/L
G7-1	0	6.035	0.00	ND	ND	507	1.185x10 ⁻²
G7-2	66.7	6.028	7.00	1.057	7.992x10 ⁻⁷	507	1.187x10 ⁻²
G7-3	114.0	6.029	11.25	1.069	8.084x10 ⁻⁷	566	1.322x10 ⁻²
G7-4	143.4	6.031	15.50	1.180	8.921x10 ⁻⁷	521	1.224x10 ⁻²

ND - not detected

initial seed material 5.303 g

Table A.36 Data from experiment G8

Sample #	elapsed time hours	pH	cumulative CaCdCl ₂ titrated mL	[Cd _T] mg/L	[Cd ²⁺] mol/L	[Ca _T] mg/L	[Ca ²⁺] mol/L
G8-1	0	6.035	0.00	ND	ND	507	1.190x10 ⁻²
G8-2	95.9	6.026	8.35	1.493	1.128x10 ⁻⁶	529	1.240x10 ⁻²
G8-3	143.4	6.027	12.60	1.460	1.104x10 ⁻⁶	551	1.295x10 ⁻²
G8-4	186.0	6.027	16.30	1.522	1.151x10 ⁻⁶	588	1.383x10 ⁻²

ND - not detected

initial seed material 5.269 g

Table A.37 Data from experiment G9

Sample #	elapsed time hours	pH	cumulative CaCdCl ₂ titrated mL	[Cd _T] mg/L	[Cd ²⁺] mol/L	[Ca _T] mg/L	[Ca ²⁺] mol/L
G9-1	0	6.032	0.00	ND	ND	535	1.257x10 ⁻²
G9-2	51.9	6.035	10.75	1.822	1.377x10 ⁻⁶	544	1.277x10 ⁻²
G9-3	69.9	6.038	14.50	1.833	1.385x10 ⁻⁶	544	1.278x10 ⁻²
G9-4	93.7	6.041	19.25	1.554	1.175x10 ⁻⁶	548	1.285x10 ⁻²

ND - not detected

initial seed material 5.013 g

Table A.38 Data from experiment G10

Sample #	elapsed time hours	pH	cumulative CaCdCl ₂ titrated mL	[Cd _T] mg/L	[Cd ²⁺] mol/L	[Ca _T] mg/L	[Ca ²⁺] mol/L
G10-1	0	6.037	0.00	ND	ND	511	1.199x10 ⁻²
G10-2	96.8	6.033	4.30	1.009	7.629x10 ⁻⁷	539	1.265x10 ⁻²
G10-3	166.7	6.028	7.35	0.773	5.843x10 ⁻⁷	539	1.266x10 ⁻²
G10-4	195.2	6.030	8.65	0.993	7.508x10 ⁻⁷	516	1.213x10 ⁻²

ND - not detected

initial seed material 5.032 g

Table A.39 Data from experiment G11

Sample #	elapsed time hours	pH	cumulative CaCdCl ₂ titrated mL	[Cd _T] mg/L	[Cd ²⁺] mol/L	[Ca _T] mg/L	[Ca ²⁺] mol/L
G11-1	0	6.018	0.00	2.299	1.738x10 ⁻⁶	532	1.250x10 ⁻²
G11-2	42.5	6.042	9.25	1.431	1.081x10 ⁻⁶	535	1.254x10 ⁻²
G11-3	69.7	6.040	15.00	1.406	1.063x10 ⁻⁶	536	1.257x10 ⁻²
G11-4	94.3	6.037	23.40	1.650	1.247x10 ⁻⁶	553	1.299x10 ⁻²

initial seed material 5.152 g

Table A.40 Data from experiment G12

Sample #	elapsed time hours	pH	cumulative CaCdCl ₂ titrated mL	[Cd _T] mg/L	[Cd ²⁺] mol/L	[Ca _T] mg/L	[Ca ²⁺] mol/L
G12-1	0	6.020	0.00	0.0301	2.281x10 ⁻⁸	538	1.265x10 ⁻²
G12-2	43.6	6.022	4.20	0.869	6.572x10 ⁻⁷	516	1.213x10 ⁻²
G12-3	71.6	6.010	5.95	1.199	9.072x10 ⁻⁷	494	1.165x10 ⁻²
G12-4	95.5	6.005	7.40	1.425	1.078x10 ⁻⁶	509	1.199x10 ⁻²
G12-5*	115.8	6.003	8.70	1.673	1.266x10 ⁻⁶	513	1.210x10 ⁻²

* syringe tip filter torn
initial seed material 4.301 g

Table A.41 Data from experiment H1

Sample #	time hours	pH	cumulative CaCdCl ₂ titrated mL	[Cd _T] mg/L	[Cd ²⁺] mol/L	[Ca _T] mg/L	[Ca ²⁺] mol/L
H1-1	0.0	6.010	0.00	0.030	2.298x10 ⁻⁸	492	1.160x10 ⁻²
H1-2	22.5	6.042	5.75	0.619	4.681x10 ⁻⁷	536	1.259x10 ⁻²
H1-3	44.6	6.035	10.25	0.164	1.241x10 ⁻⁷	535	1.257x10 ⁻²
H1-4	67.5	6.037	20.25	0.172	1.297x10 ⁻⁷	532	1.250x10 ⁻²

initial seed material 5.017 g

Table A.42 Data from experiment H2[†]

Sample #	time minutes	pH	cumulative CaCdCl ₂ titrated mL	[Cd _T] mg/L	[Cd ²⁺] mol/L	[Ca _T] mg/L	[Ca ²⁺] mol/L
H2-1	0	6.014	0.00	0.709	5.367x10 ⁻⁷	485	1.141x10 ⁻²
H2-2	39	6.126	11.25	0.564	4.245x10 ⁻⁷	642	1.485x10 ⁻²
H2-3	58	6.128	17.75	0.536	4.036x10 ⁻⁷	671	1.553x10 ⁻²
H2-4	73	6.125	22.50	0.551	4.148x10 ⁻⁷	636	1.472x10 ⁻²

[†] aqueous phase supersaturated with respect to aragonite
initial seed material 4.899 g

Table A.43 Data from experiment H3

Sample #	time hours	pH	cumulative CaCdCl ₂ titrated mL	[Cd _T] mg/L	[Cd ²⁺] mol/L	[Ca _T] mg/L	[Ca ²⁺] mol/L
H3-1	0.0	6.017	0.00	0.0200	1.511x10 ⁻⁸	544	1.282x10 ⁻²
H3-2	47.7	6.029	4.30	0.0892	6.743x10 ⁻⁸	539	1.265x10 ⁻²
H3-3	95.1	6.026	8.45	0.0926	7.001x10 ⁻⁸	560	1.316x10 ⁻²
H3-4	143.9	6.024	13.05	0.126	9.526x10 ⁻⁸	549	1.290x10 ⁻²

initial seed material 5.021 g

Table A.44 Data from experiment H4†

Sample #	time minutes	pH	cumulative CaCdCl ₂ titrated mL	[Cd _T] mg/L	[Cd ²⁺] mol/L	[Ca _T] mg/L	[Ca ²⁺] mol/L
H4-1	0	6.008	0.00	0.0819	6.608x10 ⁻⁸	542	1.277x10 ⁻²
H4-2	41	6.226	11.50	3.11	2.498x10 ⁻⁶	902	2.051x10 ⁻²
H4-3	108	6.227	30.50	1.33	1.072x10 ⁻⁶	929	2.111x10 ⁻²
H4-4	143	6.221	40.25	1.33	1.057x10 ⁻⁶	919	2.088x10 ⁻²

† aqueous phase supersaturated with respect to aragonite

initial seed material 1.407 g

Table A.45 Data from experiment H5

Sample #	time hours	pH	cumulative CaCdCl ₂ titrated mL	[Cd _T] mg/L	[Cd ²⁺] mol/L	[Ca _T] mg/L	[Ca ²⁺] mol/L
H5-1	0	6.028	0.00	0.0106	8.030x10 ⁻⁹	520	1.222x10 ⁻²
H5-2	27.3	6.085	5.75	0.314	1.524x10 ⁻⁷	574	1.337x10 ⁻²
H5-3	44.9	6.046	14.75	0.158	1.197x10 ⁻⁷	543	1.274x10 ⁻²
H5-4	72.6	6.053	20.75	0.138	1.046x10 ⁻⁷	518	1.212x10 ⁻²

initial seed material 1.348 g

Table A.46 Data from experiment H6†

Sample #	time hours	pH	cumulative CaCdCl ₂ titrated mL	[Cd _T] mg/L	[Cd ²⁺] mol/L	[Ca _T] mg/L	[Ca ²⁺] mol/L
H6-1	0	6.000	0.00	0.0132	9.968x10 ⁻⁹	508	1.199x10 ⁻²
H6-2	46.0	6.154	7.85	ND	ND	374	8.827x10 ⁻³
H6-3	66.6	6.171	11.35	0.0268	2.010x10 ⁻⁸	271	6.229x10 ⁻³
H6-4	92.1	6.245	15.70	0.00484	3.623x10 ⁻⁹	219	1.959x10 ⁻³

† CaCl₂ syringe broke during experiment, replacement syringe leaked around plunger

ND - not detected

initial seed material 1.260 g

Table A.47 Data from experiment H7†

Sample #	elapsed time hours	pH	cumulative CaCdCl ₂ titrated mL	[Cd _T] mg/L	[Cd ²⁺] mol/L	[Ca _T] mg/L	[Ca ²⁺] mol/L
H7-1	0	5.999	0.00	0.0331	2.507x10 ⁻⁸	524	1.238x10 ⁻²
H7-2	3.65	6.126	10.75	0.783	5.894x10 ⁻⁷	699	1.618x10 ⁻²
H7-3	5.12	6.131	14.75	0.756	5.682x10 ⁻⁷	717	1.659x10 ⁻²
H7-4	6.92	6.123	19.75	0.711	5.357x10 ⁻⁷	660	1.528x10 ⁻²

† aqueous phase supersaturated with respect to aragonite

initial seed material 1.269 g

Table A.48 Data from experiment H8†

Sample #	elapsed time hours	pH	cumulative CaCdCl ₂ titrated mL	[Cd _T] mg/L	[Cd ²⁺] mol/L	[Ca _T] mg/L	[Ca ²⁺] mol/L
H8-1	0	6.008	0.00	0.197	1.493x10 ⁻⁷	505	1.191x10 ⁻²
H8-2	42.6	6.160	10.10	0.230	1.730x10 ⁻⁷	400	9.231x10 ⁻³
H8-3	49.1	6.155	11.70	0.210	1.582x10 ⁻⁷	419	9.647x10 ⁻³
H8-4	64.8	6.162	15.30	0.206	1.547x10 ⁻⁷	408	9.386x10 ⁻³

† CaCl₂ replacement syringe leaked around plunger

initial seed material 1.256 g

Table A.49 Data from experiment H9

Sample #	elapsed time hours	pH	cumulative CaCdCl ₂ titrated mL	[Cd _T] mg/L	[Cd ²⁺] mol/L	[Ca _T] mg/L	[Ca ²⁺] mol/L
H9-1	0	6.009	0.00	0.0303	2.296x10 ⁻⁸	507	1.196x10 ⁻²
H9-2	18.2	6.106	19.40	0.497	3.749x10 ⁻⁷	611	1.420x10 ⁻²
H9-3	22.0	6.100	23.15	0.468	3.532x10 ⁻⁷	600	1.394x10 ⁻²
H9-4	27.1	6.106	28.65	0.494	3.724x10 ⁻⁷	609	1.414x10 ⁻²

initial seed material 1.275 g

Table A.50 Data from experiment H10

Sample #	elapsed time hours	pH	cumulative CaCdCl ₂ titrated mL	[Cd _T] mg/L	[Cd ²⁺] mol/L	[Ca _T] mg/L	[Ca ²⁺] mol/L
H10-1	0	6.017	0.00	0.0393	2.975x10 ⁻⁸	515	1.213x10 ⁻²
H10-2	45.9	6.032	9.85	0.121	9.149x10 ⁻⁸	531	1.246x10 ⁻²
H10-3	73.7	6.029	16.00	0.128	9.694x10 ⁻⁸	518	1.217x10 ⁻²
H10-4	97.6	6.028	22.00	0.123	9.337x10 ⁻⁸	521	1.225x10 ⁻²

initial seed material 5.074 g

Table A.51 Data from experiment H12

Sample #	time hours	pH	cumulative CaCdCl ₂ titrated mL	[Cd _T] mg/L	[Cd ²⁺] mol/L	[Ca _T] mg/L	[Ca ²⁺] mol/L
H12-1	0	6.027	0.00	0.0041	3.078x10 ⁻⁹	505	1.188x10 ⁻²
H12-2	18.6	6.055	10.80	0.113	9.268x10 ⁻⁸	522	1.223x10 ⁻²
H12-3	49.5	6.045	15.05	0.183	1.384x10 ⁻⁷	530	1.244x10 ⁻²
H12-4	72.8	6.051	23.30	0.0392	2.961x10 ⁻⁸	526	1.231x10 ⁻²

initial seed material 4.998 g

Appendix B
Data From XPS Analyses

Table B.1 XPS Atomic concentration table, multiplex scans.

FileName	Sample	C1s	CH	O1s	Ca2p	Cd3d5
		[0.314]	[0.314]	[0.733]	[1.927]	[4.148]
adv1863.spe	E6	16.66	6.55	56.92	0.08	19.78
adv1864.spe	E10	16.46	5.61	57.66	0.20	20.07
adv1865.spe	E12uw	17.45	6.49	55.99	0.19	19.89
adv1866.spe	E12w	16.52	6.28	57.00	0.11	20.09
adv1867.spe	E13	16.56	5.81	57.56	0.10	19.97
adv1868.spe	Calcite	17.07	9.26	57.85	15.82	0.01
adv1869.spe	Otavite	17.22	6.25	56.58	0.04	19.90
adv1870.spe	F1	16.76	6.40	56.97	0.94	18.93
adv1871.spe	F4	17.41	6.40	56.04	0.32	19.83
adv1872.spe	F7	17.02	5.33	57.59	0.31	19.75
adv1873.spe	F9	14.94	5.53	60.20	0.08	19.26
adv1874.spe	#37	16.65	8.82	57.86	13.53	3.14
adv1875.spe	#40	18.15	5.95	58.82	15.32	1.76
adv1876.spe	H1	17.77	8.11	58.03	15.87	0.23
adv1877.spe	G5	16.95	11.07	55.65	11.49	4.84

Table B.1 XPS Atomic concentration table, multiplex scans, con't.

FileName	Sample	C1s	CH	O1s	Ca2p	Cd3d5
		[0.314]	[0.314]	[0.733]	[1.927]	[4.148]
adv1878.spe	G7	17.02	8.46	58.13	13.96	2.43
adv1879.spe	G8	17.23	7.96	58.44	13.74	2.63
adv1880.spe	G10	17.74	9.85	56.32	14.08	2.01
adv1881.spe	H2	18.52	7.25	57.71	16.21	0.31
adv1882.spe	H3	18.45	7.20	58.11	16.14	0.12
adv1883.spe	H4	18.17	9.02	56.28	16.22	0.32
adv2186.spe	G4	17.90	11.08	54.24	12.34	4.43
adv2187.spe	G8	17.90	9.28	56.04	14.02	2.78
adv2188.spe	A3w	17.61	9.36	56.30	13.95	2.78
adv2189.spe	A3uw	17.97	10.18	55.29	13.71	2.85
adv2190.spe	G12	17.60	10.34	55.77	14.22	2.06
adv2191.spe	F13	17.75	6.95	55.40	0.30	19.61
adv2192.spe	E7	17.86	6.68	55.60	0.16	19.70
adv2193.spe	F8	17.16	6.13	56.71	0.38	19.63
adv2194.spe	F3	17.80	7.25	55.39	0.40	19.16
adv2195.spe	F12	17.52	6.90	55.73	0.41	19.43
adv2196.spe	F14	17.55	6.68	55.83	0.35	19.58
adv2197.spe	F11	17.57	6.33	55.99	0.38	19.73
adv2198.spe	A4uw	17.98	5.93	55.61	0.31	20.16
adv2199.spe	F10	17.77	7.36	55.03	0.20	19.64
adv2200.spe	F5	18.30	5.69	55.59	0.42	20.00
adv2201.spe	F6	17.77	6.08	55.63	0.35	20.17
adv2202.spe	E9	17.62	5.64	56.36	0.18	20.20

Table B.1 XPS Atomic concentration table, multiplex scans, con't

FileName	Sample	C1s	CH	O1s	Ca2p	Cd3d5
		[0.314]	[0.314]	[0.733]	[1.927]	[4.148]
adv2203.spe	E4	18.51	6.33	54.99	0.16	20.01
adv2204.spe	E11	18.23	6.22	55.35	0.20	20.00
adv2205.spe	A4w	18.22	5.47	56.13	0.25	19.92
adv2206.spe	F2	14.59	12.35	59.30	0.31	13.45
adv2207.spe	E8	17.82	5.02	56.71	0.17	20.27
adv2208.spe	E1	17.06	6.90	56.26	0.08	19.71
adv2209.spe	E14	17.74	5.77	56.40	0.22	19.88
adv2210.spe	E3	18.83	4.99	55.96	0.17	20.06
adv2162.spe	H8	15.35	15.05	55.31	14.06	0.23
adv2163.spe	H5	18.04	7.87	57.65	16.25	0.19
adv2164.spe	H10	18.27	7.75	57.36	16.45	0.18
adv2165.spe	H9	17.28	12.40	54.47	15.48	0.36
adv2166.spe	G2	17.43	10.93	55.06	11.95	4.63
adv2167.spe	H12w	18.25	10.26	55.45	15.91	0.14
adv2168.spe	H12uw	17.61	12.33	54.38	15.59	0.09
adv2169.spe	H7	17.47	10.83	55.63	15.71	0.36
adv2170.spe	G6	18.03	9.67	55.52	12.34	4.44
adv2171.spe	G9	18.63	7.02	57.19	13.97	3.19
adv2172.spe	G11	18.35	7.65	57.04	13.79	3.17
adv2173.spe	G5	17.18	11.46	54.78	11.54	5.05

Table B.2 XPS Atomic Concentration Table, Survey Scans

FileName	Sample	Cl s	O 1s	Na KLL	S 2p	Cl 2p	Ca 2p	Cd 3d5
		[0.314]	[0.733]	[0.000]	[0.368]	[0.954]	[1.927]	[4.148]
adv1884.spe	E6	25.80	54.31	1.12	0.59	0.22	0.11	17.84
adv1885.spe	E10	26.40	54.64	0.52	0.21	0.23	0.14	17.82
adv1886.spe	E12uw	25.48	52.14	3.11	0.32	1.03	0.15	17.73
adv1887.spe	E12w	25.69	55.28	0.33	0.43	0.18	0.10	17.99
adv1888.spe	E13	25.16	55.64	0.47	0.53	0.18	0.08	17.93
adv1889.spe	Calcite	27.56	55.91	1.14	0.33	0.37	14.55	0.02
adv1890.spe	Otavite	26.35	55.09	0.00	0.15	0.14	0.04	18.23
adv1891.spe	F1	26.73	54.51	0.22	0.19	0.24	0.88	17.19
adv1892.spe	F4	26.57	54.40	0.24	0.32	0.14	0.30	17.95
adv1893.spe	F7	24.84	56.50	0.00	0.47	0.11	0.35	17.72
adv1894.spe	F9	24.63	57.70	0.00	0.40	0.17	0.40	16.66
adv1895.spe	#37	28.28	55.44	0.43	0.33	0.55	12.24	2.62
adv1896.spe	#40	26.48	56.24	0.99	0.22	0.48	14.15	1.44
adv1897.spe	H1	26.79	55.44	1.73	0.59	0.57	14.66	0.19
adv1898.spe	G5	27.33	53.00	3.10	1.22	0.73	10.39	4.13

Table B.2 XPSAtomic Concentration Table, Survey Scans, con't.

FileName	Sample	C1s	O1s	Na KLL	Si2p	S2p	Cl2p	Ca2p	Cd3d5
		[0.314]	[0.733]	[0.000]	[0.368]	[0.717]	[0.954]	[1.927]	[4.148]
adv1899.spe	G7	24.51	56.55	1.99	1.58	0.05	0.48	12.87	1.97
adv1900.spe	G8	25.97	55.71	2.61	0.49	0.03	0.58	12.44	2.17
adv1901.spe	G10	26.90	54.37	1.69	1.57	0.05	0.53	13.24	1.66
adv1902.spe	H2	27.78	55.47	0.99	0.19	0.02	0.38	14.92	0.24
adv1903.spe	H3	26.27	57.32	0.00	0.90	0.02	0.11	15.27	0.10
adv1904.spe	H4	28.70	53.50	0.68	0.24	0.15	0.78	14.69	0.26
adv2304.spe	G4	28.73	54.50	1.73	0.42	0.34	0.88	9.38	4.03
adv2305.spe	F13	25.43	56.04	0.39	0.14	0.08	0.28	0.23	17.41
adv2306.spe	E7	25.65	55.82	0.13	0.12	0.12	0.27	0.09	17.80
adv2307.spe	G8	27.77	56.78	1.38	0.21	0.20	0.59	10.39	2.69
adv2308.spe	F8	23.80	57.47	0.06	0.23	0.09	0.17	0.02	17.96
adv2309.spe	A3w	27.24	59.53	0.24	0.06	0.23	0.18	9.97	2.54
adv2310.spe	A3uw	28.06	56.16	1.69	0.07	0.38	0.63	10.36	2.65
adv2311.spe	G12	27.31	57.41	1.29	0.44	0.14	0.54	10.82	2.06
adv2312.spe	F3	23.98	57.34	0.00	0.24	0.15	0.14	0.29	17.87

Table B.2 XPSAtomic Concentration Table, Survey Scans, con't.

FileName	Sample	C1s	O1s	Na KLL	Si2p	S2p	Cl2p	Ca2p	Cd3d5
		[0.314]	[0.733]	[0.000]	[0.368]	[0.717]	[0.954]	[1.927]	[4.148]
adv12313.spe	F12	23.81	57.16	0.12	0.11	0.12	0.22	0.28	18.19
adv12314.spe	F14	23.66	57.54	0.15	0.16	0.10	0.08	0.29	18.02
adv12315.spe	F11	23.91	57.38	0.10	0.19	0.07	0.19	0.26	17.90
adv12211.spe	A4uw	24.24	50.15	2.01	5.69	0.00	1.20	0.27	16.44
adv12212.spe	F10	25.48	51.28	0.33	5.71	0.00	0.31	0.20	16.69
adv12213.spe	F5	24.63	51.58	0.07	6.02	0.00	0.20	0.36	17.14
adv12214.spe	F6	25.68	51.17	0.09	5.90	0.05	0.18	0.36	16.56
adv12215.spe	E9	24.85	52.55	0.04	5.52	0.08	0.17	0.12	16.68
adv12216.spe	E4	25.45	51.53	0.05	5.59	0.05	0.11	0.16	17.06
adv12217.spe	E11	24.52	52.06	0.22	5.74	0.01	0.15	0.13	17.18
adv12218.spe	A4w	24.62	52.07	0.42	5.61	0.03	0.21	0.14	16.90
adv12219.spe	F2	26.60	57.99	0.23	3.93	0.00	0.14	0.21	10.90
adv12220.spe	E8	24.05	52.70	0.21	5.92	0.04	0.10	0.18	16.80
adv12221.spe	E1	25.20	52.36	0.14	5.63	0.00	0.15	0.17	16.35
adv12222.spe	E14	23.50	54.41	0.15	4.75	0.07	0.19	0.08	16.87

Table B.2 XPSAtomic Concentration Table, Survey Scans, con't.

FileName	Sample	C1s	O1s	Na KLL	Si2p	S2p	Cl2p	Ca2p	Cd3d5
		[0.314]	[0.733]	[0.000]	[0.368]	[0.717]	[0.954]	[1.927]	[4.148]
advf2223.spe	E3	23.96	53.22	0.17	5.94	0.02	0.12	0.07	15.60
advf2174.spe	H8	33.99	50.75	0.44	0.99	0.26	0.17	13.18	0.22
advf2175.spe	H5	27.91	54.77	0.33	1.02	0.14	0.11	15.56	0.16
advf2176.spe	H10	27.88	55.13	0.00	1.26	0.09	0.05	15.45	0.15
advf2177.spe	H9	32.25	51.91	0.25	0.61	0.26	0.16	14.27	0.30
advf2178.spe	G2	29.83	50.95	1.62	2.36	0.11	0.66	10.63	3.85
advf2179.spe	H12w	30.76	53.37	0.14	0.18	0.15	0.07	15.21	0.12
advf2180.spe	H12uw	31.39	50.95	1.65	0.18	0.30	0.90	14.54	0.09
advf2181.spe	H7	29.99	53.35	0.52	0.38	0.25	0.15	15.06	0.29
advf2182.spe	G6	28.23	52.66	1.20	2.42	0.08	0.70	10.99	3.73
advf2183.spe	G9	26.70	53.96	1.44	1.82	0.10	0.74	12.59	2.65
advf2184.spe	G11	27.81	53.33	1.19	2.07	0.07	0.61	12.30	2.62
advf2185.spe	G5	29.68	50.60	1.69	2.81	0.17	0.78	10.10	4.17

Appendix C
Data from XRD Analyses

Table C.1 D-spacings for calcite seed material.

D-spacing	intensity	h	k	l	D-spacing	intensity	h	k	l
3.85026	7.5	1	0	2	1.58714	1.5	1	0	10
3.03414	100.0	1	0	4	1.52518	7.5	2	1	4
2.84296	2.8	0	0	6	1.51778	3.8	2	0	8
2.49369	9.21	1	1	0	1.50967	3.6	1	1	9
2.28438	17.8	1	1	3	1.47326	2.7	2	1	5
2.09436	15.9	2	0	2	1.44046	8.8	3	0	0
1.92722	6.9	2	0	4	1.42219	4.3	0	0	12
1.91244	22.4	1	0	8	1.35682	2.0	2	1	7
1.87519	26.1	1	1	6	1.33919	3.5	2	0	10
1.62584	4.3	2	1	1	1.29681	4.4	2	1	8
1.60405	11.8	2	1	2	1.28495	1.3	3	0	6

Table C.2 D-spacings for otavite seed material.

D-spacing	intensity	h	k	l	D-spacing	intensity	h	k	l
3.78224	58.7	1	0	2	1.60652	1.4	2	1	1
2.94791	100.0	1	0	4	1.58369	17.9	2	1	2
2.71552	3.4	0	0	6	1.52211	5.2	1	0	10
2.46580	33.1	1	1	0	1.50089	13.4	2	1	4
2.24558	6.3	1	1	3	1.47386	6.1	2	0	8
2.06585	31.3	2	0	2	1.42371	10.7	3	0	0
1.89115	17.8	2	0	4	1.35771	3.6	0	0	12
1.83798	29.0	1	0	8	1.32659	0.6	2	1	7
1.82599	43.4	1	1	6	1.29534	4.7	2	0	10

Table C.3 D-spacings for sample G4.

D-spacing	intensity	h	k	l	D-spacing	intensity	h	k	l
3.84383	14.9	1	0	2	1.58467	2.5	1	0	10
3.02876	100.0	1	0	4	1.52330	9.8	2	1	4
2.84055	1.9	0	0	6	1.51565	5.9	2	0	8
2.49007	26.2	1	1	0	1.50712	4.3	1	1	9
2.28283	28.6	1	1	3	1.47105	2.5	2	1	5
2.09186	31.3	2	0	2	1.43838	9.8	3	0	0
1.92403	10.0	2	0	4	1.41959	4.5	0	0	12
1.90941	23.1	1	0	8	1.35436	1.7	2	1	7
1.87280	25.0	1	1	6	1.33659	2.2	2	0	10
1.62348	3.9	2	1	1	1.29496	4.2	2	1	8
1.60195	17.6	2	1	2	1.28323	0.6	3	0	6

Table C.4 D-spacings for sample F13.

D-spacing	intensity	h	k	l	D-spacing	intensity	h	k	l
3.77948	58.9	1	0	2	1.58241	21.5	2	1	2
2.94577	100.0	1	0	4	1.52301	6.0	1	0	10
2.71550	3.6	0	0	6	1.49992	17.2	2	1	4
2.46360	38.1	1	1	0	1.47346	7.1	2	0	8
2.24362	6.6	1	1	3	1.45926	1.0	1	1	9
2.06394	32.0	2	0	2	1.44614	0.5	2	1	5
1.88936	15.9	2	0	4	1.42272	11.4	3	0	0
1.83786	25.0	1	0	8	1.35799	3.6	0	0	12
1.82505	37.6	1	1	6	1.32592	0.5	2	1	7
1.60531	1.5	2	1	1	1.29530	4.4	2	0	10

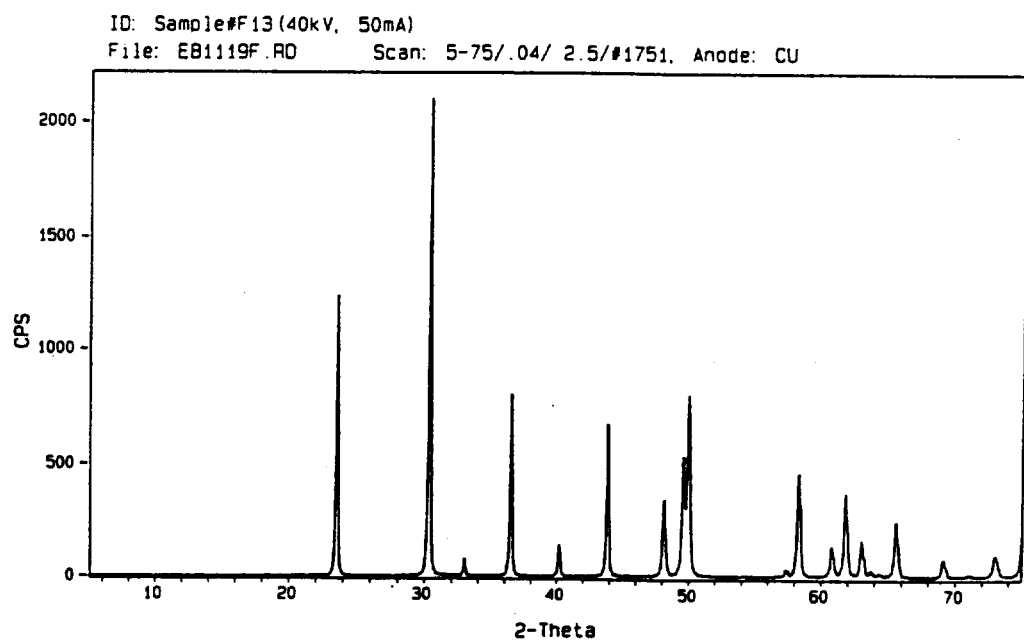
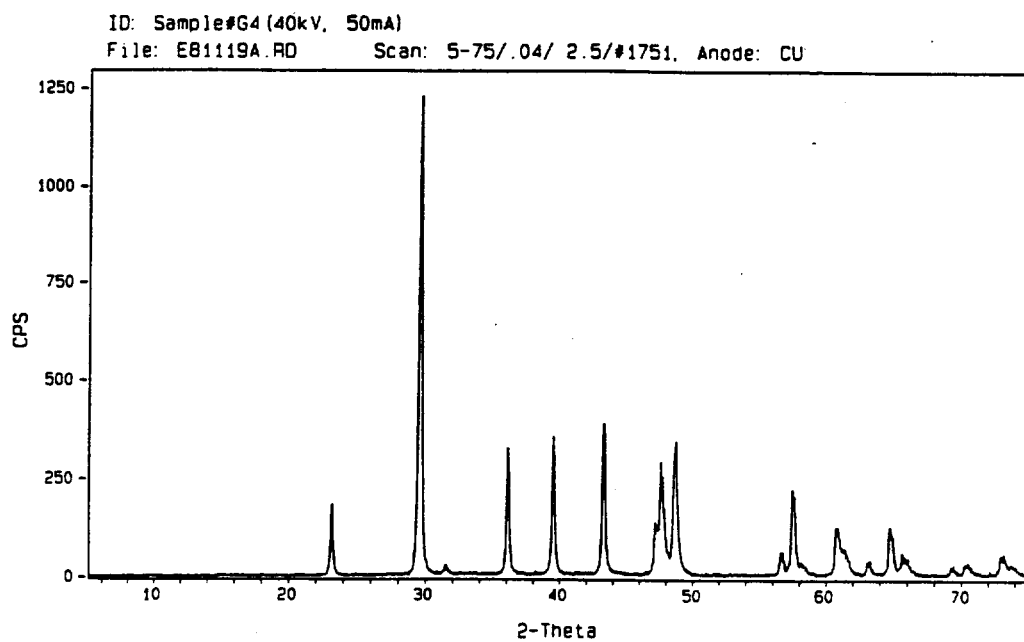


Figure C.1 XRD spectra for samples G4 and F13.

Appendix D

MeTran Source Code

! Last change: DJB 3 Nov 98 10:48 am

=====

! MeTran.F90 -- requires MeTranGV.F90

!
! 1-D advective-dispersive transport of a divalent
! metal cation (Me²⁺) in a saturated column of sand
! including the following mass transfer processes:
! - linear adsorption to sand
! - surface partitioning to calcite
! - solid state diffusion into calcite

!
! version 1.04 -- September 1998

!
! developed by: David J. Brush
! University of Waterloo
! Environmental Group
! Dept. of Civil Engineering

! The user may modify the code and give it to third parties,
! provided that an acknowledgement to the original code is retained.

! revision notes:

! 1.01 - misc. bugs
! 1.02 - misc. bugs, improved convergence criteria
! & new values for numColum and delTimeMax
! 1.03 - added Crank-Nicolson method of time integration
! & added comments to source code
! 1.04 - diffusion OFF when lenCalc < or = 0

=====

! main program

```

!-----
program MeTran
  use globalVariables ! use global variables module in MeTranGV.F90
  implicit none
  iError=0          ! initialize counters & flags
  numScreen=0
  iScreen=1
  iAlocate=0
  call screenOut()
  call inputListFile()
  if (iError>0) stop
  do iSim=1,numSim    ! multiple simulation loop
    iError=0          ! re-initialize error counter
    call inputDataFile()
    if (iError>0) cycle ! skip simulation if errors
    call dataCheck()
    if (iError>0) cycle
    call initialize()
    call screenOut()
    call timeSerOut(0)
    do                ! time loop
      cOld=c          ! update primary arrays
      xOld=x
      call timeStep()
      call solveSystem()
      call totalMass()
      call timeSerOut(1)
      call screenOut()
      if (iTimeEnd>0) exit ! end time loop
      if (iTimeOff==1) then ! turn off source if req.'d
        aqueMe=0.0
        iTimeOff=2
      end if
    end do
    call profileOut()
    call performOut()
  end do
end program MeTran

```

```

!=====
! solveSystem
! -routine to solve concentration and mole fraction corrections
! -full Newton-Raphson iteration is used for non-linear problems

```

```

! (surface partitioning with or without solid state diffusion)
! -1D column profile solved directly with TDMA solver
! -quasi-2D calcite field solved by lines with TDMA solver
! -convergence (for non-linear problems) is obtained when the
! the sum of absolute residuals is reduced by several orders of
! magnitude or the change between iterations becomes small
! (e.g., if normTol = 1.e-4 then the residuals are reduced
! by at least 4 orders from the initial value)
!-----
subroutine solveSystem()
  use globalVariables
  implicit none
  interface
    subroutine tdmaSolver(soln,coefP,coefW,coefE,src)
      real (kind=8), intent (in), dimension (:) :: coefP, coefW, coefE, src
      real (kind=8), intent (in out), dimension (:) :: soln
    end subroutine tdmaSolver
  end interface
  integer :: i,j
  real (kind=8) :: absumMasResOld, absumMasResOld2, residNorm

  normTol=1.0e-4 ! set normalized convergence tolerance

  call coefCalcite()
  call srcColumn()
  absumMasResOld=absumMasResid ! set old abs. sum of mass residuals
  absumMasResOld2=absumMasResid ! used for convergence crit.

  iNewt=0
  do ! solution loop
    iNewt=iNewt+1
    call coefColumn()
    call tdmaSolver(cDel,cCoef,cCoefW,cCoefE,cSrc)
    do i=1,numColum ! correct current concentration
      c(i)=c(i)+cDel(i)
    end do
    if (iSoliDif>0) then ! check for diffusion
      do i=1,numColum ! solve calcite profile line by line
        call srcCalcite(i)
        call tdmaSolver (xDel,xCoef,xCoefW,xCoefE,xSrc)
        do j=1,numCalc ! correct current mole fraction
          x(i,j)=x(i,j)+xDel(j)
        end do
      end do
    end do
  end do

```

```

end if
call srcColumn()
! calculate residual norm
residNorm=abs(absumMasResOld-absumMasResid)/absumMasResOld2
absumMasResOld=absumMasResid
if (residNorm<normTol) exit ! check for convergence
if (iNewt==maxNewt) then ! check for the maximum Newton iteration
  if (maxNewt>1) numNoConv=numNoConv+1
  exit
end if
end do
call boundaryCalc()
numNewt=numNewt+iNewt
end subroutine solveSystem

```

```

=====
! coefColumn
! -routine to calculate matrix coefs. for the concentration
! correction using the Newton-Raphson (NR) method
! -central weighting (CDS) is used (numColumn is selected in
! routine dataCheck so that CDS remains stable)
! -Crank-Nicolson (CN) method of time integration is used
! (delTimeMax is selected in routine dataCheck to ensure
! CN stability and to reduce numerical dispersion)
!-----
subroutine coefColumn()
  use globalVariables
  implicit none
  integer :: i
  real (kind=8) :: difCoef, advCoef, const, constb, volume
! set constants
difCoef=porosity*areaColum/delColum*disper*delTime*0.5
advCoef=porosity*areaColum*velocity*delTime*0.25
volume =porosity*areaColum*delColum
! base coefs.
i=1
  cCoefW(i)=0.0
  cCoefE(i)=difCoef-advCoef
  cCoef(i) =difCoef+advCoef+volume
do i=2,numColumn-1
  cCoefW(i)=difCoef+advCoef
  cCoefE(i)=difCoef-advCoef
  cCoef(i)= cCoefW(i)+cCoefE(i)+volume

```

```

end do
i=numColum
  cCoefW(i)=difCoef+advCoef
  cCoefE(i)=0.0
  cCoef(i)= cCoefW(i)+cCoefE(i)+volume
! add adsorption contribution
if (iAdsorb>0) then
  volume=areaColum*delColum
  const=(1.0-fraCalc)*volume*bulkDens*adsorbK
  do i=1,numColum
    cCoef(i)=cCoef(i)+const
  end do
end if
! add surface partitioning contribution
if (iSurfPart>0) then
  const=areaCalc*molSurfCalc*fwhtMe
  constB=aqueCa/surfDist
  do i=1,numColum
    cCoef(i)=cCoef(i)+const*constB/(c(i)+constB)**2
  end do
! add solid diffusion contribution
if (iSoliDif>0) then
  const=densCalc*fwhtMe/(fwhtCa+fwhtCO3) &
    *areaCalc/delCalc*2.0*soliDifus*delTime*0.5
  do i=1,numColum
    cCoef(i)=cCoef(i)+const*constB/(c(i)+constB)**2
  end do
end if
end if
end subroutine coefColumn

```

```

!=====
! coefCalcite
! -routine to calculate matrix coefs. for the mole fraction
! correction using the NR method
! -CDS & CN methods are used
!-----
subroutine coefCalcite()
  use globalVariables
  implicit none
  integer :: i
  real (kind=8) :: difCoef, volume

```



```

! check for solid state diffusion
if (iSoliDif>0) then
  difCoef=areaCalc*soliDifus/delCalc*delTime*0.5
  volume= areaCalc*delCalc
  i=1
  xCoefW(i)=0.0
  xCoefE(i)=difCoef
  xCoef(i)=3.0*difCoef+volume
do i=2,numCalc-1
  xCoefW(i)=difCoef
  xCoefE(i)=difCoef
  xCoef(i)=2.0*difCoef+volume
end do
i=numCalc
  xCoefW(i)=difCoef
  xCoefE(i)=0.0
  xCoef(i)=difCoef+volume
end if
end subroutine coefCalcite

```

```

=====
! srcColumn
! -routine to calculate the source terms (-'ve residuals)
! for the concentration correction
! -central weighting (CDS) is used (numColumn is selected in
! routine dataCheck so that CDS remains stable)
! -Crank-Nicolson method (CNM) of time integration is used
! (delTimeMax is selected in routine dataCheck to ensure
! CNM stability and to reduce numerical dispersion)
!-----
subroutine srcColumn()
  use globalVariables
  implicit none
  integer :: i
  real (kind=8) :: difCoef, advCoef, const, constb, volume

! set constants
difCoef=porosity*areaColum/delColum*disper*delTime*0.5
advCoef=porosity*areaColum*velocity*delTime*0.25
volume =porosity*areaColum*delColum
! base source terms
i=1
  cSrc(i)=- (volume*(c(i)-cOld(i))      &

```

```

+advCoef*(c(i+1)+c(i)-2.0*aqueMe) &
-difCoef*(c(i+1)-c(i)) &
+advCoef*(cOld(i+1)+cOld(i)-2.0*aqueMe) &
-difCoef*(cOld(i+1)-cOld(i))
do i=2,numColum-1
  cSrc(i)=-(volume*(c(i)-cOld(i)) &
+advCoef*(c(i+1)-c(i-1)) &
-difCoef*(c(i+1)-2.0*c(i)+c(i-1)) &
+advCoef*(cOld(i+1)-cOld(i-1)) &
-difCoef*(cOld(i+1)-2.0*cOld(i)+cOld(i-1)))
end do
i=numColum
  cSrc(i)=-(volume*(c(i)-cOld(i)) &
+advCoef*(c(i)-c(i-1)) &
+difCoef*(c(i)-c(i-1)) &
+advCoef*(cOld(i)-cOld(i-1)) &
+difCoef*(cOld(i)-cOld(i-1)))
! add adsorption contribution
if (iAdsorb>0) then
  volume=areaColum*delColum
  const=(1.0-fraCalc)*volume*bulkDens*adsorbK
  do i=1,numColum
    cSrc(i)=cSrc(i)-const*(c(i)-cOld(i))
  end do
end if
! add surface partitioning contribution
if (iSurfPart>0) then
  const=areaCalc*molSurfCalc*fwhtMe
  constB=aqueCa/surfDist
  do i=1,numColum
    cSrc(i)=cSrc(i)-const*(c(i)/(c(i)+constB) &
-cOld(i)/(cOld(i)+constB))
  end do
! add solid state diffusion contribution
if (iSoliDif>0) then
  const=densCalc*fwhtMe/(fwhtCa+fwhtCO3) &
*areaCalc/delCalc*2.0*soliDifus*delTime*0.5
  do i=1,numColum
    cSrc(i)=cSrc(i)-const*(c(i)/(c(i)+constB)-x(i,1)) &
-const*(cOld(i)/(cOld(i)+constB)-xOld(i,1))
  end do
end if
end if
! calculate the absolute sum of mass residuals

```

```

    absumMasResid=0.0
    do i=1,numColum
        absumMasResid=absumMasResid+abs(cSrc(i))
    end do
end subroutine srcColumn

```

```

=====
! srcCalcite
! -routine to calculate the source terms for the mole fraction
! correction
! -CDS & CN methods are used
!-----
subroutine srcCalcite(i)
    use globalVariables
    implicit none
    real (kind=8) :: difCoef, volume, constB
    integer :: i,j

! set constants
    difCoef=areaCalc/delCalc*soliDifus*delTime*0.5
    volume=areaCalc*delCalc
    constB=aqueCa/surfDist
! source terms
    j=1
        xSrc(j)=- (volume*(x(i,j)-xOld(i,j)) &
            -difCoef*(x(i,j+1)-3.0*x(i,j)+2.0*c(i)/(c(i)+constB)) &
            -difCoef*(xOld(i,j+1)-3.0*xOld(i,j) &
                +2.0*cOld(i)/(cOld(i)+constB)))
    do j=2,numCalc-1
        xSrc(j)=- (volume*(x(i,j)-xOld(i,j)) &
            -difCoef*(x(i,j+1)-2.0*x(i,j)+x(i,j-1)) &
            -difCoef*(xOld(i,j+1)-2.0*xOld(i,j)+xOld(i,j-1)))
    end do
    j=numCalc
        xSrc(j)=- (volume*(x(i,j)-xOld(i,j)) &
            +difCoef*(x(i,j)-x(i,j-1)) &
            +difCoef*(xOld(i,j)-xOld(i,j-1)))
end subroutine srcCalcite

```

```

=====
! timeStep

```

```

! -routine to select time step and assign time related
! parameters and indices
!-----
subroutine timeStep()
  use globalVariables
  implicit none

! initialize time step and set time target
  delTime=delTimeMax
  timeTarget=min(time+delTime,timeEnd,timeOff,timeOut)+1.0e-3
! end time target is met
  if (timeTarget>=timeEnd) then
    delTime=timeEnd-time
    iTimeEnd=1
    iTimeOut=1
    if (timeTarget>=timeOut) timeOut=timeOut+delTimeOut
    iScreen=1
! source off time target is met
  else if (timeTarget>=timeOff) then
    delTime=timeOff-time
    timeOff=timeEnd+delTimeMax
    iTimeOff=1
    iTimeOut=1
    if (timeTarget>=timeOut) timeOut=timeOut+delTimeOut
! output time target is met
  else if (timeTarget>=timeOut) then
    delTime=timeOut-time
    timeOut=timeOut+delTimeOut
    iTimeOut=1
! no target is met
  else
    iTimeOut=0
  end if
! set time and time index
  time=time+delTime
  iTime=iTime+1
! check for screen output
  if (time>timeEnd*real(numScreen-1)/4.0) then
    iScreen=1
  end if
end subroutine timeStep

```

```

!=====

```

```

! totalMass
! -routine to calculate the total mass in the system
!-----
subroutine totalMass()
  use globalVariables
  implicit none
  integer :: i,j
  real (kind=8) :: const, constB, volume

! accumulative mass in and out
totMasIn= totMasIn +porosity*areaColum*velocity*aqueMe*delTime
totMasOut=totMasOut+porosity*areaColum*velocity*delttime &
          *0.5*(c(numColum)+cOld(numColum))
! zero storage mass terms
totMasAque=0.0
totMasAds=0.0
totMasPart=0.0
totMasDif=0.0
! set constant
volume=porosity*areaColum*delColum
! aqueous phase mass
do i=1,numColum
  totMasAque=totMasAque+volume*c(i)
end do
! mass adsorbed onto sand
if (iAdsorb>0) then
  volume=areaColum*delColum
  const=(1.0-fraCalc)*volume*bulkDens*adsorbK
  do i=1,numColum
    totMasAds=totMasAds+const*c(i)
  end do
end if
! mass partitioned into calcite
if (iSurfPart>0) then
  const=areaCalc*molSurfCalc*fwhtMe
  constB=aqueCa/surfDist
  do i=1,numColum
    totMasPart=totMasPart+const*c(i)/(c(i)+constB)
  end do
! mass diffused into calcite
if (iSoliDif>0) then
  const=areaCalc*delCalc*densCalc*fwhtMe/(fwhtCa+fwhtCO3)
  do i=1,numColum
    do j=1,numCalc

```

```

        totMasDif=totMasDif+const*x(i,j)
    end do
end do
end if
end if
! sum storage mass terms
totMasStor=totMasAque+totMasAds+totMasPart+totMasDif
! calc. mass balance
totMasResid=totMasIn-totMasOut-totMasStor
end subroutine totalMass

```

```

=====
! boundaryCalc
! -routine to calculate the boundary concentrations and mole
! fractions
!-----
subroutine boundaryCalc()
    use globalVariables
    implicit none
    integer :: i,j
    real (kind=8) :: difCoef, advCoef

    difCoef=2.0*porosity*areaColum/delColum*disper
    advCoef=porosity*areaColum*velocity
    ! inflow type 3 boundary:  $-D \frac{dC}{dx} + v C = v C_0$ 
    i=0
    c(i)=(difCoef*c(i+1)+advCoef*aqueMe)/(difCoef+advCoef)
    ! outflow type 2 boundary:  $dC/dx=0$ 
    i=numColum
    c(i+1)=c(i)
    ! check for solid diffusion
    if (iSoliDif>0) then
        ! interior type 2 boundary:  $dX/dy=0$ 
        j=numCalc
        x(i,j+1)=x(i,j)
    end if

end subroutine boundaryCalc

```

```

=====
! tdmaSolver
! -tri-diagonal matrix solver -- assumes the east and west

```

```

!   coefs. are defined as positive
!-----
subroutine tdmaSolver(soln,coefP,coefW,coefE,src)
  implicit none
  real (kind=8), intent (in), dimension (:) :: coefP, coefW, coefE, src
  real (kind=8), intent (in out), dimension (:) :: soln
  integer :: iEnd,i
  real (kind=8) :: const
  real (kind=8), dimension (size(coefP)) :: work

  iEnd=size(coefP)
! decomposition & forward substitution
  i=1
  const=coefP(i)
  soln(i)=src(i)/const
  do i=2,iEnd
    work(i)=-coefE(i-1)/const
    const=coefP(i)+coefW(i)*work(i)
    soln(i)=(src(i)+coefW(i)*soln(i-1))/const
  end do
! back-substitution
  do i=iEnd-1,1,-1
    soln(i)=soln(i)-work(i+1)*soln(i+1)
  end do
end subroutine tdmaSolver

```

```

!=====
! inputListFile
!   -routine to read input list file and report errors
!   to error file: errors.txt
!-----
subroutine inputListFile()
  use globalVariables
  implicit none
  integer :: i

  open(iLst,file=fileList)
  open(iErr,file=fileErr)
  write(iErr,"(a,/)" )>>> MeTran errors file <<<'

  numLine=1
  read(iLst,"(a60)",err=10,end=10) textLine
  numLine=numLine+1

```

```

read(iLst,*,err=10,end=10) numSim
if (numSim<1) then          ! check value of numSim
  close(iLst)
  write(iErr,"(/,'error: numSim < 1 on line',i3,' of listing file: ',a)") numLine, fileList
  iError=1
  return
end if
allocate(fileIn(numSim),fileOut(numSim))  ! allocate filename arrays
do i=1,numSim          ! read simulation filenames
  numLine=numLine+1
  read(iLst,*,err=10,end=10) fileIn(i)
  numLine=numLine+1
  read(iLst,*,err=10,end=10) fileOut(i)
end do
close(iLst)
return          ! return if no errors encountered

10 close(iLst)    ! report read error
write(iErr,"(/,'read error on line',i3,' of listing file: ',a)") numLine, fileList
iError=1
return
end subroutine inputListFile

```

```

=====
! inputDataFile
! -routine to read input file(s) data & write the input data
! and/or input file read errors to the output file
! -errors in opening the files are reported in errors.txt
!-----
subroutine inputDataFile()
  use globalVariables
  implicit none

  open(iIn,file=fileIn(iSim),err=5)
  open(iOut,file=fileOut(iSim),err=6)
  write(iOut,"(a//,a,a,/)" '>>> MeTran output file <<<', &
    'echo from input file: ', trim(fileIn(iSim)))
  numLine=1
  read(iIn,"(a60)",err=10,end=10) textLine
  numLine=numLine+1
  read(iIn,"(a60)",err=10,end=10) textLine
  numLine=numLine+1
  read(iIn,*,err=10,end=10) velocity

```



```

write(iOut,"(1p,a24,g12.4,a)") 'velocity:', velocity, '[cm/d]'
numLine=numLine+1
read(iIn,*,err=10,end=10) lenColum
write(iOut,"(1p,a24,g12.4,a)") 'lenColum:', lenColum, '[cm]'
numLine=numLine+1
read(iIn,*,err=10,end=10) radColum
write(iOut,"(1p,a24,g12.4,a)") 'radColum:', radColum, '[cm]'
numLine=numLine+1
read(iIn,*,err=10,end=10) bulkDens
write(iOut,"(1p,a24,g12.4,a)") 'bulkDens:', bulkDens, '[g/cm^3]'
numLine=numLine+1
read(iIn,*,err=10,end=10) bulkSurfArea
write(iOut,"(1p,a24,g12.4,a)") 'bulkSurfArea:', bulkSurfArea, '[m^2/g]'
numLine=numLine+1
read(iIn,*,err=10,end=10) porosity
write(iOut,"(1p,a24,g12.4,a)") 'porosity:', porosity, '[-]'
numLine=numLine+1
read(iIn,*,err=10,end=10) dispsiv
write(iOut,"(1p,a24,g12.4,a)") 'dispsiv:', dispsiv, '[cm]'
numLine=numLine+1
read(iIn,*,err=10,end=10) tortuos
write(iOut,"(1p,a24,g12.4,a)") 'tortuos:', tortuos, '[-]'
numLine=numLine+1
read(iIn,"(a60)",err=10,end=10) textLine
numLine=numLine+1
read(iIn,*,err=10,end=10) aqueMe
write(iOut,"(1p,a24,g12.4,a)") 'aqueMe:', aqueMe, '[mg/L]'
numLine=numLine+1
read(iIn,*,err=10,end=10) aqueDifus
write(iOut,"(1p,a24,g12.4,a)") 'aqueDifus:', aqueDifus, '[cm^2/s]'
numLine=numLine+1
read(iIn,*,err=10,end=10) adsorbK
write(iOut,"(1p,a24,g12.4,a)") 'adsorbK:', adsorbK, '[mL/g]'
numLine=numLine+1
read(iIn,*,err=10,end=10) surfDist
write(iOut,"(1p,a24,g12.4,a)") 'surfDist:', surfDist, '[-]'
numLine=numLine+1
read(iIn,*,err=10,end=10) soliDifus
write(iOut,"(1p,a24,g12.4,a)") 'soliDifus:', soliDifus, '[cm^2/s]'
numLine=numLine+1
read(iIn,*,err=10,end=10) fwhtMe
write(iOut,"(1p,a24,g12.4,a)") 'fwhtMe:', fwhtMe, '[g/mol]'
numLine=numLine+1
read(iIn,"(a60)",err=10,end=10) textLine

```

```

numLine=numLine+1
read(iIn,*,err=10,end=10) fraCalc
write(iOut,"(1p,a24,g12.4,a)") 'fraCalc:', fraCalc, '[-]'
numLine=numLine+1
read(iIn,*,err=10,end=10) lenCalc
write(iOut,"(1p,a24,g12.4,a)") 'lenCalc:', lenCalc, '[A]'
numLine=numLine+1
read(iIn,*,err=10,end=10) densCalc
write(iOut,"(1p,a24,g12.4,a)") 'densCalc:', densCalc, '[g/cm^3]'
numLine=numLine+1
read(iIn,*,err=10,end=10) molSurfCalc
write(iOut,"(1p,a24,g12.4,a)") 'molSurfCalc:', molSurfCalc, '[mol/cm^2]'
numLine=numLine+1
read(iIn,*,err=10,end=10) aqueCa
write(iOut,"(1p,a24,g12.4,a)") 'aqueCa:', aqueCa, '[mg/L]'
numLine=numLine+1
read(iIn,"(a60)",err=10,end=10) textLine
numLine=numLine+1
read(iIn,*,err=10,end=10) timeOff
write(iOut,"(1p,a24,g12.4,a)") 'timeOff:', timeOff, '[d]'
numLine=numLine+1
read(iIn,*,err=10,end=10) timeEnd
write(iOut,"(1p,a24,g12.4,a)") 'timeEnd:', timeEnd, '[d]'
numLine=numLine+1
read(iIn,*,err=10,end=10) delTimeOut
write(iOut,"(1p,a24,g12.4,a)") 'delTimeOut:', delTimeOut, '[d]'
numLine=numLine+1
read(iIn,*,err=10,end=10) distCalcProf
write(iOut,"(1p,a24,g12.4,a)") 'distCalcProf:', distCalcProf, '[cm]'
close(iIn)
return
    ! report open file error in error file
5 write(iErr,"(/,'open error input file: ',a)") trim(fileIn(iSim))
  iError=1
  return
    ! report open file error in error file
6 write(iErr,"(/,'open error output file: ',a)") trim(fileOut(iSim))
  iError=1
  return
    ! report input file read error in output file
10 close(iIn)
  write(iErr,"(/,'read error on line',i3,' of input file: ',a)") numLine, trim(fileIn(iSim))
  write(iOut,"(/,'read error on line',i3,' of input file: ',a)") numLine, trim(fileIn(iSim))
  close(iOut)

```

```

iError=1
return
end subroutine inputDataFile

```

```

=====
! dataCheck
! -check input data for obvious errors, check/assign mass transfer
! control parameters, auto select several parameters (numColum,
! numCalc & delTimeMax), & convert input data units
! -errors are reported in the output file
!-----
subroutine dataCheck()
  use globalVariables
  implicit none

  ! check data for obvious errors
  iError=0
  write(iOut,"(/a)") 'check input data for errors:'
  if (velocity<=0.0) then
    iError=iError+1
    write(iOut,"(24x,a)") 'velocity <= 0'
  end if
  if (lenColum<=0.0) then
    iError=iError+1
    write(iOut,"(24x,a)") 'lenColum <= 0'
  end if
  if (radColum<=0.0) then
    iError=iError+1
    write(iOut,"(24x,a)") 'radColum <= 0'
  end if
  if (bulkDens<=0.0) then
    iError=iError+1
    write(iOut,"(24x,a)") 'bulkDens <= 0'
  end if
  if (bulkSurfArea<=0.0) then
    iError=iError+1
    write(iOut,"(24x,a)") 'bulkSurfArea <= 0'
  end if
  if (porosity<=0.0.or.porosity>1.0) then
    iError=iError+1
    write(iOut,"(24x,a)") 'porosity <= 0 or > 1'
  end if
  if (dispsiv<=0.0) then

```

```
iError=iError+1
write(iOut,"(24x,a)") 'dispsiv <= 0'
end if
if (tortuos<=0.0.or.tortuos>1.0) then
  iError=iError+1
  write(iOut,"(24x,a)") 'tortuos <= 0 or > 1'
end if
if (aqueMe<=0.0) then
  iError=iError+1
  write(iOut,"(24x,a)") 'aqueMe <= 0'
end if
if (aqueDifus<0.0) then
  iError=iError+1
  write(iOut,"(24x,a)") 'aqueDifus < 0'
end if
if (fwhtMe<=0) then
  iError=iError+1
  write(iOut,"(24x,a)") 'fwhtMe <= 0'
end if
if (densCalc<=0.0) then
  iError=iError+1
  write(iOut,"(24x,a)") 'densCalc <= 0'
end if
if (molSurfCalc<=0.0) then
  iError=iError+1
  write(iOut,"(24x,a)") 'molSurfCalc <= 0'
end if
if (aqueCa<=0.0) then
  iError=iError+1
  write(iOut,"(24x,a)") 'aqueCa <= 0'
end if
if (timeOff<=0) then
  iError=iError+1
  write(iOut,"(24x,a)") 'timeOff <= 0'
end if
if (timeEnd<=0) then
  iError=iError+1
  write(iOut,"(24x,a)") 'timeEnd <= 0'
end if
if (delTimeOut<=0.or.delTimeOut>timeEnd) then
  iError=iError+1
  write(iOut,"(24x,a)") 'delTimeOut <= 0 or > timeEnd'
end if
if (iError==0) then
```

```

write(iOut,"(20x,i3,a)") iError,' errors'
else
write(iOut,"(20x,i3,a)") iError,' errors ==> simulation STOPPED'
end if

! check simulation control parameters
if (iError==0) then
write(iOut,"(/a)") 'check control parameters:'
if (adsorbK<=0.0.or.fraCalc>=1.0) then
write(iOut,"(a36,a)") 'adsorbK <= 0 or fraCalc >= 1:', &
' ==> adsorption to sand is OFF'
if(fraCalc>1.0) fraCalc=1.0
iAdsorb=0
else
write(iOut,"(a36,a)") 'adsorbK > 0 and fraCalc < 1:', &
' ==> adsorption to sand is ON'
iAdsorb=1
end if
iSoliDif=1
if (surfDist<=0.0.or.fraCalc<=0.0) then
write(iOut,"(a36,a,/36x,a)") 'surfDist <= 0 or fraCalc <= 0:', &
' ==> surface partitioning is OFF', &
' ==> solid state diffusion is OFF'
if(fraCalc<0.0) fraCalc=0.0
iSurfPart=0
iSoliDif=0
maxNewt=1
else
write(iOut,"(a36,a)") 'surfDist > 0 and fraCalc > 0:', &
' ==> surface partitioning is ON'
iSurfPart=1
maxNewt=10
if (soliDifus<=0.0.or.lenCalc<=0.0) then
write(iOut,"(a36,a)") 'soliDifus <= 0 or lenCalc <= 0:', &
' ==> solid state diffusion is OFF'
iSoliDif=0
else
write(iOut,"(a36,a)") 'soliDifus > 0 and lenCalc > 0:', &
' ==> solid state diffusion is ON'
iSoliDif=1
end if
end if
if (timeOff<timeEnd) then
write(iOut,"(a36,a)") 'timeOff < timeEnd:', &

```

```

        ' ==> Me2+ source is pulsed'
else
  write(iOut,"(a36,a)") 'timeOff >= timeEnd:', &
    ' ==> Me2+ source is continuous'
end if

! assign/calculate remaining parameters
areaColum=pi*radColum**2
disper=velocity/8.64e+4*dispsiv+aqueDifus*tortuos
peColum=velocity/8.64e+4*lenColum/disper
numColum=max(nint(lenColum/dispsiv),20)
delColum=lenColum/real(numColum)
peGrid= peColum/real(numColum)
delTimeCFL=delColum/velocity
delTimeMax=min(delTimeCFL,delTimeOut)
areaCalc=fraCalc*bulkSurfArea*bulkDens*delColum*areaColum
if (iSoliDif>0) then
  numCalc=max(min(nint(lenCalc/3.0),10),1)
  delCalc=lenCalc/real(numCalc)
  iCalcProf=nint(distCalcProf/delColum)
  if (iCalcProf<1) iCalcProf=1
  if (iCalcProf>numColum) iCalcProf=numColum
else
  numCalc=0.0
  delCalc=0.0
  iCalcProf=0
end if

write(iOut,"(/a)") 'assign remaining parameters:'
write(iOut,"(1p,a36,g12.4,a)") 'column dispersion: ',disper,' [cm^2/s]'
write(iOut,"(1p,a36,g12.4,a)") 'column Peclet no.: ',peColum,' [-]'
write(iOut,"(1p,a36,i8)") '# column increments: ',numColum
write(iOut,"(1p,a36,g12.4,a)") 'grid Peclet no.: ',peGrid,' [-]'
write(iOut,"(1p,a36,g12.4,a)") 'column increment: ',delColum,' [cm]'
write(iOut,"(1p,a36,i8)") '# calcite increments: ',numCalc
write(iOut,"(1p,a36,g12.4,a)") 'calcite increment: ',delCalc,' [A]'
write(iOut,"(1p,a36,g12.4,a)") 'Courant time step: ',delTimeCFL,' [d]'
write(iOut,"(1p,a36,g12.4,a)") 'max. time step: ',delTimeMax,' [d]'

! unit conversion
velocity=velocity/8.64e+6      input   simulation
                                ! cm/s   => m/s
lenColum=lenColum*1.0e-2      ! cm    => m
radColum=radColum*1.0e-2      ! cm    => m
bulkDens=bulkDens*1.0e+6      ! g/cm^3 => g/m^3

```

```

dispsiv=dispsiv*1.0e-2      ! cm  => m
adsorbK=adsorbK*1.0e-6     ! mL/g  => m^3/g
aqueDifus=aqueDifus*1.0e-4 ! cm^2/s => m^2/s
soliDifus=soliDifus*1.0e-4 ! cm^2/s => m^2/s
lenCalc=lenCalc*1.0e-10   ! A    => m
densCalc=densCalc*1.0e+6   ! g/cm^3 => g/m^3
molSurfCalc=molSurfCalc*1.0e+4 ! mol/cm^2 => mol/m^2
timeOff=timeOff*8.64e+4    ! d    => s
timeEnd=timeEnd*8.64e+4   ! d    => s
delTimeOut=delTimeOut*8.64e+4 ! d    => s
areaColum=areaColum*1.0e-4 ! cm^2  => m^2
disper=disper*1.0e-4      ! cm^2/s => m^2/s
delColum=delColum*1.0e-2   ! cm    => m
delCalc=delCalc*1.0e-10   ! A    => m
delTimeCFL=delTimeCFL*8.64e+4 ! d    => s
delTimeMax=delTimeMax*8.64e+4 ! d    => s
distCalcProf=distCalcProf*1.0e-2 ! cm  => m
end if
close(iErr)
end subroutine dataCheck

```

```

=====
! initialize
! -routine to allocate and initialize simulation arrays &
! initialize parameters and indices
!-----
subroutine initialize()
  use globalVariables
  implicit none
  integer :: i,j

  ! check if arrays have been previously allocated
  if (iAlocate>0) then
    deallocate(c, cOld)
    deallocate(x, xOld)
    deallocate(cDel, cCoef, cCoefW, cCoefE, cSrc)
    deallocate(xDel, xCoef, xCoefW, xCoefE, xSrc)
  end if
  ! allocate column arrays
  i=numColum
  allocate(c(0:i+1), cOld(0:i+1))
  allocate(cDel(i), cCoef(i), cCoefW(i), cCoefE(i), cSrc(i))
  ! allocate calcite arrays

```

```

if (iSoliDif>0) then
  i=numColum
  j=numCalc
  allocate(x(i,j+1), xOld(i,j+1))
  allocate(xDel(i), xCoef(j), xCoefW(j), xCoefE(j), xSrc(j))
else
  i=0
  j=0
  allocate(x(i,j+1), xOld(i,j+1))
  allocate(xDel(i), xCoef(j), xCoefW(j), xCoefE(j), xSrc(j))
end if
iAlocate=1 ! set allocation flag
! zero all arrays
c=0.0
cOld=0.0
cDel=0.0
cCoef=0.0
cCoefW=0.0
cCoefE=0.0
cSrc=0.0
x=0.0
xOld=0.0
xDel=0.0
xCoef=0.0
xCoefW=0.0
xCoefE=0.0
xSrc=0.0
! initialize indices & parameters
iTimeOut=0
iTimeOff=0
iTimeEnd=0
iTime=0
numNoConv=0
numNewt=0
time=0.0
delTime=delTimeMax
timeOut=delTimeOut
totMasIn=0.0
totMasOut=0.0
end subroutine initialize

```

```

=====
! timeSerOut

```



```

! -routine to output time series data
!-----
subroutine timeSerOut(iflag)
  use globalVariables
  implicit none
  integer :: iflag
! output headings
  if (iflag==0) then
    write(iOut,"(//a)") 'time series output:'
    write(iOut,"(9a12)") ",','cumulative','pore', &
      'sand','calcite','calcite',"
    write(iOut,"(9a12)") ",','outflow','inflow','water','surface', &
      'surface','diffusion','residual'
    write(iOut,"(9a12)") 'time','conc.','- outflow','mass','mass','mass', &
      'mass','mass'
    write(iOut,"(9a12)") '[d],[mg/L],[g],[g],[g],[g]' &
      '[g],[g]'
! output values
    else if(iTimeOut>0) then
      write(iOut,"(1p,8e12.4)") time/8.64e+4,c(numColum), &
        totMasIn-totmasout,totMasAque, &
        totMasAds,totMasPart, &
        totMasDif,totMasResid
    end if
end subroutine timeSerOut

```

```

!=====
! profileOut
! -routine to output column and calcite profile data
!-----
subroutine profileOut()
  use globalVariables
  implicit none
  integer :: i,j
  real (kind=8) :: volume, adsConst, surfConst, difConst
  real (kind=8) :: xSum, const, constB
  real :: distColum, conc, aqueMass,adsMass,surfMass,difMass
  real :: distCalc, xProf, masProf, xAvg, masAvg
! output column profile headings
  write(iOut,"(//a)") 'column profile at end of simulation: '
  write(iOut,"(12x,7a12)") ",','pore','pore','sand','calcite','calcite'
  write(iOut,"(12x,7a12)") 'column','water','water','surface', &
    'surface','diffusion'

```

```

write(iOut,"(12x,7a12)") 'distance','conc.','mass','mass', &
      'mass','mass'
write(iOut,"(12x,7a12)") [cm],[mg/L],[g],[g],[g],[g]'
! output column profile values
conc=c(0)
write(iOut,"(1p,12x,7e12.4)") 0.0,conc
distColum=delColum*50.0
volume=areaColum*delColum*porosity
adsConst=(1.0-fraCalc)*areaColum*delColum*bulkDens*adsorbK
surfConst=areaCalc*molSurfCalc*fwhtMe
difConst=areaCalc*delCalc*densCalc*fwhtMe/(fwhtCa+fwhtCO3)
constB=aqueCa/surfDist
do i=1,numColum
  aqueMass=volume*c(i)
  adsMass=adsConst*c(i)
  if (iSurfPart>0) then
    surfMass=surfConst*c(i)/(c(i)+constB)
    difMass=0.0
    if (iSoliDif>0) then
      do j=1,numCalc
        difMass=difMass+difConst*x(i,j)
      end do
    end if
  end if
  conc=c(i)
  write(iOut,"(1p,12x,6e12.4)") distColum,conc,aqueMass, &
    adsMass,surfMass,difMass
  distColum=distColum+delColum*100.0
end do
conc=c(numColum+1)
write(iOut,"(1p,12x,6e12.4)") lenColum*100.0,conc

! check for solid state diffusion
if (iSoliDif>0) then
  ! output calcite profile headings
  write(iOut,"(//a)") 'calcite profile at end of simulation:'
  write(iOut,"(1p,a60,e12.4,a)") 'user specified column location of calcite profile: ', &
    distCalcProf*100.0, '[cm]'
  write(iOut,"(1p,a60,e12.4,a)") 'nearest calculated column location of calcite profile: ',
&
    (real(iCalcProf)-0.5)*delColum*100.0, '[cm]'
  write(iOut,"(24x,2a24)") 'specified location ',column average '
  write(iOut,"(12x,5a12)") 'calcite','mole','mole'
  write(iOut,"(12x,5a12)") 'distance','fraction','mass','fraction','mass'

```

```

write(iOut,"(12x,5a12)") [A]','[-]','[g]','[-]','[g]'
! output calcite profile values
xSum=0.0
const=areaCalc*molSurfCalc*fwhtMe
constB=aqueCa/surfDist
xProf=c(iCalcProf)/(c(iCalcProf)+constB)
masProf=xProf*const
do i=1,numColum
  xSum=xSum+c(i)/(c(i)+constB)
end do
xAvg=xSum/real(numColum)
masAvg=xAvg*const
write(iOut,"(1p,12x,5e12.4)") 0.0,xProf,masProf,xAvg,masAvg
const=areaCalc*delCalc*densCalc*fwhtMe/(fwhtCa+fwhtCO3)
distCalc=delCalc*0.5e+10
do j=1,numCalc
  xProf=x(iCalcProf,j)
  masProf=xProf*const
  xSum=0.0
  do i=1,numColum
    xSum=xSum+x(i,j)
  end do
  xAvg=xSum/real(numColum)
  masAvg=xAvg*const
  write(iOut,"(1p,12x,5e12.4)") distCalc,xProf,masProf,xAvg,masAvg
  distCalc=distCalc+delCalc*1.e+10
end do
distCalc=lenCalc*1.e+10
write(iOut,"(1p,12x,2e12.4,12x,e12.4)") distCalc,xProf,xAvg
end if

end subroutine profileOut

```

```

=====
! performOut
! -routine to output simulation performance parameters
! =====
subroutine performOut()
  use globalVariables
  implicit none
  real :: avgNewt

  if (iTime>0) then

```

```

    avgNewt=real(numNewt)/real(iTime)
else
    avgNewt=0.0
end if
write(iOut,"(//a)") 'simulation performance: '
write(iOut,"(a36,i8)") 'total time steps: ',iTime
write(iOut,"(a36,i8)") 'total non-converged steps: ',numNoConv
write(iOut,"(a36,g12.4,/)") 'avg. Newton iter. per step: ',avgNewt
close(iOut)
end subroutine performOut

```

```

=====
! screenOut
! -routine to output screen information
!-----
subroutine screenOut()
    use globalVariables
    implicit none

! check screen output flag
if (iScreen>0) then
! check screen output index
if (numScreen==0) then
    write(iScr,"(//5x,a)") '>>> MeTran v1.04 -- University of Waterloo 1998 <<<<'
    numScreen=numScreen+1
    iScreen=1
else if (numScreen==1) then
    write(iScr,"(/a,i2,a,i2,a)") '---- simulation ',iSim,' of ',numSim, &
    '-----'
    write(iScr,"(a40,a)") 'input file: ', trim(fileIn(iSim))
    write(iScr,"(a40,a)") 'output file: ', trim(fileOut(iSim))
    write(iScr,"(a40,i8)") '# column increments: ',numColum
    write(iScr,"(a40,i8)") '# calcite increments: ',numCalc
    write(iScr,"(1p,a40,g12.4)") 'column Peclet no.: ',peColum
    write(iScr,"(1p,a40,g12.4,a)") 'simulation end time: ',timeEnd/8.64e+4,' [d]'
    write(iScr,"(1p,a40,g12.4,a)") 'max. time step: ',delTimeMax/8.64e+4,' [d]'
    write(iScr,"(a40,i8)") 'approx. # time steps: ',nint(timeEnd/delTimeMax)
    write(iScr,"(/a40,a)") 'processing complete: ', ' 0 %'
    numScreen=numScreen+1
    iScreen=0
else if (numScreen==2) then
    write(iScr,"(40x,a)") ' 25 %'
    numScreen=numScreen+1

```

```
    iScreen=0
  else if (numScreen==3) then
    write(iScr,"(40x,a)" ' 50 %'
    numScreen=numScreen+1
    iScreen=0
  else if (numScreen==4) then
    write(iScr,"(40x,a)" ' 75 %'
    numScreen=numScreen+1
    iScreen=0
  else if (numScreen==5) then
    write(iScr,"(40x,a)" ' 100 %'
    numScreen=1
    iScreen=1
  end if
end if
end subroutine screenOut
```

Biography

The author was born, raised and educated near the western edge of the Allegheny Mountains. As an undergraduate, she spent a summer in the Chemistry Department at Dartmouth College as a National Science Foundation-Research Experience for Undergraduates (NSF-REU) intern. After graduating from Allegheny College in 1993 with a B.S. magna cum laude in Chemistry, she headed west to attend the Oregon Graduate Institute. While in the Pacific Northwest, she studied Environmental Science, Aikido and the off road limitations of an '88 Dodge Omni. Upon completion of her Ph.D. in Environmental Science and Engineering, the author plans to take the Omni on one last great adventure returning to the Appalachian Mountains. She intends to ease into the non-student lifestyle with a post-doc at the Oak Ridge National Laboratory. It is her eventual goal to teach at a liberal arts college.

Publications

Pavlick, A. and Pankow, J. F. (1999) The solid solution/aqueous solution partitioning of cadmium to calcite. *Abstracts of Papers*, Northwest Regional ACS Meeting, June 20-23.

Pankow, J. F., B. T. Mader, L. M. Isabelle, W. Luo, A. Pavlick, and C. Liang (1997) Conversion of nicotine in tobacco smoke to its volatile and available free-base form through the action of gaseous ammonia, *Environmental Science and Technology*, **31**, 2428-2433.

Sheffield, A. E. and A. Pavlick (1993) Surface area and compositional analysis of atmospheric particles, *Abstracts of Papers*, Eastern Analytical Symposium, November 14-19.